

Electronic Supplementary Information

Multifunctional 3-Cyanopyridine Compounds: Synthesis Based on Tandem Reaction with 100% Atomic Economy and Their Applications

Xi-Ying Cao^a, Zhong-Hao Li^a, Xiao-Hui Cao^{*b}, Zong Li^a, Chu-Ming Pang^{*c}, Zu-Qi Zhang^a,
Zhao-Yang Wang^{*a}

^a School of Chemistry, South China Normal University; Guangzhou Key Laboratory of Analytical Chemistry for Biomedicine; GDMPA Key Laboratory for Process Control and Quality Evaluation of Chiral Pharmaceuticals; Key Laboratory of Theoretical Chemistry of Environment, Ministry of Education, Guangzhou, 510006, P. R. China.

^b School of Pharmacy, Guangdong Pharmaceutical University, Guangzhou 510006, P. R. China.

^c School of Materials Science and Engineering, South China University of Technology, Guangzhou 510640, P. R. China.

*Corresponding authors: wangzy@scnu.edu.cn; nkallwar@126.com; 202210183286@mail.scut.edu.cn

Contents

1. General Information	1
1.1. Conventional Reagents and Equipments	1
1.2. Activation of Strain and Preparation of Bacterial Suspension.....	1
1.3. Minimum Inhibitory Concentration (MIC) and Minimum Bactericidal Concentration (MBC) Assays	1
2. Experimental Part.....	3
2.1. Experimental Procedure for Compounds 3a-3k and 4a-4t	3
2.2. Characterization Data for All Products 3a-3k and 4a-4t	4
2.3. Characterization Spectra for All Products 3a-3k and 4a-4t	16
2.4. Data of Single-crystal X-ray Analysis.....	70
2.5. Investigations of the Reaction Mechanism.....	72
2.6. Gram Scale Experiment.....	74
3. Computational Details	75
3.1. Absolute Energies and Energy Corrections	75
3.2. Coordinations.....	77
4. Optical Property Characterization.....	85
4.1. Photophysical Properties of 3d , 3g , 3i , 3j , 4g and 4h	85
4.2. Fluorescence Emission Spectra and UV-Vis Absorption Spectra of Compounds 3d , 3g , 3i , 3j , 4g , and 4h	86
4.3. Assessment of AIE Properties for Compounds 3d , 3g , 3i , 3j , 4g , and 4h	89
4.4. Dual-state Emission Testing of Six Representative Compounds.....	92
4.5. The Responses of Compounds 3d and 4g to Metal Ions	93
5. Antimicrobial Activity Assays	114
6. References	115

1. General Information

1.1. Conventional Reagents and Equipments

Melting point (m.p.) was performed on an X-5 digital melting point apparatus without correcting. Flash column chromatography was performed using 200-300 mesh silica gel. The ¹H and ¹³C NMR spectra were acquired on a 600 MHz Bruker spectrometer. High resolution mass spectra (HR-MS) were recorded on the MAT95XP high resolution mass spectrometry (Thermo Fisher Technologies, USA). UV-Visible absorbance spectra were performed on UV-2700 ultraviolet spectrometer (SHIMADZU, Japan). The fluorescence spectra were measured by F-4600 fluorescence spectrometer (HITACHI, Japan). The single crystal structure was determined by Agilent Gemini E type X-ray single crystal diffraction (Agilent, USA) using Mo as a target. The biosafety cabinet adopts Suzhou Antai Air Technology Co., LTD., whose model is BSC-1003.

All reagents and solvents were purchased from commercial sources and used without further purification. Different benzopyranonitriles **1** were synthesized as the reported method in our lab.^[1]

1.2. Activation of Strain and Preparation of Bacterial Suspension

As reported in reference,^[2] the streak plate method was employed to disperse *Escherichia coli* ATCC 43894 and *Staphylococcus aureus* ATCC 25923, which were stored frozen at -80 °C, onto LB agar plates. These plates were then incubated at 37 °C in a biochemical incubator for 24 h. Single colonies were selected from the agar plates by using an inoculation loop and inoculated into 2 mL of liquid LB broth, followed by incubation for 12 h. Subsequently, 50 µL of the bacterial suspension was diluted 1:100 and used for further expansion to the logarithmic growth phase.

1.3. Minimum Inhibitory Concentration (MIC) and Minimum Bactericidal Concentration (MBC) Assays

As reported in references,^[3, 4] the bacterial suspension, cultured to the logarithmic phase, was diluted with LB broth to an OD₆₀₀ = 0.1 for subsequent use. A stock solution of the test compound was prepared at a concentration of 4 mg/mL by dissolving 8 mg of the compound. Serial dilutions were performed in a 96-well plate by using LB broth to achieve a range of concentrations (180 µL). An equal volume (20 µL) of the diluted bacterial suspension was then added to each well, resulting in final compound concentrations of 2000, 1000, 500, 250, 125, 62.5, 31.25, 15.625, and 7.8125 µg/mL. The plates were incubated at 37 °C (18 h for *E.*

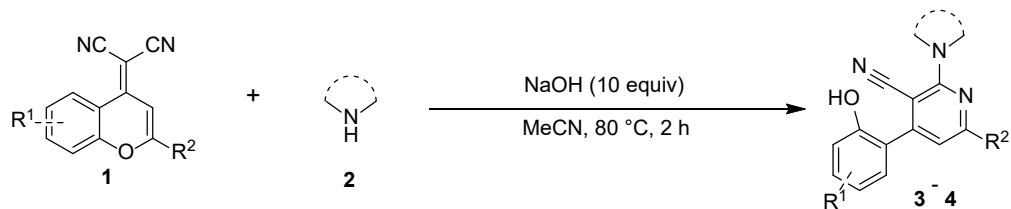
coli and 18-20 h for *S. aureus*).

The Minimum Inhibitory Concentration (MIC) was defined as the lowest concentration of the compound at which no visible bacterial growth was observed. A bacterial suspension without the compound served as a negative control, while LB broth without bacteria or compound served as a positive control. Each concentration was tested in triplicate, and the experiment was technically repeated three times to confirm the MIC values for each bacterium.

The Minimum Bactericidal Concentration (MBC) was determined as the lowest concentration of the compound required to completely kill the bacteria. From the MIC assay, 100 μ L of the wells that showed no turbidity were plated onto agar plates. After incubation at 37 °C for 24 h, the MBC was defined as the lowest concentration at which no bacterial colonies were observed.

2. Experimental Part

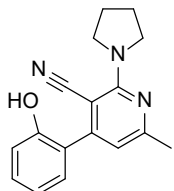
2.1. Experimental Procedure for Compounds 3a-3k and 4a-4t



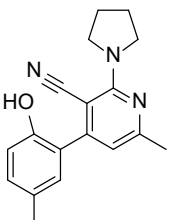
To a 25 mL round-bottom flask, benzopyranonitrile **1** (0.3 mmol), pyrrolidine **2** (3 mmol), and NaOH (3 mmol) were added and dissolved in 4 mL of MeCN. The mixture was stirred at 80 °C for 2 h. After completion of the reaction, the solvent was evaporated under reduced pressure. The residue was dissolved in an appropriate amount of water, and the pH of the solution was adjusted to neutral with HCl (6 M). The aqueous phase was extracted with dichloromethane (15×3). The organic phases were combined, dried over anhydrous sodium sulfate, and concentrated under reduced pressure. The resulted crude product was further purified by column chromatography (petroleum ether/ethyl acetate = 10/1, v/v) to afford **3a-3j** and **4a-4t**.

By the way, in the following control experiments, we also used the above method to synthesized product **3k** only using piperidine instead of pyrrolidine (see **Scheme S1, Eq. 2** in other part of **ESI** in the following).

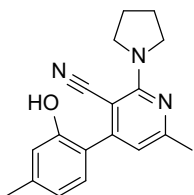
2.2. Characterization Data for All Products 3a-3k and 4a-4t



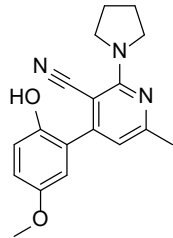
4-(2-Hydroxyphenyl)-6-methyl-2-(pyrrolidin-1-yl)nicotinonitrile (3a): Yellowish solid, m.p. 169.0-170.4 °C, yield: 96%; **¹H NMR** (600 MHz, CDCl₃), δ, ppm: 1.91 (*t*, *J* = 6.6 Hz, 4H), 2.47 (*s*, 3H), 3.55 (*t*, *J* = 6.6 Hz, 4H), 6.95 (*s*, 1H), 7.18-7.24 (*m*, 2H), 7.40-7.45 (*m*, 1H), 7.85 (*d*, *J* = 7.8 Hz, 1H); **¹³C NMR** (150 MHz, CDCl₃), δ, ppm: 25.2, 25.5, 50.5, 96.2, 103.4, 117.1, 117.2, 123.7, 123.9, 131.3, 144.7, 152.6, 158.0, 158.1, 160.0; **ESI-HRMS**, *m/z*: Calcd for C₁₇H₁₈N₃O [M+H]⁺, 208.1444, found: 208.1441.



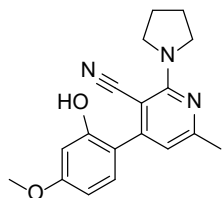
4-(2-Hydroxy-5-methylphenyl)-6-methyl-2-(pyrrolidin-1-yl)nicotinonitrile (3b): White solid, m.p. 142.9-143.7 °C, yield: 95%; **¹H NMR** (600 MHz, CDCl₃), δ, ppm: 1.91 (*t*, *J* = 6.6 Hz, 4H), 2.38 (*s*, 3H), 2.48 (*s*, 3H), 3.55 (*t*, *J* = 6.6 Hz, 4H), 6.95 (*s*, 1H), 7.12 (*d*, *J* = 8.4 Hz, 1H), 7.23 (*d*, *J* = 8.4 Hz, 1H), 7.64 (*s*, 1H); **¹³C NMR** (150 MHz, CDCl₃), δ, ppm: 21.0, 25.2, 25.5, 50.5, 96.3, 103.4, 116.8, 123.7, 132.3, 133.4, 144.7, 150.7, 158.1, 158.2, 161.8; **ESI-HRMS**, *m/z*: Calcd for C₁₈H₂₀N₃O [M-H]⁺, 294.1601, found: 294.1596.



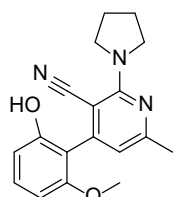
4-(2-Hydroxy-4-methylphenyl)-6-methyl-2-(pyrrolidin-1-yl)nicotinonitrile (3c): Yellow solid, m.p.: 215.8-217.3 °C, yield: 89%; **¹H NMR** (600 MHz, CDCl₃), δ, ppm: 1.96 (*t*, *J* = 6.6 Hz, 4H), 2.31 (*s*, 3H), 2.42 (*s*, 3H), 3.80 (*t*, *J* = 6.6 Hz, 4H), 5.92 (*b*, 1H), 6.45 (*s*, 1H), 6.74 (*s*, 1H), 6.81 (*d*, *J* = 7.8 Hz, 1H), 7.10 (*d*, *J* = 7.8 Hz, 1H); **¹³C NMR** (150 MHz, CDCl₃), δ, ppm: 21.4, 25.0, 25.7, 49.5, 87.7, 113.0, 117.2, 119.2, 121.7, 122.0, 130.0, 141.1), 152.6, 153.7, 158.0, 161.8; **ESI-HRMS**, *m/z*: Calcd for C₁₈H₂₀N₃O [M+H]⁺: 294.1601, Found: 294.1595.



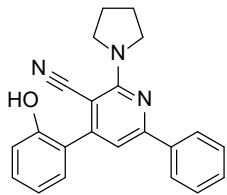
4-(2-Hydroxy-5-methoxyphenyl)-6-methyl-2-(pyrrolidin-1-yl)nicotinonitrile (3d): White solid, m.p.: 165.8-168.2 °C, yield: 95%; **¹H NMR** (600 MHz, CDCl₃), δ, ppm: 1.95 (*t*, *J* = 6.6 Hz, 4H), 2.41 (*s*, 3H), 3.78 (*s*, 3H), 3.79 (*t*, *J* = 6.6 Hz, 4H), 5.96 (*b*, 1H), 6.45 (*s*, 1H), 6.74 (*s*, 1H), 6.81-6.84 (*m*, 2H); **¹³C NMR** (150 MHz, CDCl₃), δ, ppm: 25.0, 25.7, 49.5, 55.9, 87.5, 113.0, 115.0, 116.5, 117.7, 119.0, 125.5, 146.8, 153.4, 153.7, 157.8, 161.8; **ESI-HRMS**, *m/z*: Calcd for C₁₈H₂₀N₃O₂ [M+H]⁺: 310.1550, Found: 310.1545.



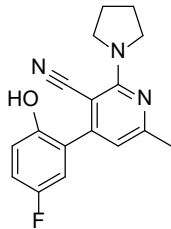
4-(2-Hydroxy-4-methoxyphenyl)-6-methyl-2-(pyrrolidin-1-yl)nicotinonitrile (3e): White solid, m.p.: 198.3-199.1 °C, yield: 93%; **¹H NMR** (600 MHz, CDCl₃), δ, ppm: 1.96 (*t*, *J* = 6.6 Hz, 4H), 2.41 (*s*, 3H), 3.75 (*s*, 3H), 3.79 (*t*, *J* = 6.6 Hz, 4H), 6.44 (*s*, 1H), 6.46 (*s*, 1H), 6.55 (*d*, *J* = 8.4 Hz, 1H), 7.12 (*d*, *J* = 8.4 Hz, 1H); **¹³C NMR** (150 MHz, CDCl₃), δ, ppm: 25.0, 25.7, 49.5, 55.4, 87.8, 102.2, 106.8, 113.2, 117.6, 119.4, 131.1, 153.7, 154.3, 158.1, 161.7, 161.7; **ESI-HRMS**, *m/z*: Calcd for C₁₈H₂₀N₃O₂ [M+H]⁺: 310.1550, Found: 310.1545.



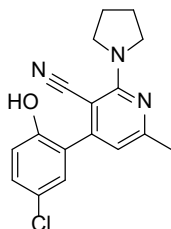
4-(2-Hydroxy-6-methoxyphenyl)-6-methyl-2-(pyrrolidin-1-yl)nicotinonitrile (3f): White solid, m.p.: 162.6-164.3 °C, yield: 42%; **¹H NMR** (600 MHz, CDCl₃), δ, ppm: 1.98 (*t*, *J* = 6.6 Hz, 4H), 2.44 (*s*, 3H), 3.74-3.86 (*m*, 7H), 6.43 (*s*, 1H), 6.58-6.62 (*m*, 2H), 7.25 (*t*, *J* = 7.8 Hz, 1H); **¹³C NMR** (150 MHz, CDCl₃), δ, ppm: 24.8, 25.6, 49.3, 56.00, 89.2, 103.3, 109.3, 113.4, 113.9, 118.7, 130.3, 150.0, 153.6, 157.4, 157.7, 161.2; **ESI-HRMS**, *m/z*: Calcd for C₁₈H₂₀N₃O₂ [M+H]⁺: 310.1550, Found: 310.1545.



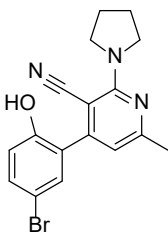
4-(2-Hydroxyphenyl)-6-phenyl-2-(pyrrolidin-1-yl)nicotinonitrile (3g): White solid, m.p.: 221.4-223.4 °C, yield: 72%; **¹H NMR** (600 MHz, CDCl₃), δ, ppm: 2.05 (*t*, *J* = 6.6 Hz, 4H), 3.96 (*t*, *J* = 6.6 Hz, 4H), 5.37 (*s*, 1H), 6.98 (*d*, *J* = 8.4 Hz, 1H), 7.04-7.10 (*m*, 1H), 7.12 (*s*, 1H), 7.30-7.37 (*m*, 2H), 7.45-7.50 (*m*, 3H), 8.06-8.10 (*m*, 2H); **¹³C NMR** (150 MHz, CDCl₃), δ, ppm: 20.5, 21.3, 61.5, 105.3, 115.7, 116.8, 117.2, 118.4, 125.0, 135.9, 136.2, 151.1, 153.1, 161.7; **ESI-HRMS**, *m/z*: Calcd for C₂₂H₂₀N₃O [M+H]⁺: 342.1601, Found: 342.1596.



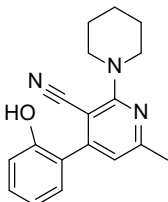
4-(5-Fluoro-2-hydroxyphenyl)-6-methyl-2-(pyrrolidin-1-yl)nicotinonitrile (3h): Yellowish solid, m.p.: 171.8-173.2 °C, yield: 89%; **¹H NMR** (600 MHz, CDCl₃), δ, ppm: 1.97 (*t*, *J* = 6.6 Hz, 4H), 2.42 (*s*, 3H), 3.80 (*t*, *J* = 6.6 Hz, 4H), 5.91 (*b*, 1H), 6.42 (*s*, 1H), 6.81-6.85 (*m*, 1H), 6.90-6.93 (*m*, 1H), 6.95-6.99 (*m*, 1H); **¹³C NMR** (150 MHz, CDCl₃), δ, ppm: 25.1, 25.7, 49.4, 87.1, 112.7, 116.5 (*d*, *J* = 23.9 Hz), 117.1 (*d*, *J* = 22.8 Hz), 117.6 (*d*, *J* = 8.0 Hz), 118.9, 125.9 (*d*, *J* = 7.7 Hz), 148.9 (*d*, *J* = 2.3 Hz), 152.4, 156.7 (*d*, *J* = 238.2 Hz), 157.8, 162.3; **¹⁹F NMR** (564 MHz, CDCl₃), δ, ppm: -123.8; **ESI-HRMS**, *m/z*: Calcd for C₁₇H₁₇N₃OF [M+H]⁺: 298.1350, Found: 298.1345.



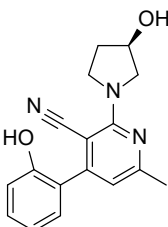
4-(5-Chloro-2-hydroxyphenyl)-6-methyl-2-(pyrrolidin-1-yl)nicotinonitrile (3i): Yellow-green solid, m.p.: 188.9-190.4 °C, yield: 82%; **¹H NMR** (600 MHz, CDCl₃), δ, ppm: 1.97 (*t*, *J* = 6.6 Hz, 4H), 2.42 (*s*, 3H), 3.79 (*t*, *J* = 6.6 Hz, 4H), 6.40 (*s*, 1H), 6.78 (*d*, *J* = 8.4 Hz, 1H), 7.16 (*s*, 1H), 7.18 (*d*, *J* = 8.4 Hz, 1H); **¹³C NMR** (150 MHz, CDCl₃), δ, ppm: 25.1, 25.7, 49.4, 87.1, 112.8, 117.9, 119.0, 125.4, 126.5, 129.7, 130.5, 151.7, 152.4, 157.7, 162.4; **ESI-HRMS**, *m/z*: Calcd for C₁₇H₁₇N₃OCl [M+H]⁺: 314.1055, Found: 314.1048.



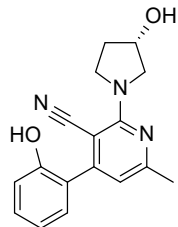
4-(5-Bromo-2-hydroxyphenyl)-6-methyl-2-(pyrrolidin-1-yl)nicotinonitrile (3j): White solid, m.p.: 209.3-210.1 °C, yield: 75%; **1H NMR** (600 MHz, CDCl₃), δ, ppm: 1.96 (*t*, *J* = 6.6 Hz, 4H), 2.41 (*s*, 3H), 3.78 (*t*, *J* = 6.6 Hz, 4H), 6.40 (*s*, 1H), 6.68 (*d*, *J* = 9.0 Hz, 1H), 6.85 (*b*, 1H), 7.26-7.33 (*m*, 2H); **13C NMR** (150 MHz, CDCl₃), δ, ppm: 25.1, 25.7, 49.4, 87.0, 112.2, 112.9, 118.3, 119.1, 127.0, 132.5, 133.3, 152.5, 152.6, 157.6, 162.3; **ESI-HRMS**, *m/z*: Calcd for C₁₇H₁₇N₃OBr [M+H]⁺: 358.0550, Found: 358.0542.



4-(2-Hydroxyphenyl)-6-methyl-2-(piperidin-1-yl)nicotinonitrile (3k): Yellow solid, m.p.: 189.8-191.8 °C, yield: 35%; **1H NMR** (600 MHz, CDCl₃), δ, ppm: 1.63-1.72 (*m*, 6H), 2.48 (*s*, 3H), 3.50-3.55 (*m*, 4H), 7.00 (*s*, 1H), 7.19-7.25 (*m*, 2H), 7.41-7.46 (*m*, 1H), 7.86 (*d*, *J* = 8.4 Hz, 1H); **13C NMR** (150 MHz, CDCl₃), δ, ppm: 24.6, 25.2, 26.0, 50.7, 98.0, 104.9, 117.1, 117.2, 123.7, 123.9, 131.4, 145.6, 152.5, 158.5, 161.2, 161.9; **ESI-HRMS**, *m/z*: Calcd for C₁₈H₂₀N₃O [M+H]⁺: 294.1601, Found: 294.1601.

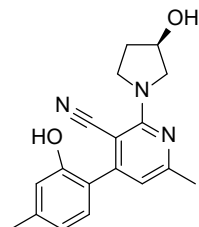


(R)-4-(2-Hydroxyphenyl)-2-(3-hydroxypyrrolidin-1-yl)-6-methylnicotinonitrile (4a): White solid, m.p.: 178.2-179.4 °C, yield: 97%; **1H NMR** (600 MHz, CDCl₃), δ, ppm: 2.01-2.08 (*m*, 2H), 2.55 (*s*, 3H), 3.28 (*d*, *J* = 12.6 Hz, 1H), 3.56-3.64 (*m*, 1H), 4.01-4.09 (*m*, 2H), 4.55-4.60 (*m*, 1H), 7.06 (*s*, 1H), 7.28-7.32 (*m*, 2H), 7.50-7.53 (*m*, 1H), 7.93 (*d*, *J* = 7.2 Hz, 1H); **13C NMR** (150 MHz, CDCl₃), δ, ppm: 25.1, 33.5, 47.7, 58.8, 70.8, 96.7, 104.1, 117.1, 117.2, 123.8, 124.0, 131.6, 145.0, 152.6, 158.1, 158.3, 162.1; **ESI-HRMS**, *m/z*: Calcd for C₁₇H₁₈N₃O₂ [M+H]⁺: 296.1394, Found: 296.1400.



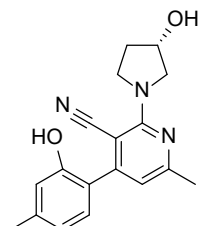
(S)-4-(2-Hydroxyphenyl)-2-(3-hydroxypyrrolidin-1-yl)-6-methylnicotinonitrile (4b):

White solid, m.p.: 163.6-164.1 °C, yield: 96%; **¹H NMR** (600 MHz, DMSO-*d*₆), δ, ppm: 2.02-2.07 (*m*, 2H), 2.43 (*s*, 3H), 3.83 (*d*, *J* = 12.0 Hz, 1H), 3.86-3.92 (*m*, 1H), 3.93-4.02 (*m*, 2H), 4.50-4.54 (*m*, 1H), 5.32 (*s*, 1H), 6.50 (*s*, 1H), 6.92 (*d*, *J* = 8.4 Hz, 1H), 6.97-7.01 (*m*, 1H), 7.20 (*d*, *J* = 8.4 Hz, 1H), 7.26-7.30 (*m*, 1H); **¹³C NMR** (600 MHz, DMSO-*d*₆), δ, ppm: 24.8, 33.4, 47.0, 57.4, 70.4, 87.8, 113.6, 116.4, 119.1, 120.3, 124.9, 130.1, 130.6, 153.2, 154.3, 157.8, 161.8; **ESI-HRMS**, *m/z*: Calcd for C₁₇H₁₈N₃O₂ [M+H]⁺: 296.1394, Found: 296.1400.



(R)-4-(2-Hydroxy-4-methylphenyl)-2-(3-hydroxypyrrolidin-1-yl)-6-methylnicotinonitrile (4c):

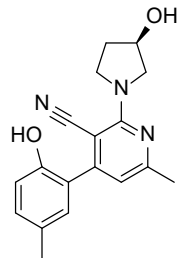
White solid, m.p.: 174.1-175.9 °C, yield: 77%; **¹H NMR** (600 MHz, CD₃OD), δ, ppm: 2.00-2.11 (*m*, 2H), 2.32 (*s*, 3H), 2.41 (*s*, 3H), 3.74 (*d*, *J* = 11.4 Hz, 1H), 3.81-3.86 (*m*, 1H), 3.90-3.98 (*m*, 2H), 4.47-4.52 (*m*, 1H), 6.53 (*s*, 1H), 6.74 (*d*, *J* = 7.8 Hz, 1H), 6.76 (*s*, 1H), 7.04 (*d*, *J* = 7.8 Hz, 1H); **¹³C NMR** (150 MHz, CD₃OD), δ, ppm: 25.1, 23.5, 33.1, 46.7, 56.9, 69.8, 87.9, 113.5, 116.1, 118.7, 120.0, 122.3, 129.7, 140.5, 154.0, 155.0, 158.0, 161.0; **ESI-HRMS**, *m/z*: Calcd for C₁₈H₂₀N₃O₂ [M+H]⁺: 310.1550, Found: 310.1559.



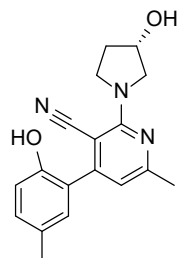
(S)-4-(2-Hydroxy-4-methylphenyl)-2-(3-hydroxypyrrolidin-1-yl)-6-methylnicotinonitrile (4d):

White solid, m.p.: 187.5-189.0 °C, yield: 79%; **¹H NMR** (600 MHz, DMSO-*d*₆), δ, ppm: 1.97-2.01 (*m*, 2H), 2.29 (*s*, 3H), 2.39 (*s*, 3H), 2.44 (*s*, 1H), 3.77 (*d*, *J* = 12.0 Hz, 1H), 3.80-3.86 (*m*, 1H), 3.88-3.99 (*m*, 2H), 4.43-4.48 (*m*, 1H), 6.45 (*s*, 1H), 6.78 (*d*, *J* = 8.4 Hz, 1H), 6.96 (*s*, 1H), 7.03 (*d*, *J* = 8.4 Hz, 1H); **¹³C NMR** (150 MHz, DMSO-*d*₆), δ, ppm: 20.4, 24.8,

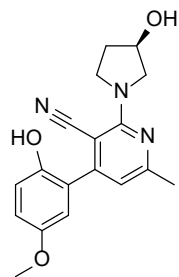
33.4, 47.0, 57.4, 70.4, 87.4, 96.5, 104.1, 113.6, 116.3, 124.7, 130.4, 131.1, 151.0, 154.4, 157.8, 161.6; **ESI-HRMS**, *m/z*: Calcd for C₁₈H₂₀N₃O₂ [M+H]⁺: 310.1550, Found: 310.1555.



(R)-4-(2-Hydroxy-5-methylphenyl)-2-(3-hydroxypyrrolidin-1-yl)-6-methylnicotinonitrile (4e): White solid, m.p.: 153.7-155.7 °C, yield: 94%; **¹H NMR** (600 MHz, CDCl₃), δ, ppm: 1.97-2.04 (*m*, 2H), 2.30 (*s*, 3H), 2.40 (*s*, 3H), 3.80 (*d*, *J* = 11.4 Hz, 1H), 3.82-3.88 (*m*, 1H), 3.90-3.99 (*m*, 2H), 4.47-4.50 (*m*, 1H), 6.47 (*s*, 1H), 6.81 (*d*, *J* = 8.4 Hz, 1H), 6.97 (*s*, 1H), 7.04 (*d*, *J* = 8.4 Hz, 1H); **¹³C NMR** (150 MHz, CDCl₃), δ, ppm: 21.4, 25.1, 33.6, 47.4, 57.9, 69.3, 88.3, 113.8, 116.8, 119.1, 120.2, 122.5, 130.3, 140.3, 154.6, 154.7, 157.9, 160.8; **ESI-HRMS**, *m/z*: Calcd for C₁₈H₂₀N₃O₂ [M+H]⁺: 310.1550, Found: 310.1559.

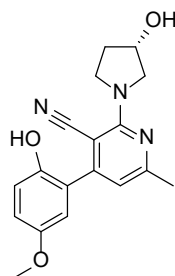


(S)-4-(2-Hydroxy-5-methylphenyl)-2-(3-hydroxypyrrolidin-1-yl)-6-methylnicotinonitrile (4f): Yellowish solid, m.p.: 177.1-179.1 °C, yield: 89%; **¹H NMR** (600 MHz, CDCl₃), δ, ppm: 1.97-2.02 (*m*, 2H), 2.29 (*s*, 3H), 2.39 (*s*, 3H), 3.77 (*d*, *J* = 12.0 Hz, 1H), 3.81-3.86 (*m*, 1H), 3.88-3.98 (*m*, 2H), 4.42-4.47 (*m*, 1H), 6.45 (*s*, 1H), 6.78 (*d*, *J* = 8.4 Hz, 1H), 6.96 (*s*, 1H), 7.03 (*d*, *J* = 8.4 Hz, 1H); **¹³C NMR** (150 MHz, CDCl₃), δ, ppm: 20.4, 24.8, 33.4, 47.0, 57.4, 70.4, 87.8, 113.6, 116.3, 119.1, 124.7, 129.3, 130.4, 131.1, 151.0, 154.4, 157.8, 161.6; **ESI-HRMS**, *m/z*: Calcd for C₁₈H₂₀N₃O₂ [M+H]⁺: 310.1550, Found: 310.1559.

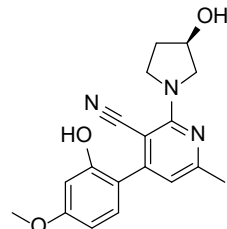


(R)-4-(2-Hydroxy-5-methylphenyl)-2-(3-hydroxypyrrolidin-1-yl)-6-methylnicotinonitrile

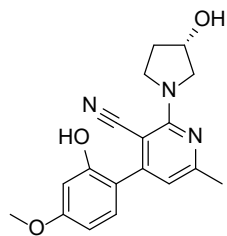
(4g): White solid, m.p.: 184.3-186.3 °C, yield: 96%; **¹H NMR** (600 MHz, CD₃OD), δ, ppm: 2.01-2.12 (*m*, 2H), 2.43 (*s*, 3H), 3.75 (*d*, *J* = 12.0 Hz, 1H), 3.76 (*s*, 3H), 3.84-3.89 (*m*, 1H) 3.91-3.99 (*m*, 2H), 4.49-4.53 (*m*, 1H), 6.55 (*s*, 1H), 6.76 (*s*, 1H), 6.83-6.88 (*m*, 2H); **¹³C NMR** (150 MHz, CD₃OD), δ, ppm: 23.5, 33.1, 46.7, 54.9, 56.9, 69.8, 87.7, 113.3, 114.9, 115.6, 116.4, 118.5, 125.5, 147.9, 152.8, 154.6, 157.9, 161.2; **ESI-HRMS**, *m/z*: Calcd for C₁₈H₂₀N₃O₃ [M+H]⁺: 326.1499, Found: 326.1503.



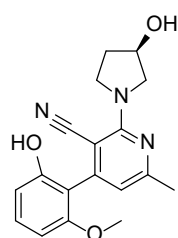
(S)-4-(2-Hydroxy-5-methylphenyl)-2-(3-hydroxypyrrolidin-1-yl)-6-methylnicotinonitrile (4h): White solid, m.p.: 191.4-193.1 °C, yield: 95%; **¹H NMR** (600 MHz, CD₃OD), δ, ppm: 2.01-2.14 (*m*, 2H), 2.42 (*s*, 3H), 3.72-3.78 (*m*, 4H), 3.83-3.88 (*m*, 1H), 3.91-3.99 (*m*, 2H), 4.48-4.52 (*m*, 1H), 6.55 (*s*, 1H), 6.76 (*s*, 1H), 6.84-6.88 (*m*, 2H); **¹³C NMR** (150 MHz, CD₃OD), δ, ppm: 23.5, 33.1, 46.7, 54.9, 56.9, 69.8, 87.7, 113.3, 114.9, 115.6, 116.4, 118.6, 125.5, 147.9, 152.8, 154.6, 157.9, 161.2; **ESI-HRMS**, *m/z*: Calcd for C₁₈H₂₀N₃O₃ [M+H]⁺: 326.1499, Found: 326.1508.



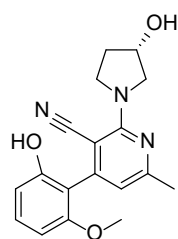
(R)-4-(2-Hydroxy-4-methylphenyl)-2-(3-hydroxypyrrolidin-1-yl)-6-methylnicotinonitrile (4i): Yellowish solid, m.p.: 194.7-196.7 °C, yield: 97%; **¹H NMR** (600 MHz, CD₃OD), δ, ppm: 2.00-2.11 (*m*, 2H), 2.39 (*s*, 3H), 3.72 (*d*, *J* = 12.0 Hz, 1H), 3.78 (*s*, 1H), 3.80-3.85 (*m*, 1H), 3.89-3.97 (*m*, 2H), 4.46-4.51 (*m*, 1H), 6.48-6.51 (*m*, 2H), 6.52 (*s*, 1H), 7.09 (*d*, *J* = 9.0 Hz, 1H); **¹³C NMR** (150 MHz, CD₃OD), δ, ppm: 23.6, 33.1, 46.7, 54.4, 56.9, 69.8, 88.0, 101.2, 104.9, 113.6, 117.8, 118.9, 130.9, 154.7, 155.4, 158.1, 161.0, 161.6; **ESI-HRMS**, *m/z*: Calcd for C₁₈H₂₀N₃O₃ [M+H]⁺: 326.1499, Found: 326.1504.



(S)-4-(2-Hydroxy-4-methylphenyl)-2-(3-hydroxypyrrolidin-1-yl)-6-methylnicotinonitrile (4j): White solid, m.p.: 203.6-204.8 °C, yield: 94%; **1H NMR** (600 MHz, DMSO-*d*₆), δ, ppm: 1.82-1.97 (*m*, 2H), 2.44 (*s*, 3H), 3.03 (*d*, *J* = 11.4 Hz, 1H), 3.38-3.47 (*m*, 1H), 3.70-3.83 (*m*, 2H), 3.86 (*s*, 1H), 4.32-4.37 (*m*, 1H), 4.89 (*b*, 1H), 6.91 (*d*, *J* = 2.4 Hz, 1H), 6.94 (*dd*, *J*₁ = 9.0 Hz, *J*₂ = 2.4 Hz, 1H), 7.24 (*s*, 1H), 8.08 (*d*, *J* = 9.0 Hz, 1H); **13C NMR** (150 MHz, DMSO-*d*₆), δ, ppm: 25.3, 33.4, 48.0, 56.3, 56.0, 69.3, 79.6, 95.4, 101.2, 110.1, 112.4, 126.2, 145.0, 154.1, 157.4, 158.2, 161.9, 162.7; **ESI-HRMS**, *m/z*: Calcd for C₁₈H₂₀N₃O₃ [M+H]⁺: 326.1499, Found: 326.1500.

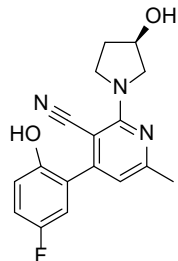


(R)-4-(2-Hydroxy-6-methylphenyl)-2-(3-hydroxypyrrolidin-1-yl)-6-methylnicotinonitrile (4k): Yellow solid, m.p.: 189.8-191.1 °C, yield: 82%; **1H NMR** (600 MHz, CD₃OD), δ, ppm: 2.00-2.12 (*m*, 2H), 2.41 (*s*, 3H), 3.72-3.77 (*m*, 4H), 3.82-3.87 (*m*, 1H), 3.89-3.99 (*m*, 2H), 4.48-4.51 (*m*, 1H), 6.47 (*d*, *J* = 5.4 Hz, 1H), 6.54-6.59 (*m*, 2H), 7.17-7.22 (*m*, 1H); **13C NMR** (150 MHz, CD₃OD), δ, ppm: 23.5, 33.1, 46.6, 54.9, 56.8, 69.8, 89.1, 102.1, 108.2, 114.1, 114.5, 118.6, 129.9, 151.9, 155.0, 157.6, 157.9, 160.8; **ESI-HRMS**, *m/z*: Calcd for C₁₈H₂₀N₃O₃ [M+H]⁺: 326.1499, Found: 326.1497.

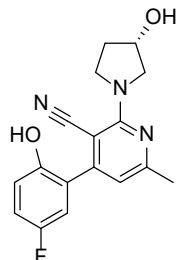


(S)-4-(2-Hydroxy-6-methylphenyl)-2-(3-hydroxypyrrolidin-1-yl)-6-methylnicotinonitrile (4l): Yellow solid, m.p.: 217.4-218.4 °C, yield: 82%; **1H NMR** (600 MHz, CD₃OD), δ, ppm: 1.99-2.10 (*m*, 2H), 2.41 (*s*, 3H), 3.72-3.76 (*m*, 4H), 3.82-3.87 (*m*, 1H), 3.89-3.98 (*m*, 2H), 4.47-4.52 (*m*, 1H), 6.47 (*d*, *J* = 5.4 Hz, 1H), 6.54-6.60 (*m*, 2H), 7.17-7.22 (*m*, 1H); **13C NMR**

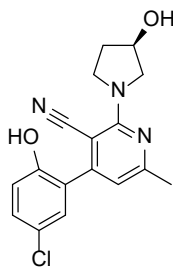
(150 MHz, CD₃OD), δ , ppm: 23.5, 33.1, 46.5, 54.9, 56.8, 69.8, 89.1, 102.1, 108.2, 114.1, 114.5, 118.6, 129.9, 151.9, 155.0, 157.6, 157.9, 160.8; **ESI-HRMS**, m/z : Calcd for C₁₈H₂₀N₃O₃ [M+H]⁺: 326.1499, Found: 326.1508.



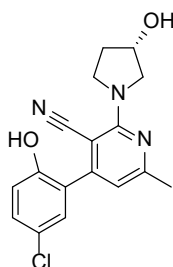
(R)-4-(5-Fluoro-2-hydroxyphenyl)-2-(3-hydroxypyrrolidin-1-yl)-6-methylnicotinonitrile (4m): Yellowish solid, m.p.: 197.2-198.7 °C, yield: 96%; **¹H NMR** (600 MHz, DMSO-*d*₆), δ , ppm: 1.87-1.99 (*m*, 2H), 2.38 (*s*, 3H), 3.59 (*d*, J = 11.4 Hz, 1H), 3.70-3.75 (*m*, 1H), 3.77-3.82 (*m*, 2H), 4.37-4.41 (*m*, 1H), 5.03 (*s*, 1H), 6.55 (*s*, 1H), 6.92-6.96 (*m*, 1H), 7.02-7.05 (*m*, 1H), 7.09-7.14 (*m*, 1H), 7.79 (*s*, 1H); **¹³C NMR** (150 MHz, DMSO-*d*₆), δ , ppm: 25.1, 33.6, 47.3, 57.8, 69.3, 87.9, 113.6, 116.6 (*d*, J = 23.6 Hz), 116.9 (*d*, J = 22.4 Hz), 117.2 (*d*, J = 8.0 Hz), 118.8, 126.0 (*d*, J = 7.8 Hz), 151.2 (*d*, J = 1.9 Hz), 153.4, 155.4 (*d*, J = 233.6 Hz), 157.7, 161.2; **¹⁹F NMR** (564 MHz, DMSO-*d*₆), δ , ppm: -126.0; **ESI-HRMS**, m/z : Calcd for C₁₇H₁₇N₃O₂ [M+H]⁺: 314.1299, Found: 314.1306.



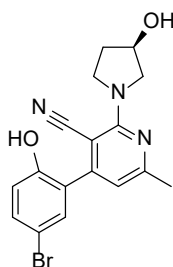
(S)-4-(5-Fluoro-2-hydroxyphenyl)-2-(3-hydroxypyrrolidin-1-yl)-6-methylnicotinonitrile (4n): Yellowish solid, m.p.: 167.8-169.4 °C, yield: 96%; **¹H NMR** (600 MHz, CD₃OD), δ , ppm: 2.01-2.11 (*m*, 2H), 2.42 (*s*, 3H), 3.75 (*d*, J = 11.4 Hz, 1H), 3.83-3.89 (*m*, 1H), 3.91-3.99 (*m*, 2H), 4.47-4.53 (*m*, 1H), 6.53 (*s*, 1H), 6.86-6.91 (*m*, 1H), 6.92-6.96 (*m*, 1H), 6.98-7.04 (*m*, 1H); **¹³C NMR** (150 MHz, CD₃OD), δ , ppm: 23.5, 33.1, 46.6, 56.9, 69.8, 87.5, 113.0, 115.9 (*d*, J = 23.9 Hz), 116.1 (*d*, J = 22.8 Hz), 116.5 (*d*, J = 8.0 Hz), 118.4, 126.0 (*d*, J = 7.7 Hz), 150.5 (*d*, J = 2.4 Hz), 153.4, 155.9 (*d*, J = 235.1 Hz), 157.8, 161.5; **¹⁹F NMR** (564 MHz, CD₃OD), δ , ppm: -127.6; ESI-HRMS, m/z : Calcd for C₁₇H₁₇N₃O₂ [M+H]⁺: 314.1299, Found: 314.1303.



(R)-4-(5-Chloro-2-hydroxyphenyl)-2-(3-hydroxypyrrolidin-1-yl)-6-methylnicotinonitrile (4o): Yellowish solid, m.p.: 195.5-197.3 °C, yield: 87%; **1H NMR** (600 MHz, CD₃OD), δ, ppm: 2.00-2.10 (*m*, 2H), 2.41 (*s*, 3H), 3.75 (*d*, *J* = 12.0 Hz, 1H), 3.82-3.87 (*m*, 1H), 3.89-3.97 (*m*, 2H), 4.47-4.51 (*m*, 1H), 6.50 (*s*, 1H), 6.90 (*d*, *J* = 8.4 Hz, 1H), 7.16 (*s*, 1H), 7.23 (*d*, *J* = 8.4 Hz, 1H); **13C NMR** (150 MHz, CD₃OD), δ, ppm: 23.6, 33.1, 46.7, 56.9, 69.8, 87.4, 113.0, 116.9, 118.4, 123.6, 126.7, 129.3, 129.6, 153.2, 153.3, 157.7, 161.5; **ESI-HRMS**, *m/z*: Calcd for C₁₇H₁₇ClN₃O₂ [M+H]⁺: 330.1004, Found: 330.1014.

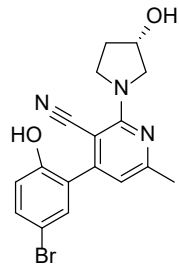


(S)-4-(5-Chloro-2-hydroxyphenyl)-2-(3-hydroxypyrrolidin-1-yl)-6-methylnicotinonitrile (4p): Yellowish solid, m.p.: 179.5-181.5 °C, yield: 87%; **1H NMR** (600 MHz, CD₃OD), δ, ppm: 1.99-2.10 (*m*, 2H), 2.41 (*s*, 3H), 3.75 (*d*, *J* = 11.4 Hz, 1H), 3.82-3.87 (*m*, 1H), 3.90-3.98 (*m*, 2H), 4.48-4.52 (*m*, 1H), 6.50 (*s*, 1H), 6.85 (*d*, *J* = 8.4 Hz, 1H), 7.29 (*s*, 1H), 7.36 (*d*, *J* = 8.4 Hz, 1H); **13C NMR** (150 MHz, CD₃OD), δ, ppm: 23.6, 33.1, 46.6, 56.9, 69.8, 87.4, 110.5, 113.0, 117.4, 118.4, 127.2, 132.2, 132.6, 153.2, 153.7, 157.7, 161.5; **ESI-HRMS**, *m/z*: Calcd for C₁₇H₁₇ClN₃O₂ [M+H]⁺: 330.1004, Found: 330.1014.

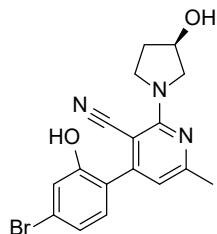


(R)-4-(5-Bromo-2-hydroxyphenyl)-2-(3-hydroxypyrrolidin-1-yl)-6-methylnicotinonitrile (4q): Yellowish solid, m.p.: 183.7-184.5 °C, yield: 85%; **1H NMR** (600 MHz, CD₃OD), δ, ppm: 2.00-2.09 (*m*, 2H), 2.43 (*s*, 3H), 3.75 (*d*, *J* = 12.0 Hz, 1H), 3.84-3.88 (*m*, 1H), 3.91-3.96

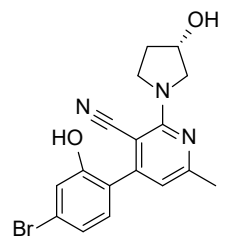
(*m*, 2H), 4.49-4.52 (*m*, 1H), 6.51 (*s*, 1H), 6.86 (*d*, *J* = 8.4 Hz, 1H), 7.30 (*s*, 1H), 7.38 (*d*, *J* = 8.4 Hz, 1H); ¹³C NMR (150 MHz, CD₃OD), δ , ppm: 23.6, 33.1, 46., 56.9, 69.8, 87.4, 110.5, 113.0, 117.4, 118.3, 127.3, 132.2, 132.6, 153.2, 153.7, 157.7, 161.6; ESI-HRMS, *m/z*: Calcd for C₁₇H₁₇BrN₃O₂ [M+H]⁺: 374.0499, Found: 374.0487.



(S)-4-(5-Bromo-2-hydroxyphenyl)-2-(3-hydroxypyrrolidin-1-yl)-6-methylnicotinonitrile (4r): Yellowish solid, m.p.: 194.5-196.3 °C, yield: 83%; ¹H NMR (600 MHz, DMSO-*d*₆), δ , ppm: 1.87-1.99 (*m*, 2H), 2.37 (*s*, 3H), 3.74 (*d*, *J* = 11.4 Hz, 1H), 3.69-3.73 (*m*, 1H), 3.76-3.81 (*m*, 2H), 4.35-4.40 (*m*, 1H), 5.02 (*s*, 1H), 6.52 (*s*, 1H), 7.08 (*d*, *J* = 8.4 Hz, 1H), 7.12 (*d*, *J* = 8.4 Hz, 1H), 7.13 (*s*, 1H), 10.33 (*s*, 1H); ¹³C NMR (150 MHz, DMSO-*d*₆), δ , ppm: 25.1, 33.6, 47.3, 57.8, 69.3, 87.8, 113.5, 118.8, 118.9, 122.3, 122.9, 124.8, 132.1, 153.5, 156.0, 157.7, 161.3; ESI-HRMS, *m/z*: Calcd for C₁₇H₁₇BrN₃O₂ [M+H]⁺: 374.0499, Found: 374.0481.



(R)-4-(4-Bromo-2-hydroxyphenyl)-2-(3-hydroxypyrrolidin-1-yl)-6-methylnicotinonitrile (4s): Yellow solid, m.p.: 196.6-198.6 °C, yield: 82%; ¹H NMR (600 MHz, CD₃OD), δ , ppm: 2.03-2.06 (*m*, 2H), 2.43 (*s*, 3H), 3.75 (*d*, *J* = 11.4 Hz, 1H), 3.84-3.88 (*m*, 1H), 3.91-3.97 (*m*, 2H), 4.50-4.53 (*m*, 1H), 6.53 (*s*, 1H), 7.09 (*d*, *J* = 8.4 Hz, 1H), 7.24 (*d*, *J* = 8.4 Hz, 1H); 7.47 (*s*, 1H); ¹³C NMR (150 MHz, CD₃OD), δ , ppm: 23.5, 33.1, 46.6, 56.9, 69.7, 87.4, 110.5, 113.0, 117.4, 118.3, 127.3, 132.2, 132.6, 153.2, 153.7, 157.7, 161.5; ESI-HRMS, *m/z*: Calcd for C₁₇H₁₇BrN₃O₂ [M+H]⁺: 374.0499, Found: 374.0488.



(S)-4-(4-Bromo-2-hydroxyphenyl)-2-(3-hydroxypyrrolidin-1-yl)-6-methylnicotinonitrile

(4t): Yellowish solid, m.p.: 187.9-189.5 °C, yield: 84%; **¹H NMR** (600 MHz, CD₃OD), δ, ppm: 2.00-2.10 (*m*, 2H), 2.41 (*s*, 3H), 3.74 (*d*, *J* = 12.0 Hz, 1H), 3.82-3.87 (*m*, 1H), 3.90-3.97 (*m*, 2H), 4.48-4.52 (*m*, 1H), 6.50 (*s*, 1H), 6.85 (*d*, *J* = 8.4 Hz, 1H), 7.29 (*s*, 1H), 7.37 (*d*, *J* = 8.4 Hz, 1H); **¹³C NMR** (150 MHz, CD₃OD), δ, ppm: 23.6, 33.1, 46.6, 56.9, 69.8, 87.4, 103.8, 110.5, 113.0, 117.4, 127.2, 132.2, 132.6, 153.2, 153.7, 157.7, 161.6; **ESI-HRMS**, *m/z*: Calcd for C₁₇H₁₇BrN₃O₂ [M+H]⁺: 374.0499, Found: 374.0489.

2.3. Characterization Spectra for All Products 3a-3k and 4a-4t

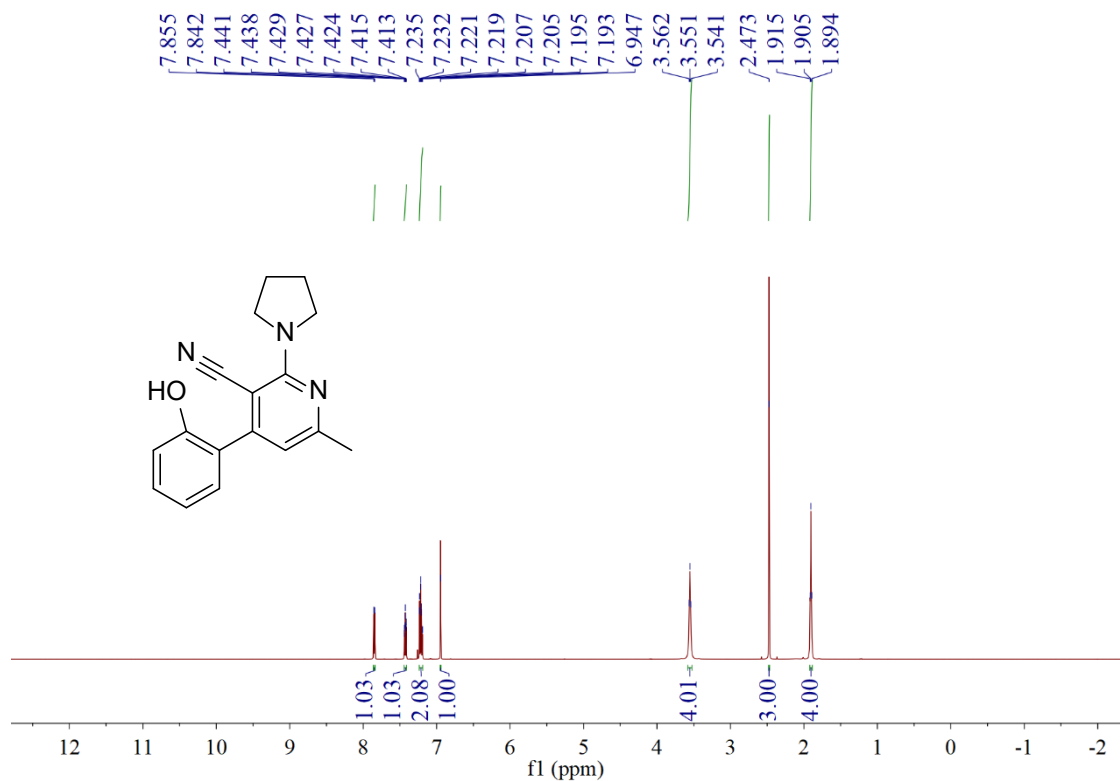


Fig. S1. ^1H NMR spectrum of compound 3a.

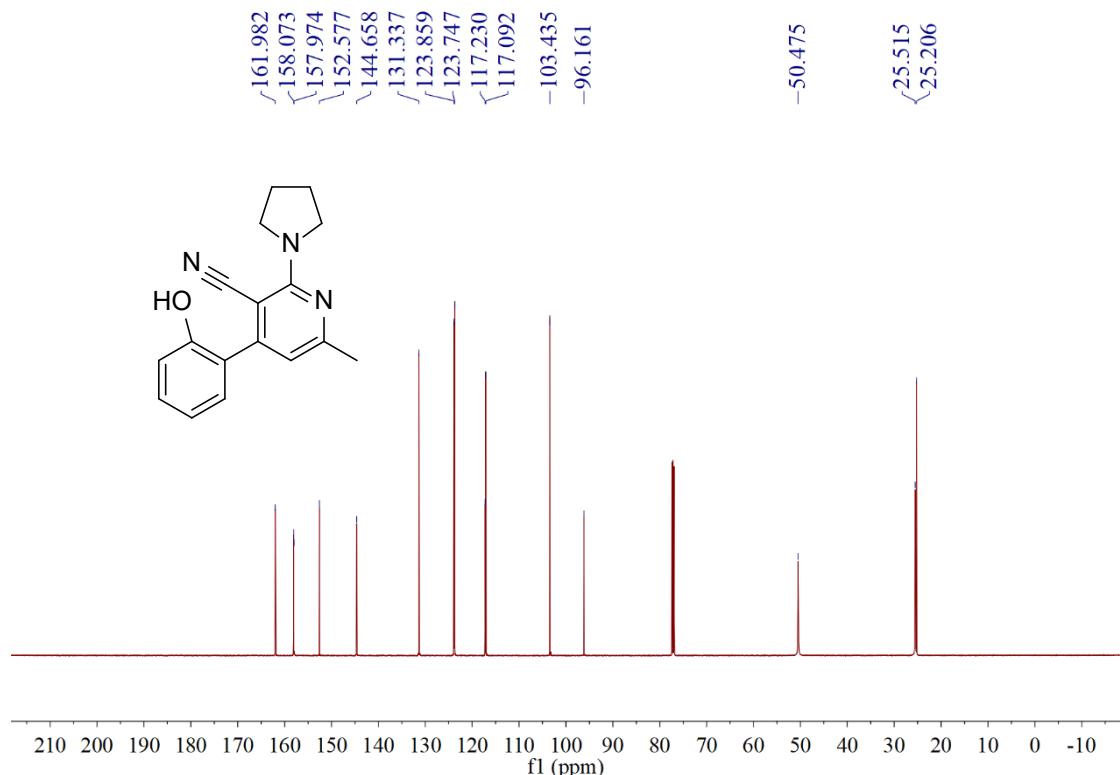


Fig. S2. ^{13}C NMR spectrum of compound 3a.

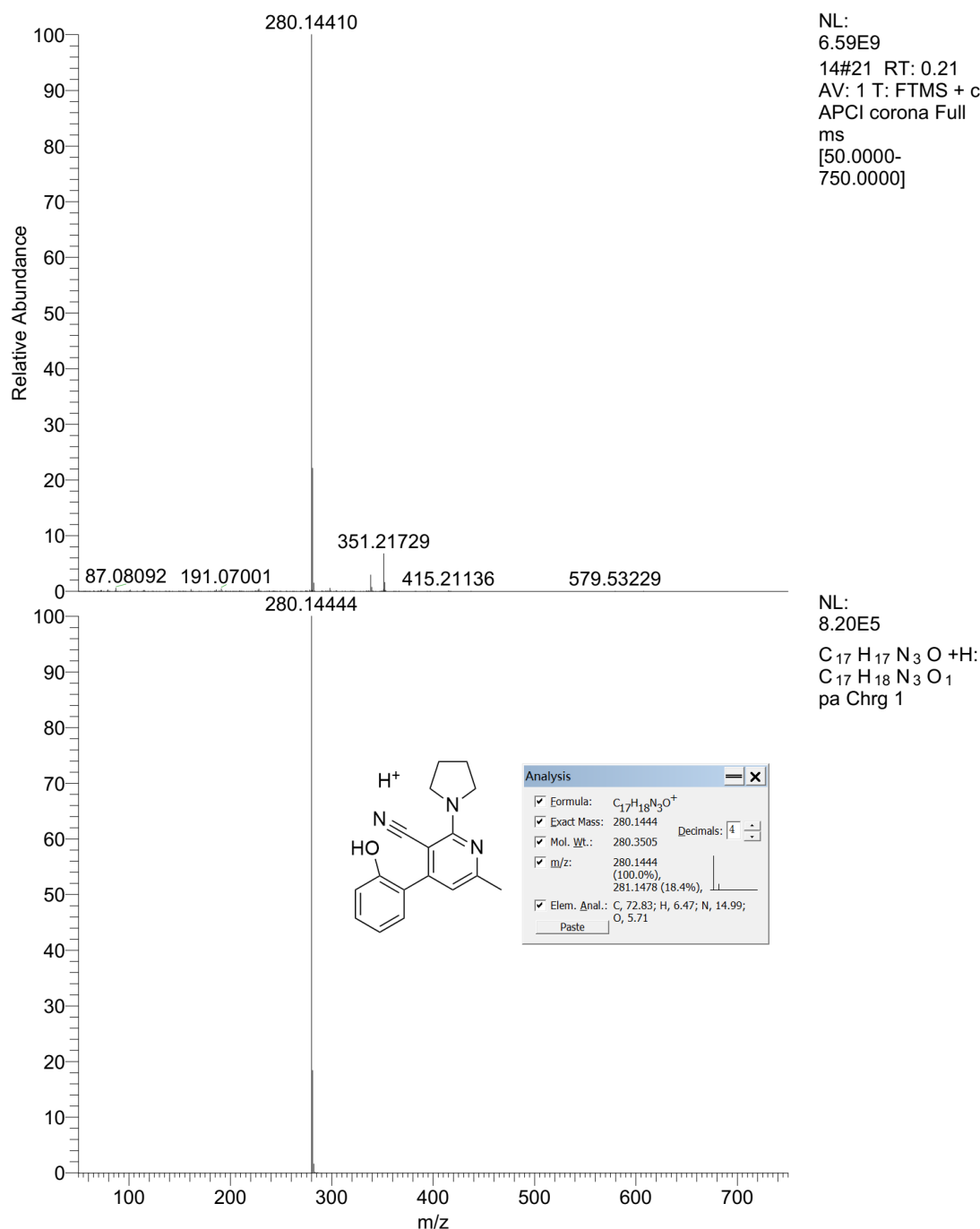


Fig. S3. HRMS spectrum of compound **3a**.

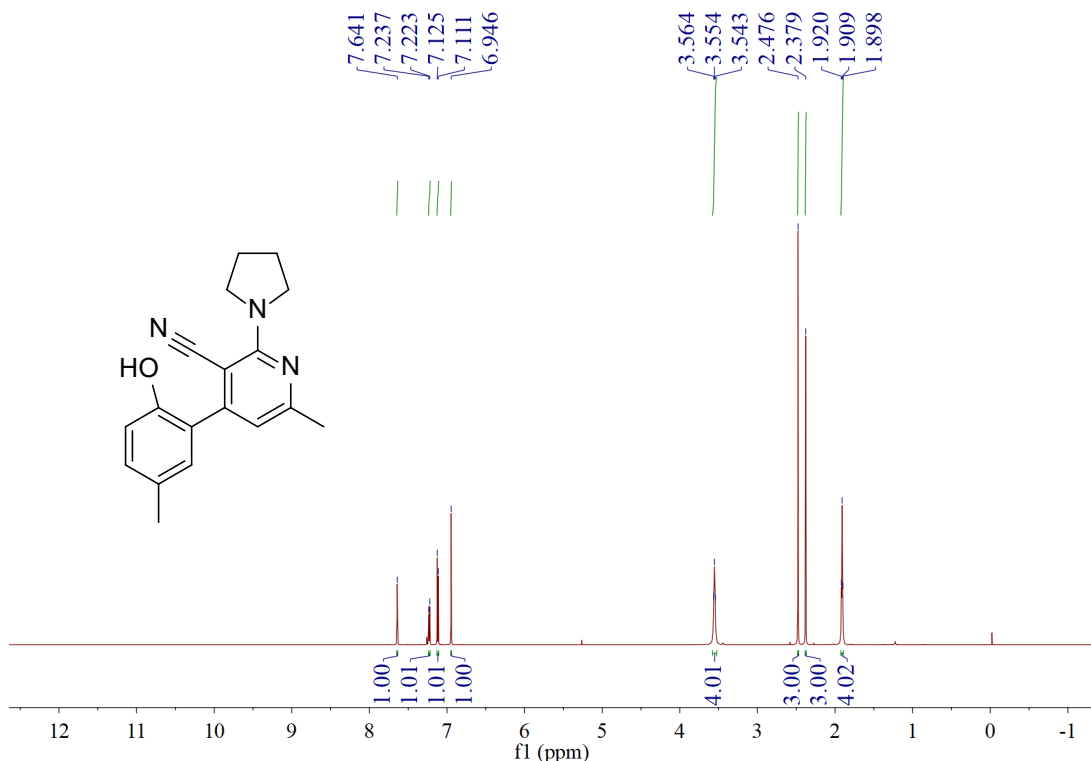


Fig. S4. ^1H NMR spectrum of compound **3b**.

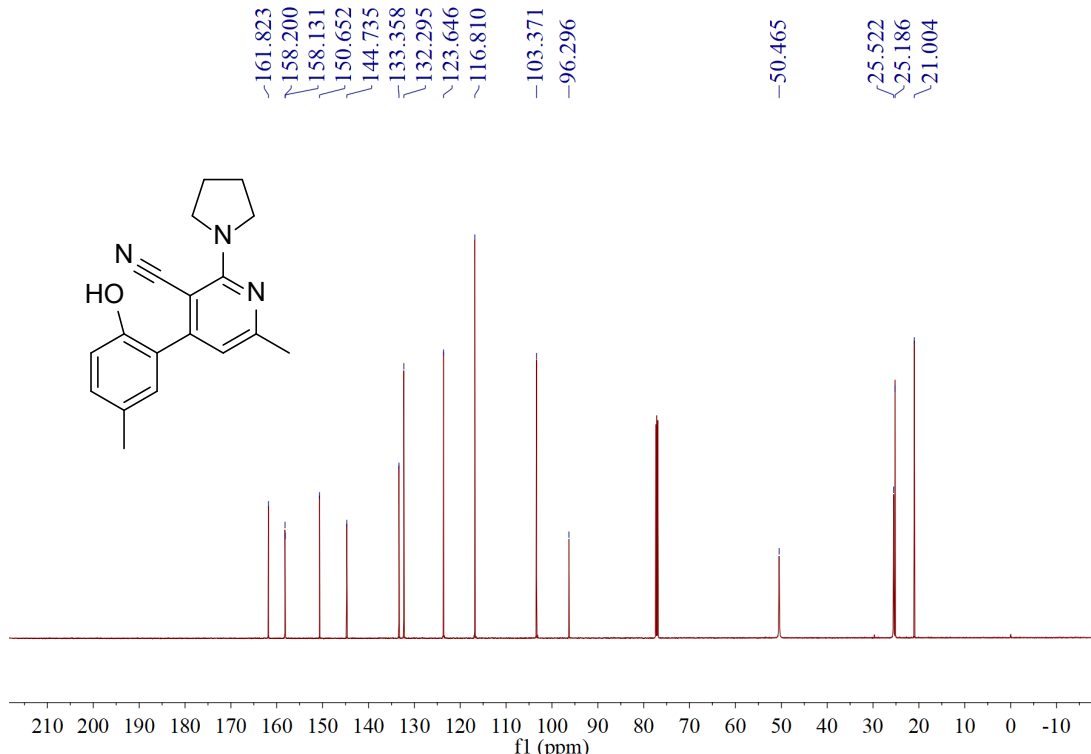


Fig. S5. ^{13}C NMR spectrum of compound **3b**.

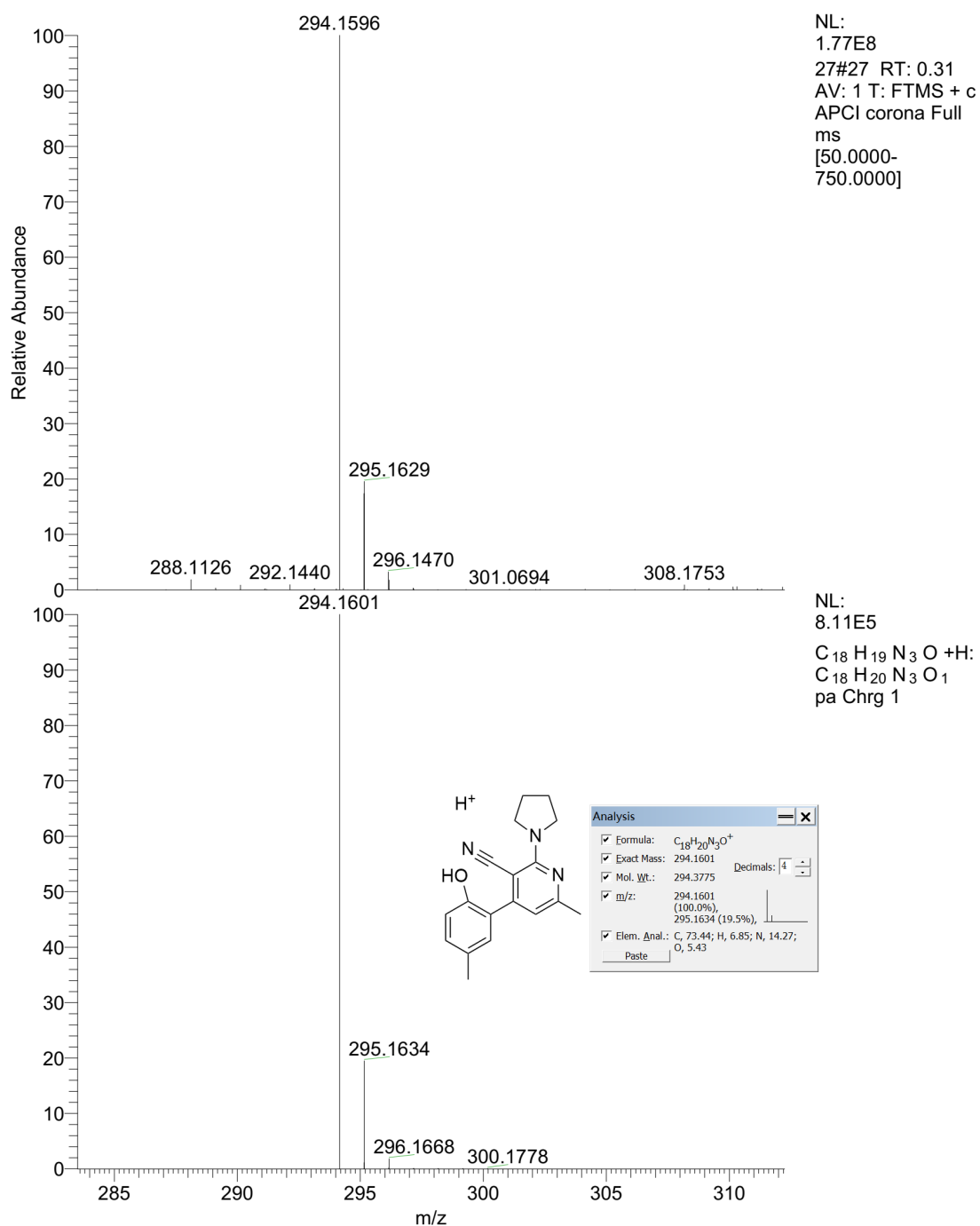


Fig. S6. HRMS spectrum of compound **3b**.

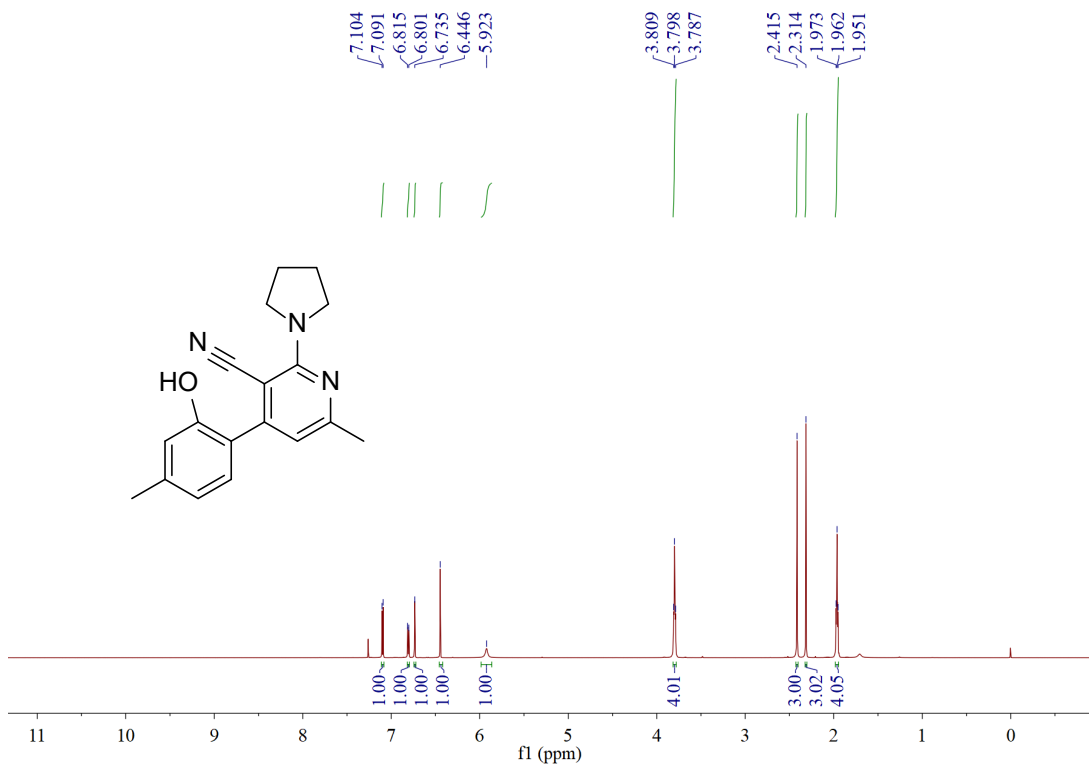


Fig. S7. ^1H NMR spectrum of compound 3c.

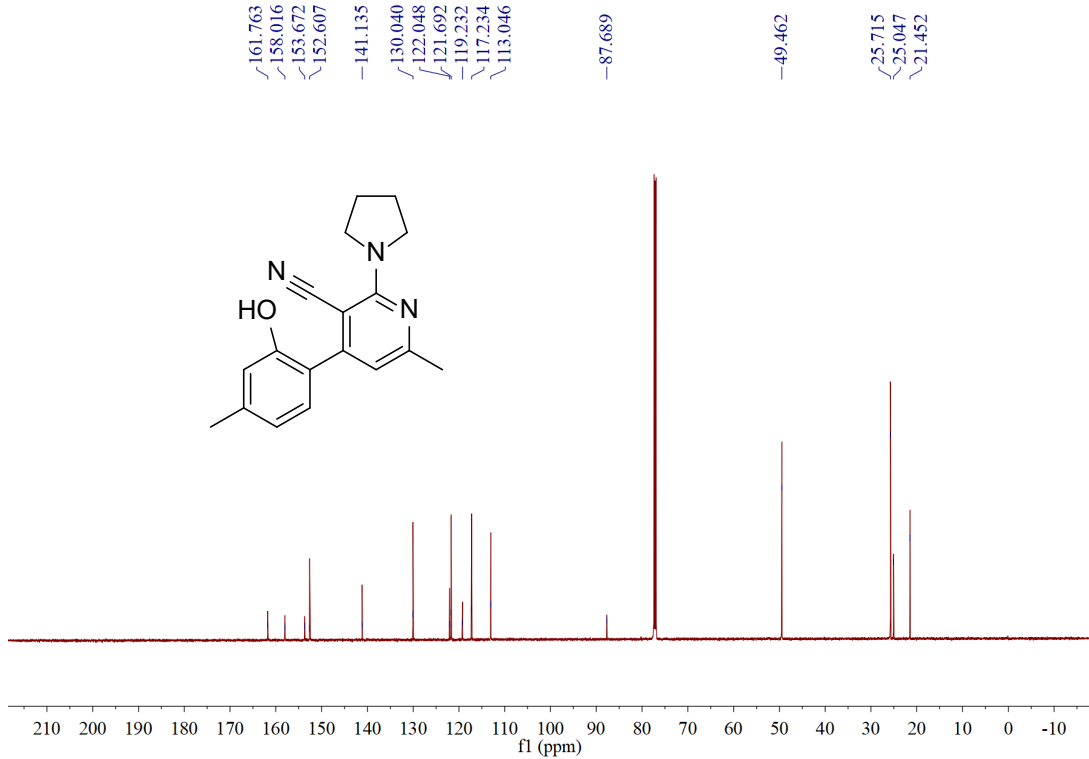


Fig. S8. ^{13}C NMR spectrum of compound 3c.

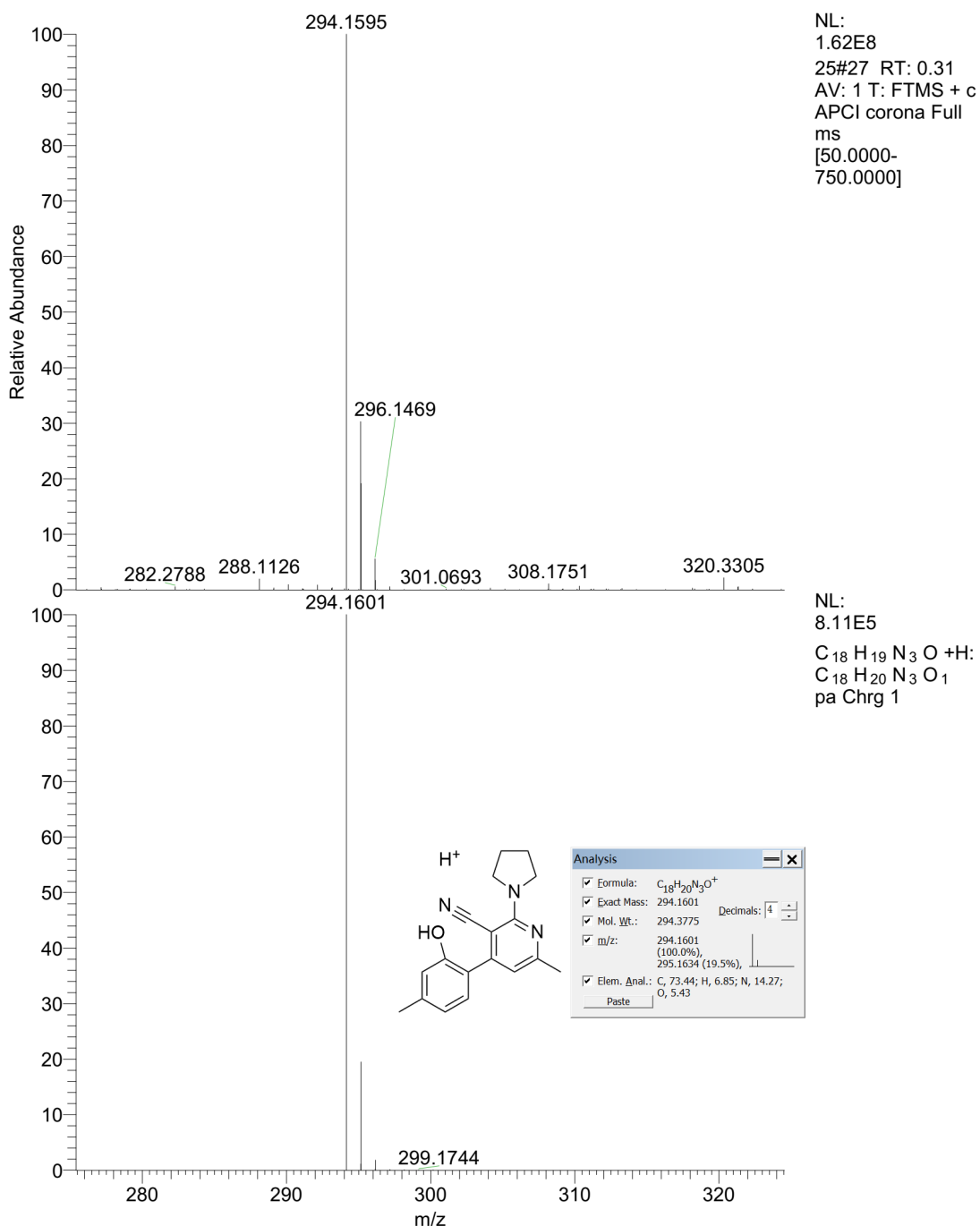


Fig. S9. HRMS spectrum of compound **3c**.

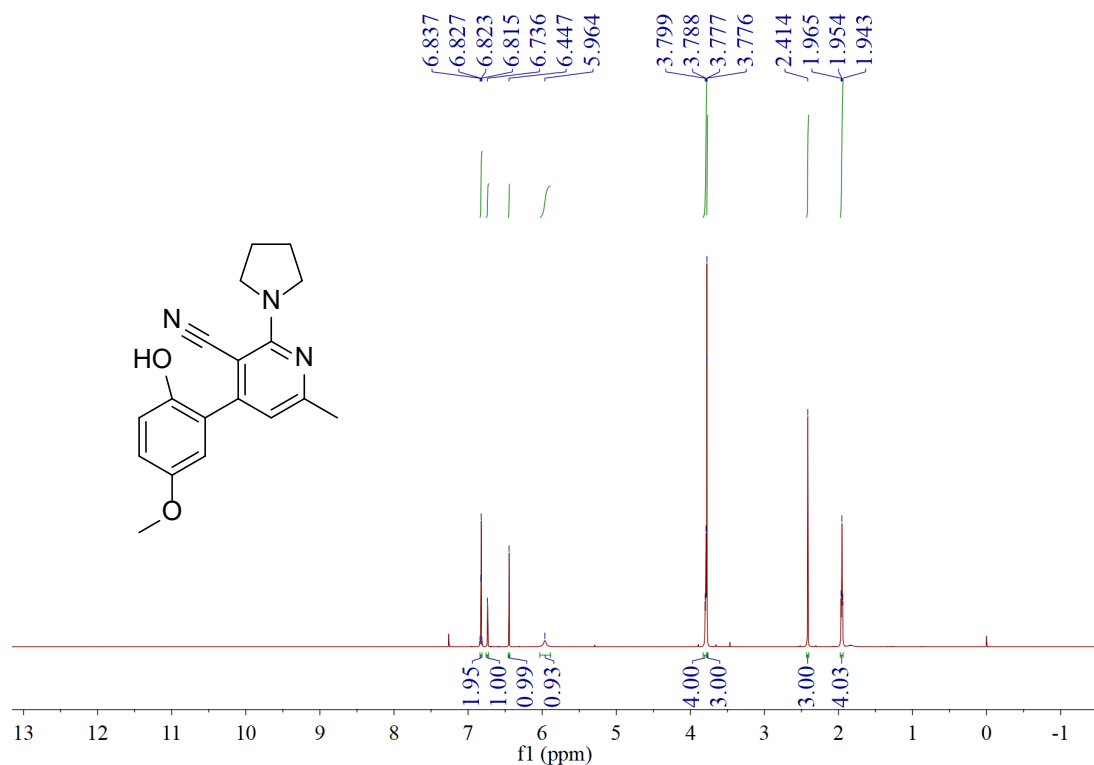


Fig. S10. ¹H NMR spectrum of compound 3d.

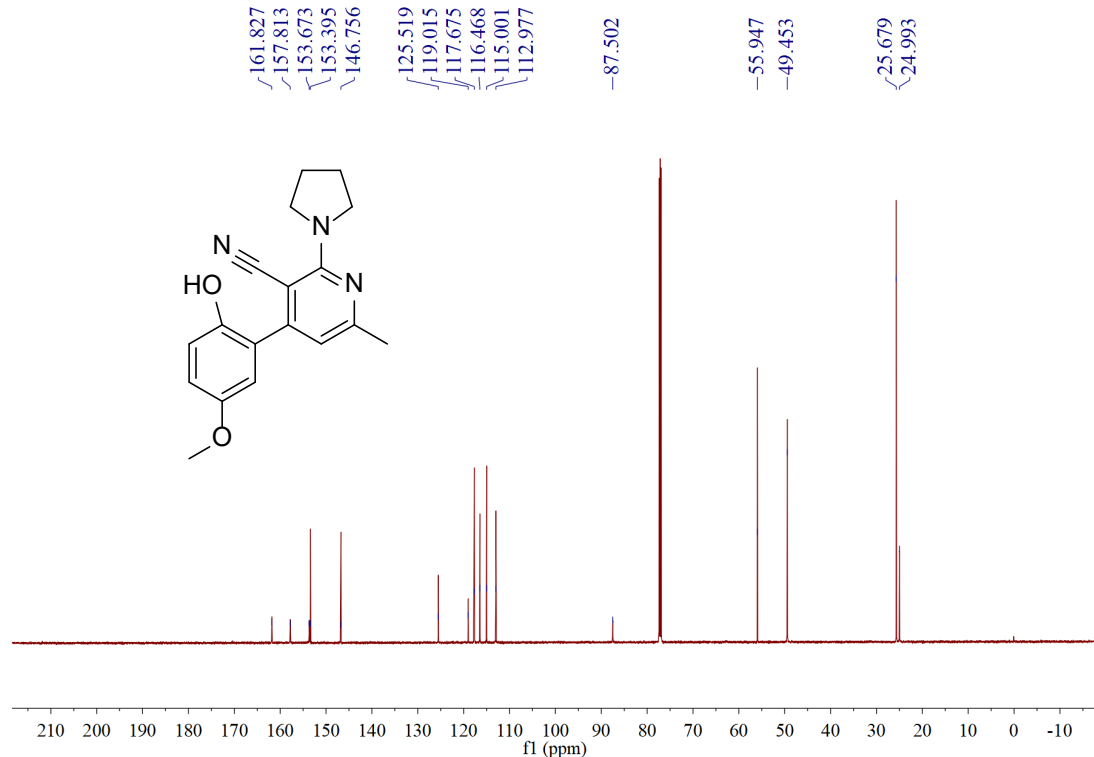


Fig. S11. ¹³C NMR spectrum of compound 3d.

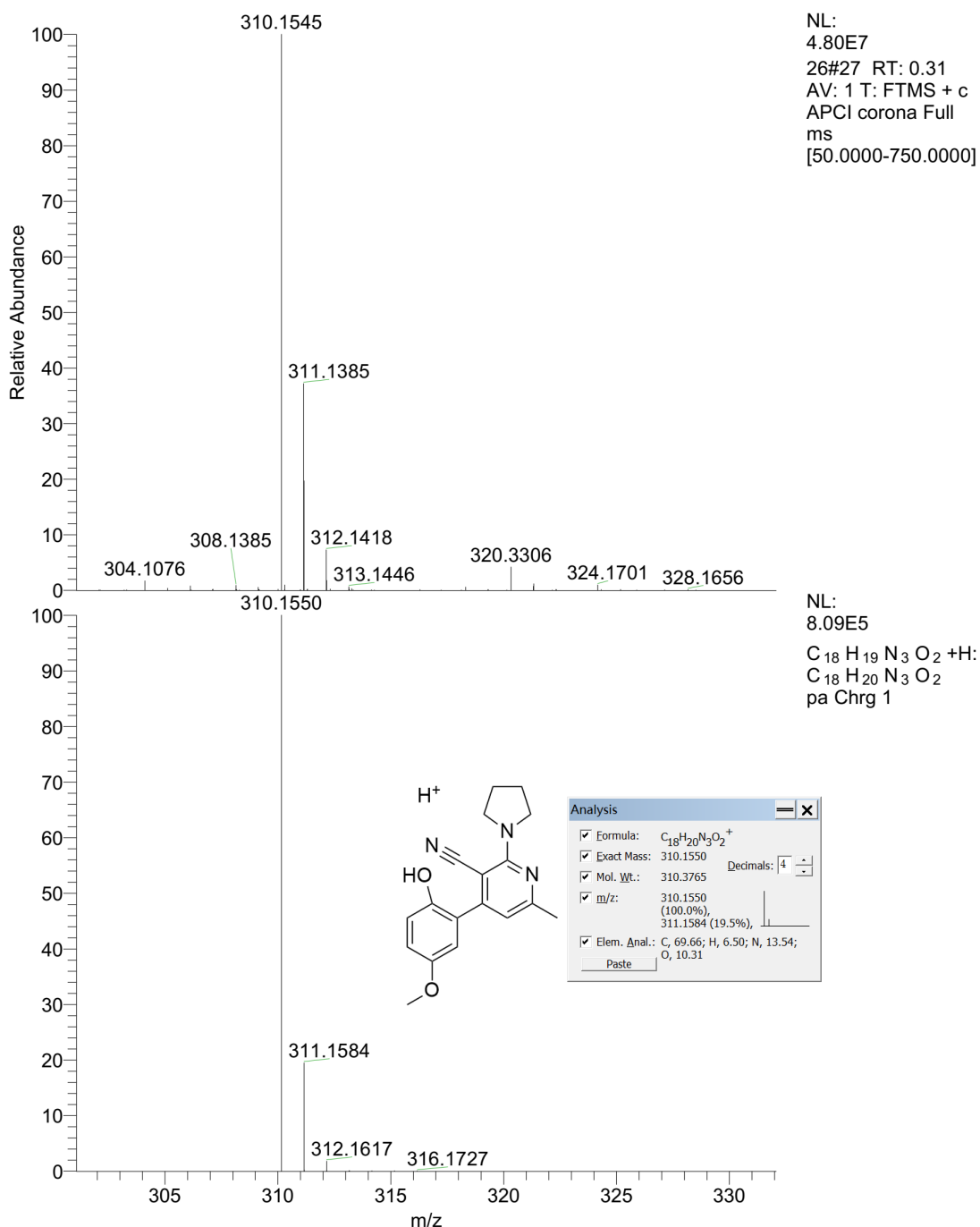


Fig. S12. HRMS spectrum of compound 3d.

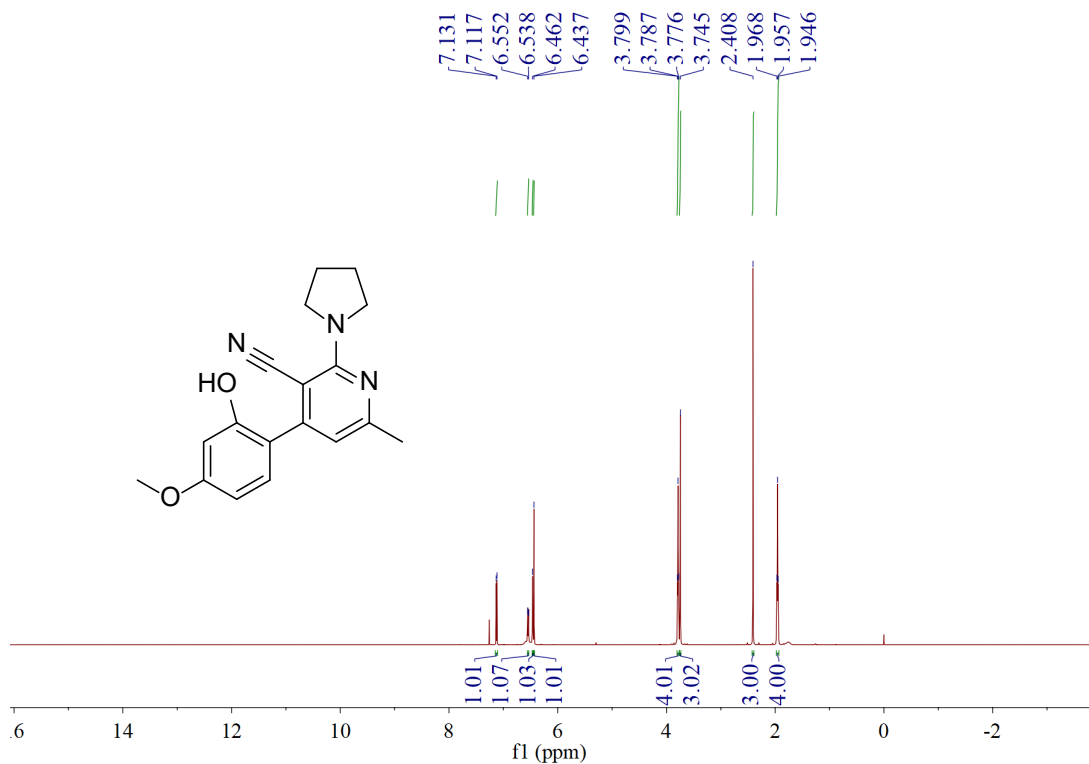


Fig. S13. ^1H NMR spectrum of compound **3e**.

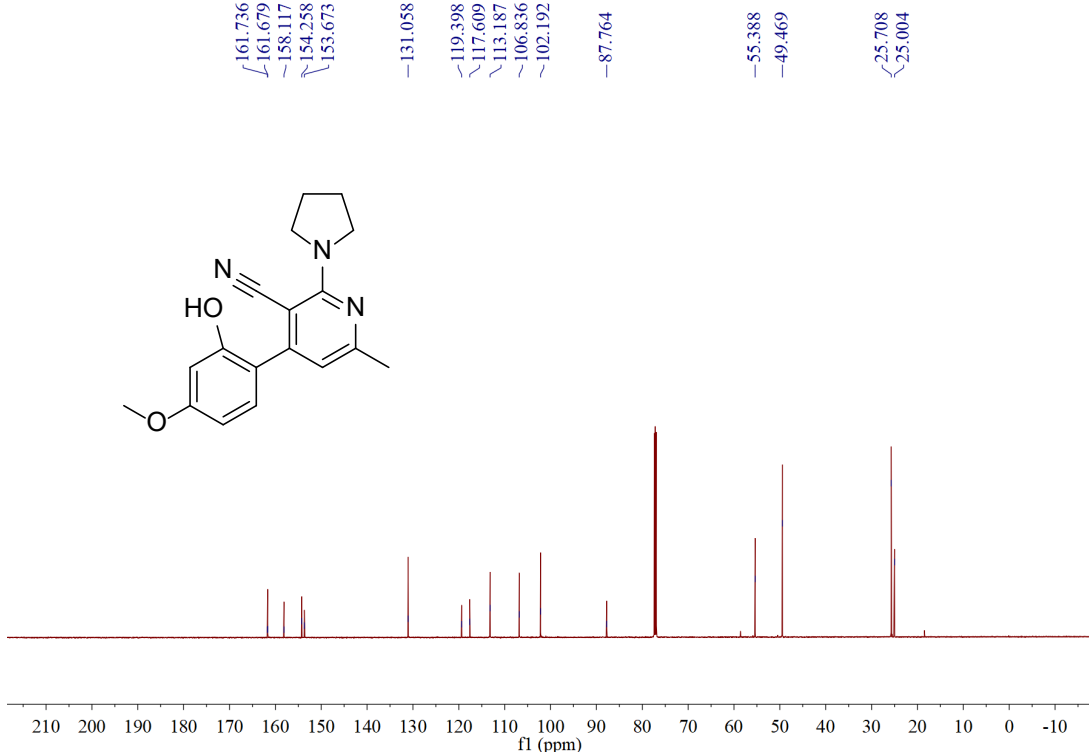


Fig. S14. ^{13}C NMR spectrum of compound **3e**.

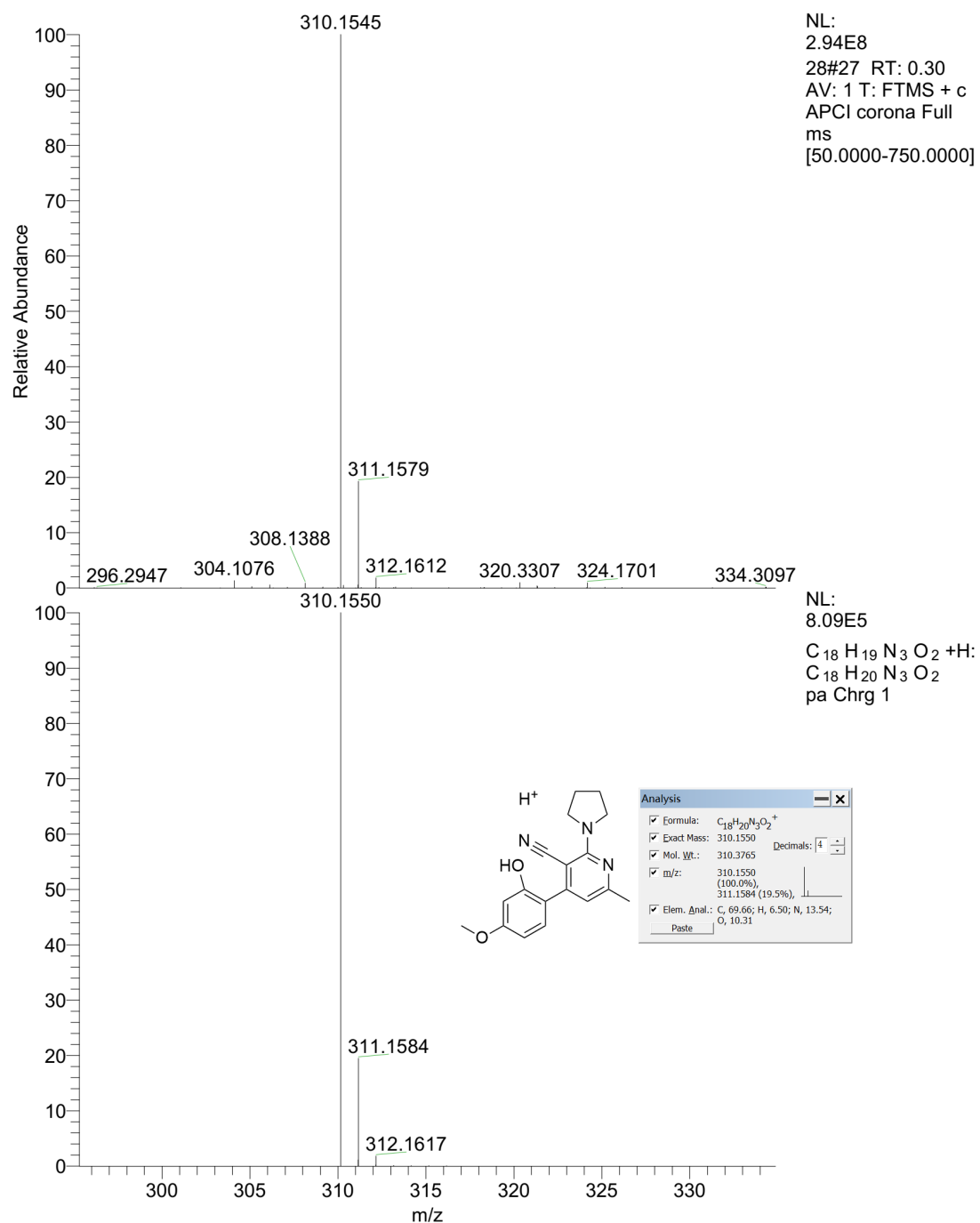


Fig. S15. HRMS spectrum of compound 3e.

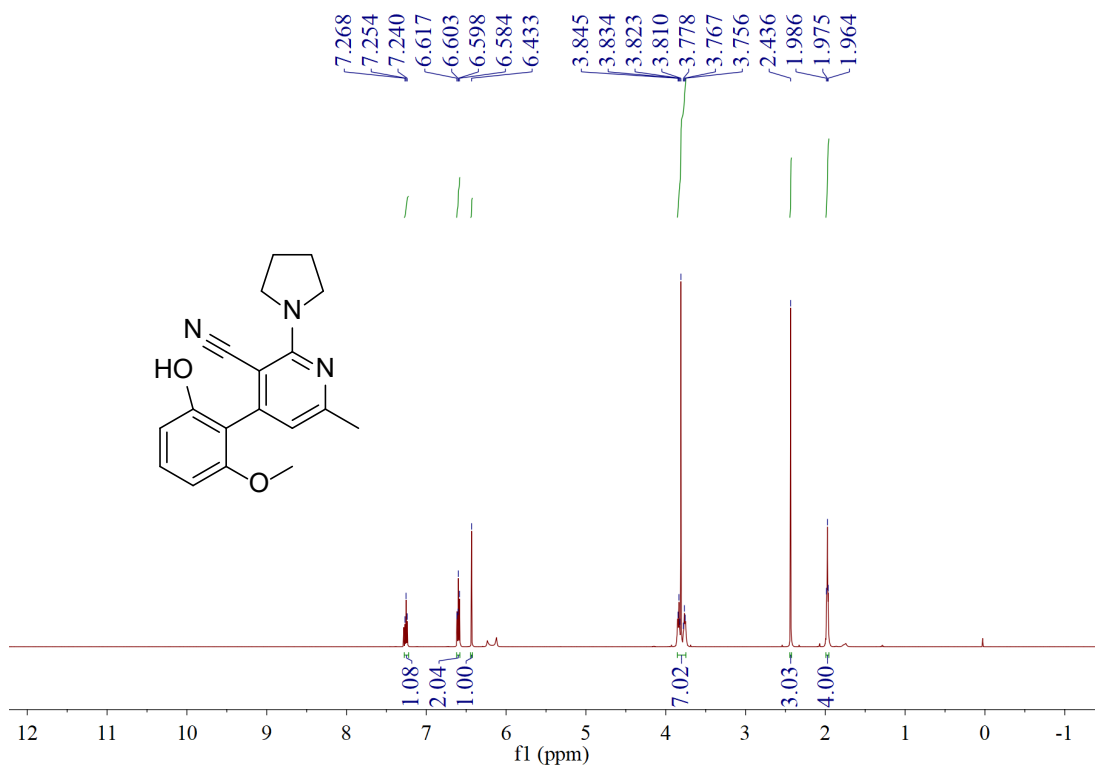


Fig. S16. ¹H NMR spectrum of compound 3f.

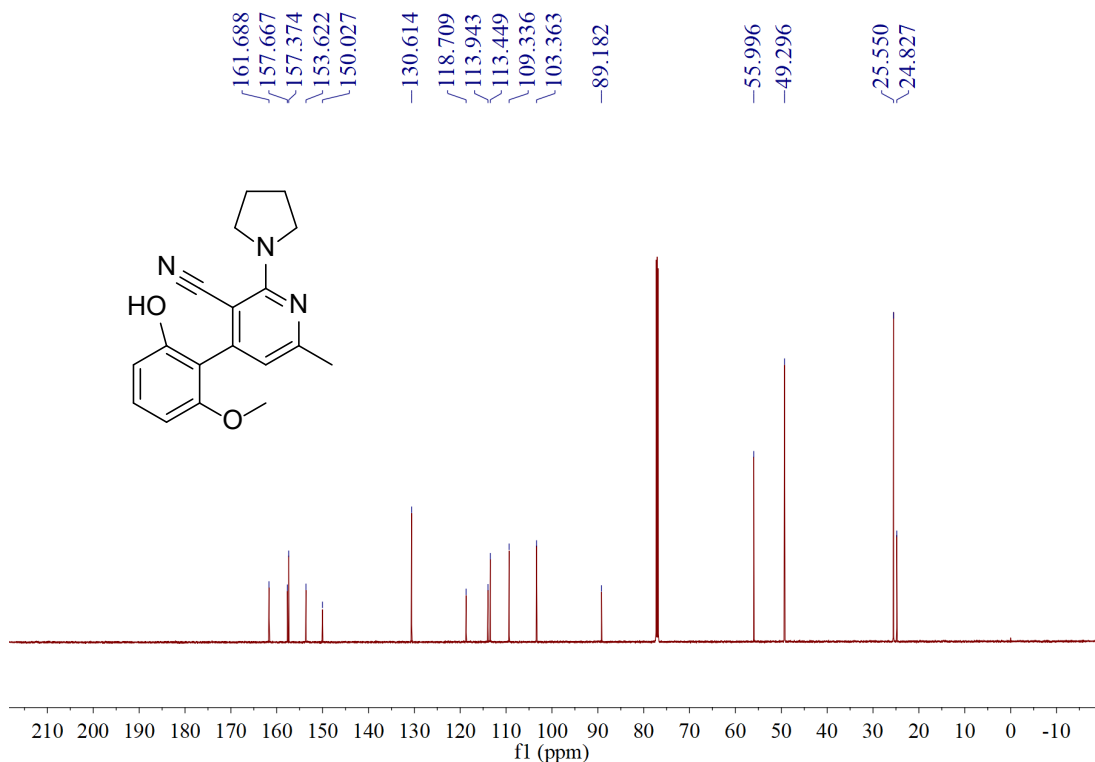


Fig. S17. ¹³C NMR spectrum of compound 3f.

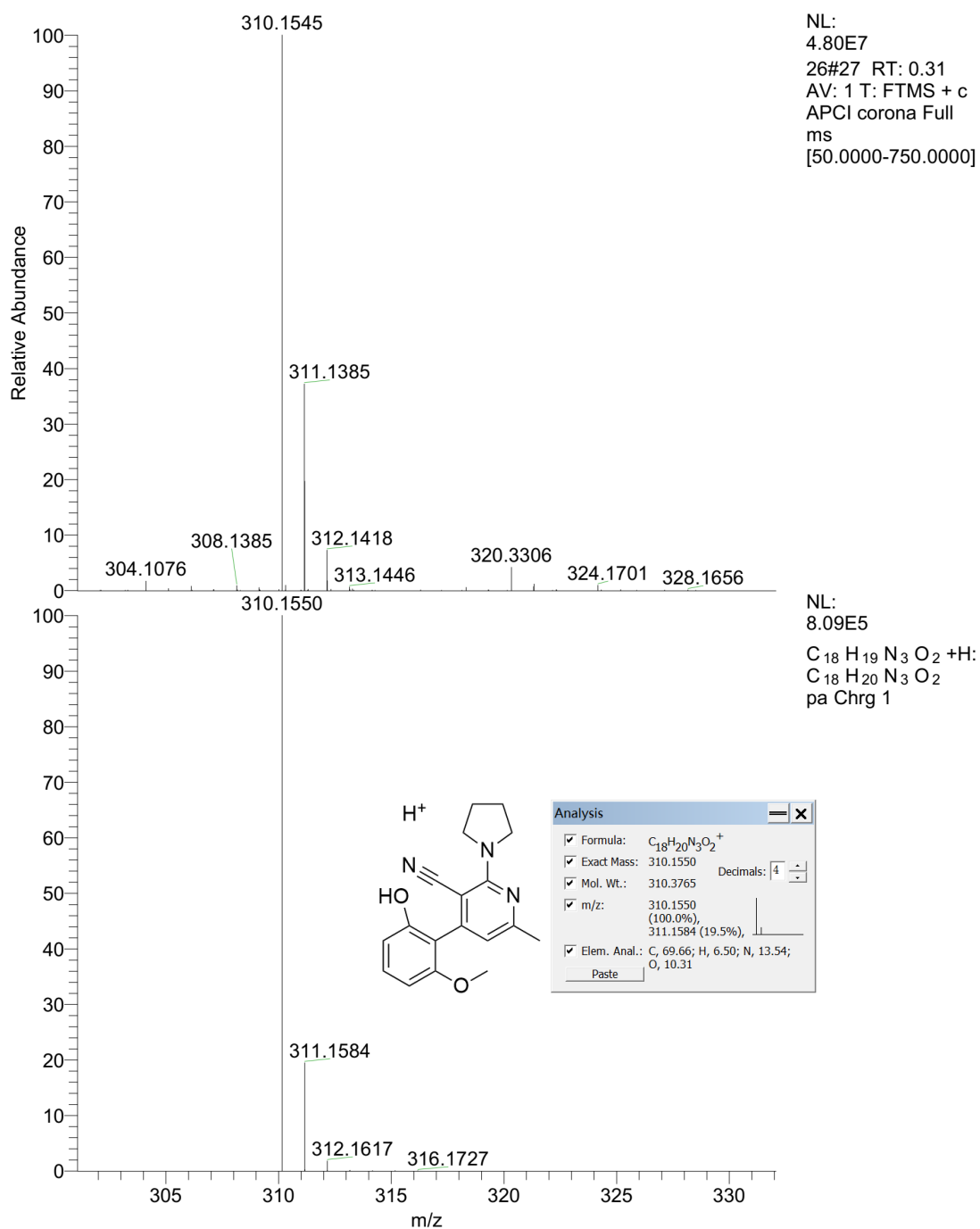


Fig. S18. HRMS spectrum of compound 3f.

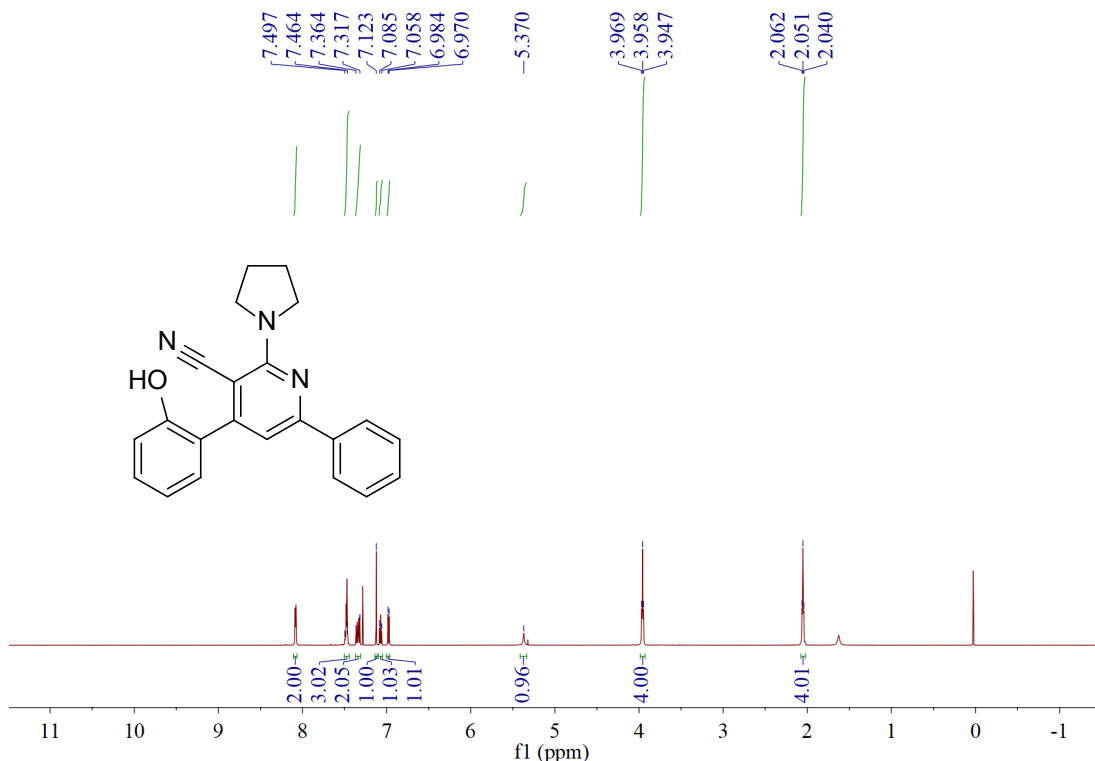


Fig. S19. ¹H NMR spectrum of compound 3g.

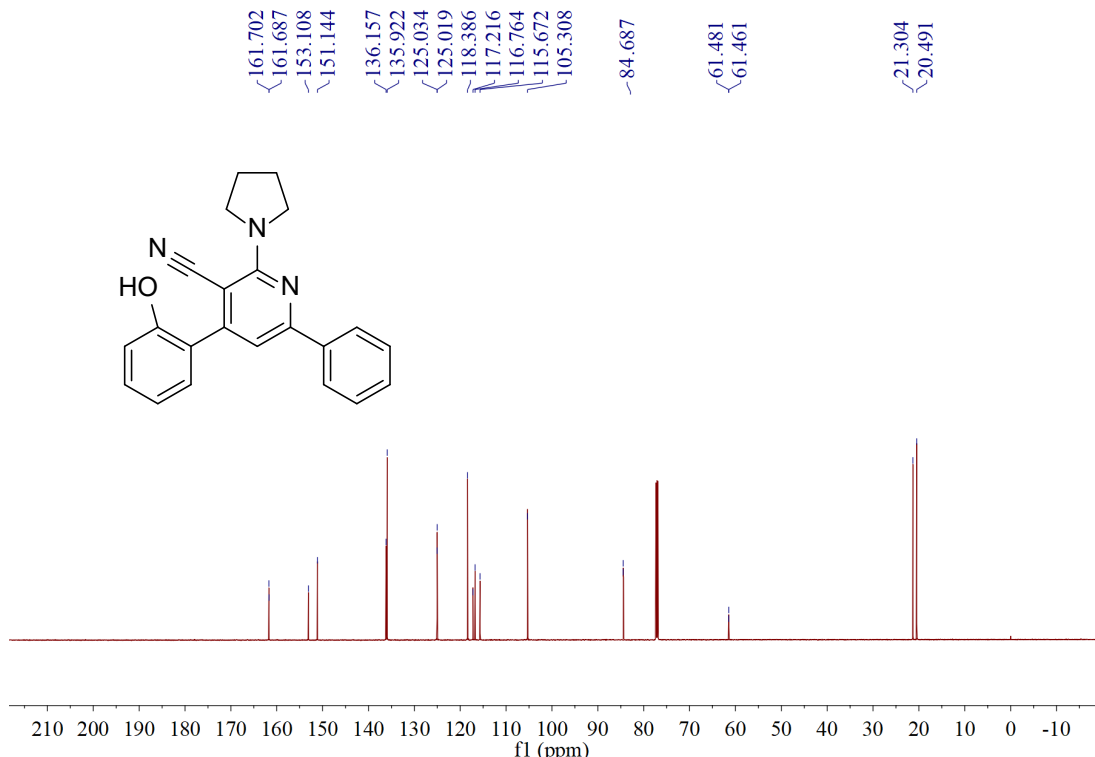


Fig. S20. ¹³C NMR spectrum of compound 3g.

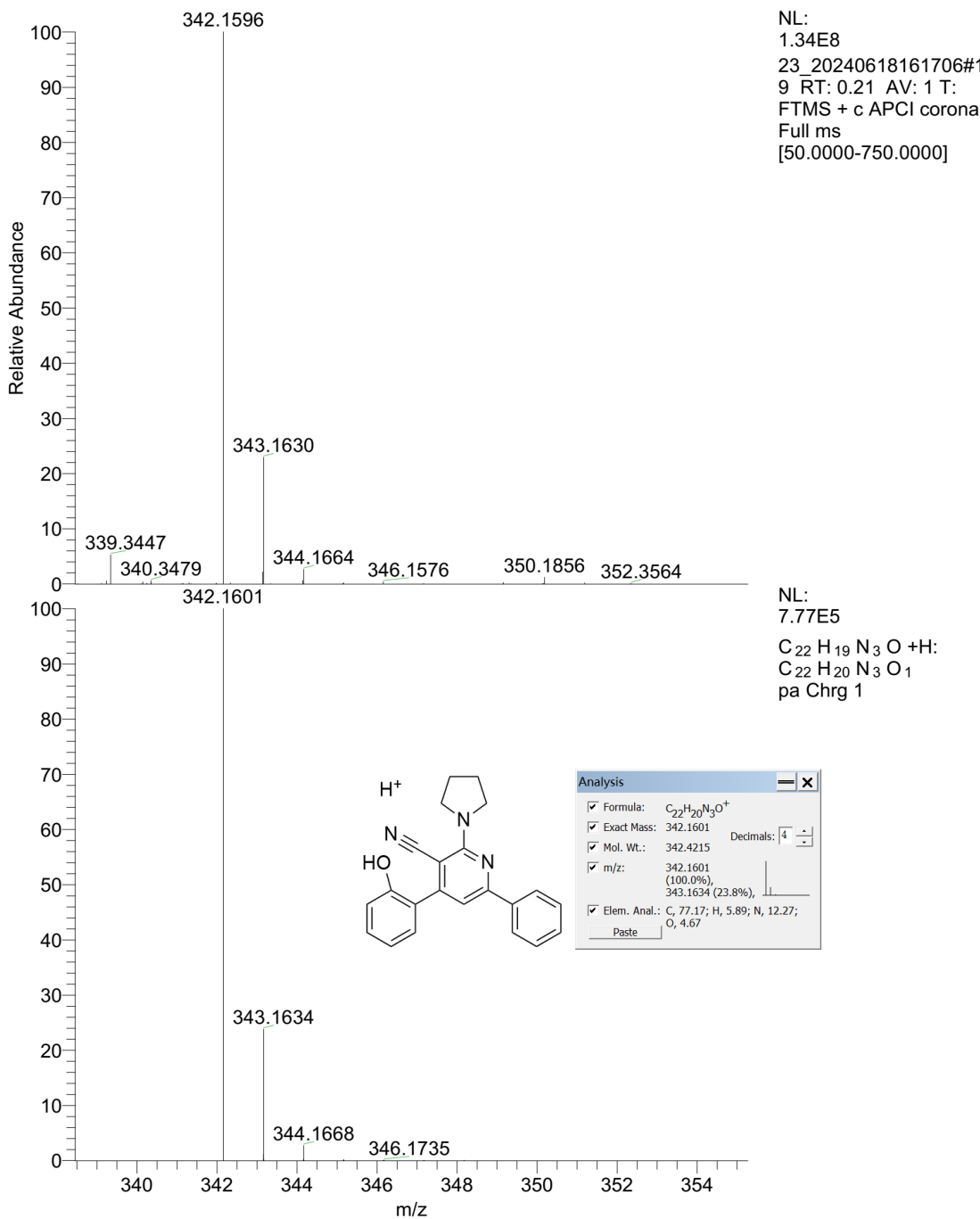


Fig. S21. HRMS spectrum of compound 3g.

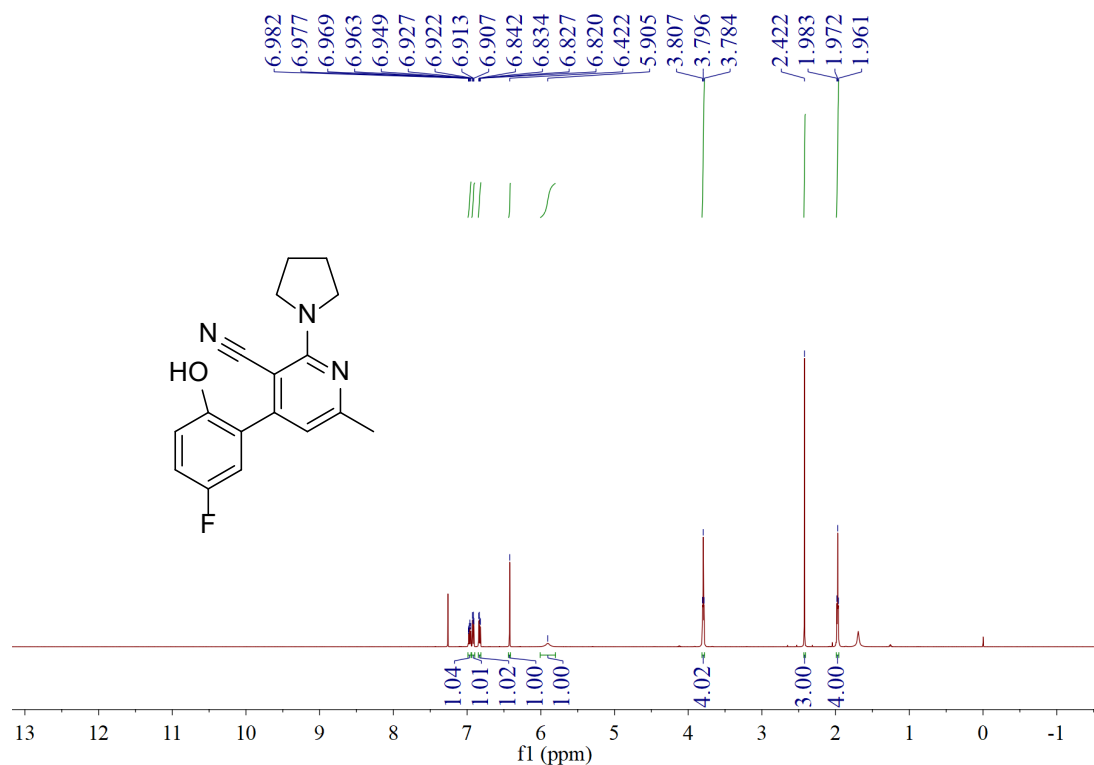


Fig. S22. ¹H NMR spectrum of compound 3h.

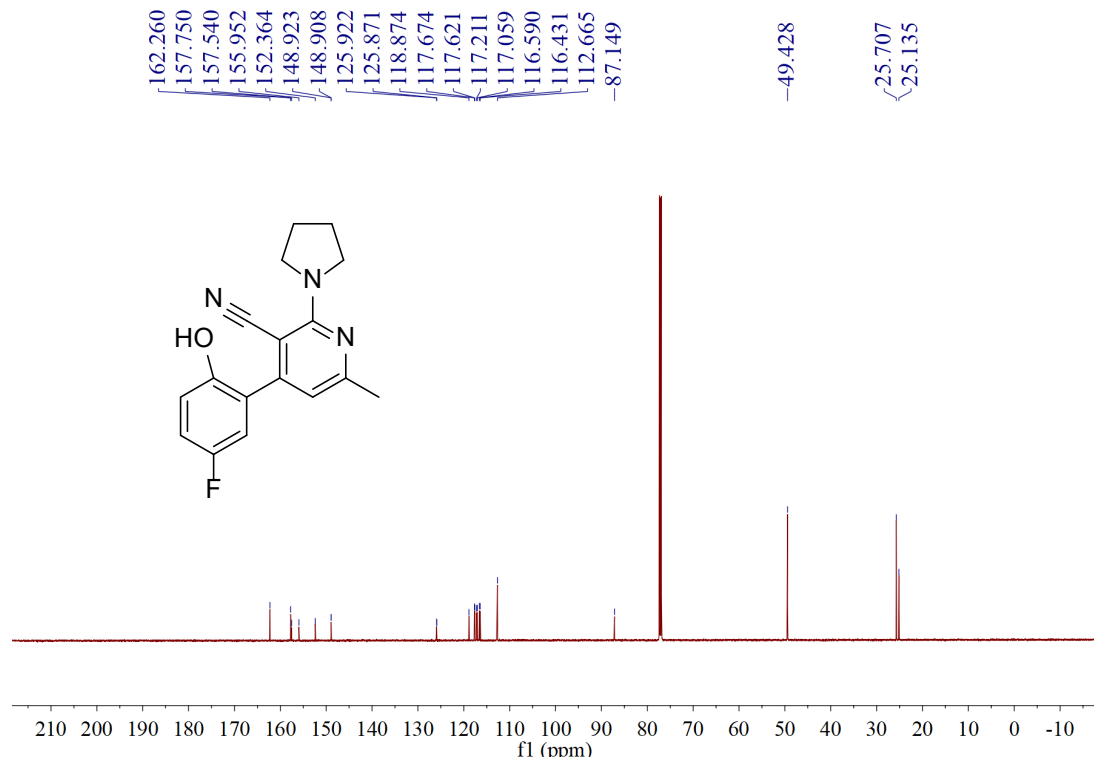


Fig. S23. ¹³C NMR spectrum of compound 3h.

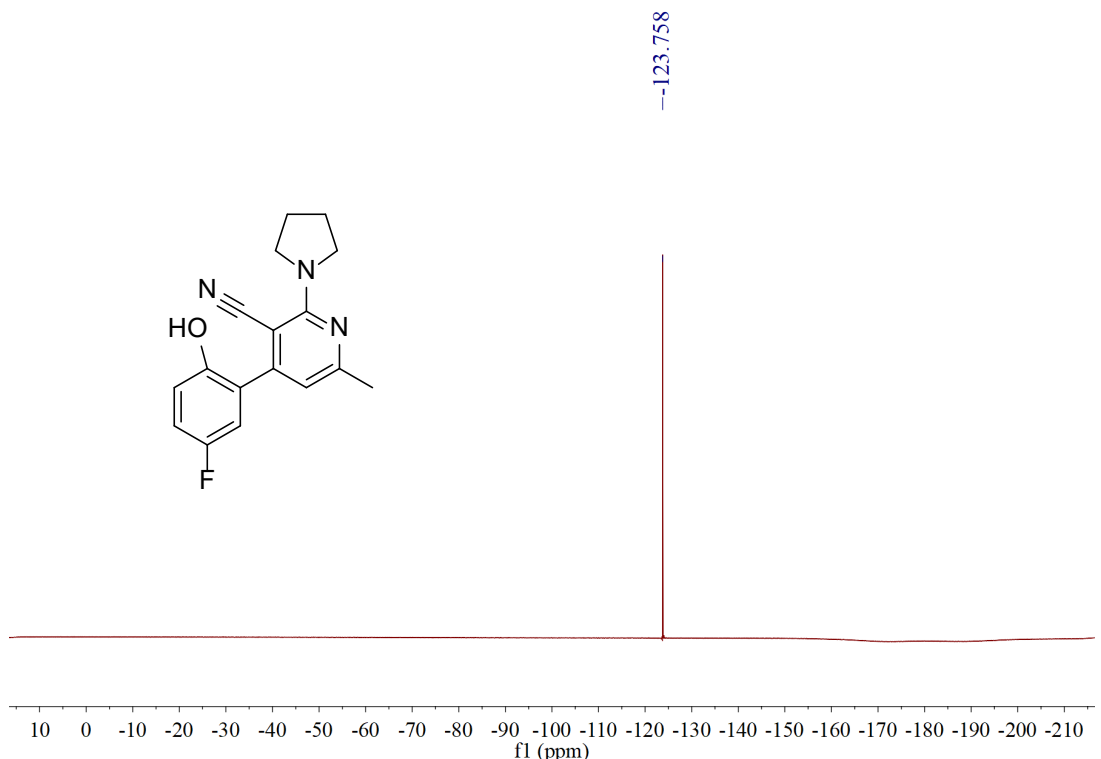


Fig. S24. ^{19}F NMR spectrum of compound 3h.

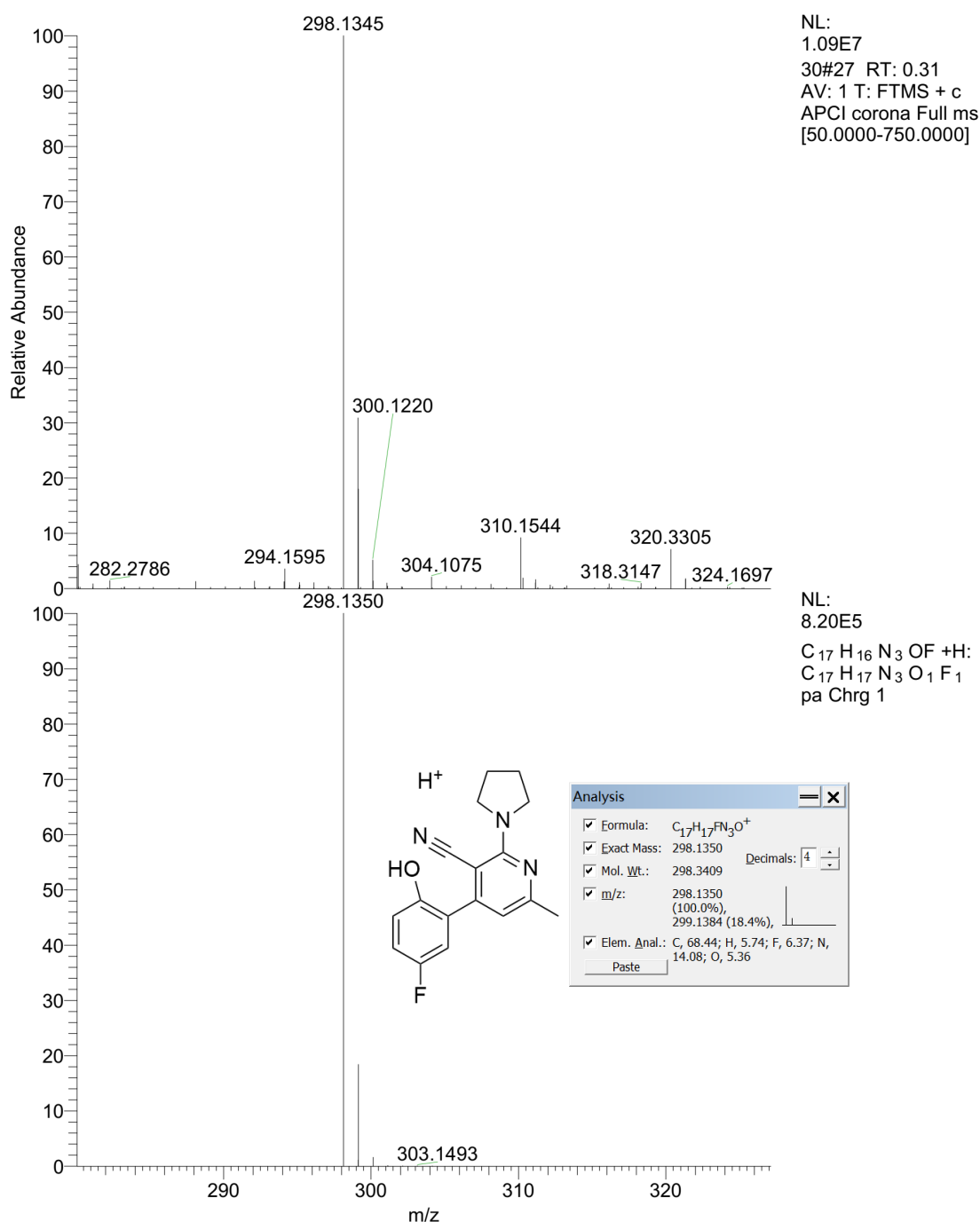


Fig. S25. HRMS spectrum of compound 3h.

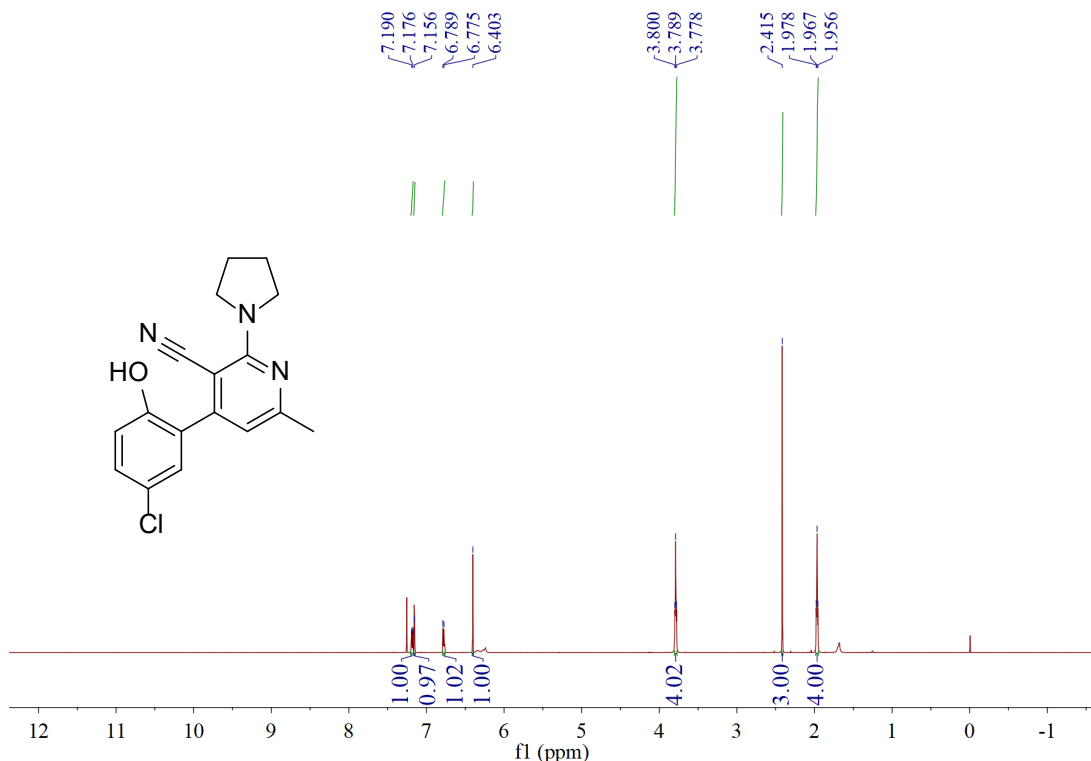


Fig. S26. ^1H NMR spectrum of compound 3i.

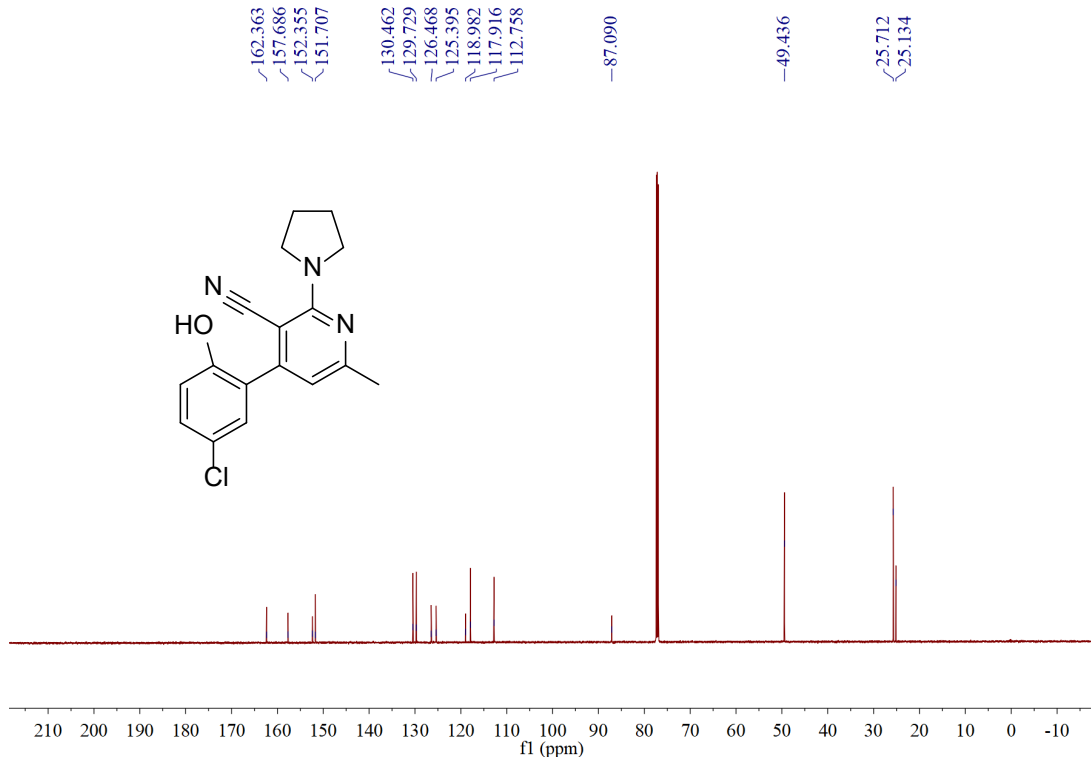


Fig. S27. ^{13}C NMR spectrum of compound 3i.

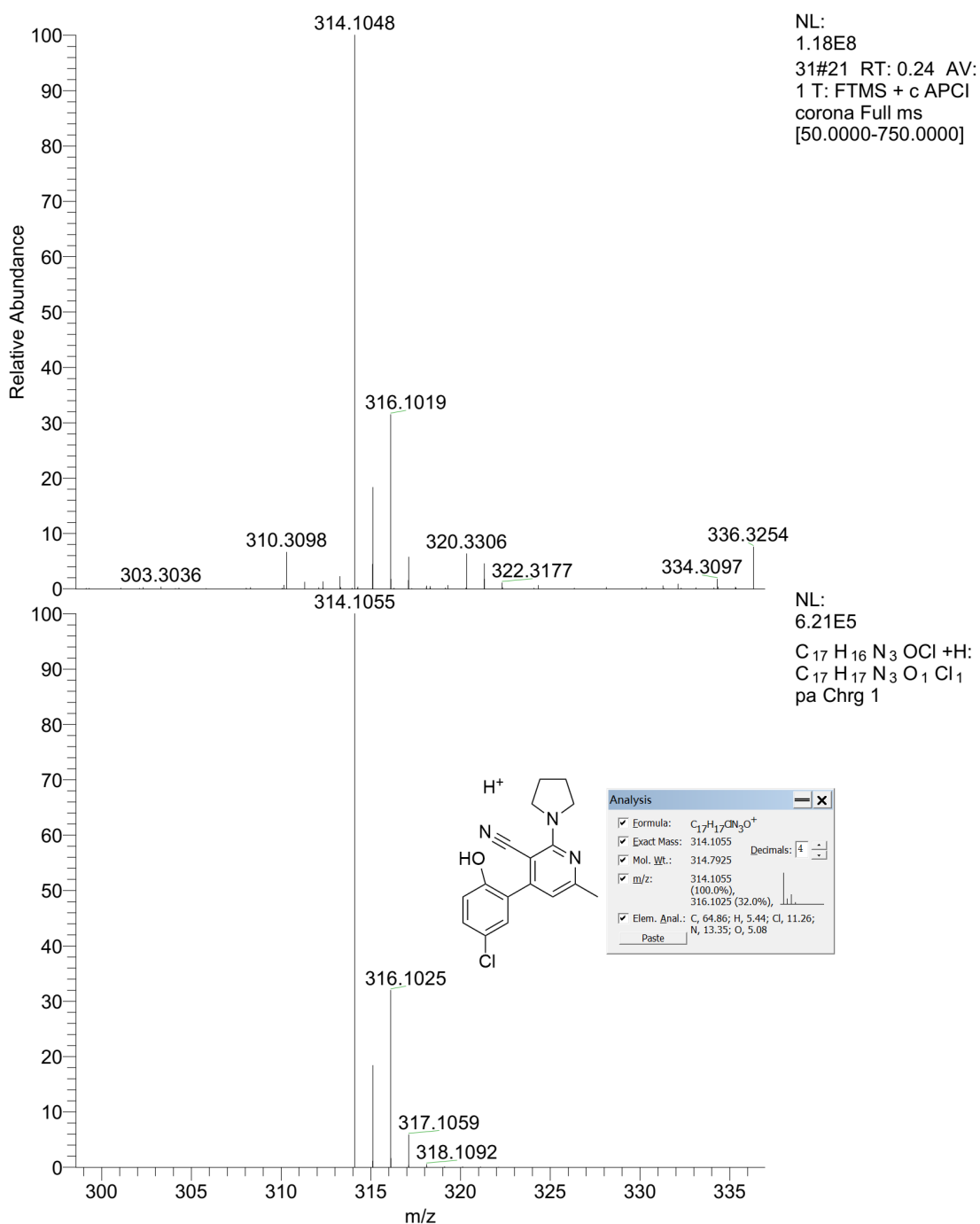


Fig. S28. HRMS spectrum of compound **3i**.

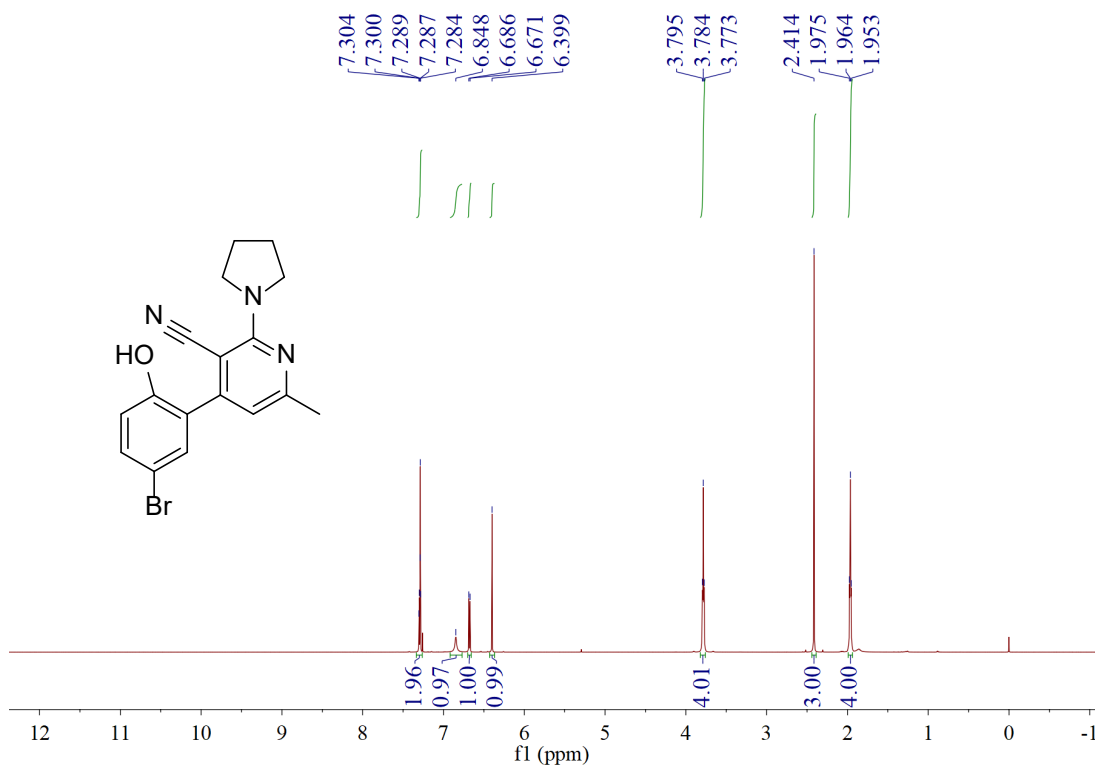


Fig. S29. ^1H NMR spectrum of compound **3j**.

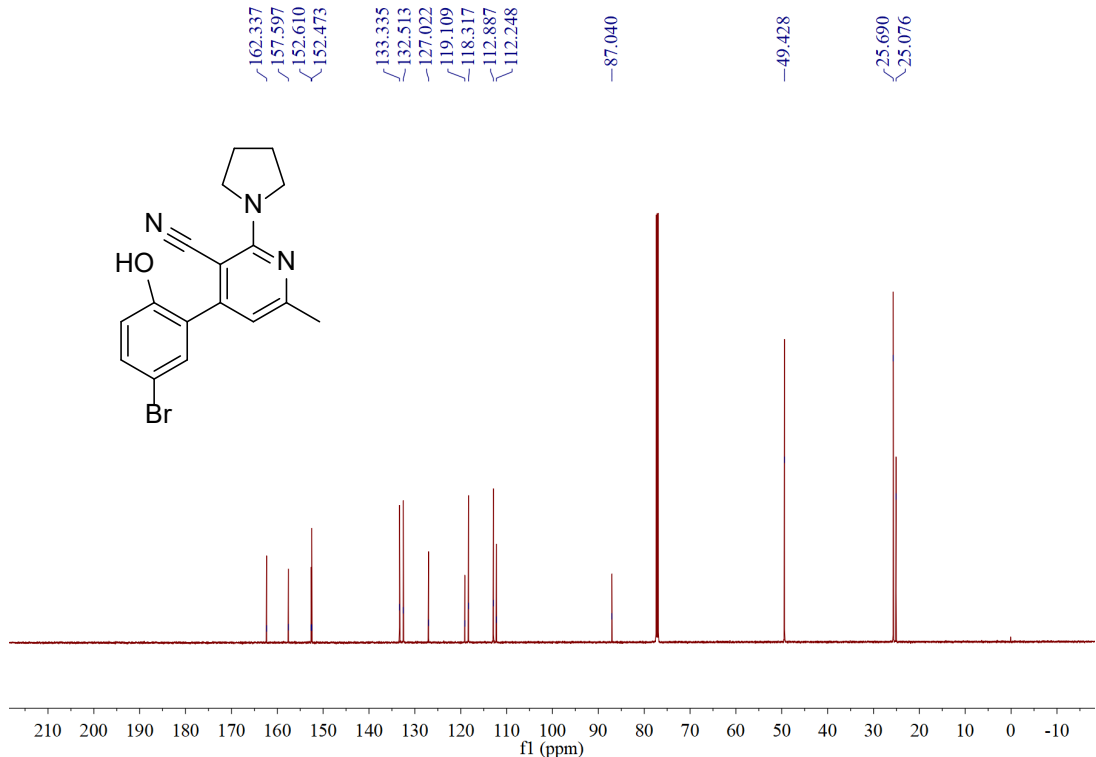


Fig. S30. ^{13}C NMR spectrum of compound **3j**.

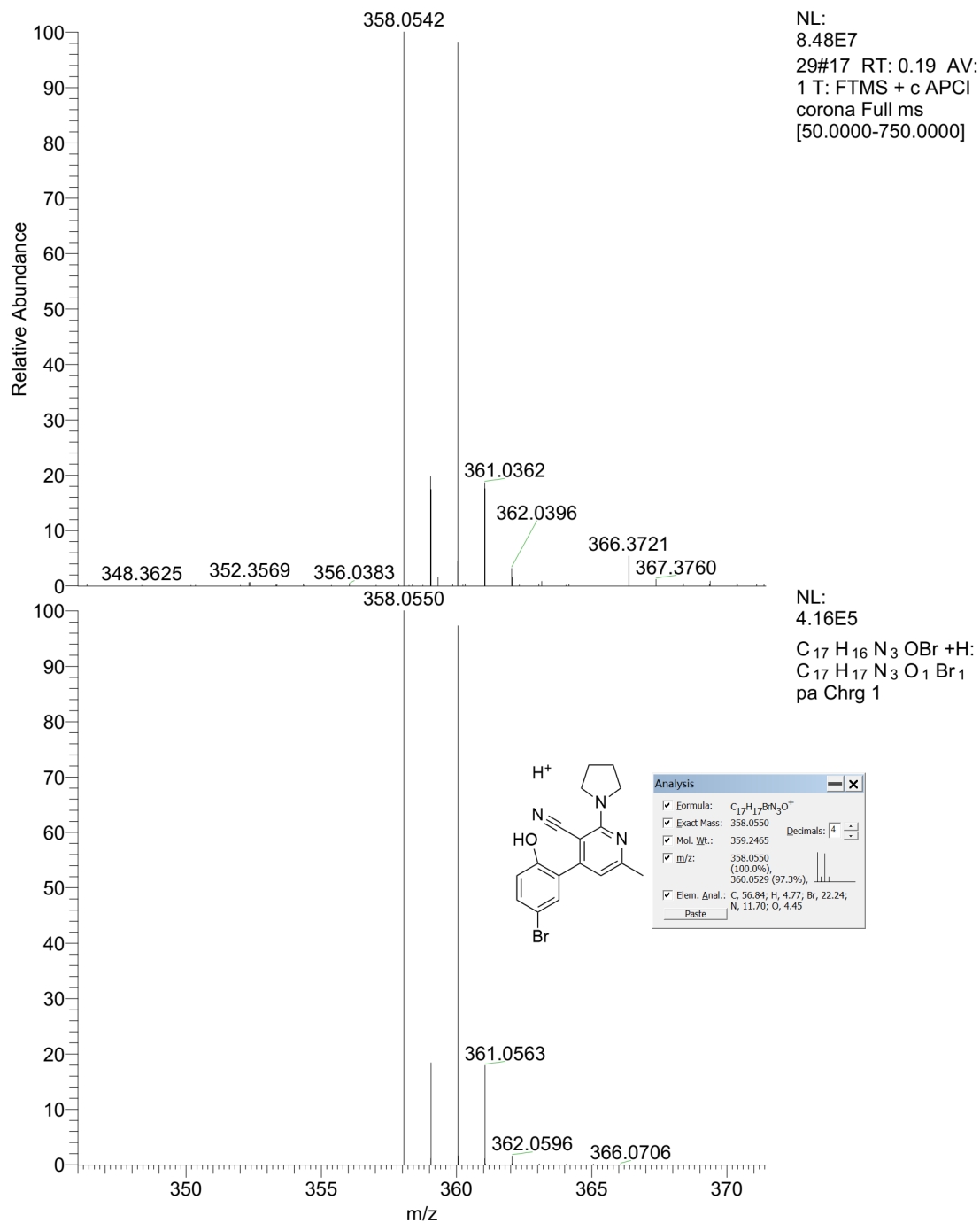


Fig. S31. HRMS spectrum of compound 3j.

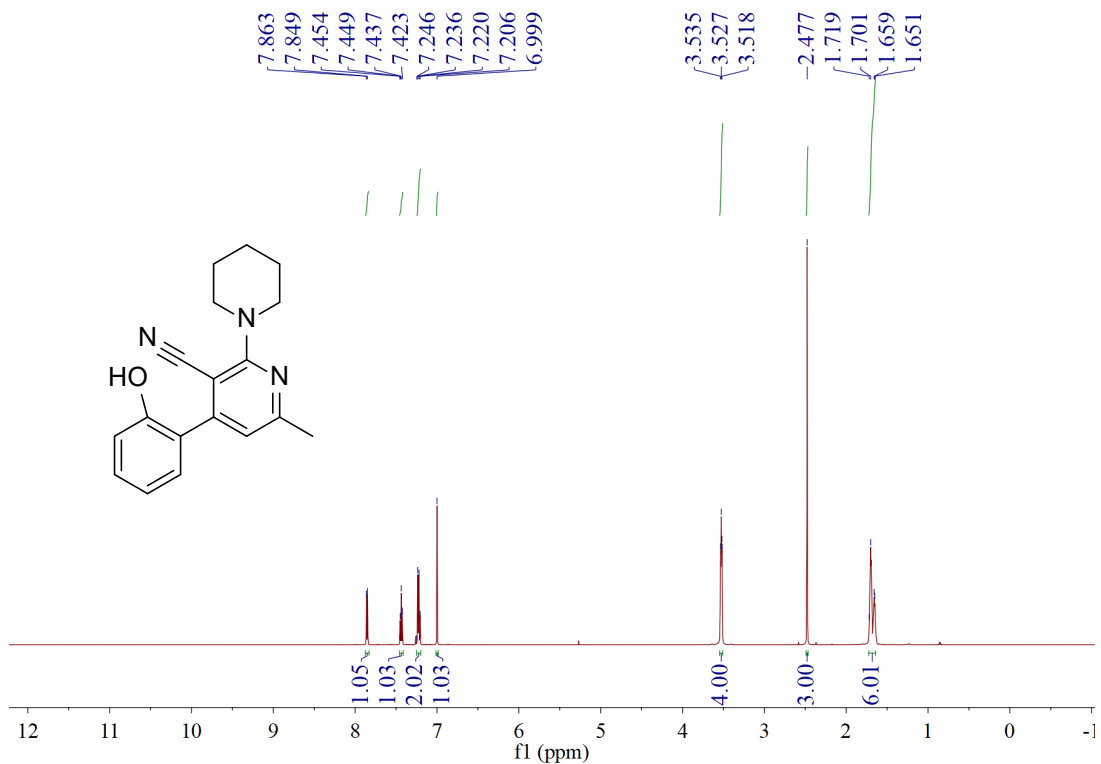


Fig. S32. ^1H NMR spectrum of compound **3k**.

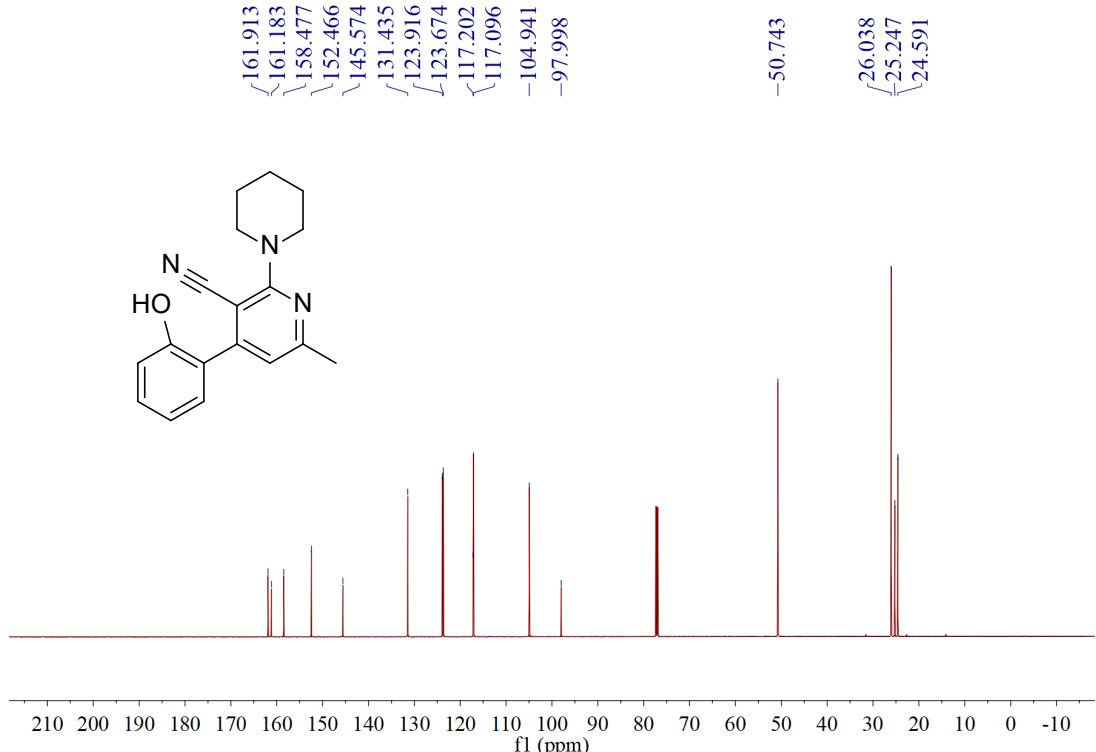


Fig. S33. ^{13}C NMR spectrum of compound **3k**.

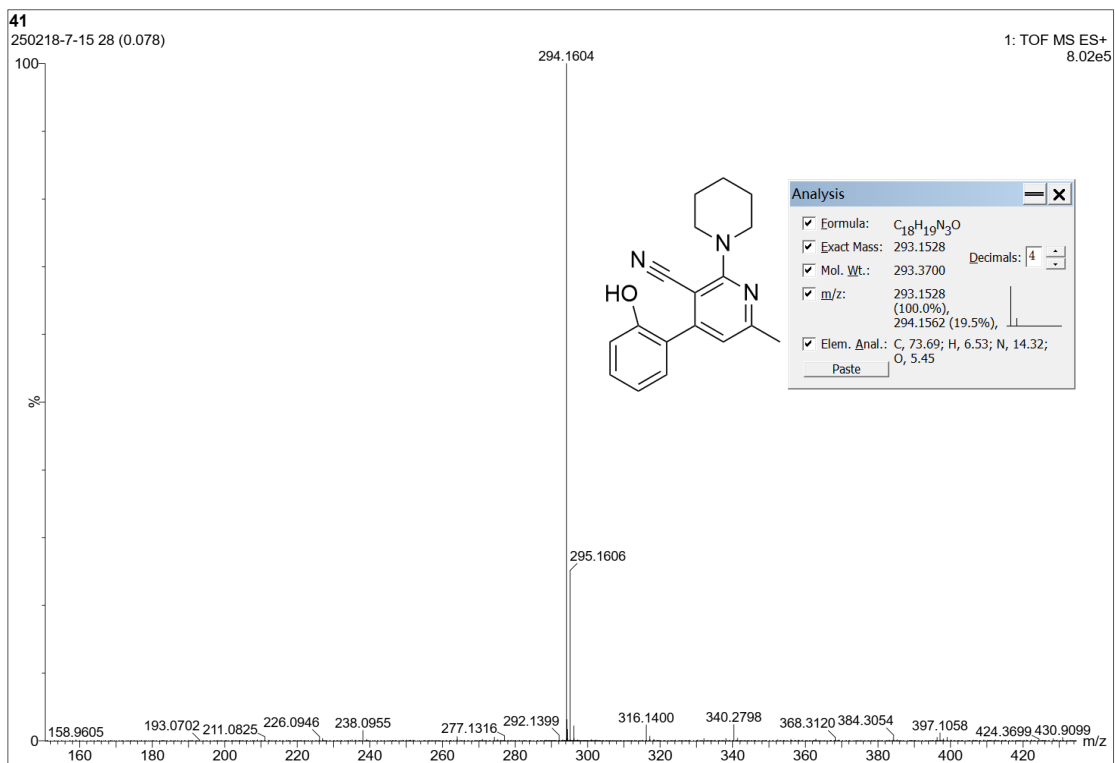


Fig. S34. HRMS spectrum of compound 3k.

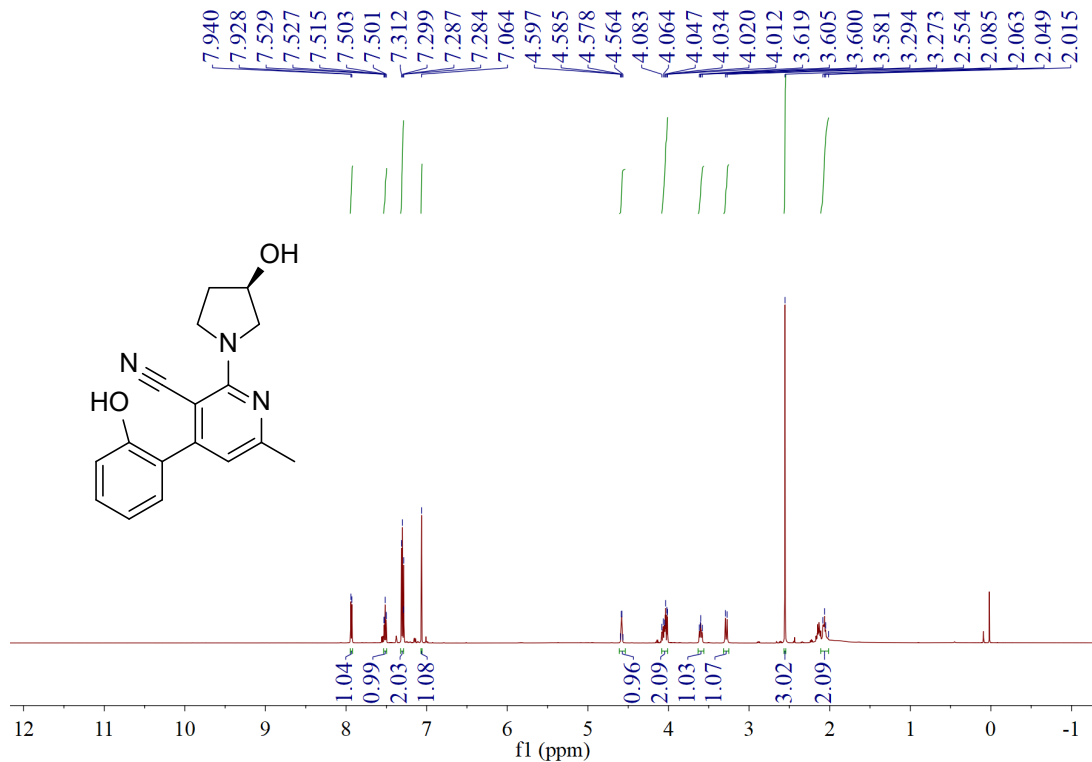


Fig. S35. ¹H NMR spectrum of compound 4a.

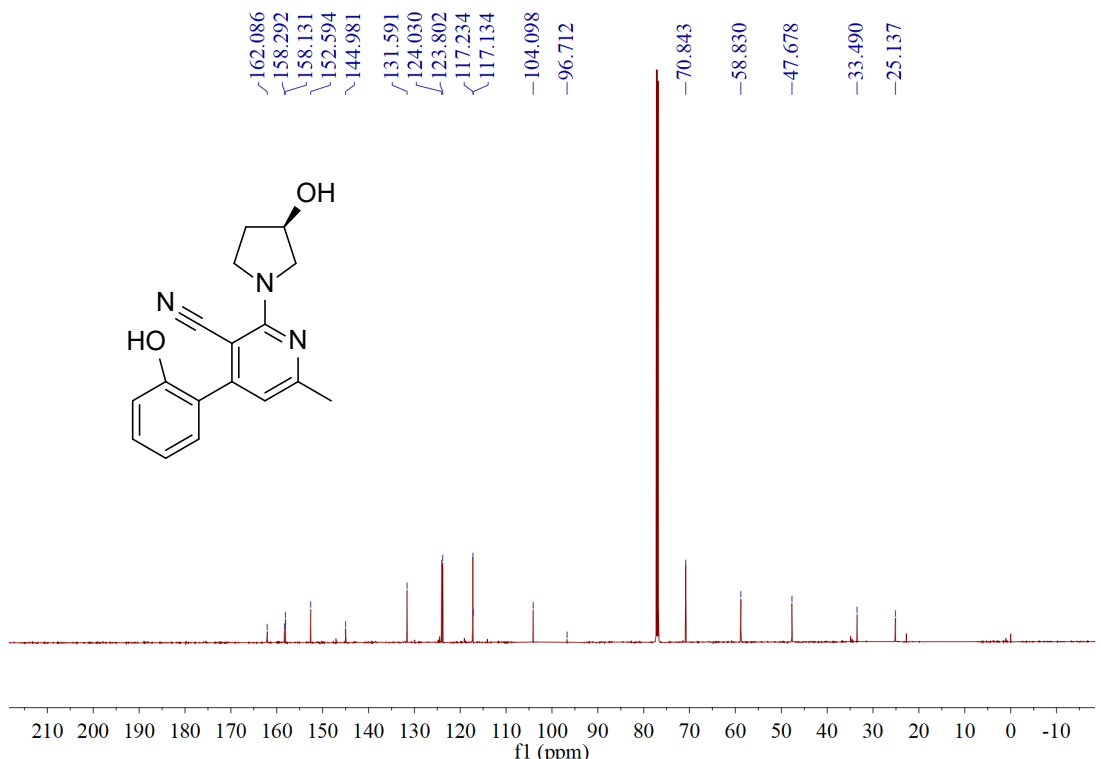


Fig. S36. ^{13}C NMR spectrum of compound 4a.

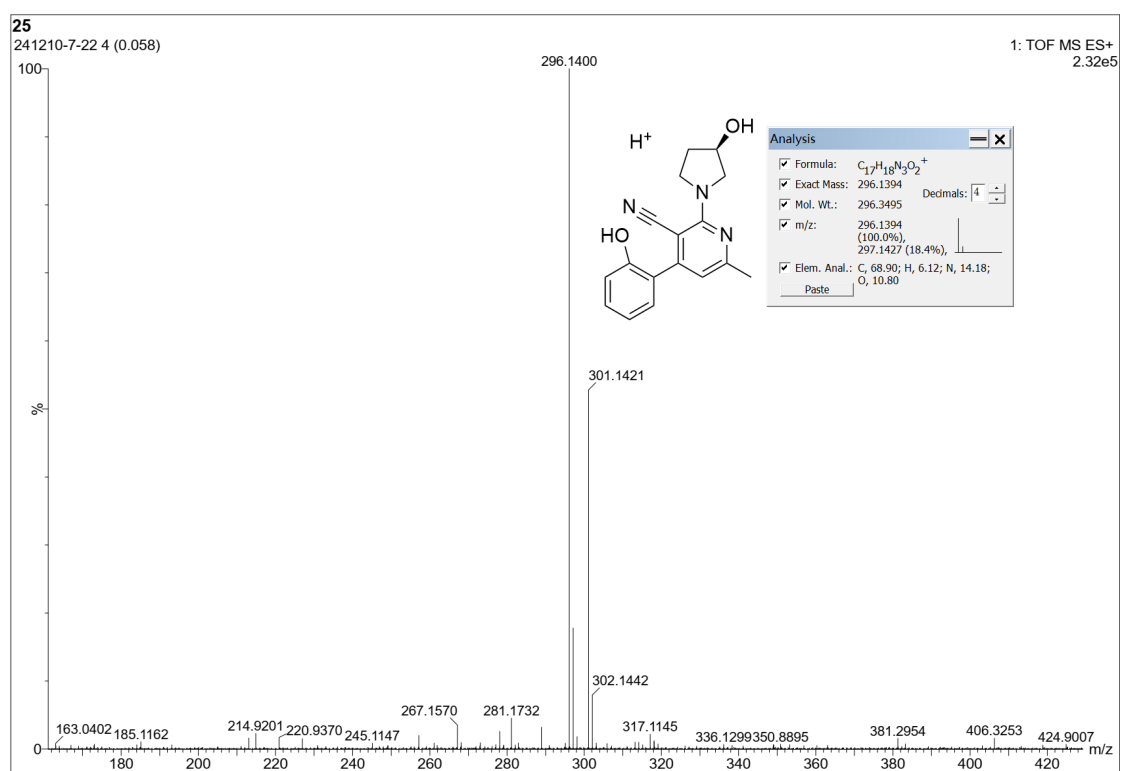


Fig. S37. HRMS spectrum of compound 4a.

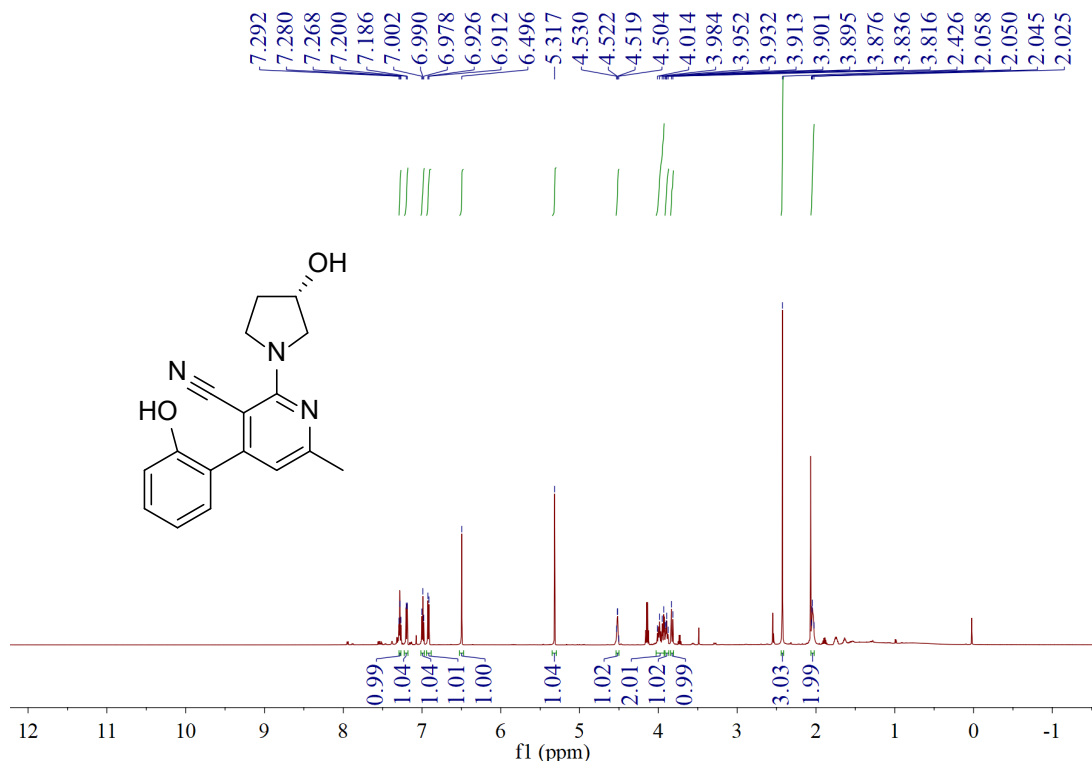


Fig. S38. ^1H NMR spectrum of compound **4b**.

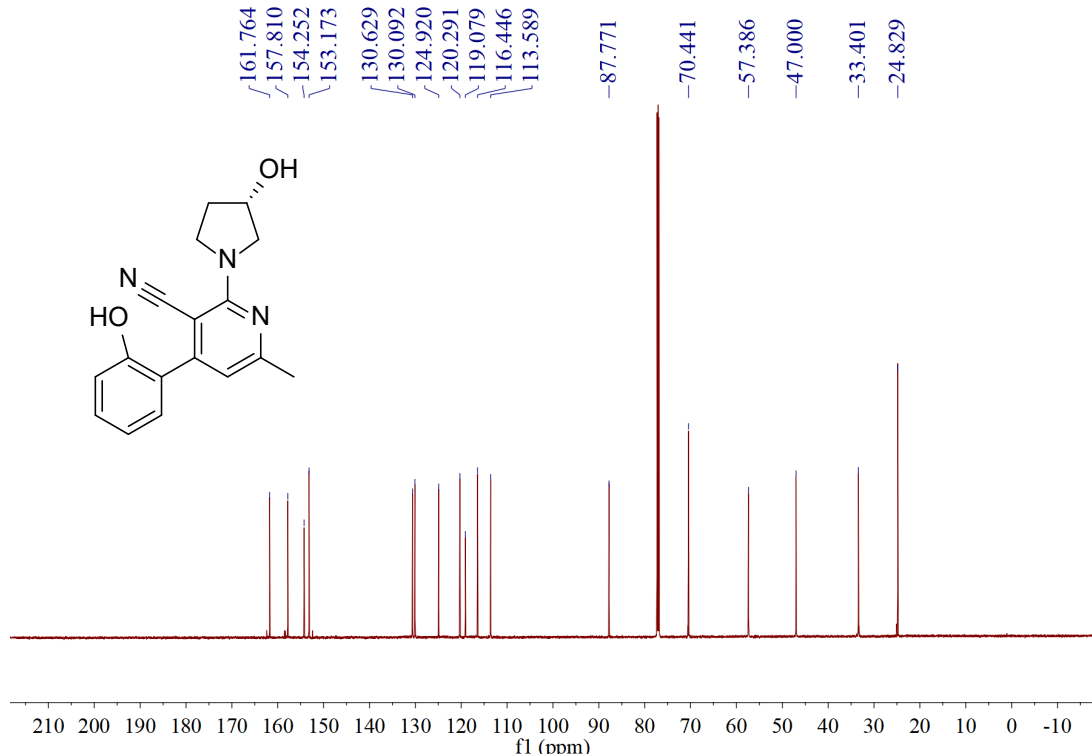


Fig. S39. ^{13}C NMR spectrum of compound **4b**.

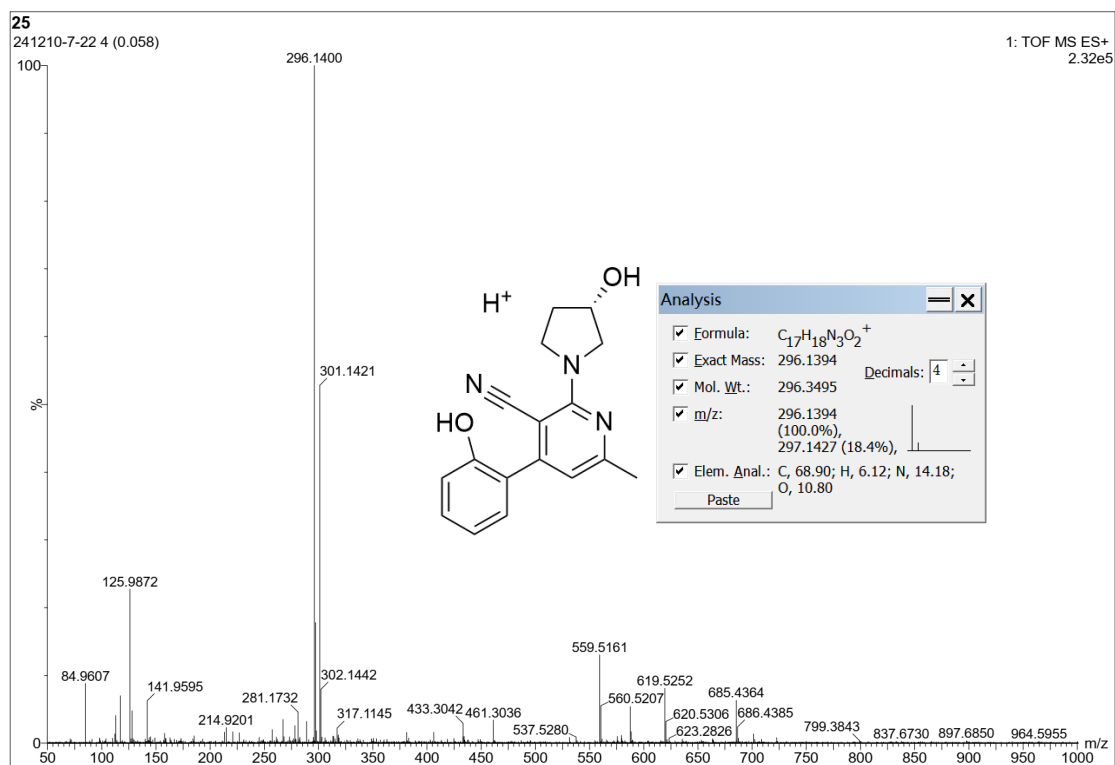


Fig. S40. HRMS spectrum of compound 4b.

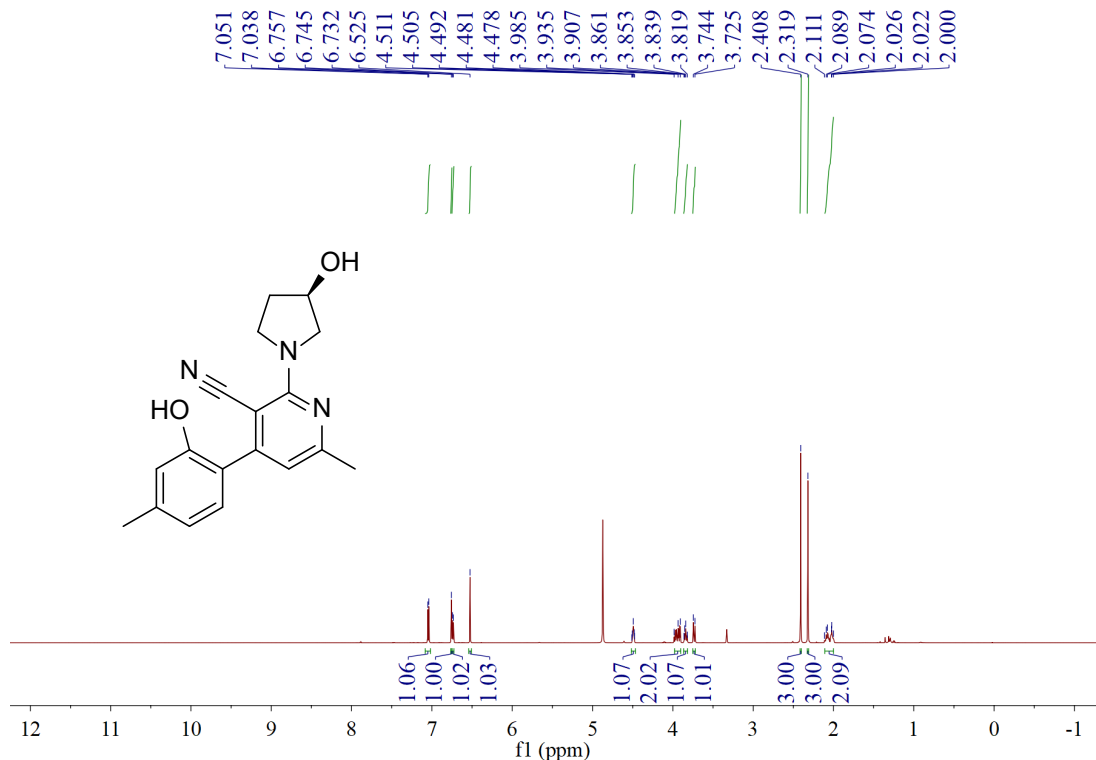


Fig. S41. ^1H NMR spectrum of compound 4c.

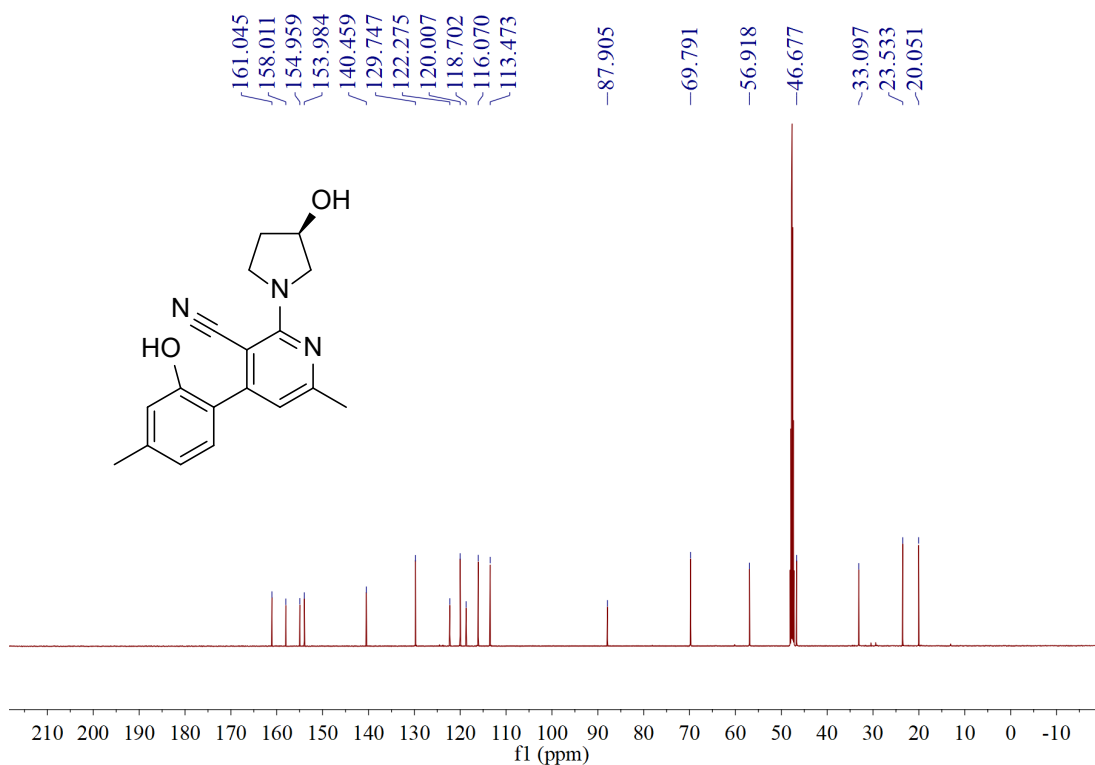


Fig. S42. ^{13}C NMR spectrum of compound **4c**.

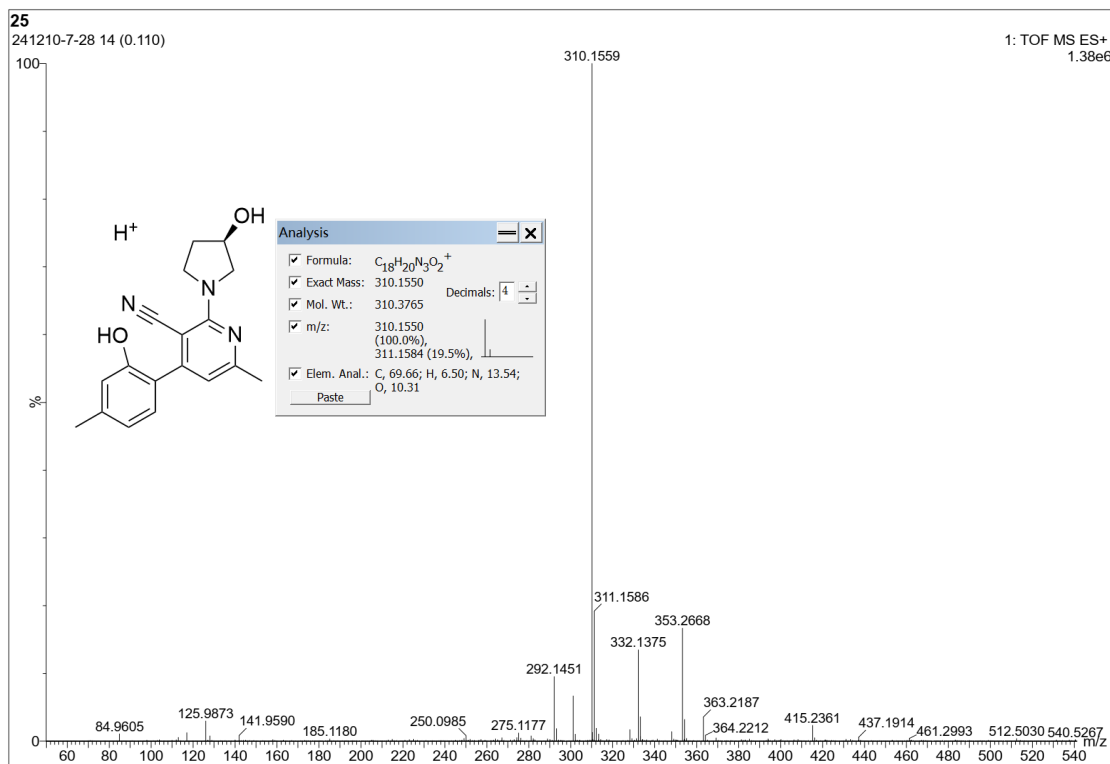


Fig. S43. HRMS spectrum of compound **4c**.

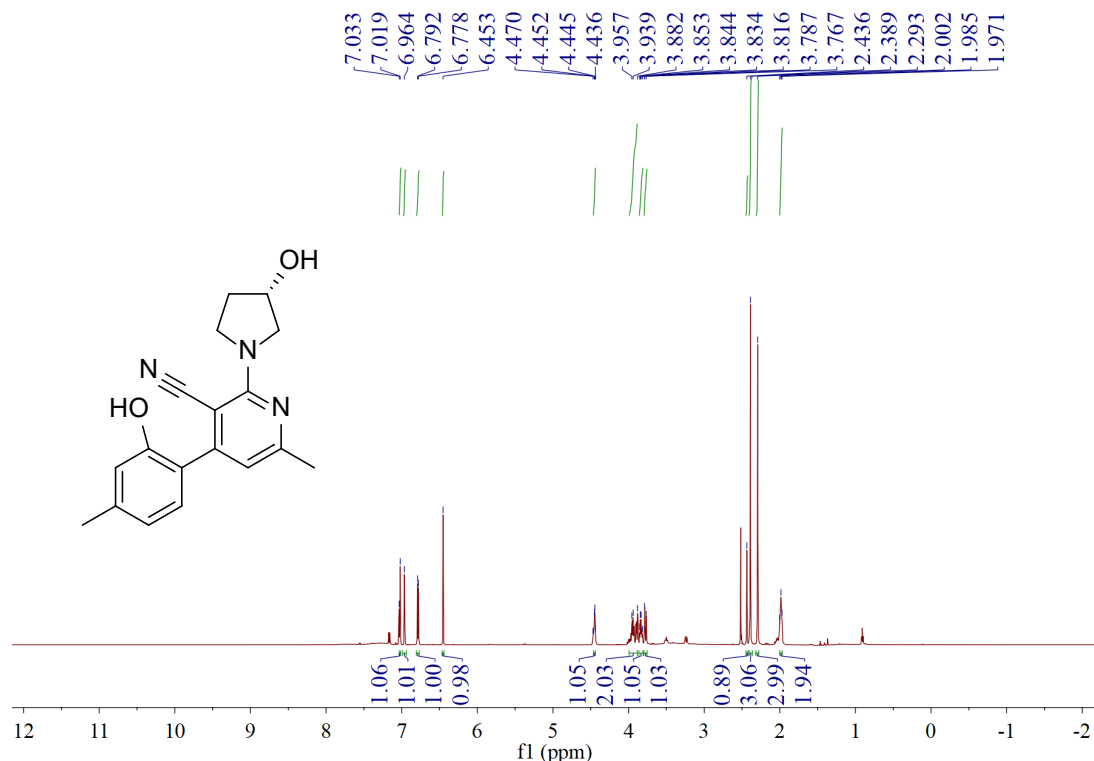


Fig. S44. ^1H NMR spectrum of compound **4d**.

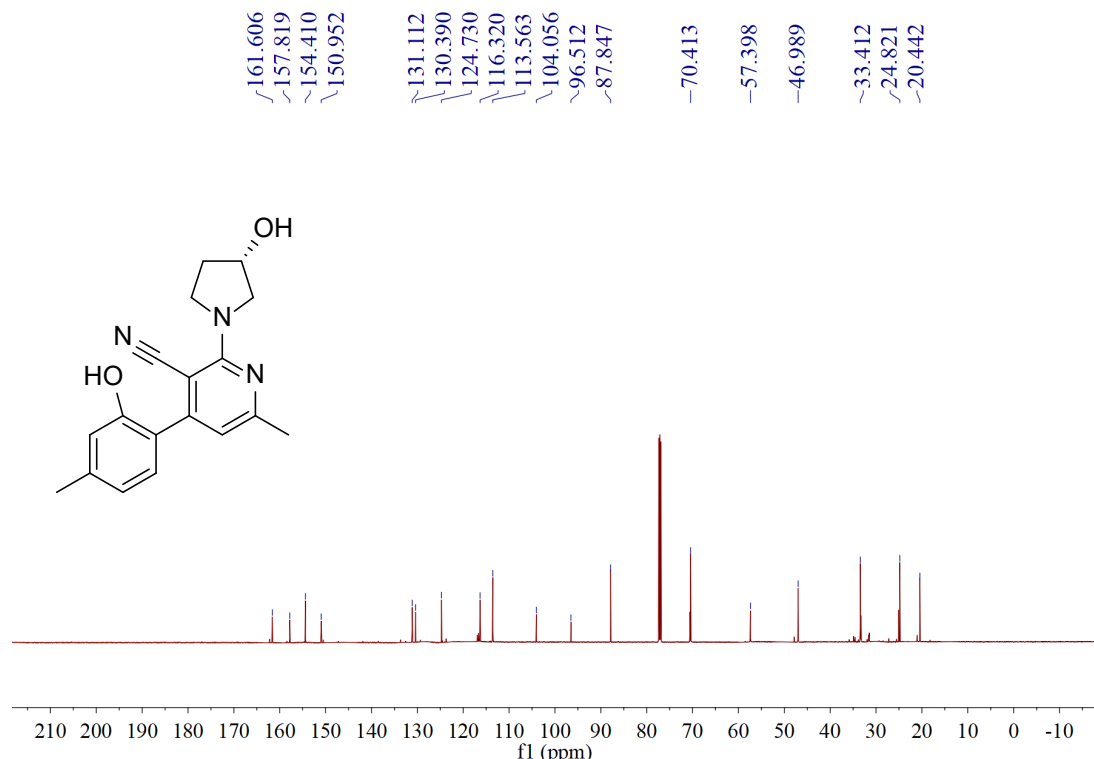


Fig. S45. ^{13}C NMR spectrum of compound **4d**.

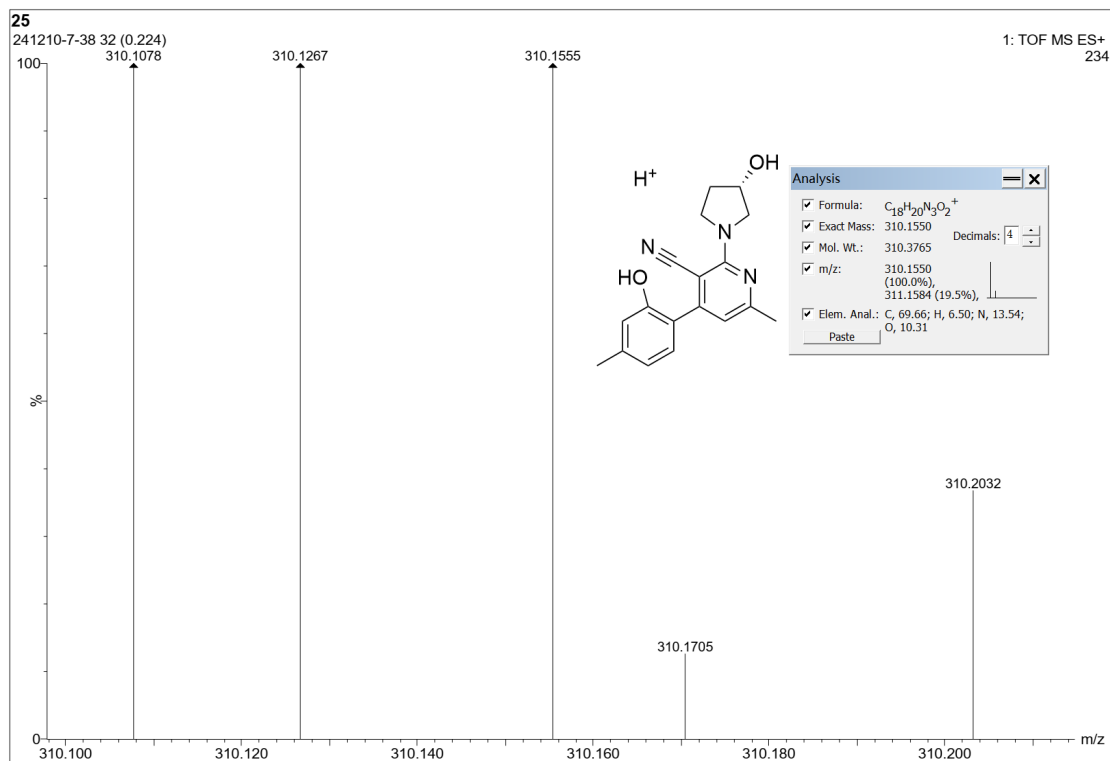


Fig. S46. HRMS spectrum of compound 4d.

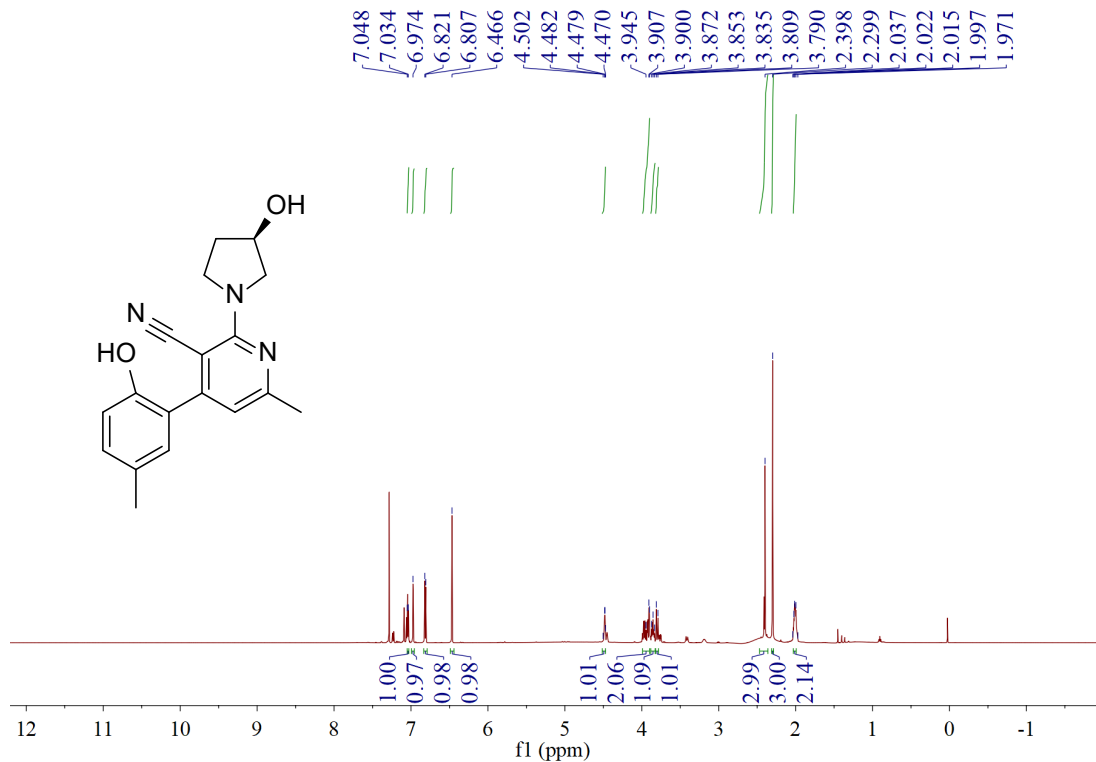


Fig. S47. ^1H NMR spectrum of compound 4e.

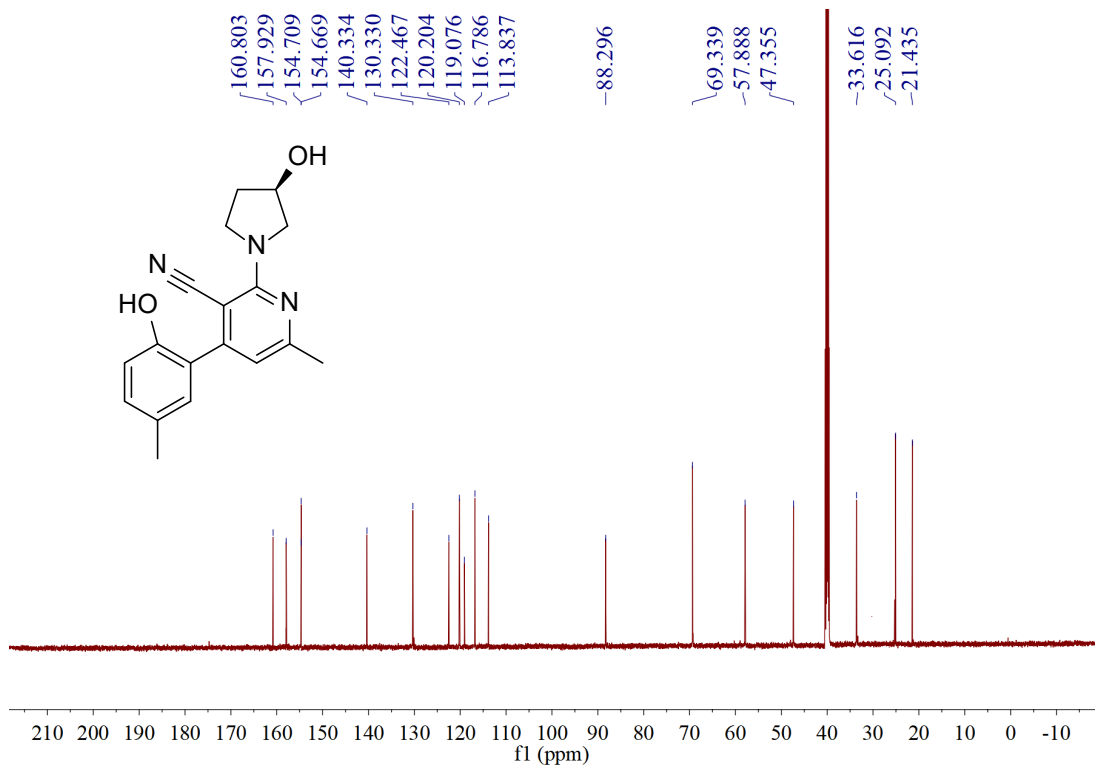


Fig. S48. ^{13}C NMR spectrum of compound 4e.

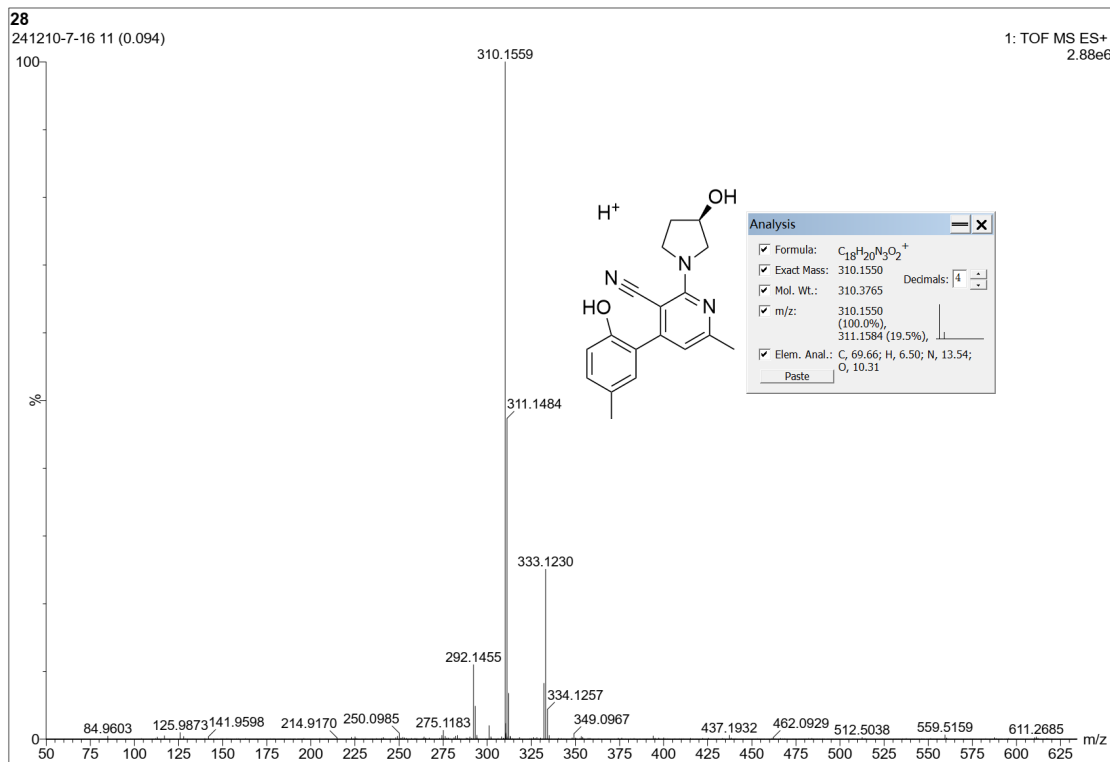


Fig. S49. HRMS spectrum of compound 4e.

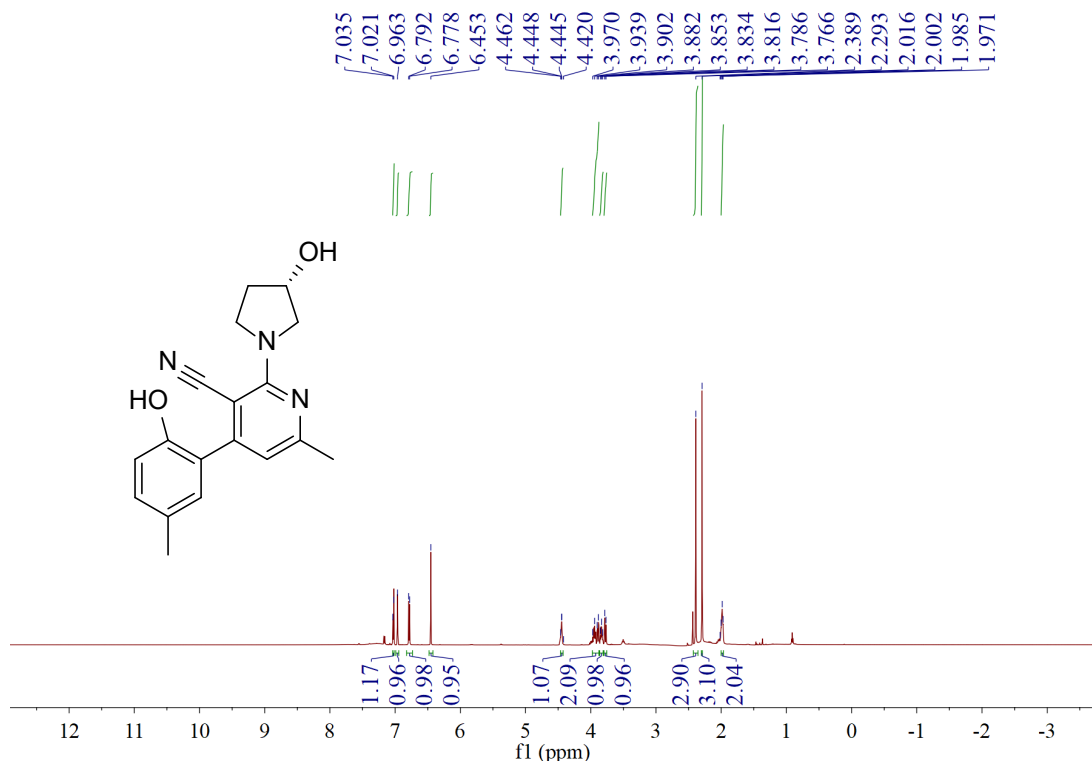


Fig. S50. ^1H NMR spectrum of compound 4f.

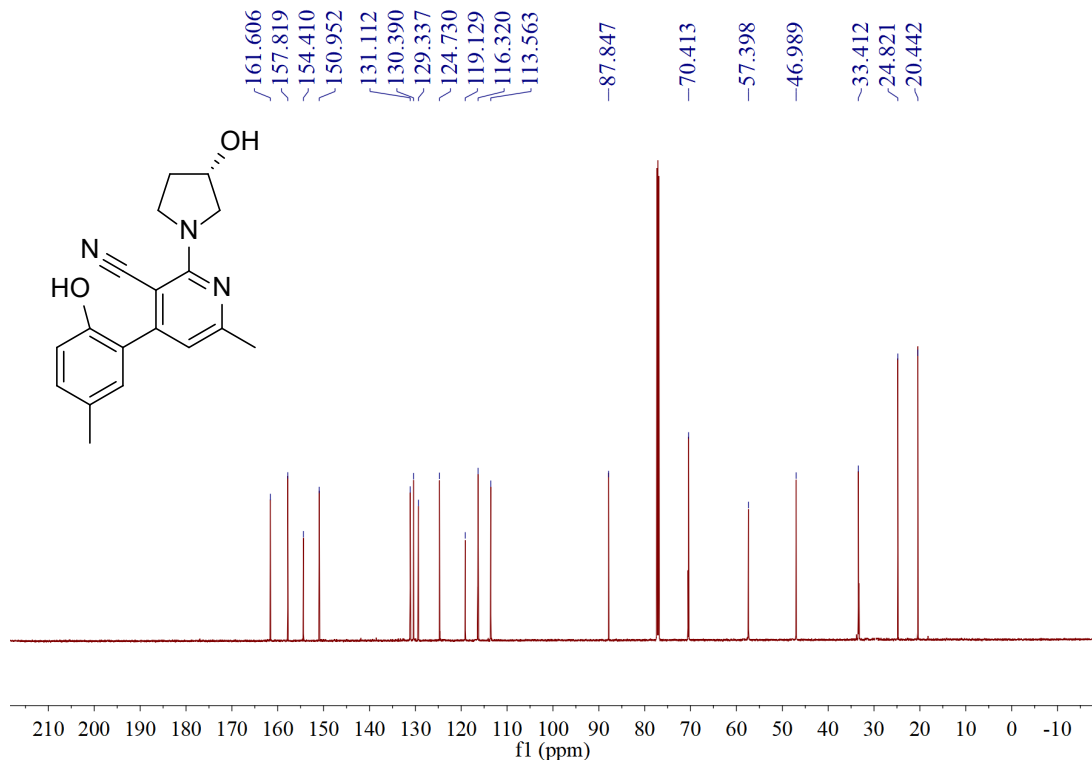


Fig. S51. ^{13}C NMR spectrum of compound 4f.

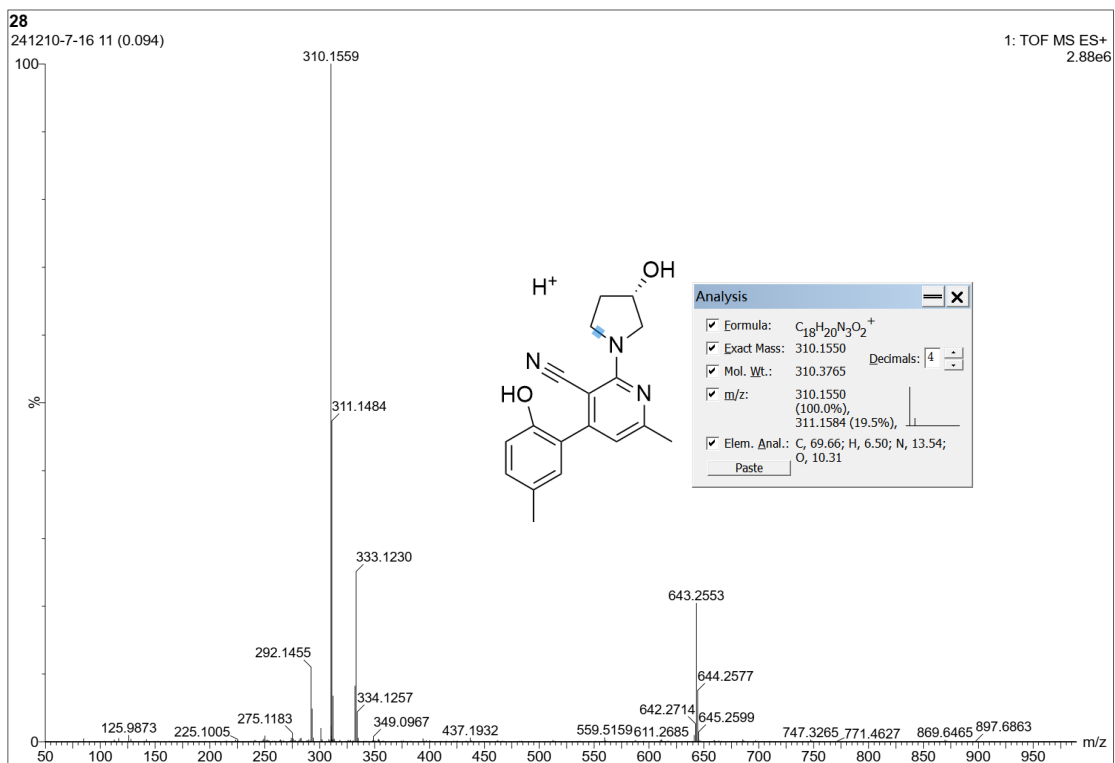


Fig. S52. HRMS spectrum of compound 4f.

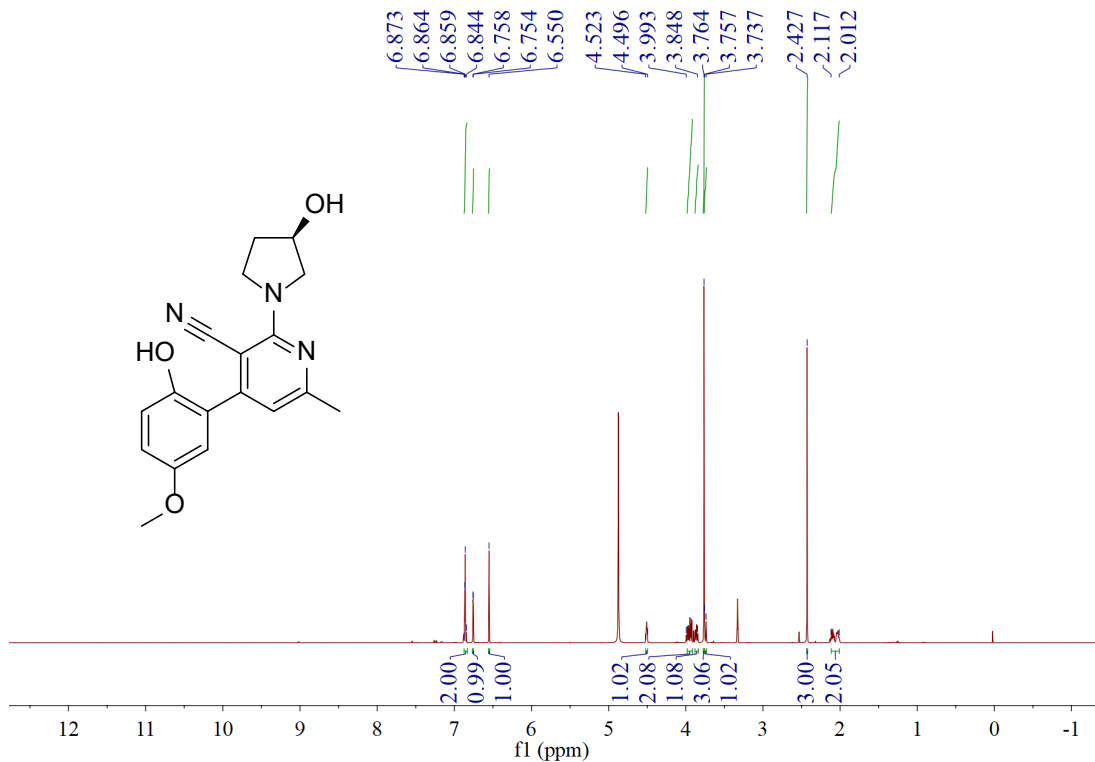


Fig. S53. ^1H NMR spectrum of compound 4g.

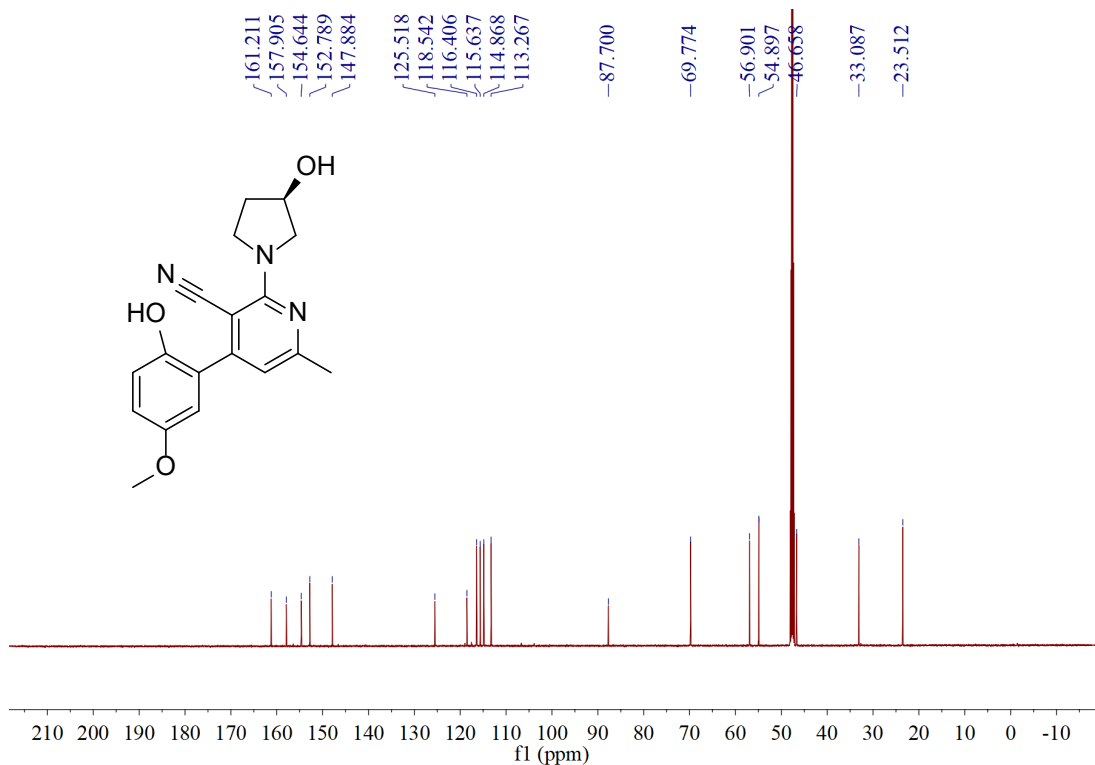


Fig. S54. ^{13}C NMR spectrum of compound **4g**.

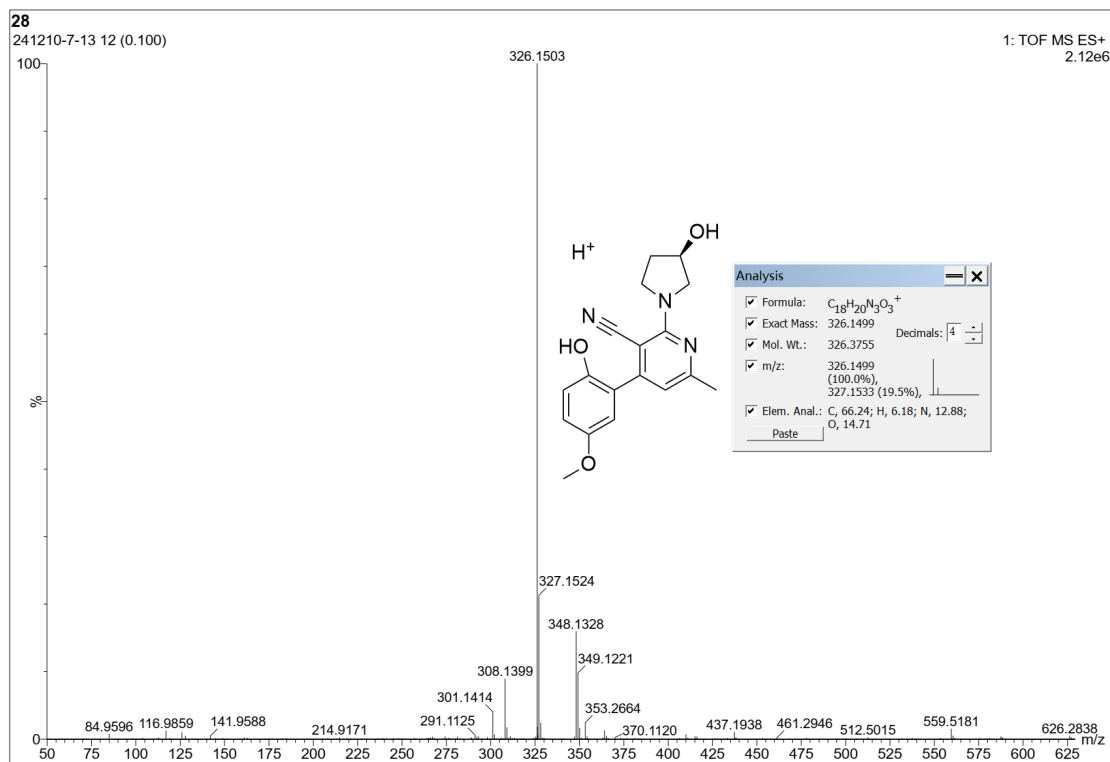


Fig. S55. HRMS spectrum of compound **4g**.

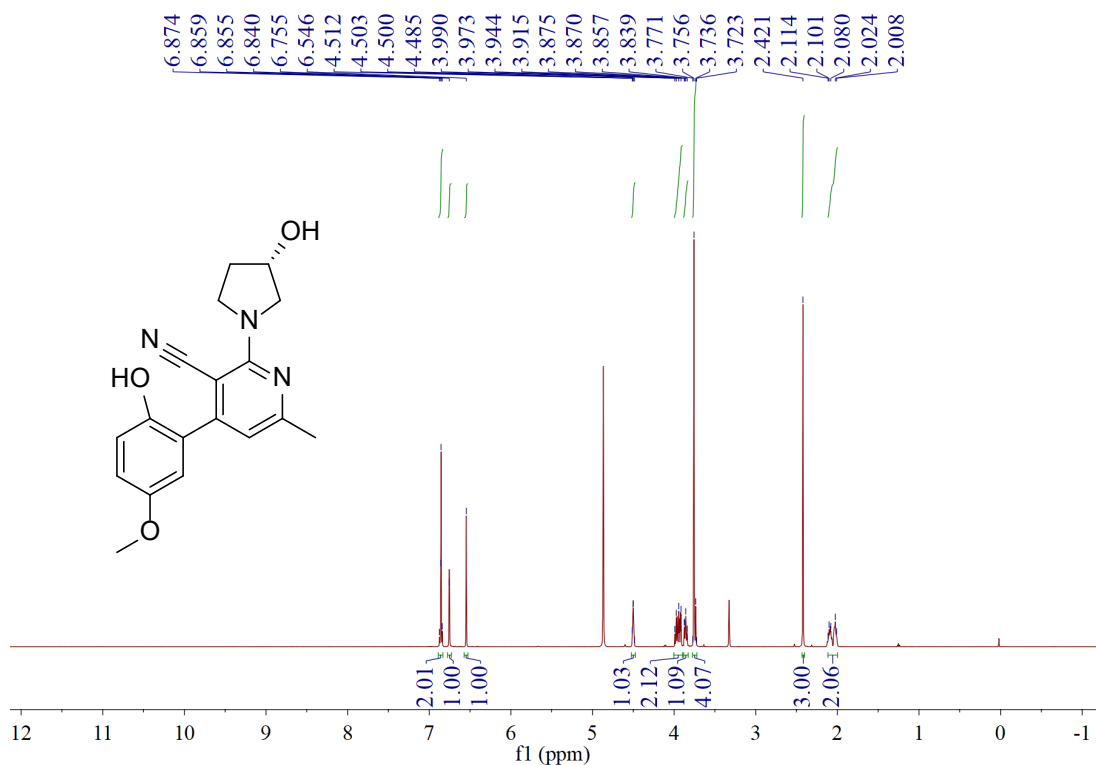


Fig. S56. ¹H NMR spectrum of compound 4h.

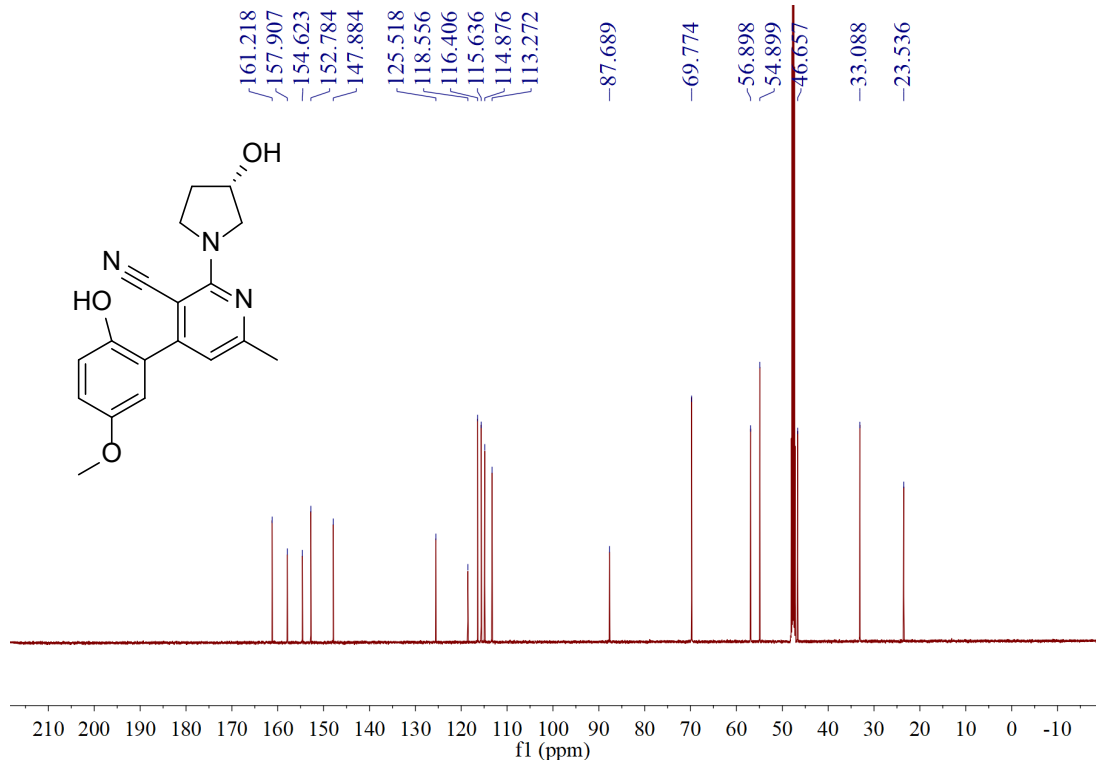


Fig. S57. ¹³C NMR spectrum of compound 4h.

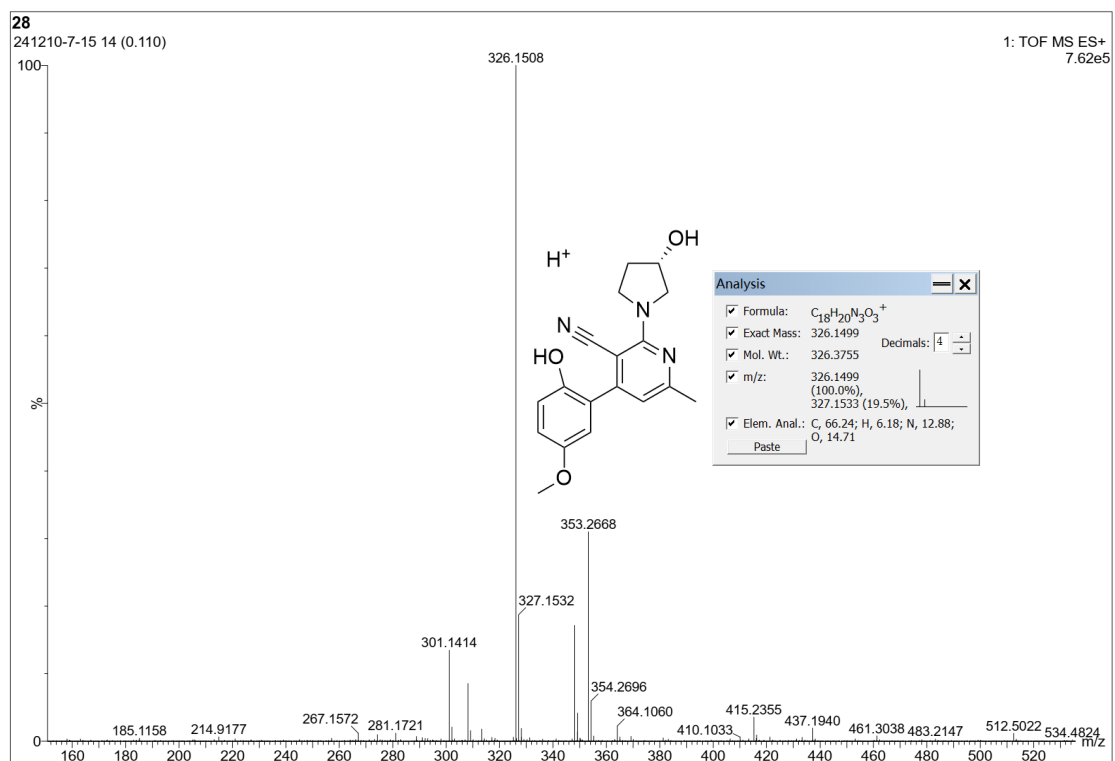


Fig. S58. HRMS spectrum of compound 4h.

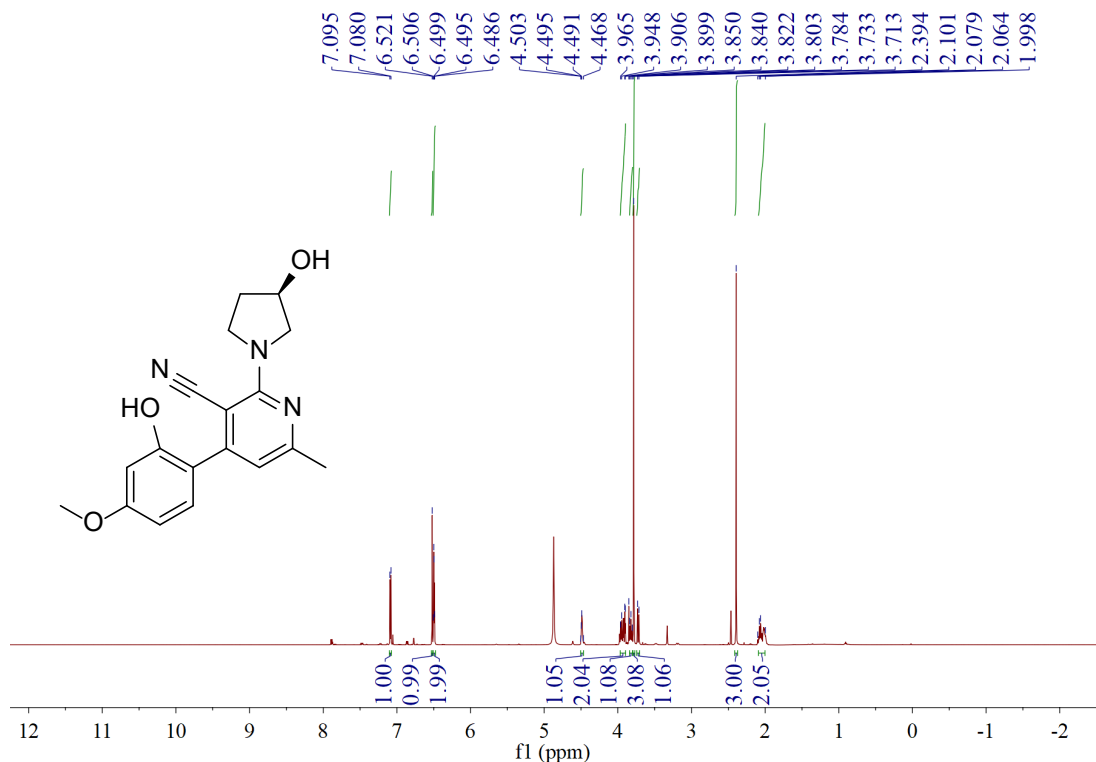


Fig. S59. ^1H NMR spectrum of compound 4i.

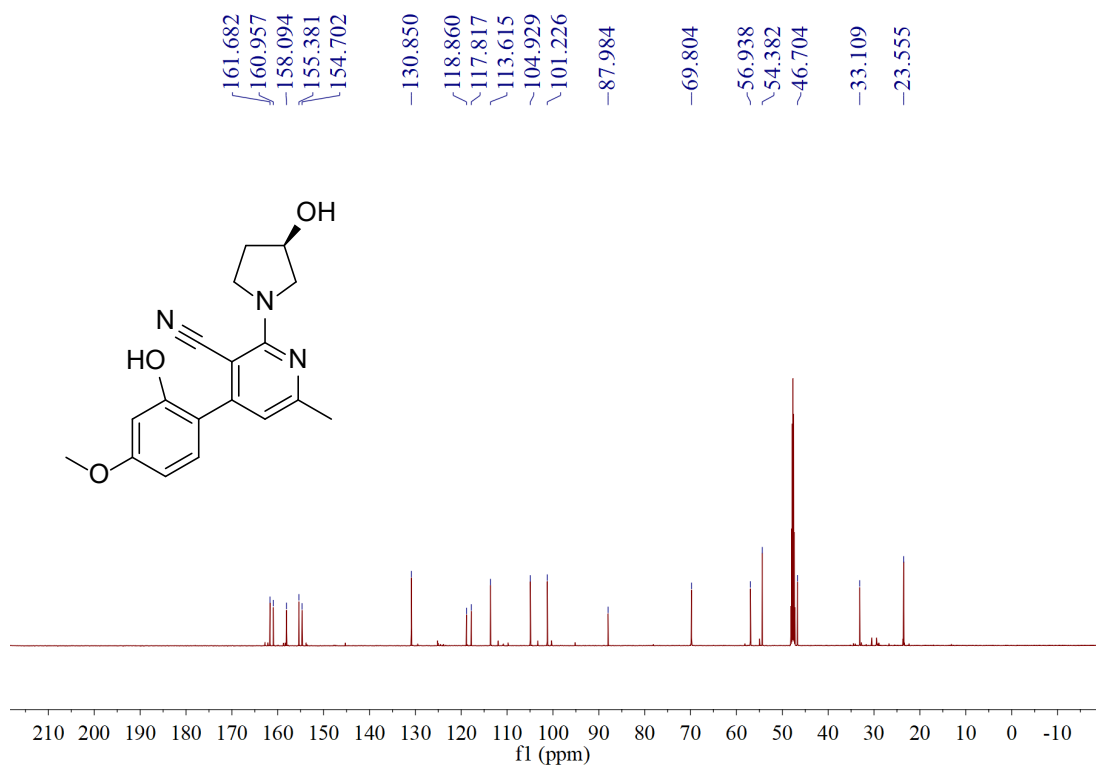


Fig. S60. ^{13}C NMR spectrum of compound 4i.

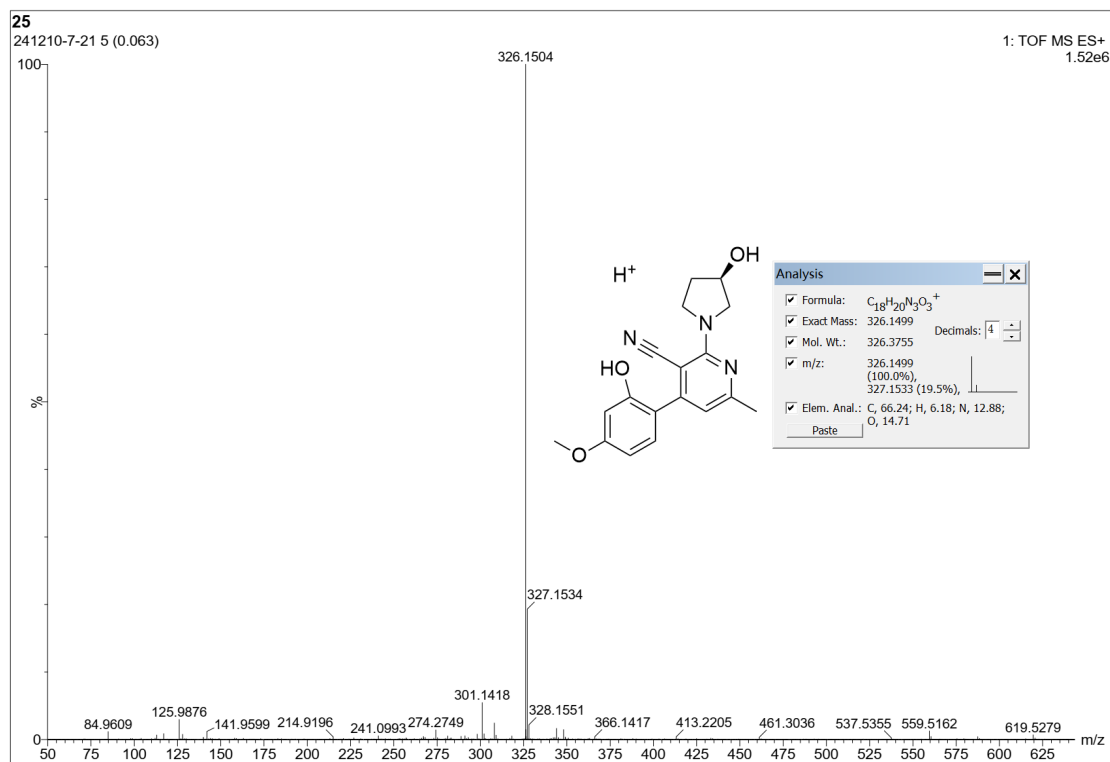


Fig. S61. HRMS spectrum of compound 4i.

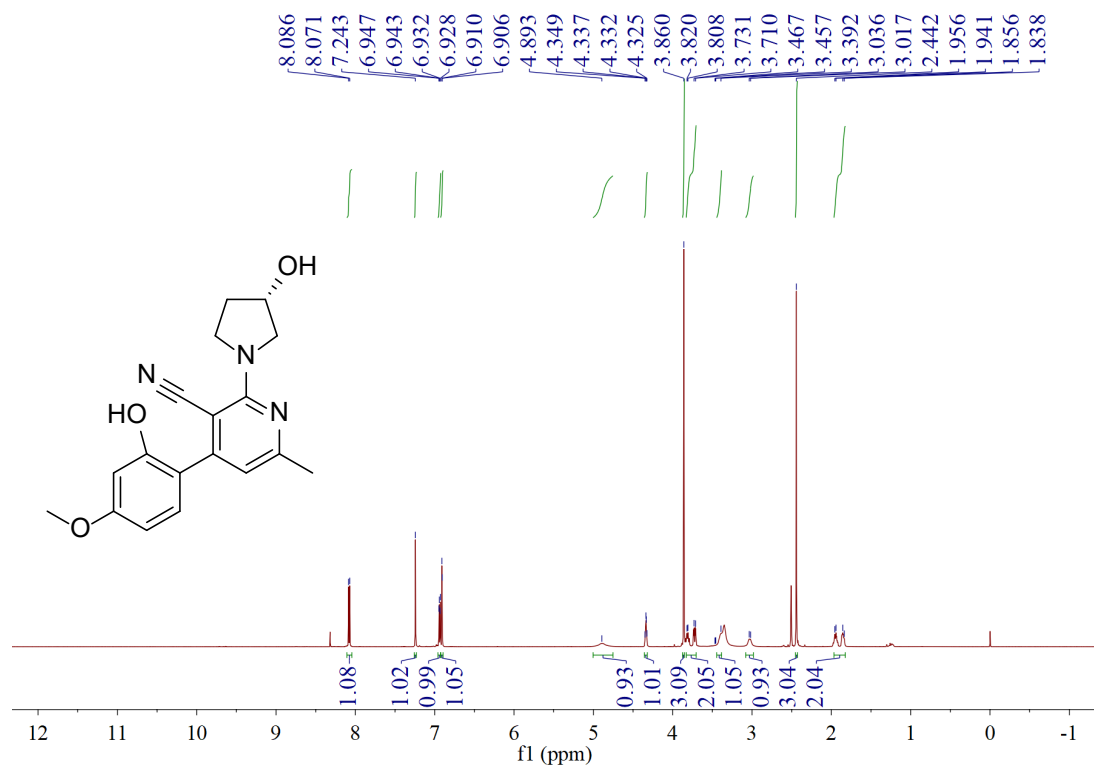


Fig. S62. ^1H NMR spectrum of compound 4j.

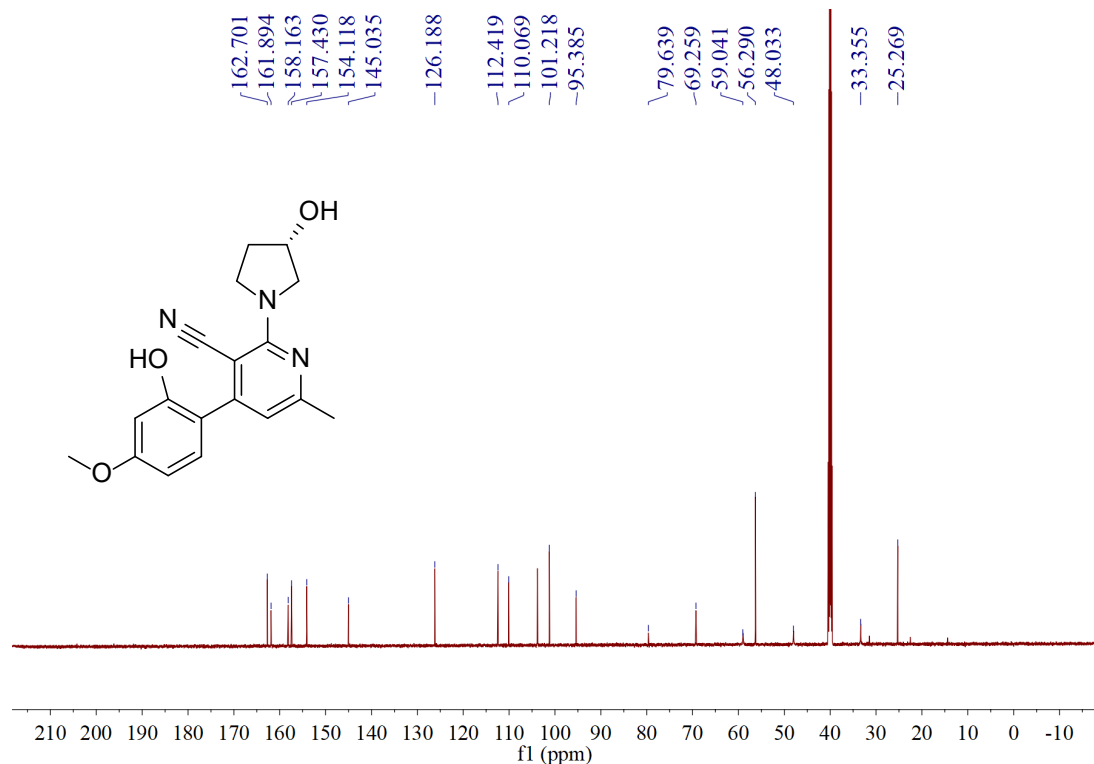


Fig. S63. ^{13}C NMR spectrum of compound 4j.

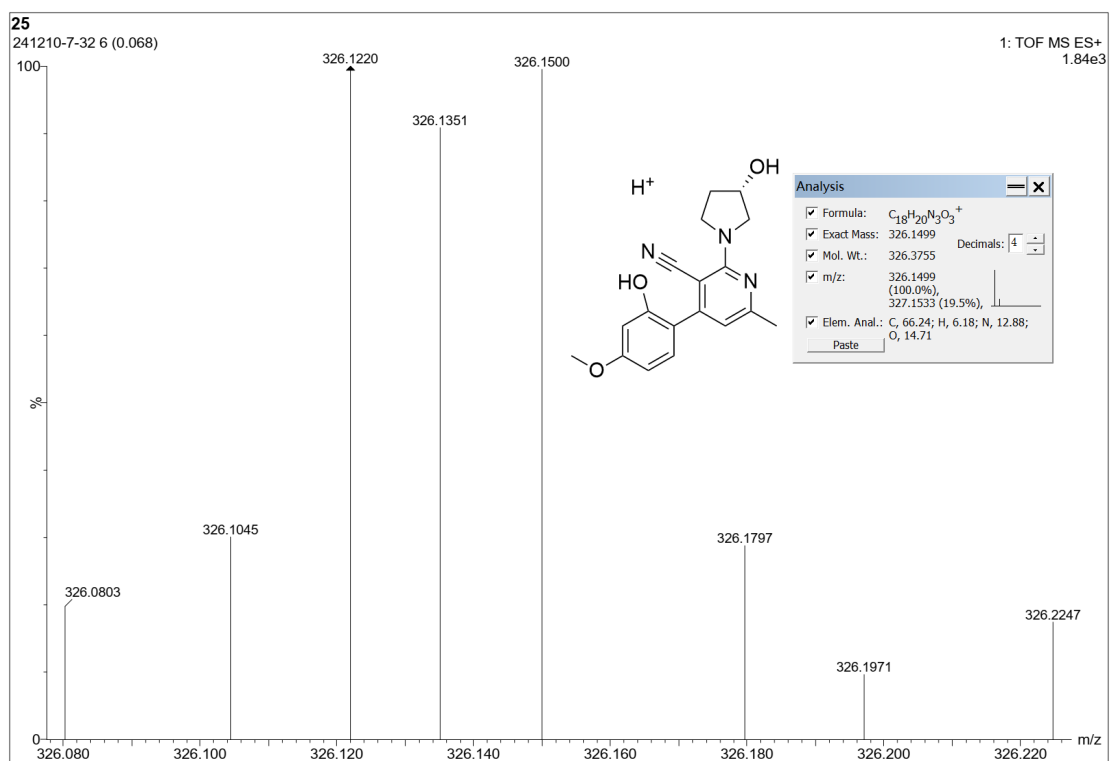


Fig. S64. HRMS spectrum of compound 4j.

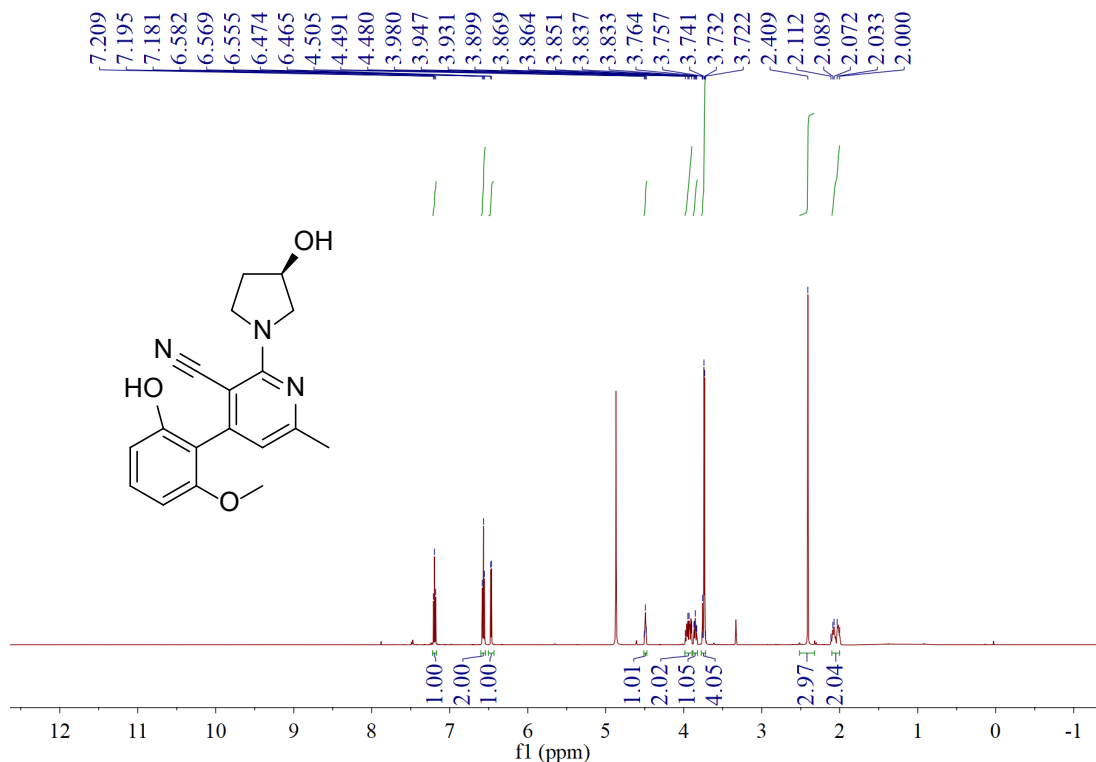


Fig. S65. ^1H NMR spectrum of compound 4k.

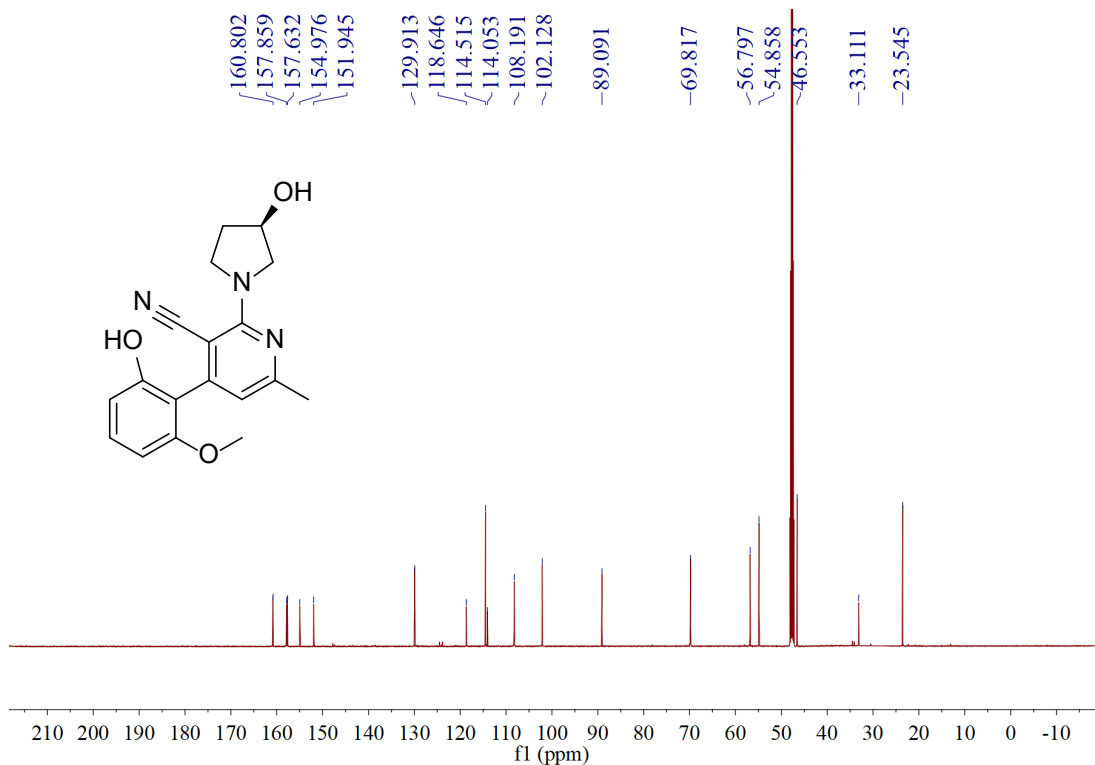


Fig. S66. ^{13}C NMR spectrum of compound **4k**.

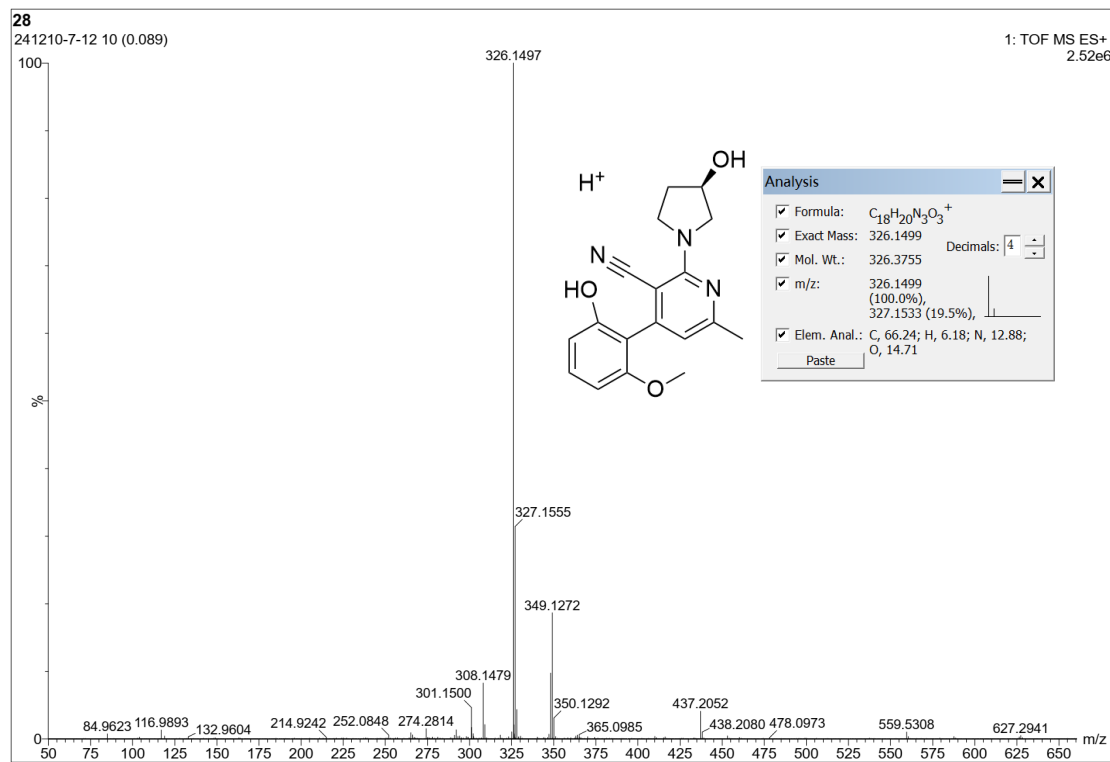


Fig. S67. HRMS spectrum of compound **4k**.

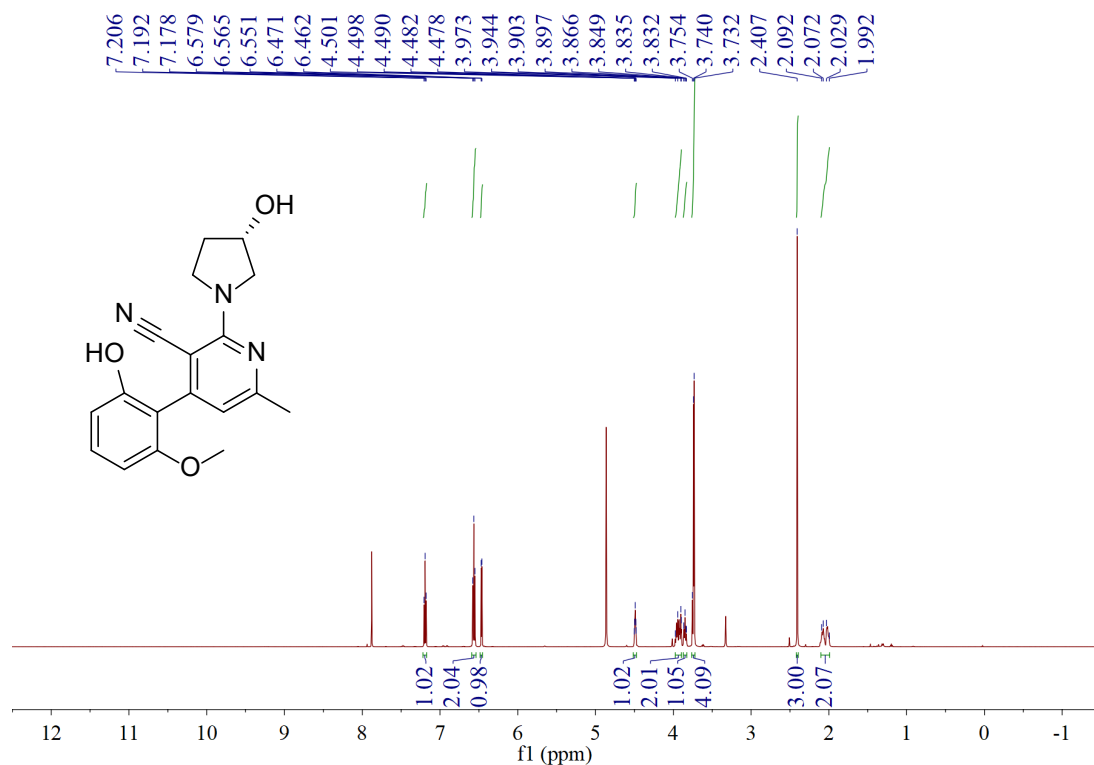


Fig. S68. ^1H NMR spectrum of compound 4l.

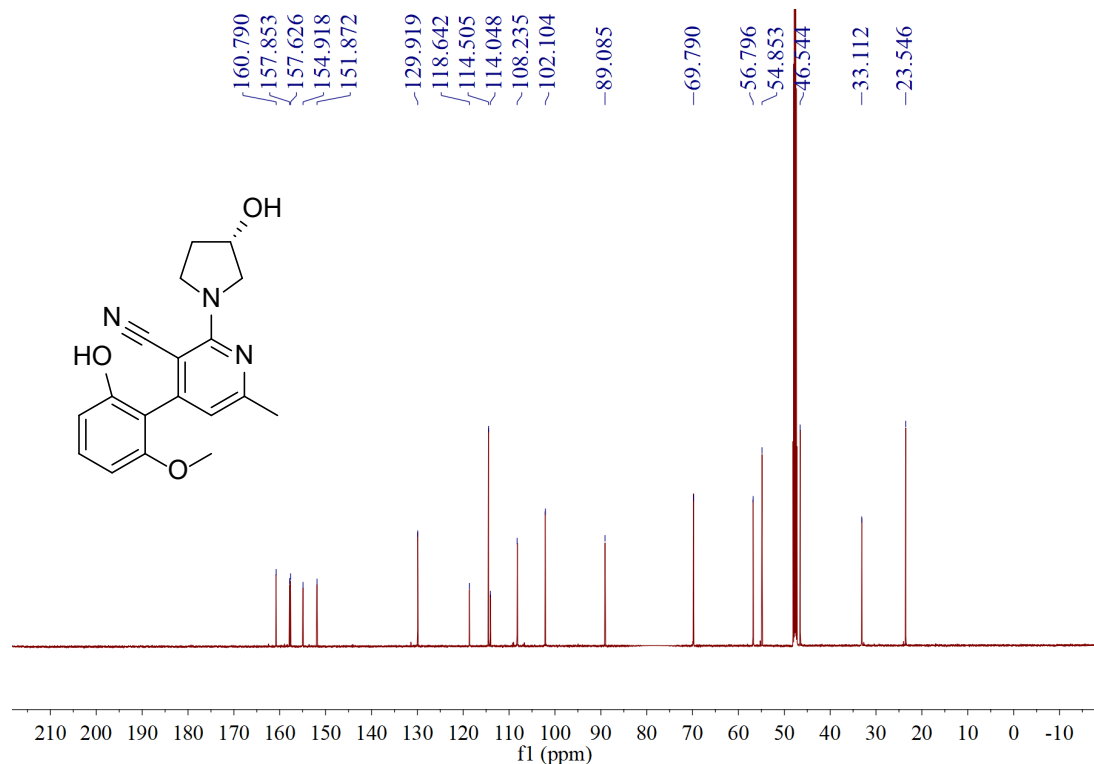


Fig. S69. ^{13}C NMR spectrum of compound 4l.

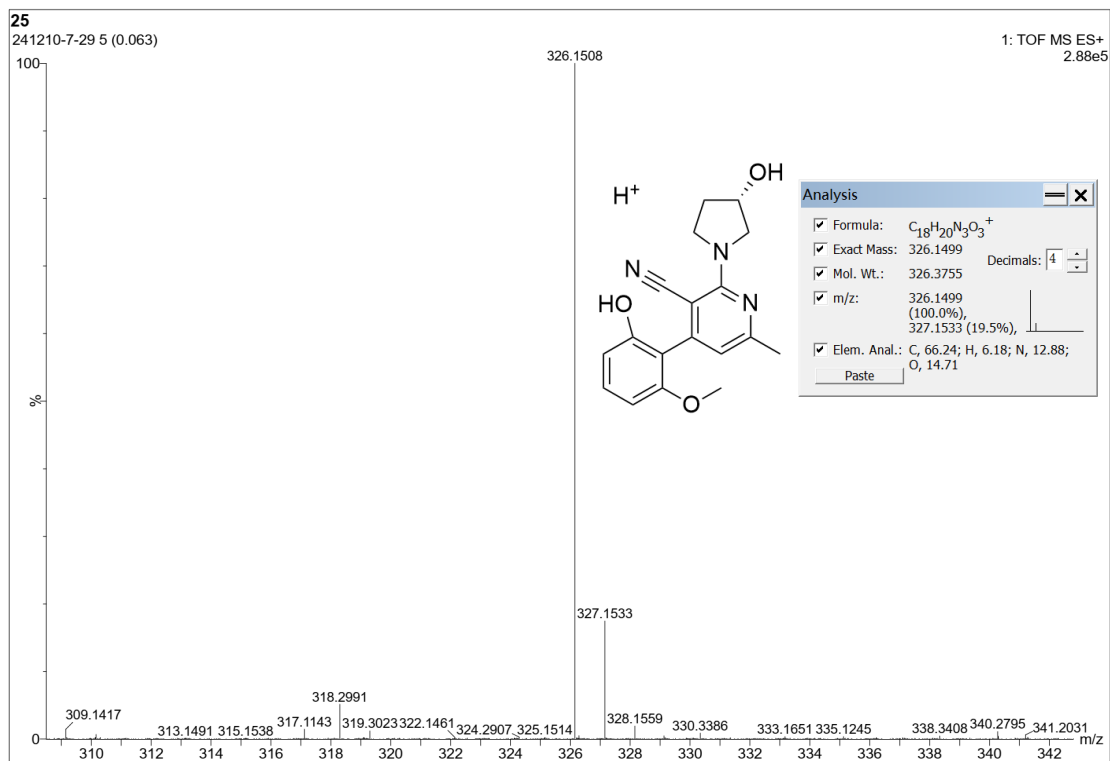


Fig. S70. HRMS spectrum of compound 4l.

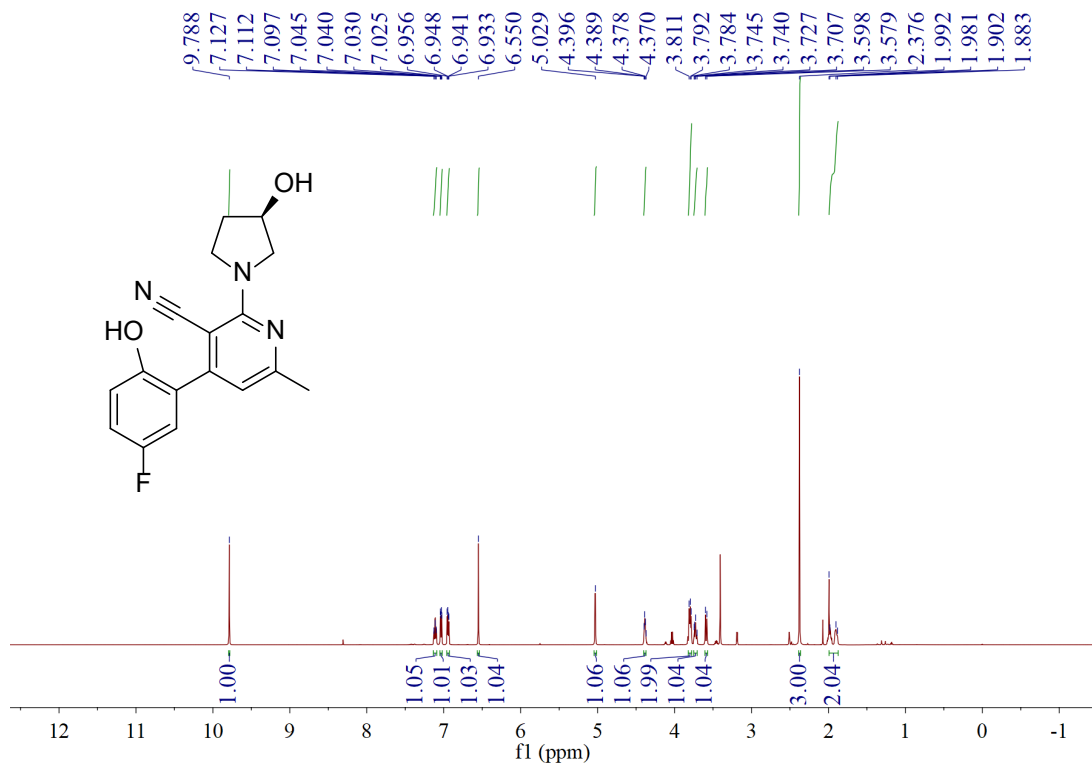


Fig. S71. 1H NMR spectrum of compound 4m.

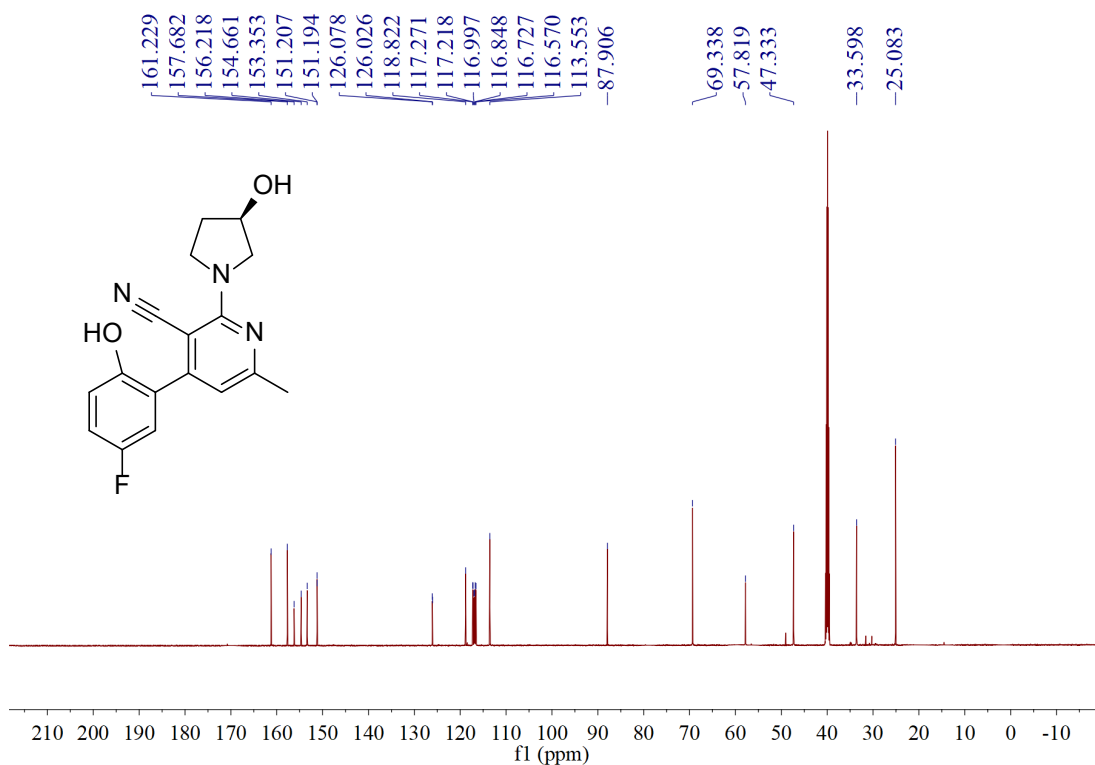


Fig. S72. ^{13}C NMR spectrum of compound **4m**.

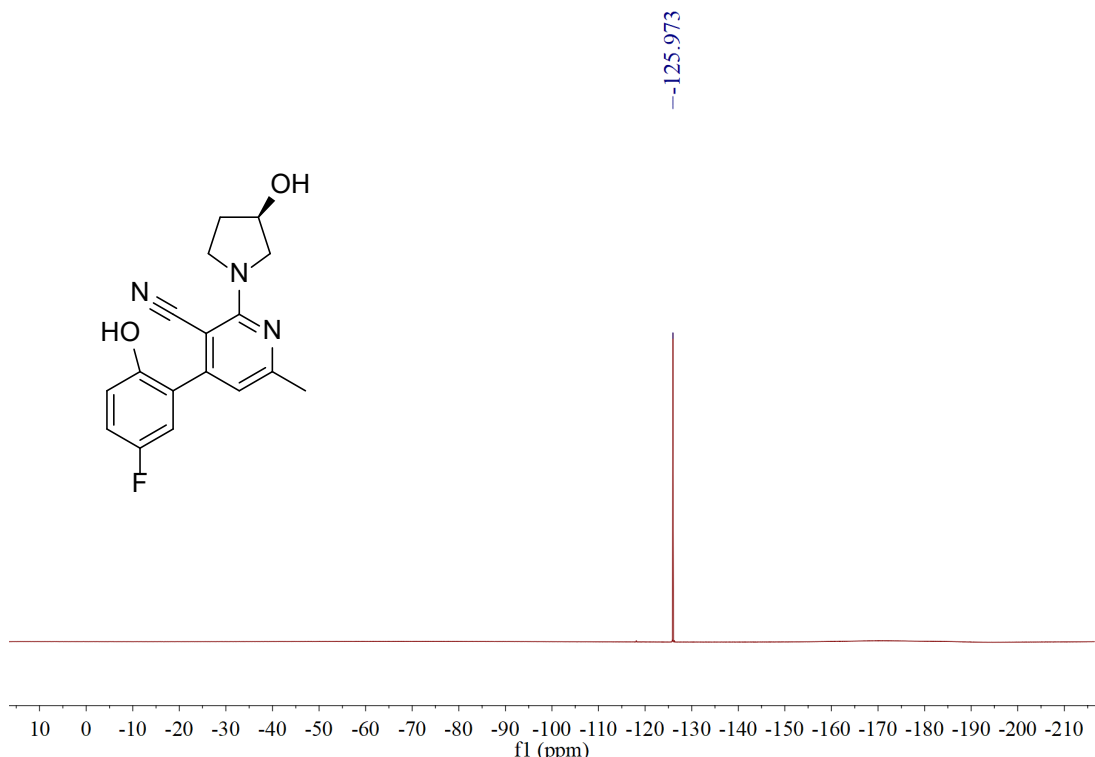


Fig. S73. ^{19}F NMR spectrum of compound **4m**.

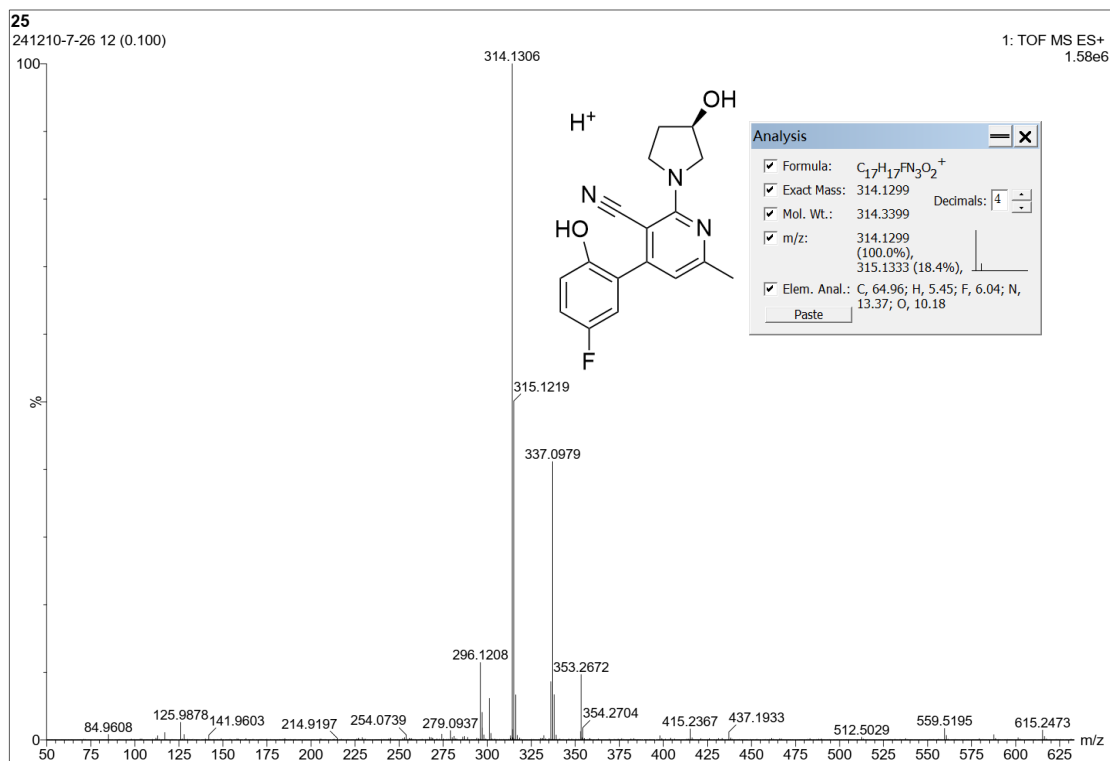


Fig. S74. HRMS spectrum of compound 4m.

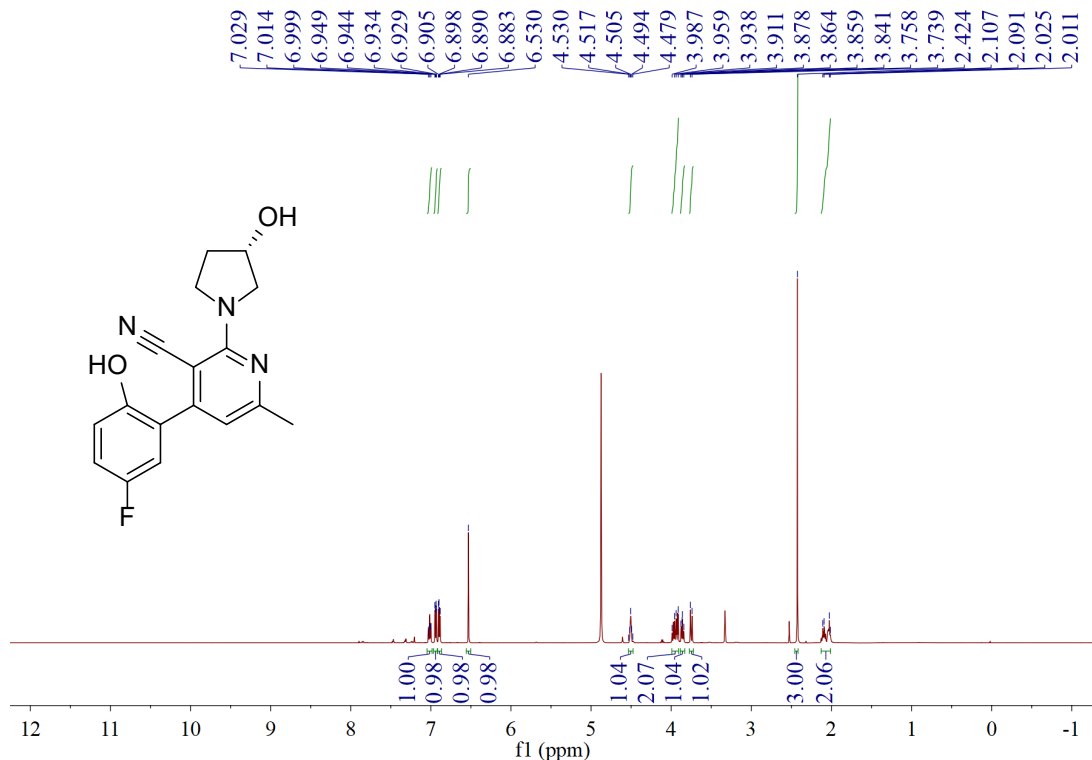


Fig. S75. ^1H NMR spectrum of compound 4n.

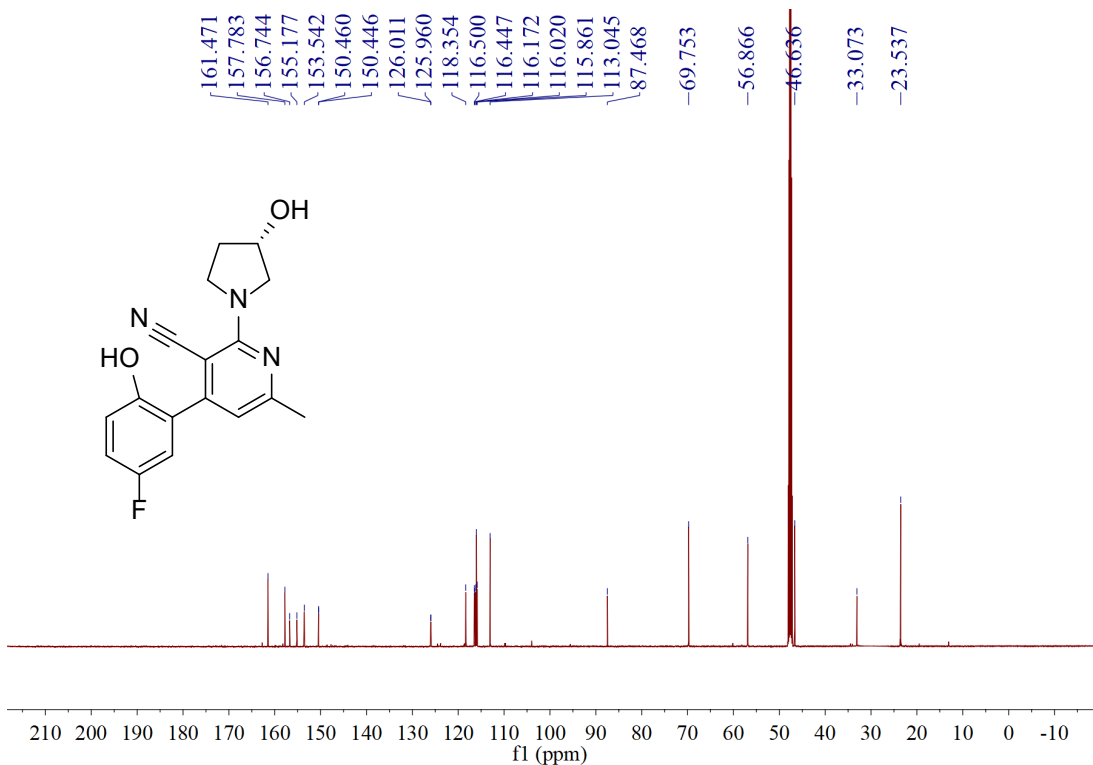


Fig. S76. ^{13}C NMR spectrum of compound 4n.

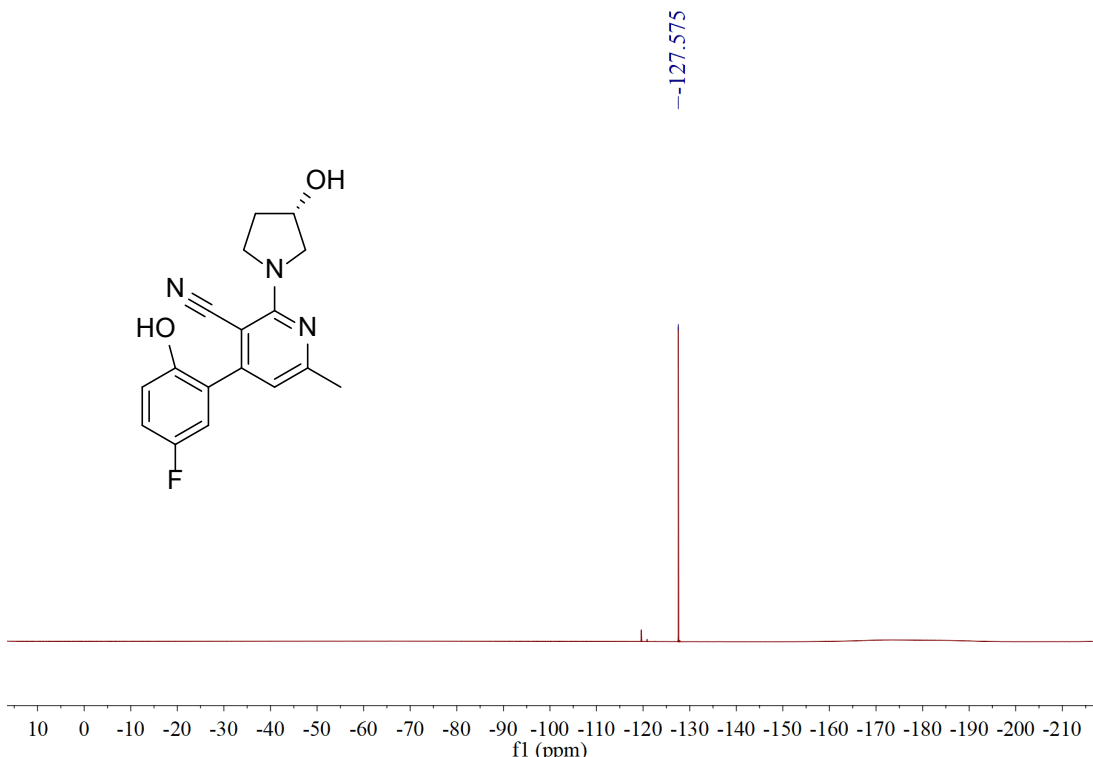


Fig. S77. ^{19}F NMR spectrum of compound 4n.

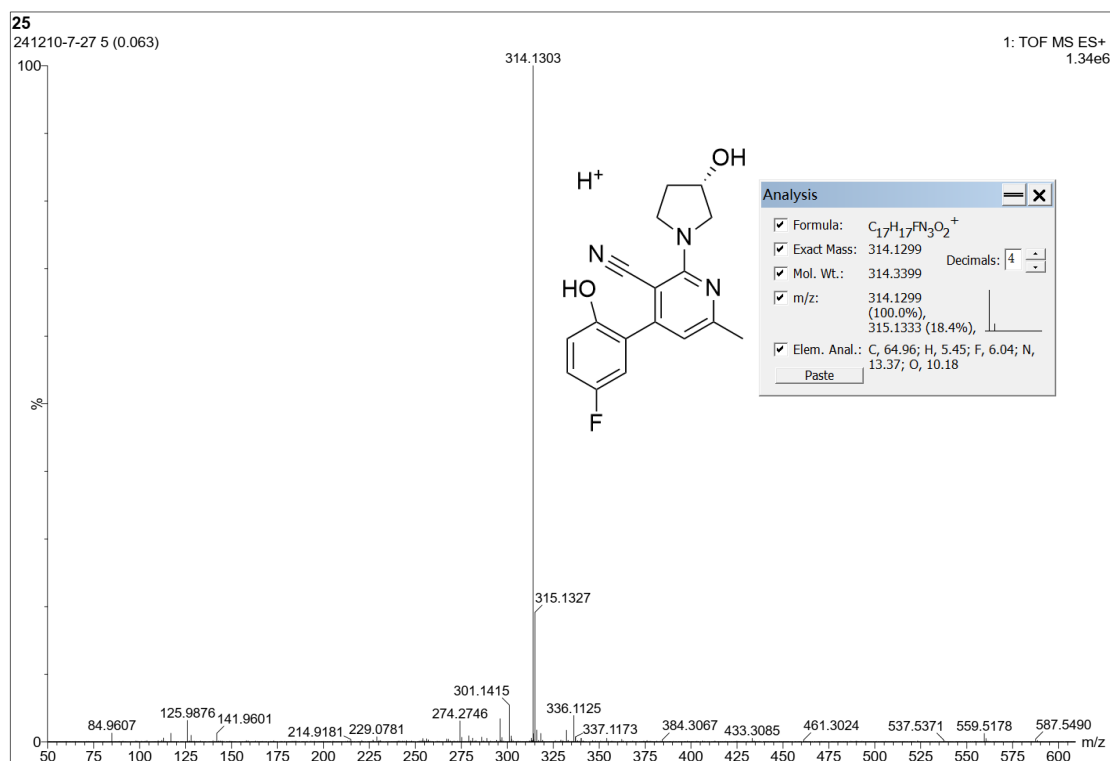


Fig. S78. HRMS spectrum of compound 4n.

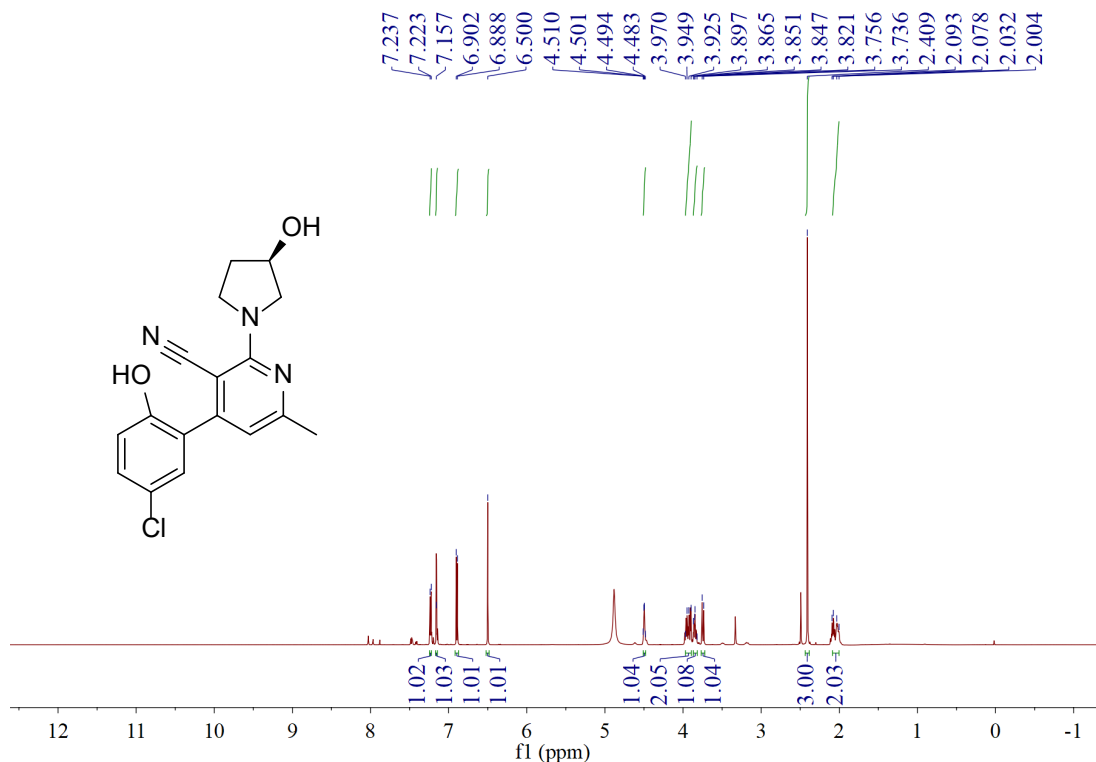


Fig. S79. ^1H NMR spectrum of compound 4o.

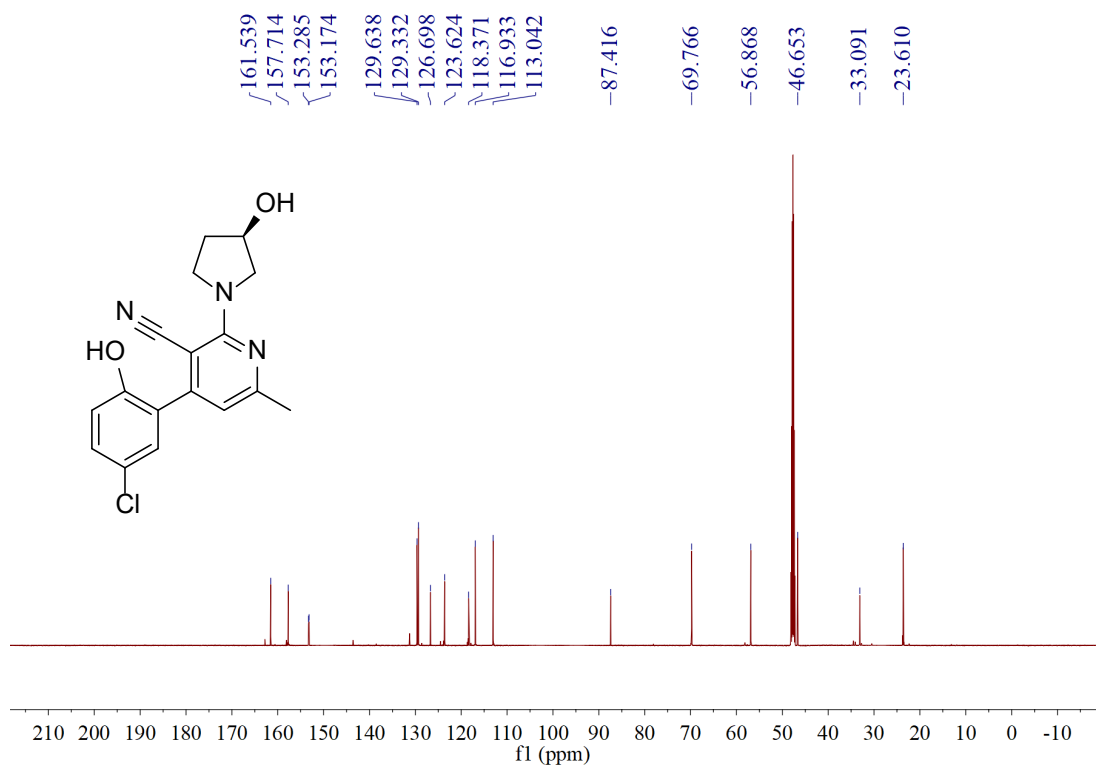


Fig. S80. ^{13}C NMR spectrum of compound **4o**.

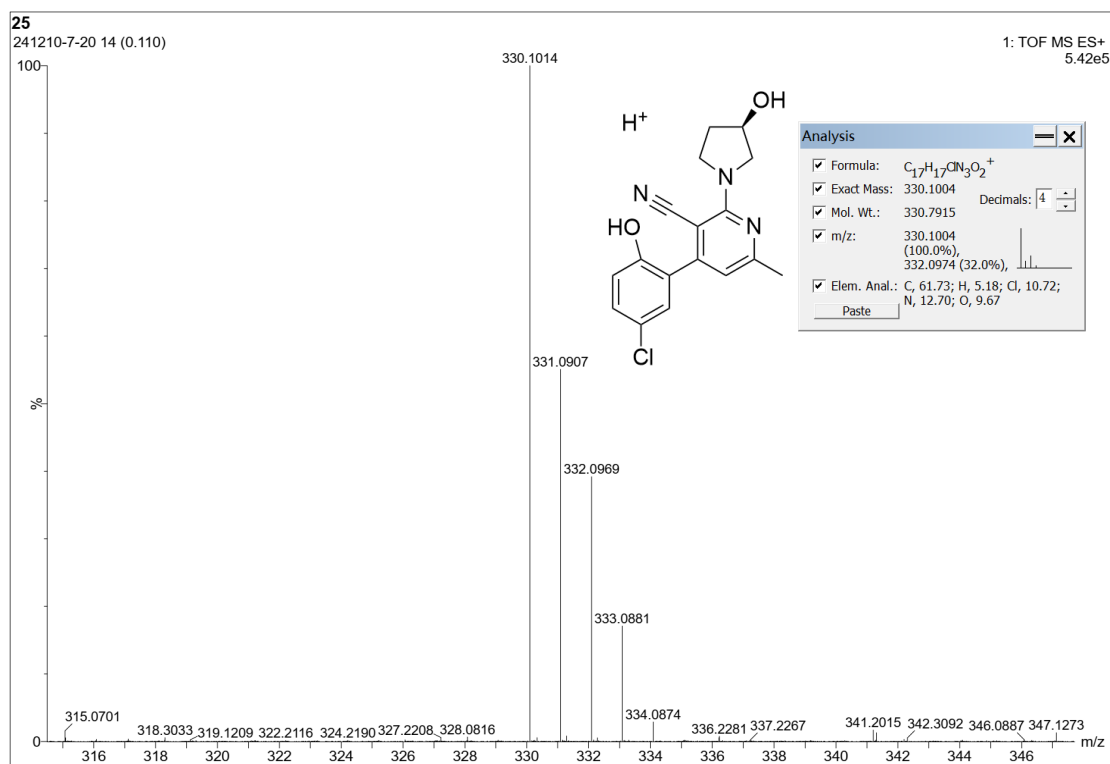


Fig. S81. HRMS spectrum of compound **4o**.

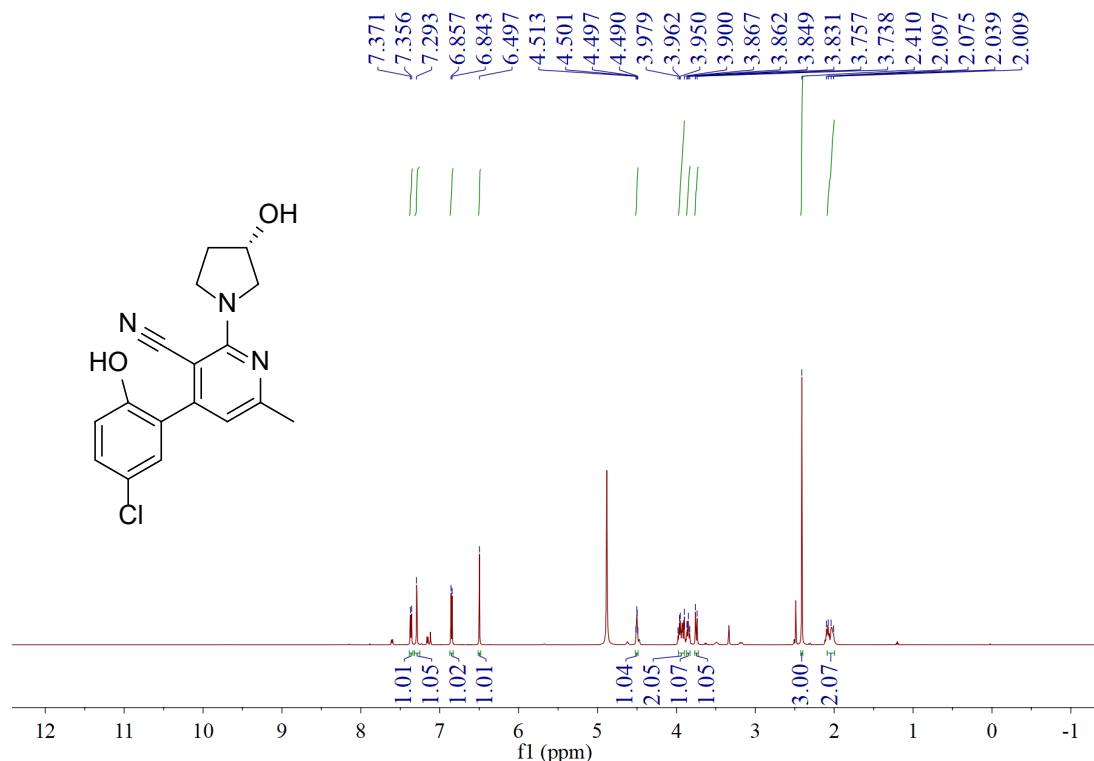


Fig. S82. ^1H NMR spectrum of compound **4p**.

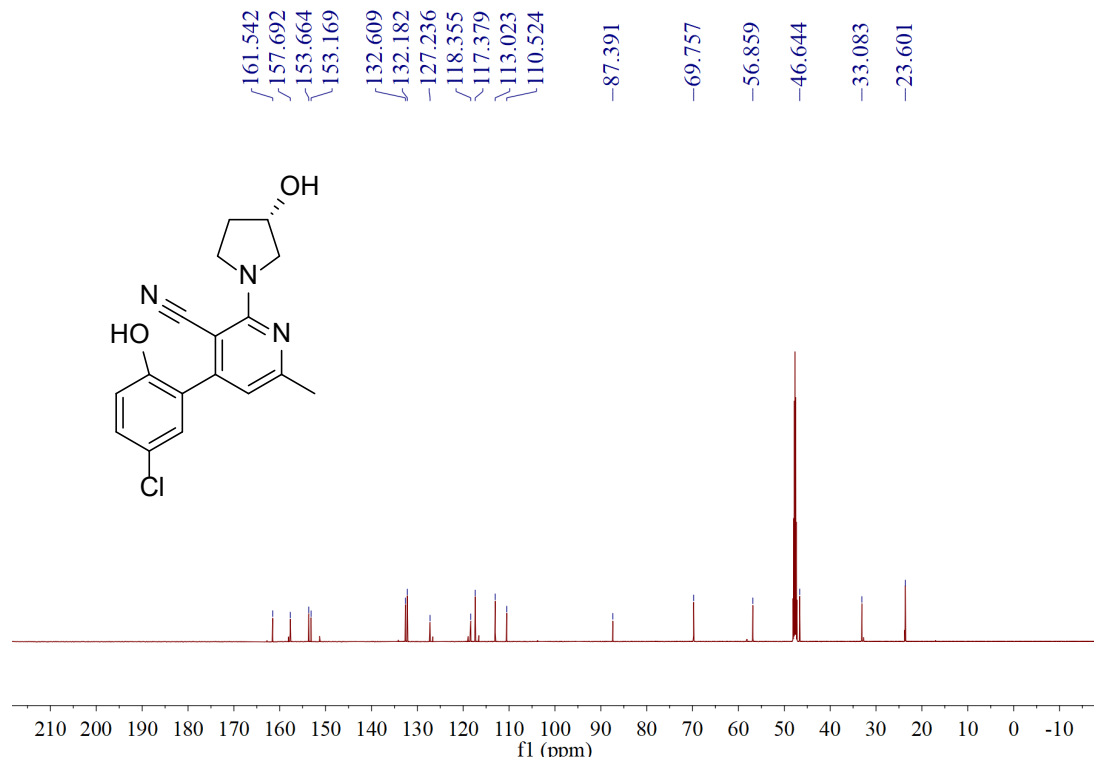


Fig. S83. ^{13}C NMR spectrum of compound **4p**.

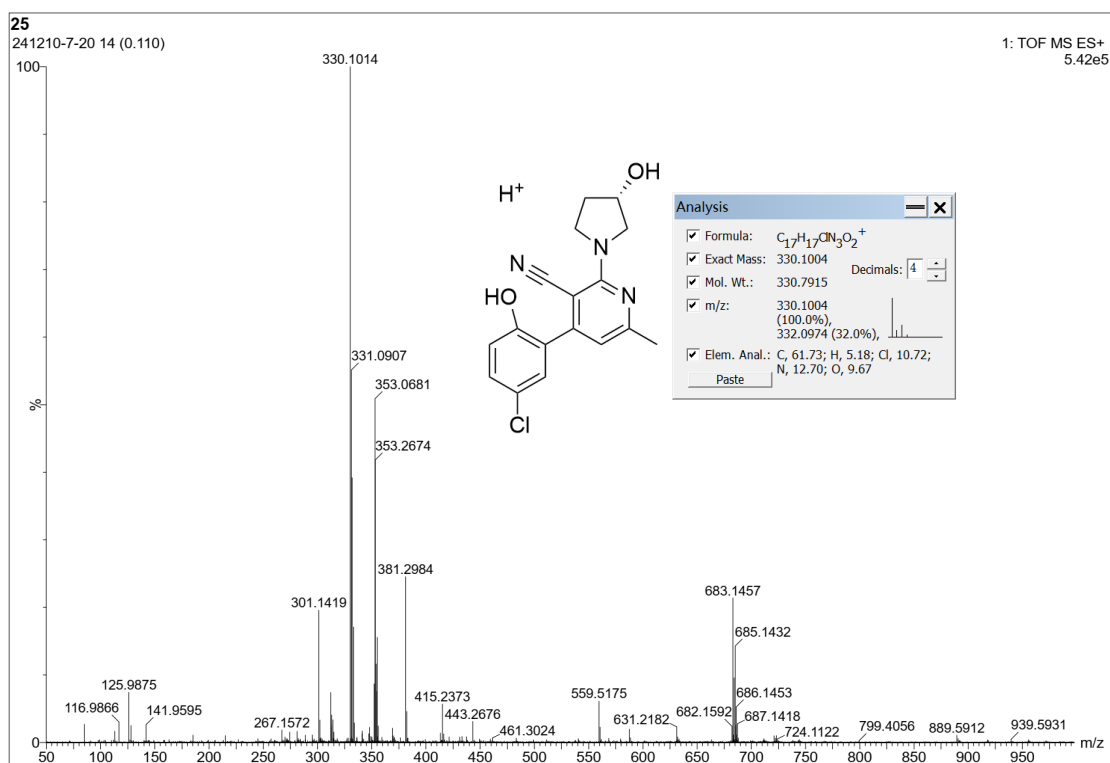


Fig. S84. HRMS spectrum of compound 4p.

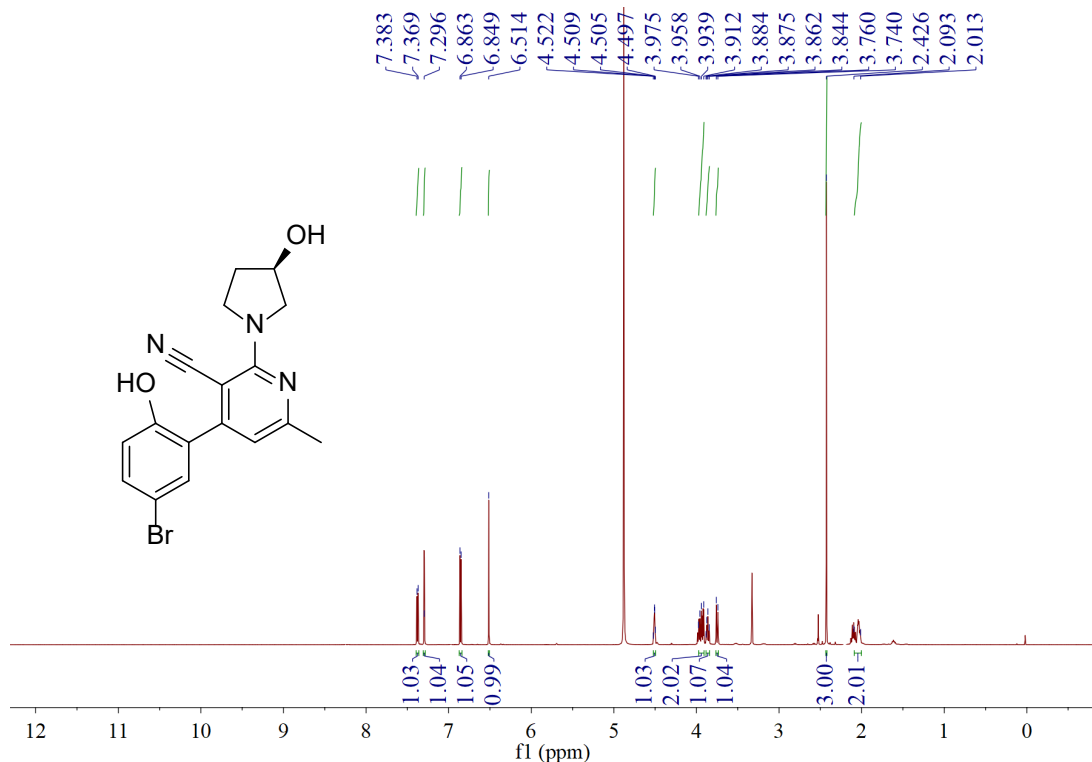


Fig. S85. ^1H NMR spectrum of compound 4q.

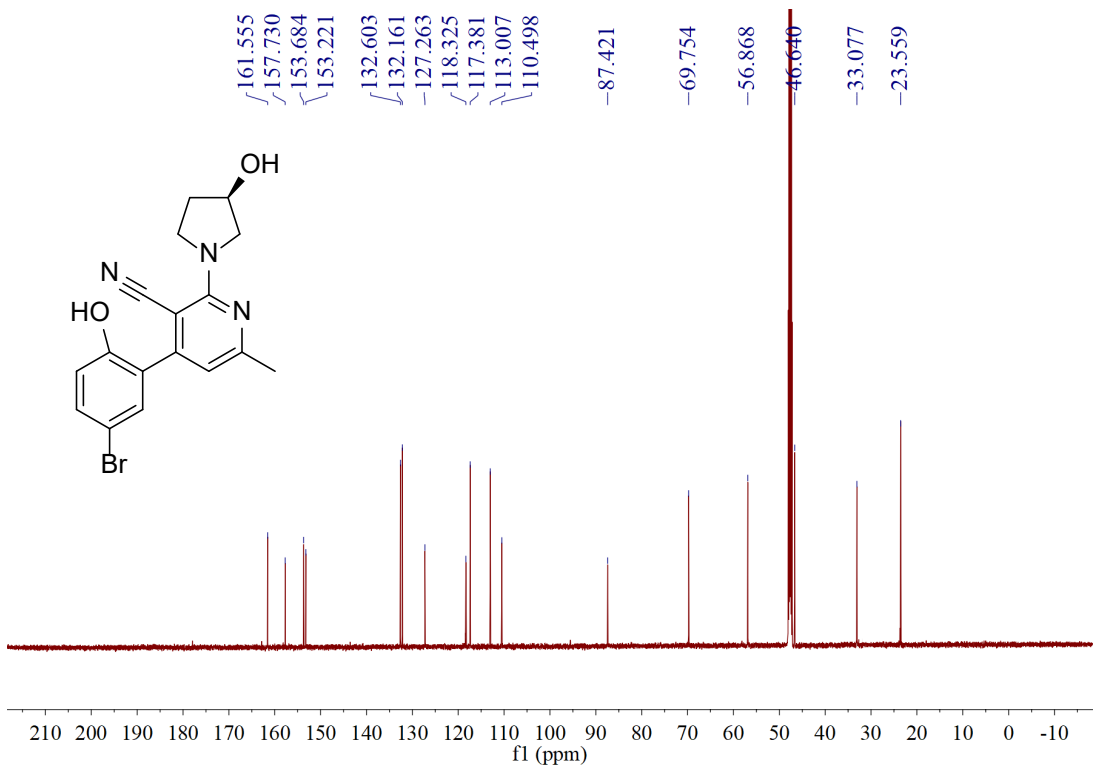


Fig. S86. ^{13}C NMR spectrum of compound 4q.

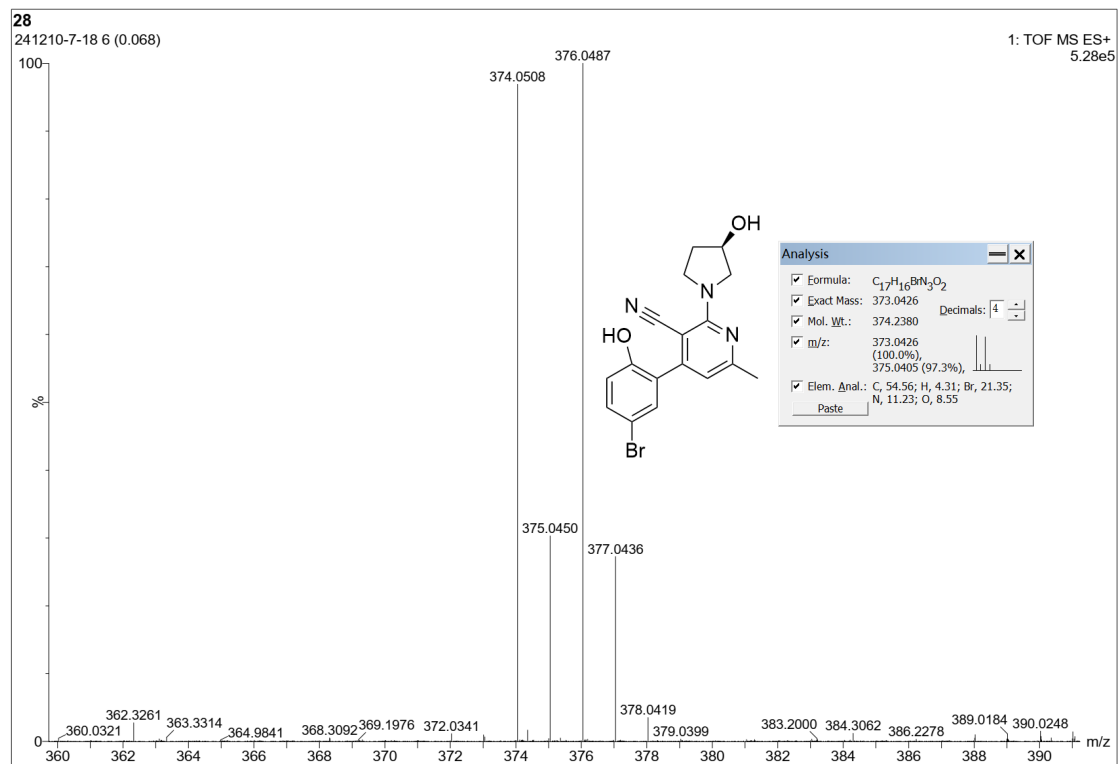


Fig. S87. HRMS spectrum of compound 4q.

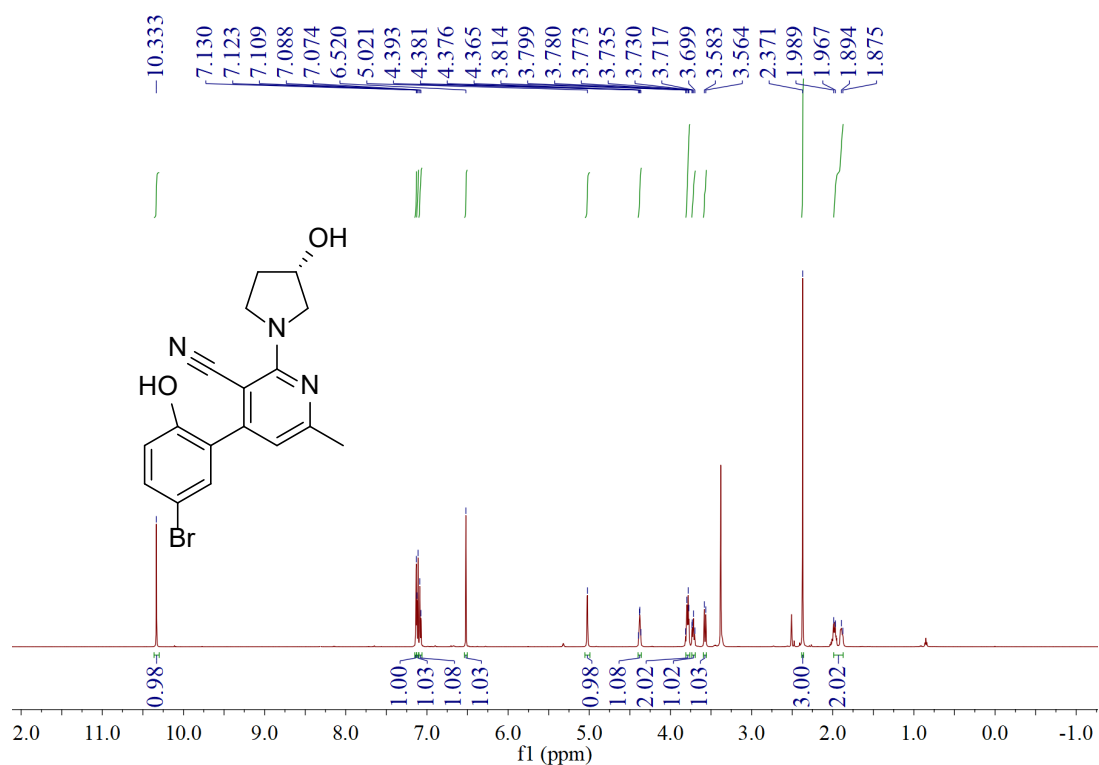


Fig. S88. ^1H NMR spectrum of compound **4r**.

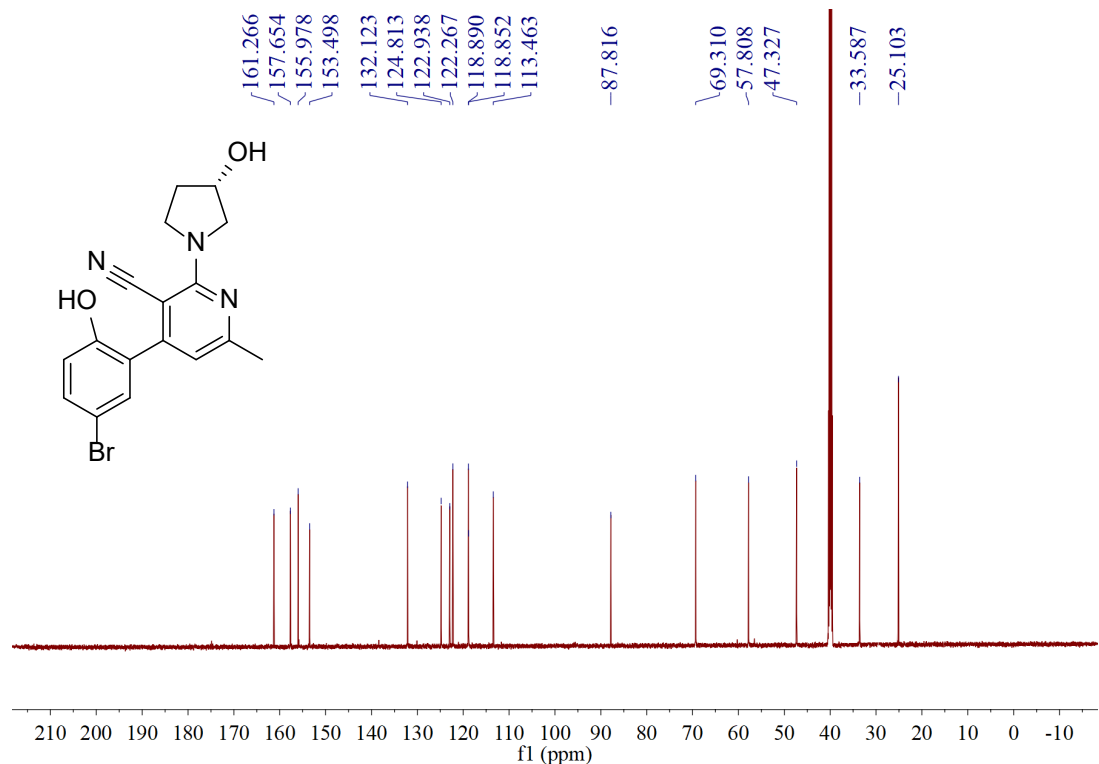


Fig. S89. ^{13}C NMR spectrum of compound **4r**.

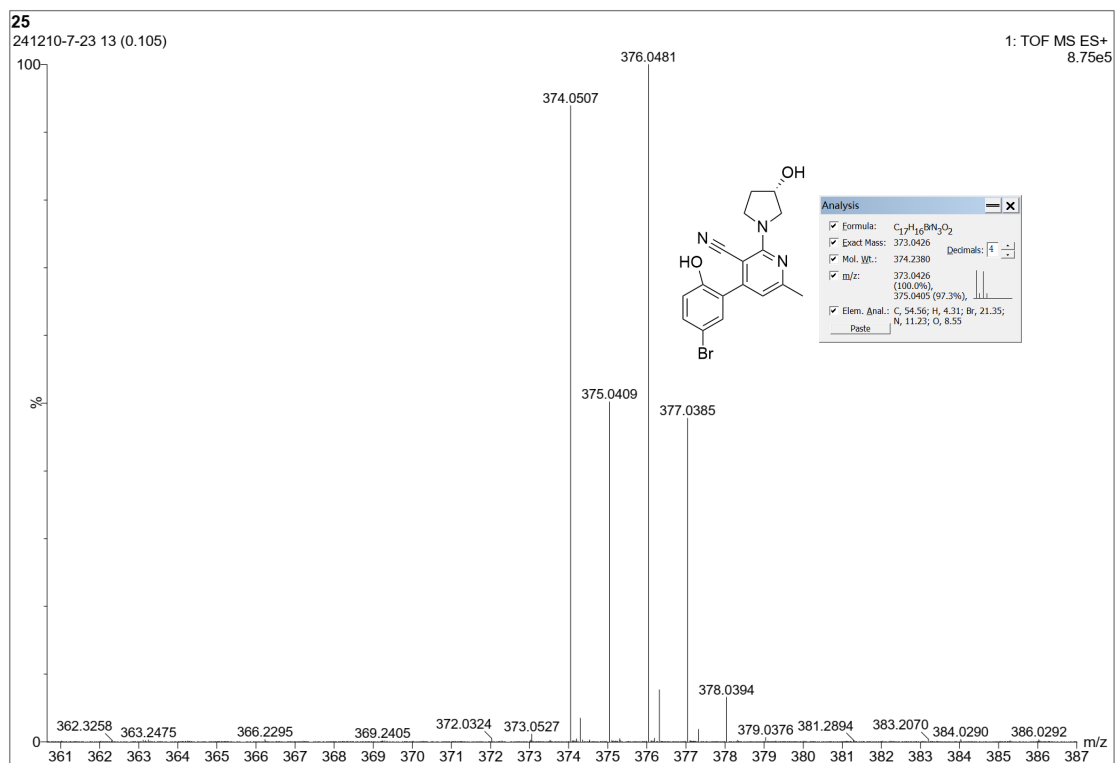


Fig. S90. HRMS spectrum of compound 4r.

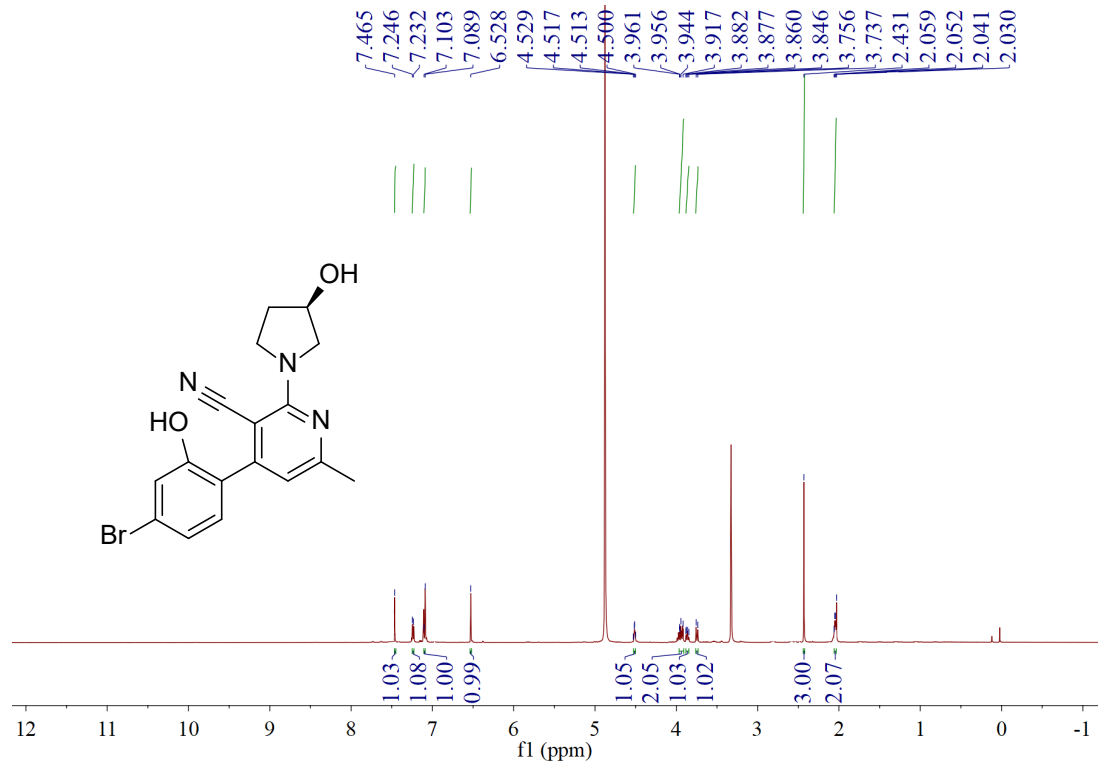


Fig. S91. ¹H NMR spectrum of compound 4s.

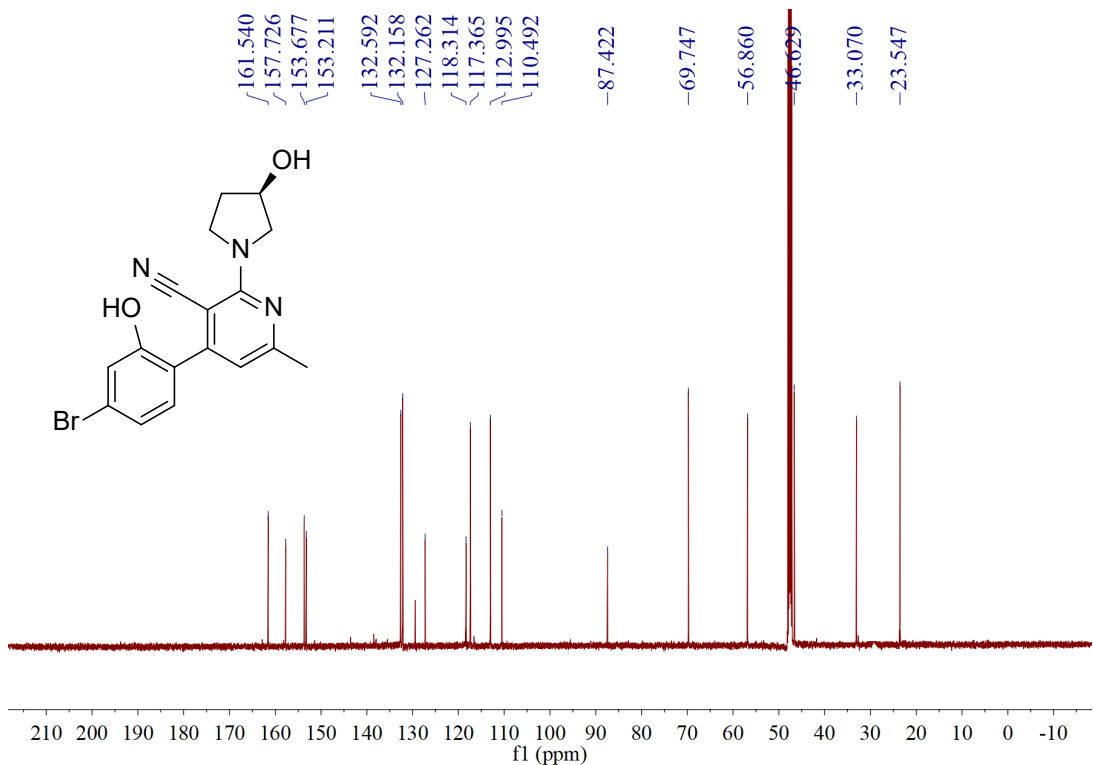


Fig. S92. ^{13}C NMR spectrum of compound **4s**.

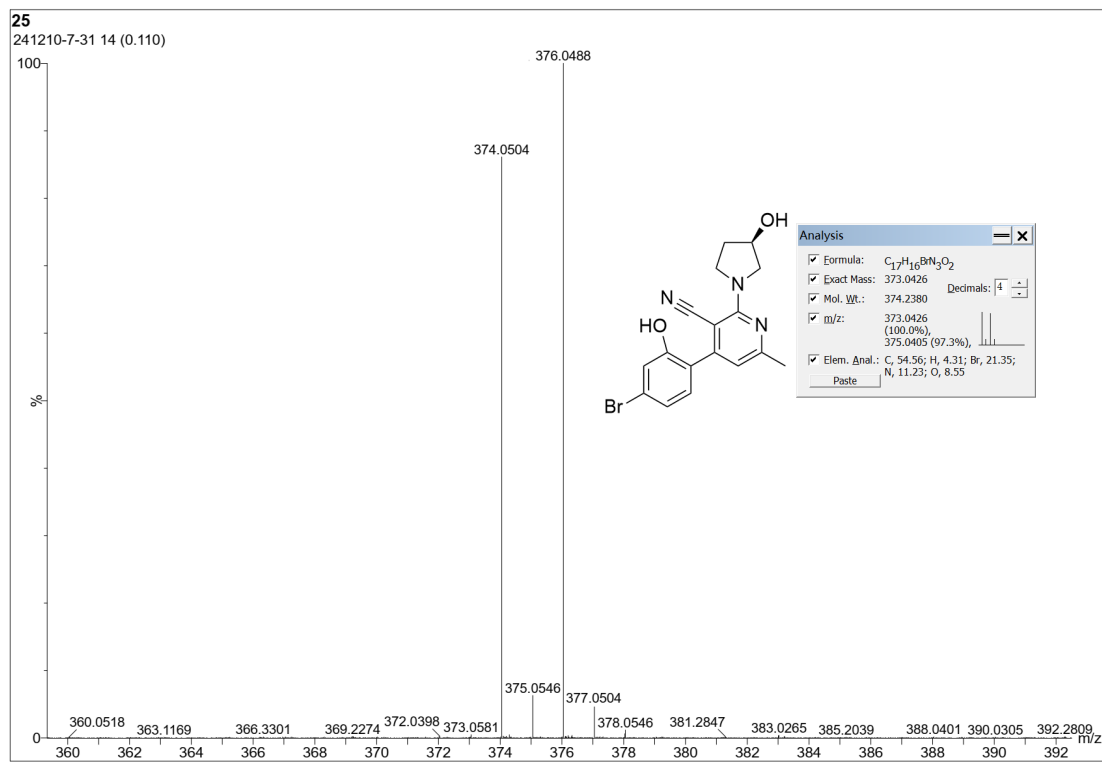


Fig. S93. HRMS spectrum of compound **4s**.

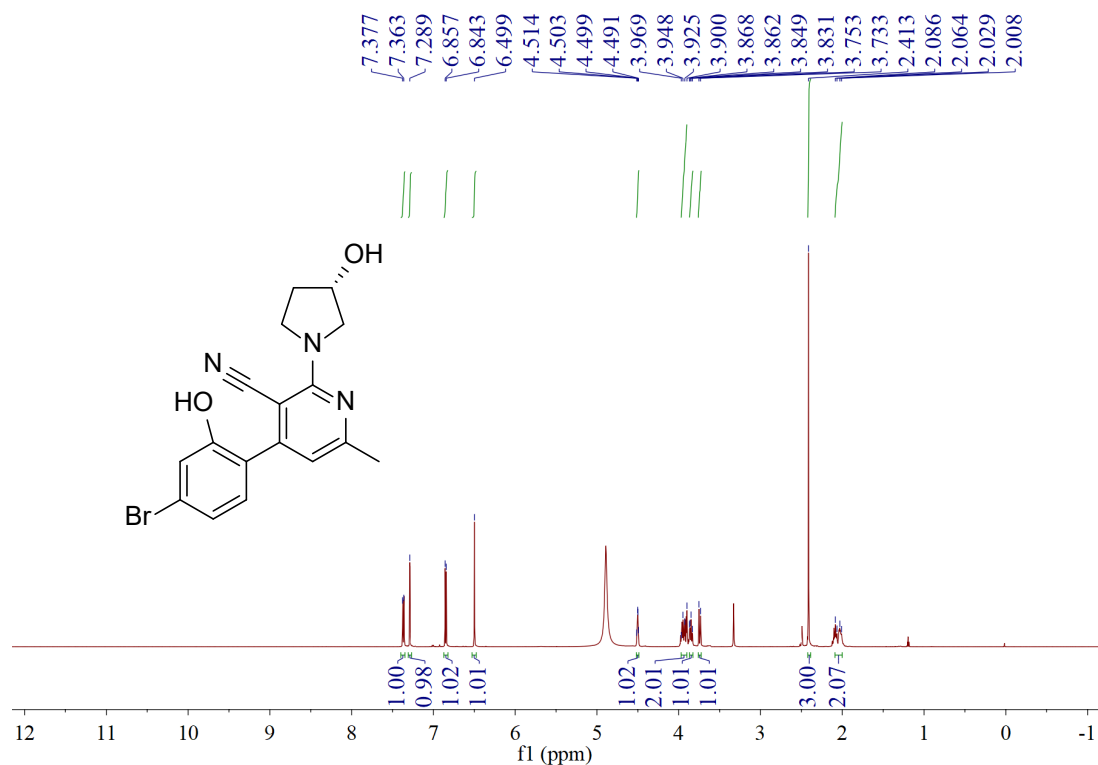


Fig. S94. ^1H NMR spectrum of compound 4t.

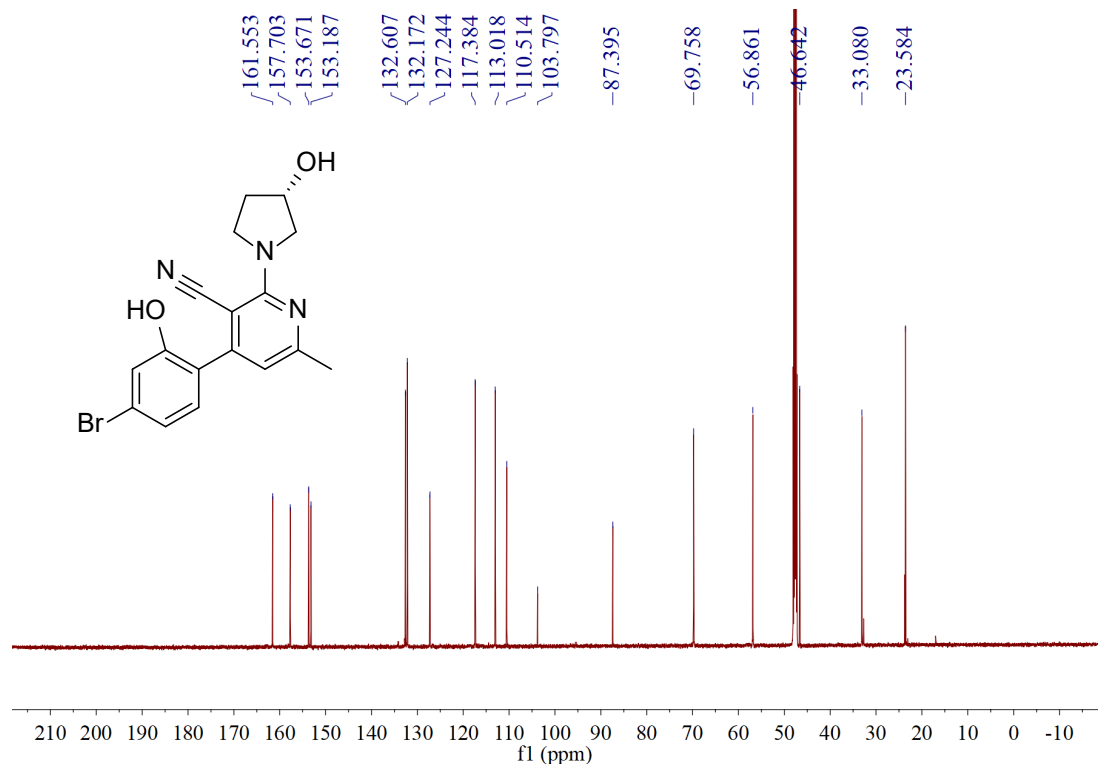


Fig. S95. ^{13}C NMR spectrum of compound 4t.

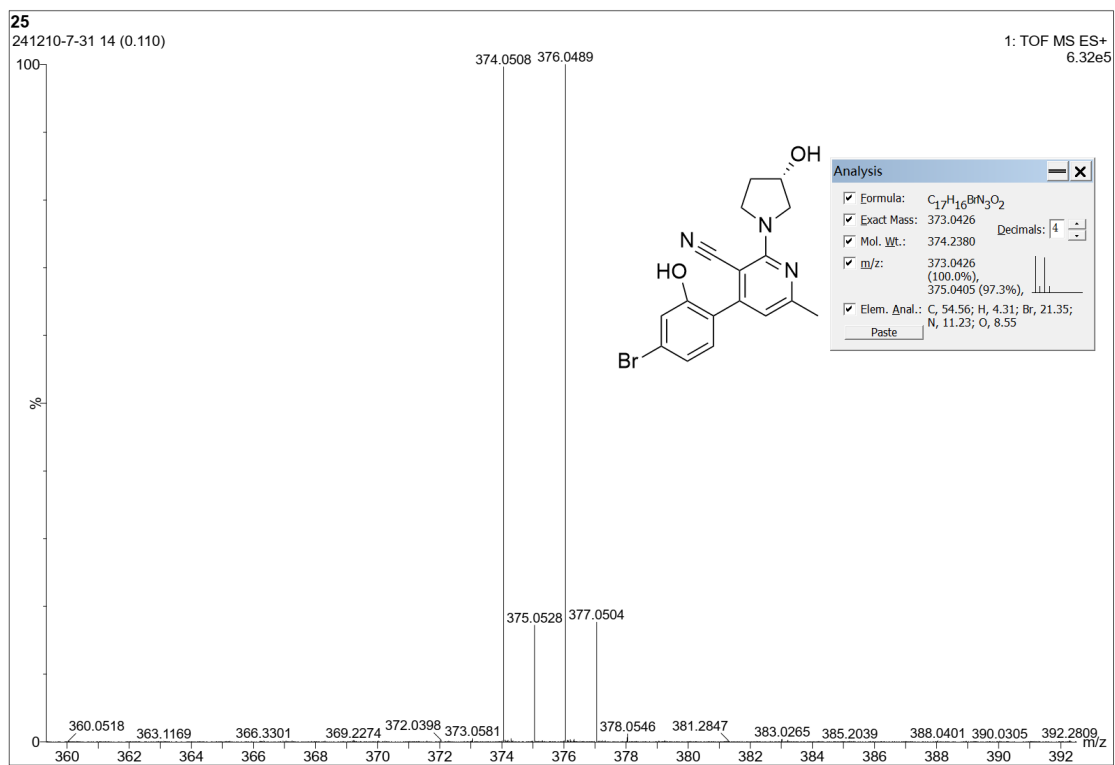


Fig. S96. HRMS spectrum of compound 4t.

2.4. Data of Single-crystal X-ray Analysis

Table S1. Crystal data and structure refinement for **3c**.

Compound	3c (CCDC: 24201345)
Empirical formula	C ₁₈ H ₁₉ N ₃ O
Formula weight	293.36
Temperature (K)	200
Wavelength (Å)	0.71073
Crystal system	monoclinic
Space group	P2 ₁ /c
Unit cell dimensions (Å, °)	$a = 12.8541(7)$, $b = 8.4683(5)$, $c = 15.3887(9)$ $\alpha = 90$, $\beta = 110.066(6)$, $\gamma = 90$
Volume (Å ³)	1573.41(17)
Z	4
Density (calculated) (g/cm ³)	1.238
Absorption coefficient (mm ⁻¹)	0.079
F(000)	624.0
Theta range for data collection	5.486 to 58.548
Index ranges	-17 ≤ h ≤ 17, -11 ≤ k ≤ 7, -20 ≤ l ≤ 20
Reflections collected	13077
Independent reflections	3816 [R _{int} = 0.0279, R _{sigma} = 0.0334]
Completeness to theta = 29.569°	0.996
Absorption correction	Multi-Scan
Max. and min. transmission	1.000 and 0.950
Refinement method	Least Squares minimisation
Data / restraints / parameters	3816/0/202
Goodness-of-fit on F ²	1.017
Final R indices [I>2sigma(I)]	R ₁ = 0.0645, wR ₂ = 0.1588
R indices (all data)	R ₁ = 0.0863, wR ₂ = 0.1742
Largest diff. peak and hole	0.51/-0.35 e.Å ⁻³

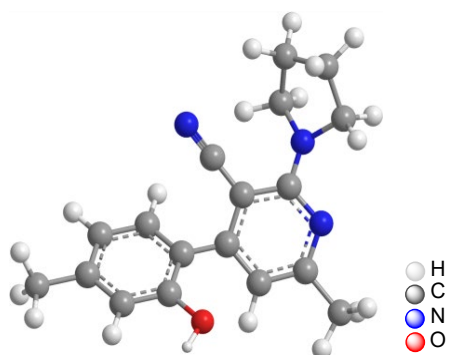
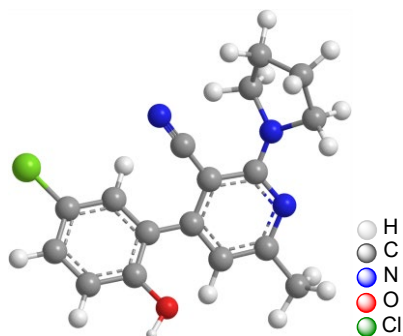


Fig. S97. The molecular structure of **3c**.

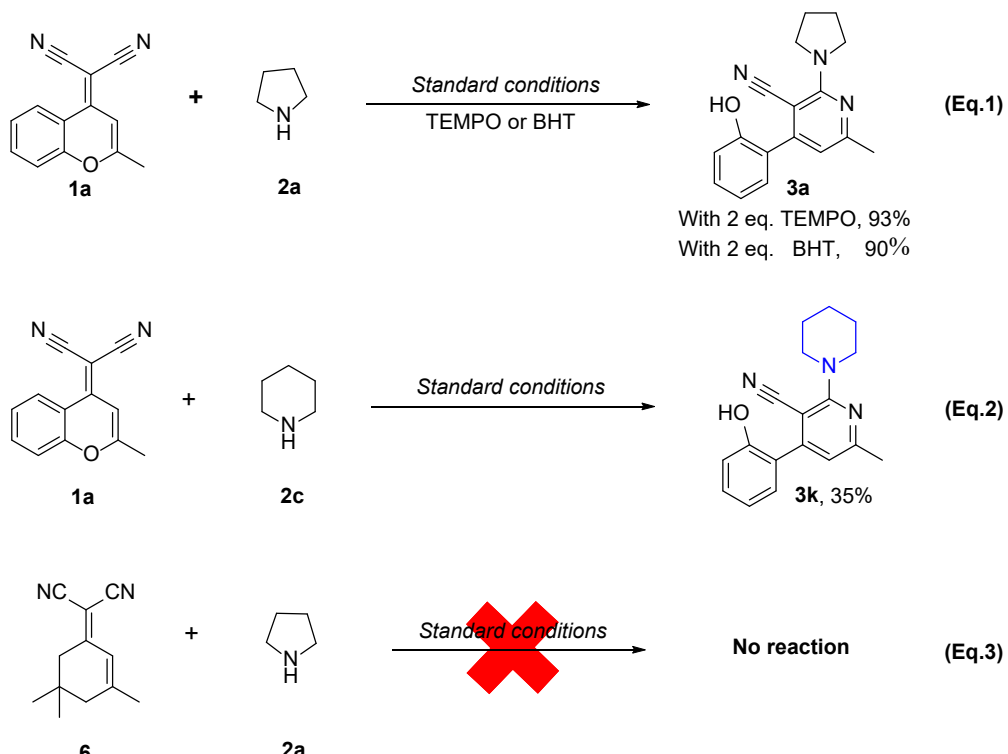
Table S2. Crystal data and structure refinement for **3i**.

Compound	3i (CCDC: 2420135)
Empirical formula	C ₁₇ H ₁₆ ClN ₃ O
Formula weight	313.78
Temperature (K)	297
Wavelength (Å)	0.71073
Crystal system	monoclinic
Space group	P2 ₁
Unit cell dimensions (Å, °)	$a = 7.1028(13)$, $b = 8.8291(16)$, $c = 12.7916(17)$ $\alpha = 90$, $\beta = 95.609(13)$, $\gamma = 90$
Volume (Å ³)	798.3(2)
Z	2
Density (calculated) (g/cm ³)	1.305
Absorption coefficient (mm ⁻¹)	0.244
F(000)	328.0
Theta range for data collection	5.616 to 58.628
Index ranges	-8 ≤ h ≤ 8, -10 ≤ k ≤ 11, -17 ≤ l ≤ 17
Reflections collected	6298
Independent reflections	3542 [R _{int} = 0.0248, R _{sigma} = 0.0486]
Completeness to theta = 25.000°	99.9 %
Absorption correction	Multi-Scan
Max. and min. transmission	1.000 and 0.744
Data / restraints / parameters	3542/97/229
Goodness-of-fit on F ²	1.029
Final R indices [I>2sigma(I)]	R ₁ = 0.0526, wR ₂ = 0.1048
R indices (all data)	R ₁ = 0.0755, wR ₂ = 0.1159
Largest diff. peak and hole	0.18/-0.18 e.Å ⁻³

**Fig. S98.** The molecular structure of **3i**.

2.5. Investigations of the Reaction Mechanism

To gain further insights into the reaction mechanism involving in the ring-opening of **1a**, several control experiments were conducted (**Scheme S1**).



Scheme S1. Control experiments.

To the reaction system, 2.0 eq. of the radical scavengers TEMPO (2,2,6,6-tetramethyl-piperidine-1-oxyl) or BHT (2,6-di-*tert*-butyl-4-methylphenol)^[5] were added separately, as depicted in **Eq. 1** of **Scheme S1**. The results indicated that the yields remained essentially unchanged, at 93% and 90%, respectively. These findings suggest that the reaction does not proceed *via* a radical process.

At the same time, in order to further validate the experimental findings, the reaction of benzopyrannitrile **1a** with piperidine (**2c**) instead of **2a** under standard conditions was investigated. It can be seen that **2c** also undergoes a similar ring-opening reaction with benzopyrannitrile **1a**, yielding the final product **3k** (**Scheme S1, Eq. 2**, its characterization data can be seen in other section in this ESI). However, due to the steric hindrance of piperidine **2c**, the yield of the ring-opening reaction (35%) is significantly lower than that observed with pyrrolidine **2a** (96%).

Furthermore, we conducted validation experiments by utilizing cyclohexenenenitrile analogs (e.g., compound **6**). The experimental results revealed that cyclohexenenenitrile

compound **6** lacking heteroatoms did not react with pyrrolidine **2a**, and no cyano-containing aromatic heterocycle products were detected (**Scheme S1, Eq. 3**). This observation suggests that the reaction mechanism may be initiated by the nucleophilic attack of pyrrolidine (or the promoter NaOH) on the C-O single bond of benzopyran-nitrile, leading to ring-opening.

As shown in **Figure 1**, the theoretical calculations were performed to elucidate the mechanism of substrate conversion to the final product under excess NaOH conditions.

Furthermore, the reaction intermediate **INT-4** (**Fig. S99**) was accurately identified through GC-MS analysis as expected, thereby validating the proposed reaction mechanism.

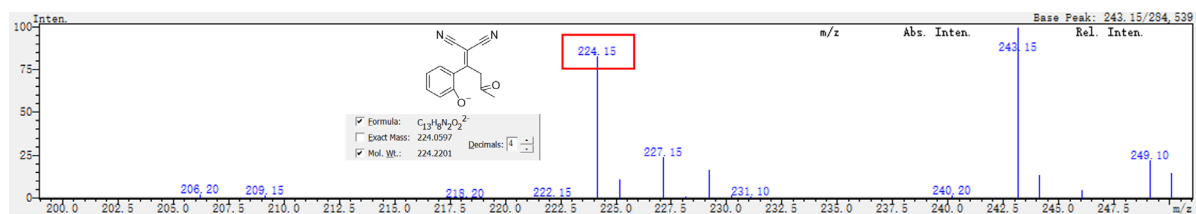


Fig. S99. GC-MS of intermediate INT-4.

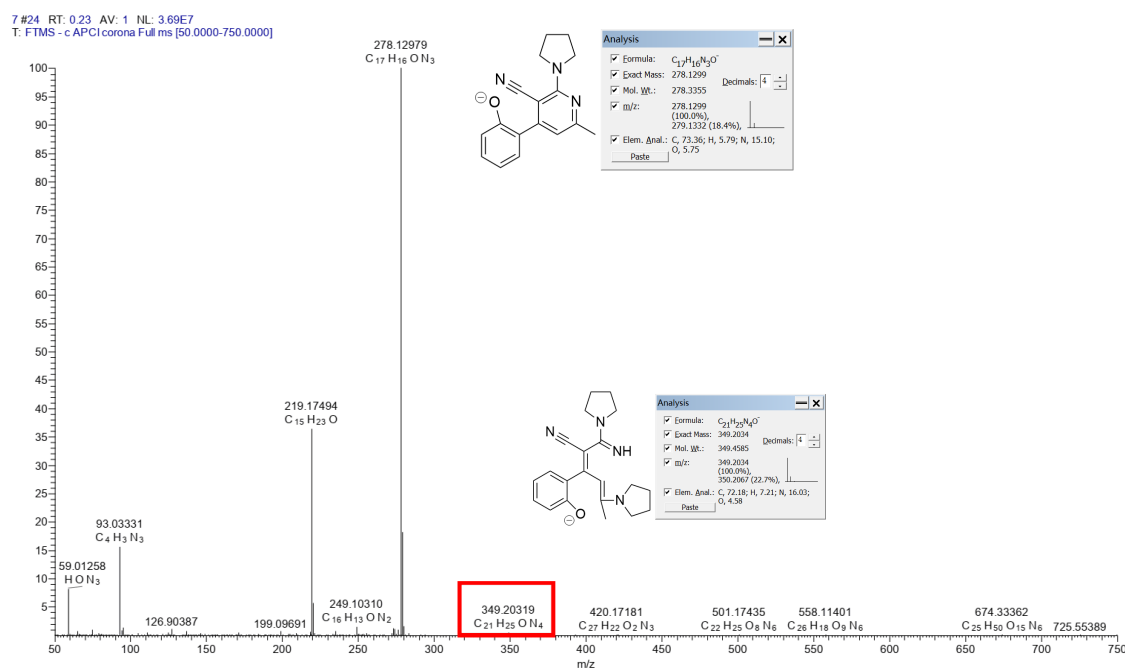


Fig. S100. The HR-MS of the detected intermediates in the control experiments.

2.6. Gram Scale Experiment

Given the broad applications of 3-cyanopyridine derivatives in fluorescent materials and biological activity, we have scaled up the reaction of benzopyranonitrile **1a** and pyrrolidine **2a** to further investigate their significant practical value. The original reaction scale of **1a** was expanded to 2 mmol and 5 mmol, respectively, to conduct the reaction on a gram scale (**Scheme S2**).



Scheme S2. The gram scale experiment.

It can be observed that the yield of compound **3a** is slightly decreased with increasing reactant loading (93%, 87% vs. 96%). Even so, the target compound **3a** is still obtained in high yields. Thus, the gram scale experiment is successful, and this transformation is practical in organic synthesis.

3. Computational Details

3.1. Absolute Energies and Energy Corrections

Quantum chemistry calculations were conducted with the Gaussian 09 software package.^[6] The structures were optimized by the density functional theory (DFT)^[7] with B3LYP-D3 functional^[8, 9] with basis set 6-31G(d)^[10] using SMD^[11] continuum solvent model (solvent = MeCN).

Frequency analyses were performed at the same level of theory to verify the stationary points to be real minima or saddle points and to obtain the thermodynamic energy corrections at 383.15 K. All transition states were confirmed by intrinsic reaction coordinate (IRC) calculations were performed to confirm the connection between two correct minima for a transition state.

In order to get more accurate electronic energies, the single point energy were calculated at the B3LYP-D3(BJ)/def2-TZVP level of theory using SMD continuum solvent model (solvent = MeCN).

Table S3. Calculated energy data and imaginary frequencies for all structure.

Structure	Energy (au)	Thermal correction to Enthalpy (au)	Thermal correction to Gibbs Free Energy (au))	Imaginary frequency (cm ⁻¹)
	B3LYP-D3bj/ def2TZVP/SMD	B3LYP-D3/6- 31G(d)/SMD	B3LYP-D3/6- 31G(d)/SMD	B3LYP-D3/6- 31G(d)/SMD
Sub	-685.218356	0.196085	0.128254	None
OH⁻	-75.93172	0.011875	-0.011992	None
INT-1	-761.214366	0.211461	0.140192	None
TS-1	-761.185099	0.208826	0.137128	-248.51
INT-2	-761.202598	0.210621	0.136543	None
TS-2	-761.201908	0.209485	0.136957	-205.94
INT-3	-761.224048	0.210813	0.135884	None
TS-3	-761.193011	0.204992	0.131996	-1384.50
INT-4	-761.213099	0.210646	0.136659	None
TS-4	-1049.83945	0.362398	0.267752	-229.90
INT-5	-1049.866198	0.365075	0.269582	None
Pyrrolidine	-212.692416	0.136163	0.102104	None
TS-5	-1049.862766	0.364729	0.273124	-116.07
INT-6	-1049.896603	0.366215	0.275195	None

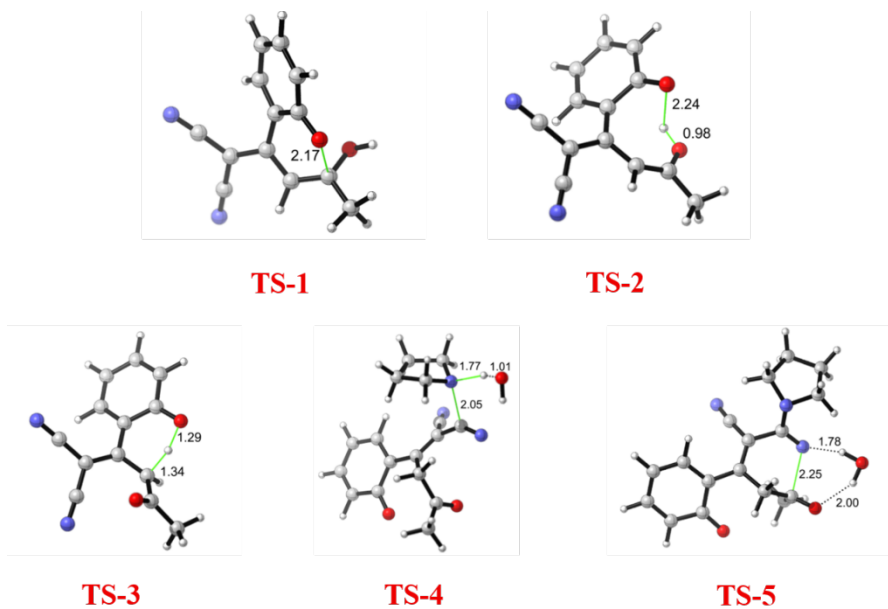


Fig. S101. Structure of transition states.

3.2. Coordinations

Sub

Charge = 0	Multiplicity = 1		
C	3.14376700	-1.73131800	0.00005800
C	3.02579500	-0.35092900	0.00001900
C	1.75248700	0.22362300	-0.00000400
C	0.56579300	-0.54634300	0.00000800
C	0.73218300	-1.95188700	0.00004700
C	1.98995200	-2.53158300	0.00007100
H	4.12832200	-2.18897300	0.00007700
H	3.89274100	0.30139000	0.00000700
C	-0.71300700	0.16255200	-0.00001600
H	-0.13263900	-2.59858400	0.00006000
H	2.07908100	-3.61342300	0.00010200
C	-0.62373800	1.59127600	-0.00004800
C	0.56433500	2.25228300	-0.00005700
H	-1.52448800	2.19210400	-0.00006500
O	1.73962200	1.59144000	-0.00003900
C	0.74469900	3.72940100	-0.00005900
H	-0.22255500	4.23577800	-0.00028100
H	1.31381600	4.03929500	0.88463800
H	1.31421000	4.03925100	-0.88451600
C	-1.98973300	-0.42728200	0.00000000
C	-2.29873300	-1.81225600	0.00004700
N	-2.62922200	-2.93190600	0.00002300
C	-3.15401100	0.39243100	-0.00003200
N	-4.11423600	1.05502500	-0.00001000

OH⁻

Charge = -1	Multiplicity = 1		
O	0.00000000	0.00000000	0.10909800
H	0.00000000	0.00000000	-0.87278100

INT-1

Charge = -1	Multiplicity = 1		
C	-2.39888100	2.65873400	0.08225400
C	-2.64731400	1.33792400	-0.28863400
C	-1.61154200	0.40205900	-0.26357000
C	-0.29379800	0.77222000	0.08947500
C	-0.08292500	2.10124600	0.49629000
C	-1.11731700	3.03676500	0.49438700
H	-3.20871400	3.38350100	0.06943100
H	-3.63903100	1.00723700	-0.58309500
C	0.75873100	-0.26402500	0.00233300
H	0.90284100	2.40882700	0.82448300
H	-0.92187100	4.05689700	0.81297200
C	0.34435300	-1.55527600	-0.07857200
C	-1.10664100	-1.92000400	-0.02273400

H	1.05181100	-2.37348200	-0.17375100
O	-1.91897300	-0.87786600	-0.62247000
C	-1.43932900	-3.17870500	-0.81482800
H	-0.90733800	-4.03212600	-0.38425900
H	-2.51706900	-3.37467100	-0.77257800
H	-1.14544700	-3.06838100	-1.86266800
C	2.18441100	0.09398100	-0.00357200
C	2.68824600	1.32447100	-0.45287200
N	3.13123300	2.34884500	-0.82196800
C	3.14627600	-0.89239300	0.27363100
N	3.93556900	-1.72626500	0.52233000
O	-1.48361200	-2.05895900	1.33935400
H	-2.40775000	-2.37324100	1.35031700

TS-1

Charge = -1	Multiplicity = 1		
C	2.65060800	-2.36940600	-0.07238200
C	2.71115900	-1.11621800	-0.65604400
C	1.68592600	-0.13057500	-0.47300400
C	0.46695100	-0.59495600	0.19253100
C	0.46152800	-1.87597700	0.78608800
C	1.53025500	-2.75544500	0.68753100
H	3.48959300	-3.05380300	-0.18701500
H	3.59207000	-0.80191300	-1.21096800
C	-0.75719800	0.20020600	0.10669400
H	-0.41075100	-2.17124600	1.36304000
H	1.49704200	-3.72336200	1.17959900
C	-0.68208400	1.59425000	-0.05410900
C	0.48752400	2.30841000	0.21313400
H	-1.46381700	2.11514700	-0.59924800
O	1.88626200	1.07066200	-0.88536700
C	0.79294900	3.62380900	-0.43367900
H	0.46088300	4.44092000	0.21972900
H	1.87364300	3.72312800	-0.57856900
H	0.29645800	3.71452400	-1.40174300
C	-2.04225600	-0.43640500	-0.02187400
C	-2.24410000	-1.79558500	-0.35069300
N	-2.45878400	-2.91115400	-0.63639200
C	-3.22357900	0.33754600	0.04303900
N	-4.19961800	0.98168900	0.10923800
O	1.13960900	2.04296800	1.36016900
H	2.04063500	2.41590400	1.30345400

INT-2

Charge = -1	Multiplicity = 1		
C	-3.62403300	-0.03039300	0.27530200
C	-2.96463700	-0.87198900	-0.58921800
C	-1.51988300	-0.86856000	-0.76136200
C	-0.80508900	0.13594200	0.05092100
C	-1.53941400	0.99173600	0.91415500
C	-2.91253400	0.91833400	1.05280100
H	-4.70726800	-0.09709000	0.37251600
H	-3.50955200	-1.60482800	-1.18144500
C	0.62920700	0.30262200	-0.05827600
H	-0.98745900	1.69164000	1.53748600
H	-3.43283700	1.55638700	1.76168700

C	1.56252100	-0.79346900	-0.16455600
C	1.41567600	-2.07055300	0.28667300
H	2.53953600	-0.56906800	-0.58039400
O	-0.96713500	-1.64494700	-1.57944400
C	2.48312800	-3.11036900	0.12633900
H	2.77935200	-3.51153200	1.10489200
H	2.09609700	-3.94973100	-0.46801500
H	3.36798400	-2.70994000	-0.37264400
C	1.19159900	1.61005400	-0.08374900
C	0.43651600	2.78613500	-0.32737200
N	-0.14288000	3.77662000	-0.55118300
C	2.58742800	1.82756900	0.04820000
N	3.73674800	2.01225100	0.15928800
O	0.30224900	-2.46503300	0.92875500
H	0.37325000	-3.41045900	1.15555200

TS-2

Charge = -1	Multiplicity = 1		
C	3.60489300	-0.25203200	-0.28937400
C	2.90845200	-1.00641900	0.62716200
C	1.46795700	-0.93479700	0.78026200
C	0.79937300	0.04305600	-0.09270400
C	1.56704600	0.80672600	-1.01086500
C	2.93578300	0.66332900	-1.13737700
H	4.68489000	-0.36687900	-0.37110100
H	3.42014800	-1.71689300	1.27300800
C	-0.62987500	0.32179800	0.04271800
H	1.04536300	1.49520400	-1.67162400
H	3.48472500	1.23161300	-1.88271100
C	-1.65933900	-0.67939200	0.09910000
C	-1.60545000	-1.99597800	-0.27819500
H	-2.65387300	-0.33598200	0.36355300
O	0.85428200	-1.67103200	1.60413400
C	-2.82208200	-2.86726400	-0.31621900
H	-2.94975400	-3.28521900	-1.32266500
H	-2.69311700	-3.71395900	0.37001100
H	-3.72454800	-2.31799100	-0.04073700
C	-1.05343100	1.67537500	0.09703400
C	-0.16459700	2.76245900	0.30675300
N	0.52571200	3.68491100	0.50107000
C	-2.42208400	2.04669400	0.02380500
N	-3.54667300	2.35824300	-0.03823900
O	-0.51744000	-2.66304300	-0.67380400
H	0.27828500	-2.12069600	-0.51278200

INT-3

Charge = -1	Multiplicity = 1		
C	3.57894900	0.11021000	-0.27556800
C	2.96369500	-0.66681300	0.67950900
C	1.52312900	-0.71707200	0.85810000
C	0.76283300	0.13171400	-0.08173400
C	1.44807200	0.93330500	-1.03223100
C	2.82460400	0.92387900	-1.15624500
H	4.66484800	0.09548700	-0.36090000
H	3.54772000	-1.28886100	1.35484200

C	-0.69189500	0.25278300	0.04416400
H	0.85668200	1.53801500	-1.71658500
H	3.31607300	1.51371300	-1.92455100
C	-1.56597700	-0.88429900	0.10697300
C	-1.28339000	-2.15799000	-0.31073100
H	-2.59023800	-0.71800400	0.42366900
O	0.98994600	-1.42713800	1.74906400
C	-2.29257100	-3.26075900	-0.28283000
H	-2.41370900	-3.68460500	-1.28735100
H	-1.93686500	-4.06996800	0.36772900
H	-3.26169500	-2.91241100	0.08012400
C	-1.27685100	1.53932500	0.08749500
C	-0.52117900	2.72834400	0.26826800
N	0.06106500	3.72690800	0.43631600
C	-2.68269200	1.73256500	0.02013900
N	-3.83845100	1.89255700	-0.03763800
O	-0.11291600	-2.57056100	-0.80894300
H	0.52229200	-1.81917900	-0.80053900

TS-3

Charge = -1	Multiplicity = 1		
C	3.95131900	-0.51212400	-0.04489900
C	3.07808900	-1.48976400	0.40196600
C	1.67134600	-1.35300200	0.25157300
C	1.17432900	-0.10008400	-0.28319300
C	2.10212700	0.86476000	-0.73470400
C	3.47101700	0.67123900	-0.63724400
H	5.02340500	-0.67168000	0.04899900
H	3.44581800	-2.41371200	0.83984400
C	-0.26502800	0.13949000	-0.26335800
H	1.72550100	1.76829100	-1.20478200
H	4.16099500	1.41880600	-1.01717800
C	-1.09230700	-1.05891900	-0.41425700
C	-2.45189800	-1.21324000	0.12550900
H	-0.91339600	-1.58501600	-1.35779000
O	0.88172800	-2.33275500	0.60659900
C	-3.29925500	-2.28838900	-0.53851500
H	-4.17820600	-2.50442300	0.07491400
H	-3.62965600	-1.93653800	-1.52528300
H	-2.72559100	-3.20886100	-0.70042300
C	-0.79259400	1.41859700	-0.02226400
C	-0.03058000	2.50771300	0.48564000
N	0.54880900	3.42045700	0.92724500
C	-2.15061100	1.74667900	-0.28777600
N	-3.24149100	2.06958800	-0.54745100
O	-2.87928900	-0.59613300	1.10337900
H	-0.27532400	-1.86381000	0.27244300

INT-4

Charge = -1	Multiplicity = 1		
C	3.83275000	-0.21334700	-0.01062800
C	3.00819200	-1.29942200	0.14297800
C	1.56410800	-1.20755200	0.04032000
C	1.02640100	0.13197000	-0.25841000
C	1.93472300	1.22251800	-0.40833500
C	3.29870000	1.07166800	-0.29781500

H	4.91113300	-0.33617800	0.07641200
H	3.40989300	-2.28731400	0.35643500
C	-0.38510900	0.31160400	-0.41932100
H	1.54386100	2.19611900	-0.68580100
H	3.96072300	1.91732500	-0.46022300
C	-1.22396800	-0.85601800	-0.87828700
C	-1.77974500	-1.69298800	0.28367100
H	-0.65609300	-1.50633300	-1.54353500
O	0.84349300	-2.22418100	0.24257000
C	-2.08162600	-3.13404700	-0.05191600
H	-2.52474600	-3.63933800	0.81030100
H	-2.77711700	-3.17835200	-0.90064000
H	-1.15677200	-3.63584700	-0.35023100
C	-1.06838900	1.51093900	-0.15695400
C	-0.51201100	2.63723400	0.50961500
N	-0.10466000	3.57415700	1.07499300
C	-2.45698000	1.65089900	-0.43380300
N	-3.59530300	1.78595300	-0.65691700
O	-2.05001400	-1.19490700	1.36233900
H	-2.10123900	-0.49889700	-1.43522200

TS-4

Charge = -2	Multiplicity = 1		
C	-3.78230100	-2.60698100	-0.17231900
C	-4.10693300	-1.26556900	-0.23447200
C	-3.12081300	-0.21207800	-0.15390300
C	-1.73324300	-0.65851000	0.00081200
C	-1.45239900	-2.04341500	0.04887600
C	-2.43951300	-3.01657700	-0.03508900
H	-4.57064500	-3.35620200	-0.24075800
H	-5.14152700	-0.94611100	-0.34699300
C	-0.65460400	0.32638100	0.04822200
H	-0.41637600	-2.36207600	0.10757600
H	-2.17648800	-4.07093300	-0.02042200
C	-0.82908200	1.58632300	-0.76552300
C	-1.51717200	2.72337200	-0.00035700
H	-1.39980700	1.38164000	-1.67349600
O	-3.46923100	1.00974700	-0.19494400
C	-2.27366100	3.70671900	-0.86912600
H	-2.68646900	4.51320500	-0.25652400
H	-1.59831500	4.13316100	-1.62335200
H	-3.07835800	3.18302400	-1.39223300
C	0.51472300	0.15779600	0.76513600
C	0.65835400	-0.84767200	1.76120400
N	0.79988400	-1.60517500	2.63976400
C	1.67388200	1.04979400	0.62061300
N	2.01016800	2.19427800	0.68614100
O	-1.36374300	2.89877600	1.19592900
H	0.14888800	1.98465200	-1.06487300
C	3.39162500	-1.56810400	0.28078900
C	2.50702800	-2.55559000	-0.54347400
C	1.99058900	-1.69340700	-1.72296800
C	2.78951200	-0.37102600	-1.57722500
H	4.34901300	1.03460500	-0.08545000
H	3.24757200	-1.67340600	1.36280700
H	4.45718900	-1.81636600	0.08580100
H	3.08770400	-3.41934800	-0.89021200

H	1.68176900	-2.94801300	0.06010700
H	2.14142700	-2.17375000	-2.69796400
H	0.91888600	-1.49784800	-1.61700400
H	3.71776300	-0.45119200	-2.18378100
H	2.24383700	0.50177200	-1.96332700
N	3.09422000	-0.20974900	-0.16250400
O	4.83187900	1.91711400	-0.07454800
H	4.05685100	2.45387700	0.17760900

Pyrrolidine

Charge = 0	Multiplicity = 1		
C	-1.15669000	-0.45284200	0.19776800
C	1.15662900	-0.45272300	0.19813200
C	0.77767600	1.02767000	-0.07106400
C	-0.77767900	1.02775000	-0.07061500
H	-2.05991000	-0.77490300	-0.32995900
H	-1.32368600	-0.60876500	1.27209800
H	1.32299000	-0.60823200	1.27262400
H	2.06016300	-0.77495700	-0.32895500
H	1.19880700	1.69975800	0.68454000
H	1.16362900	1.34907100	-1.04498100
H	-1.19822800	1.69923600	0.68584700
H	-1.16421300	1.35007600	-1.04398900
N	0.00008200	-1.27404200	-0.20887900
H	0.00026000	-1.31212200	-1.23039000

INT-5

Charge = -2	Multiplicity = 1		
C	-5.04936600	-1.26336300	-0.27402100
C	-4.78624400	0.06914500	-0.01848800
C	-3.44940000	0.62509000	0.00249300
C	-2.37267000	-0.33434900	-0.27042000
C	-2.69545600	-1.68362200	-0.53969400
C	-3.99964100	-2.16544400	-0.54506800
H	-6.08008900	-1.61803000	-0.27762400
H	-5.59675600	0.76739300	0.18531500
C	-0.97366600	0.09677500	-0.30780500
H	-1.88703200	-2.36482400	-0.79676600
H	-4.20466100	-3.20575000	-0.78389900
C	-0.61703200	1.44305100	-0.89833300
C	0.08663400	2.44173100	0.04182100
H	-1.52278200	1.94270500	-1.24833700
O	-3.25635800	1.85102800	0.26739200
C	-0.39675700	2.53036500	1.47774300
H	-0.56336200	1.54656700	1.92140200
H	0.33683200	3.08544800	2.07059300
H	-1.35373500	3.06644300	1.48911600
C	0.08248100	-0.67076000	0.13313100
C	-0.12074200	-1.79194500	0.97670800
N	-0.20327700	-2.68774400	1.72800700
C	1.51402700	-0.12745300	0.00401900
N	1.78833300	1.02097900	0.43432200
O	0.64320600	3.42394000	-0.48328900
H	0.06003700	1.31127600	-1.75220900
C	3.78617000	-0.49898300	-0.89365200
C	4.52993900	-1.25465100	0.23585400

C	3.68149000	-2.54158400	0.44652100
C	2.52526800	-2.39507900	-0.57631600
H	2.63449900	3.55509700	-0.38067300
H	3.83842600	0.58713200	-0.81858400
H	4.18197700	-0.80511100	-1.87210000
H	5.56984100	-1.47212900	-0.03115500
H	4.54195000	-0.64436800	1.14566000
H	4.25502600	-3.46071800	0.28308900
H	3.27712400	-2.58261500	1.46412700
H	2.80677700	-2.86893400	-1.52719100
H	1.59279400	-2.85178000	-0.25013800
N	2.39032100	-0.94833900	-0.81130000
O	3.45944200	3.12291100	-0.08934700
H	3.04497900	2.26135000	0.19716600

INT-6

Charge = -2	Multiplicity = 1		
C	-5.13494200	-1.20408800	-0.25746000
C	-4.87009000	0.09929800	0.11270000
C	-3.53086000	0.65137900	0.17391600
C	-2.46249400	-0.27913000	-0.21616700
C	-2.78459700	-1.60840100	-0.57738100
C	-4.08861400	-2.08389900	-0.61218600
H	-6.16588200	-1.55682400	-0.28415900
H	-5.67805200	0.77584900	0.38686900
C	-1.07305400	0.15938200	-0.26061500
H	-1.97739700	-2.26744500	-0.89064300
H	-4.29954900	-3.10130100	-0.93062600
C	-0.70174500	1.48643000	-0.87122300
C	0.52629200	2.18973900	-0.22474600
H	-1.56050100	2.15570900	-0.86382600
O	-3.32909200	1.83427900	0.57713600
C	0.23600700	2.56478900	1.25740800
H	-0.06652600	1.71824300	1.88901200
H	1.14850100	3.01256800	1.66643200
H	-0.56186500	3.31675400	1.28477300
C	-0.00607700	-0.60430400	0.16913100
C	-0.19404700	-1.76732200	0.96223400
N	-0.31049100	-2.70728800	1.64822200
C	1.38878500	-0.08377800	-0.00925700
N	1.66013300	1.16041200	-0.17566000
O	0.87669000	3.26233100	-0.95136400
H	-0.41946700	1.30729500	-1.92149700
C	3.80635900	-0.51939700	0.06421900
C	4.68717700	-1.78203400	-0.11408400
C	3.69081500	-2.96023600	-0.17019500
C	2.39417000	-2.29704500	-0.63375500
H	2.31560300	3.66288700	-0.31721100
H	4.02021700	0.03544900	0.98423100
H	3.94529000	0.18217700	-0.77031700
H	5.25078800	-1.71334700	-1.05048800
H	5.41413600	-1.89530900	0.69583900
H	4.01351200	-3.76557400	-0.83742500
H	3.53900600	-3.38476700	0.82904500
H	2.41021800	-2.12371900	-1.72378200
H	1.50706500	-2.88513100	-0.39620200
N	2.42381100	-1.02111000	0.10422700

O	3.22379300	3.65851000	0.14960600
H	3.28109500	2.69314000	0.25419000

4. Optical Property Characterization

4.1. Photophysical Properties of 3d, 3g, 3i, 3j, 4g and 4h

The photophysical properties of six compounds **3d**, **3g**, **3i**, **3j**, **4g** and **4h**, which were selected as the representative examples, were investigated.

The optical properties of all synthesized compounds are presented in **Table S4**, along with their corresponding spectra.

Table S4. The maximum emission peak of **3d**, **3g**, **3i**, **3j**, **4g** and **4h** (10^{-5} M) in solvents of different polarities.

3d			3g			3i			
Solvent	λ_{em}^a (nm)	λ_{abs}^b (nm)	$\Delta\lambda^c$ (nm)	λ_{em}^a (nm)	λ_{abs}^b (nm)	$\Delta\lambda^c$ (nm)	λ_{em}^a (nm)	λ_{abs}^b (nm)	$\Delta\lambda^c$ (nm)
Hexane	423	272, 356	66	438	264, 386	52	438	273, 348	90
DCM	431	274, 357	74	452	267, 393	59	448	275, 359	89
THF	432	271, 346	86	442	266, 390	52	448	273, 350	98
EtOAc	437	270, 347	90	453	261, 390	63	452	272, 351	101
Dioxane	436	271, 350	86	454	286, 392	62	450	280, 350	100
EtOH	439	269, 348	91	453	280, 390	63	449	271, 351	98
MeCN	440	271, 351	89	459	281, 390	69	459	273, 354	105
DMF	440	263, 348	92	460	283, 393	67	457	263, 352	105
DMSO	445	272, 350	95	465	285, 396	69	462	273, 354	108
Red shift	22			27			24		
3j			4g			4h			
Solvent	λ_{em}^a (nm)	λ_{abs}^b (nm)	$\Delta\lambda^c$ (nm)	λ_{em}^a (nm)	λ_{abs}^b (nm)	$\Delta\lambda^c$ (nm)	λ_{em}^a (nm)	λ_{abs}^b (nm)	$\Delta\lambda^c$ (nm)
Hexane	434	272, 345	89	433	-	-	434	-	-
DCM	450	274, 358	92	441	269, 338	73	442	272, 342	100
THF	445	271, 349	96	442	266, 358	84	445	270, 344	101
EtOAc	453	270, 347	106	447	267, 339	108	447	269, 344	103
Dioxane	453	280, 349	104	446	267, 343	103	448	270, 345	103
EtOH	451	269, 348	103	449	267, 360	89	457	269, 348	109
MeCN	457	272, 351	106	450	267, 358	92	454	270, 348	106
DMF	456	263, 349	107	450	262, 361	89	455	263, 349	106
DMSO	461	271, 352	109	460	268, 367	93	461	271, 350	111
Red shift	27			27			27		

4.2. Fluorescence Emission Spectra and UV-Vis Absorption Spectra of Compounds 3d, 3g, 3i, 3j, 4g, and 4h.

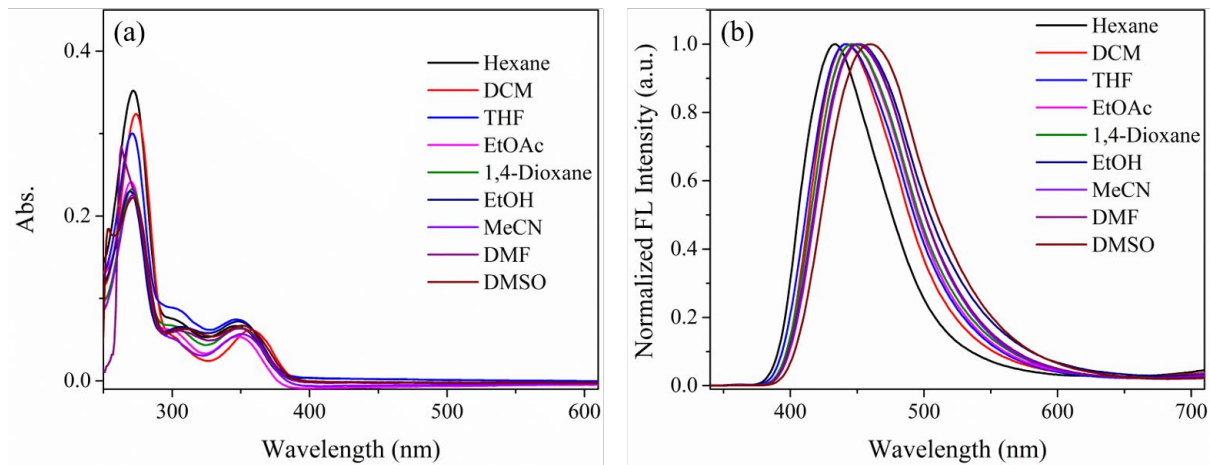


Fig. S102. (a) UV-vis absorption spectra and (b) normalized fluorescence spectra of compound **3d** (110^{-5} M, $\lambda_{\text{ex}} = 280$ nm) in solvents of different polarities.

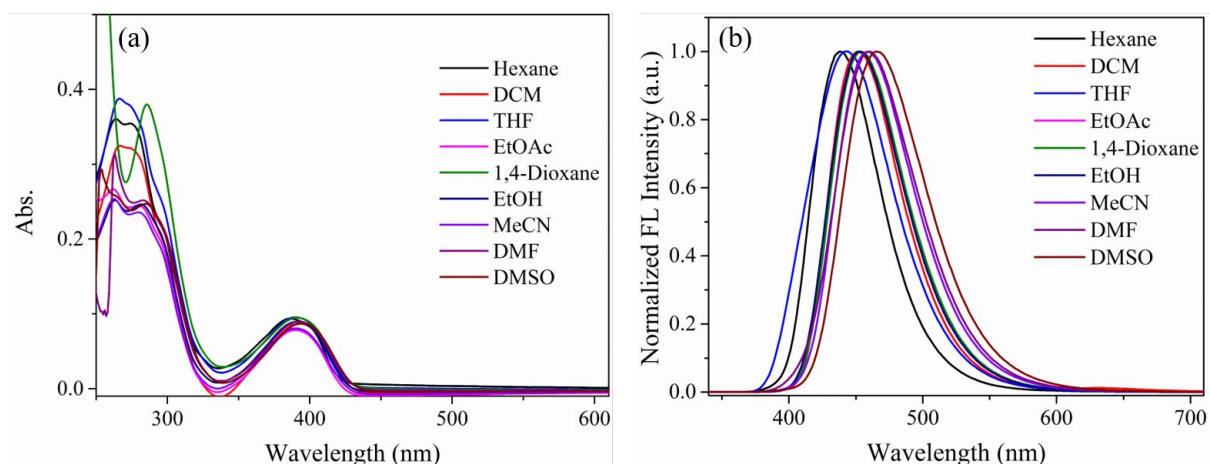


Fig. S103. (a) UV-vis absorption spectra and (b) normalized fluorescence spectra of compound **3g** (10^{-5} M, $\lambda_{\text{ex}} = 280$ nm) in solvents of different polarities.

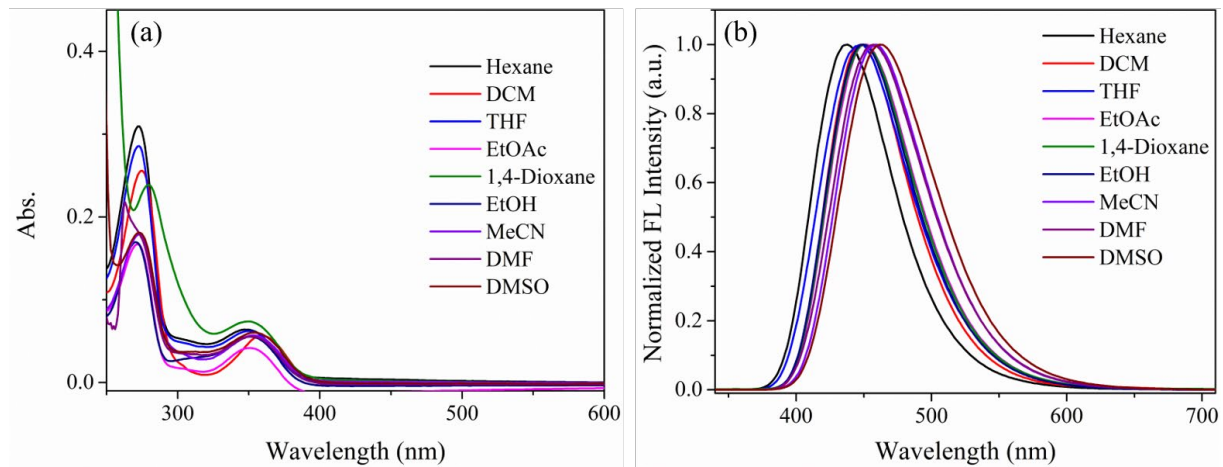


Fig. S104. (a) UV-vis absorption spectra and (b) normalized fluorescence spectra of compound **3i** (10^{-5} M, $\lambda_{\text{ex}} = 280$ nm) in solvents of different polarities.

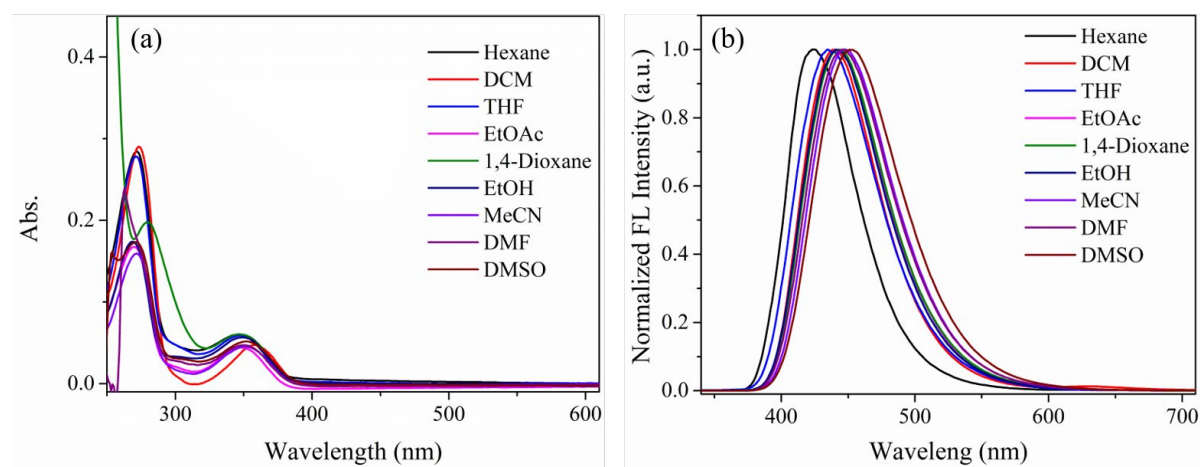


Fig. S105. (a) UV-vis absorption spectra and (b) normalized fluorescence spectra of compound **3j** (10^{-5} M, $\lambda_{\text{ex}} = 280$ nm) in solvents of different polarities.

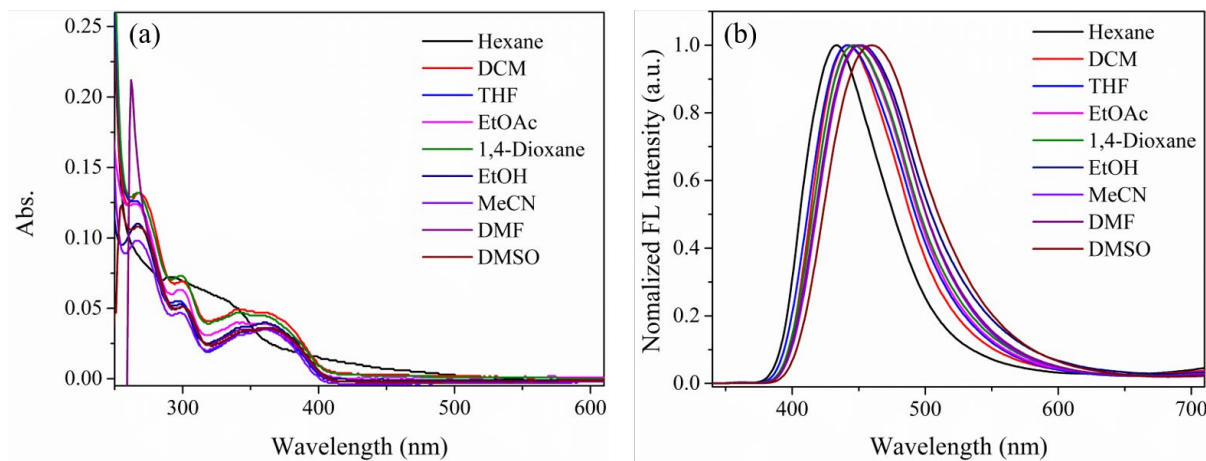


Fig. S106. (a) UV-vis absorption spectra and (b) normalized fluorescence spectra of compound **4g** (10^{-5} M, $\lambda_{\text{ex}} = 280$ nm) in solvents of different polarities.

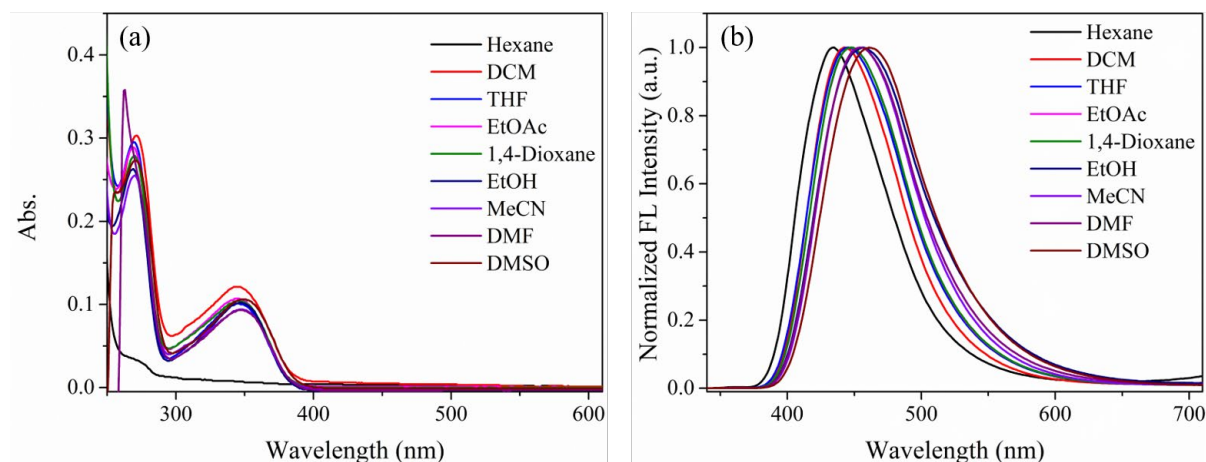


Fig. S107. (a) UV-vis absorption spectra and (b) normalized fluorescence spectra of compound **4h** (10^{-5} M, $\lambda_{\text{ex}} = 280$ nm) in solvents of different polarities.

4.3. Assessment of AIE Properties for Compounds **3d**, **3g**, **3i**, **3j**, **4g**, and **4h**.

The fluorescence intensity of compound **3g** exhibits a peak at 70% water content. Specifically, as the water fraction (f_w) is increased from 0% to 70%, the intensity of the fluorescence emission peak is increased. However, a sharp decrease in fluorescence intensity can be observed as f_w is increased from 70% to 99% (Fig. S108).

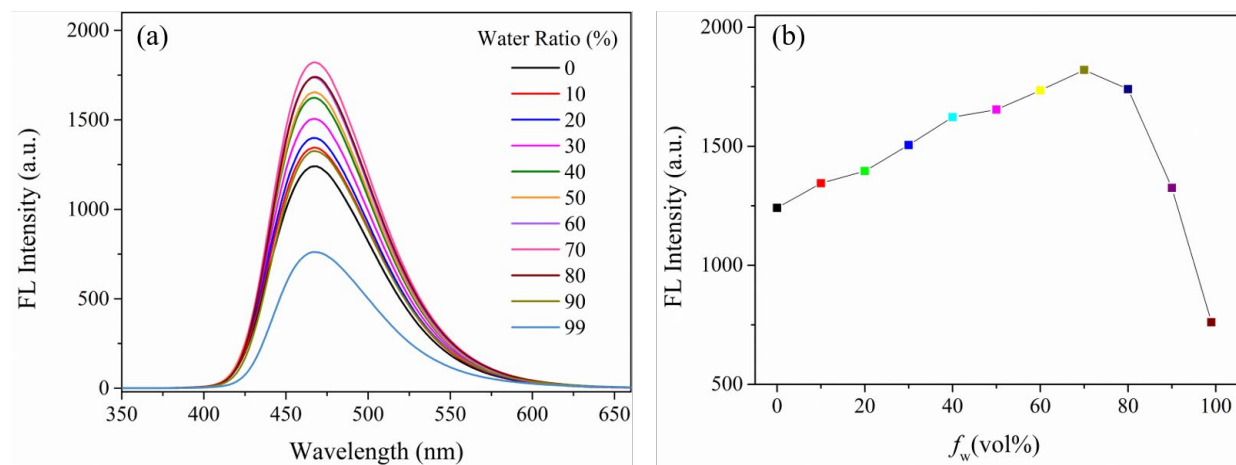


Fig. S108. (a) The fluorescence spectra of compound **3g** (10^{-5} M) and (b) plot of emission peak intensity in DMSO/H₂O systems with different water fraction (0-99% by volume).

Both compounds **3i** and **3j** (10^{-5} M) can exhibit strong blue fluorescence in DMSO. The fluorescence emission intensity is increased with increasing water content when f_w is increased from 0% to 60%. However, a sharp decrease in fluorescence intensity can be observed when f_w is increased from 60% to 99% (Figs. S109 and S110).

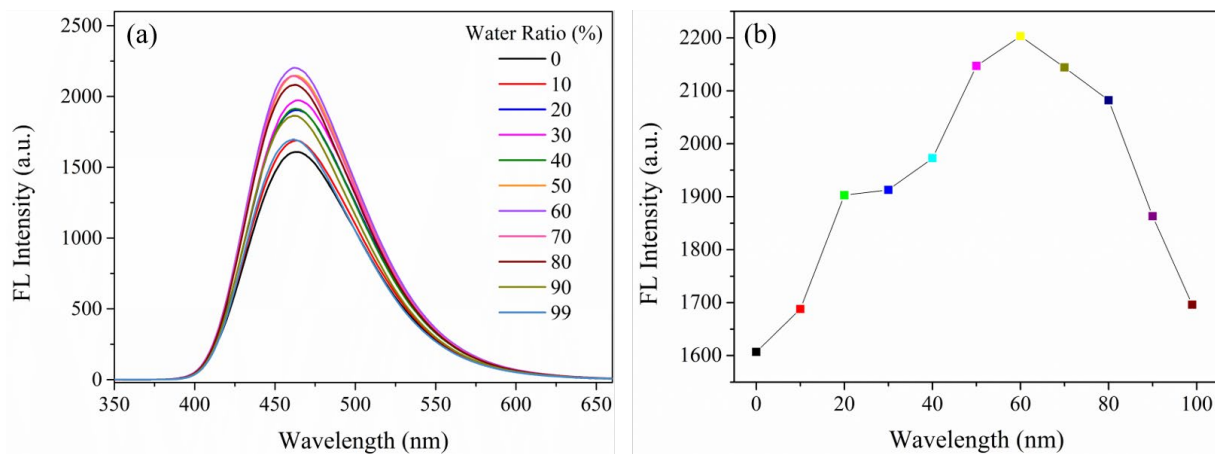


Fig. S109. (a) The fluorescence spectra of compound **3i** (10^{-5} M) and (b) plot of emission peak intensity in DMSO/H₂O systems with different water fraction (0-99% by volume).

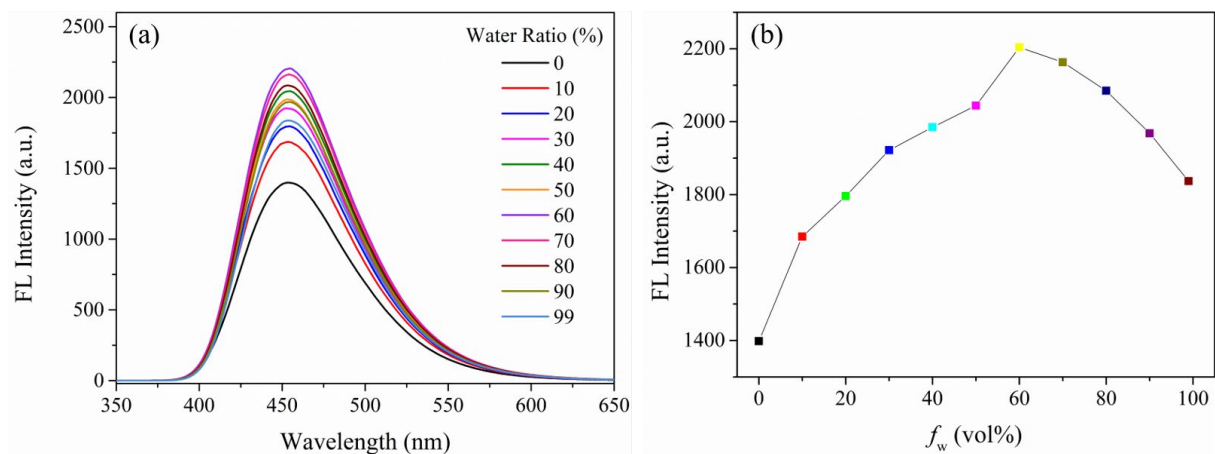


Fig. S110. (a) The fluorescence spectra of compound **3j** (10^{-5} M) and (b) plot of emission peak intensity in DMSO/H₂O systems with different water fraction (0-99% by volume).

Both compounds **4g** (Fig. S111) and **4h** (Fig. S112) can exhibit strong fluorescence in DMSO, with their emission spectra gradually decreasing as the water content increases from 0% to 99%. The fluorescence quenching of **4g** and **4h** may be attributed to the increased water content, which activates non-radiative pathways for **4g** and **4h**, leading to aggregation-caused quenching (ACQ).

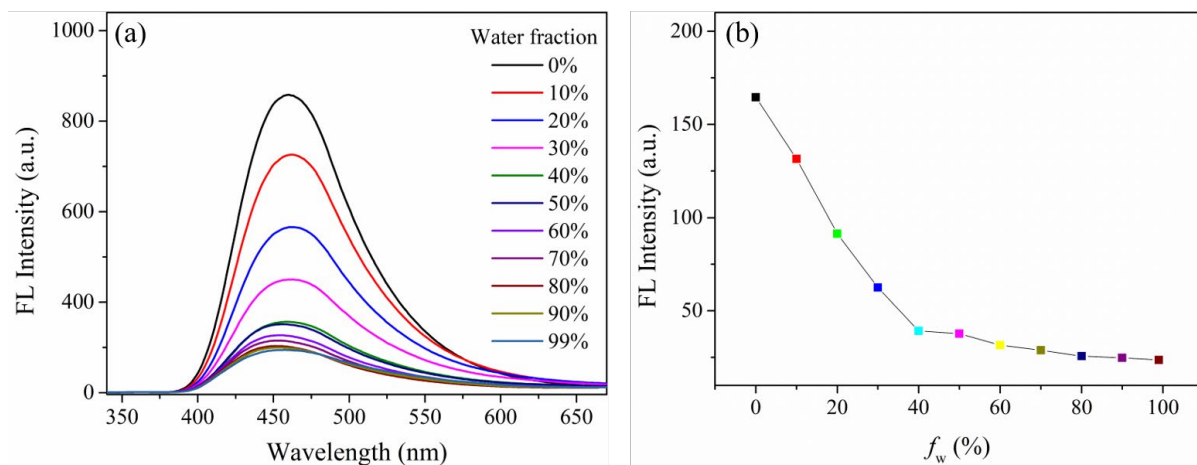


Fig. S111. (a) The fluorescence spectra of compound **4g** (10^{-5} M) and (b) plot of emission peak intensity in DMSO/H₂O systems with different water fraction (0-99% by volume).

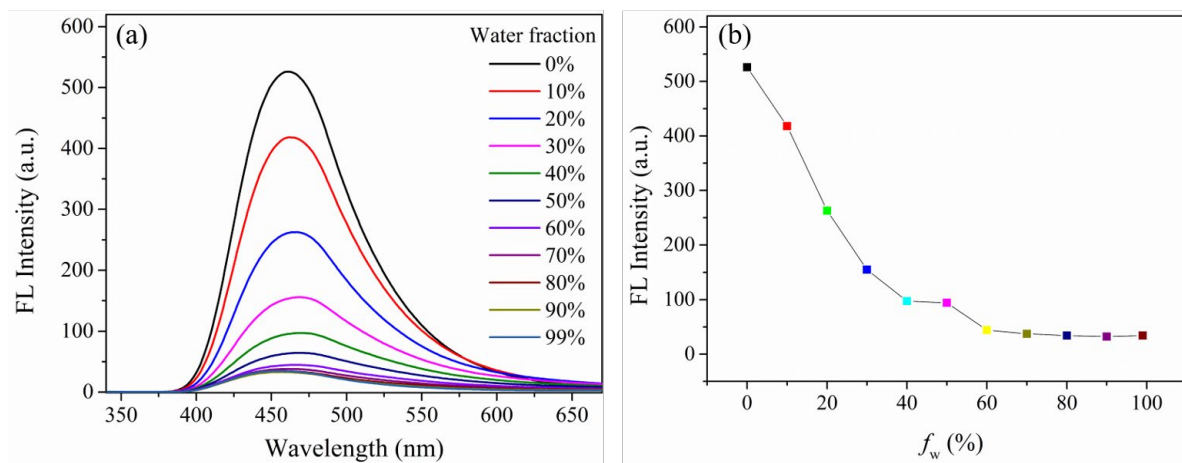
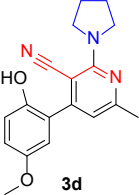
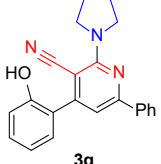
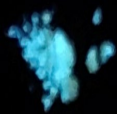
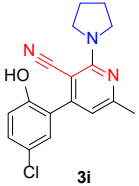
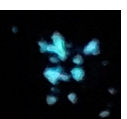
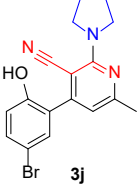
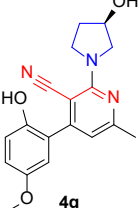
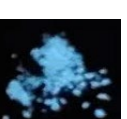
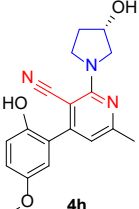
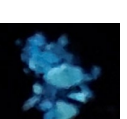


Fig. S112. (a) The fluorescence spectra of compound **4h** (10^{-5} M) and (b) plot of emission peak intensity in DMSO/H₂O systems with different water fraction (0-99% by volume).

4.4. Dual-state Emission Testing of Six Representative Compounds

Table S5. Dual-state emission and fluorescence images of six representative compounds.

Compounds	Solution	Solid	Photo images	
	λ_{em} (nm)	λ_{em} (nm)	Liquid	Solid
	445	426		
	465	467		
	462	444		
	461	458		
	460	461		
	461	451		

4.5. The Responses of Compounds **3d** and **4g** to Metal Ions

The aforementioned experiments indicate that the presence of hydroxyl groups influences the aggregation-induced emission (AIE) properties of the compounds. To comparatively assess the impact of hydroxyl groups on the probe's detection capabilities, we have selected compounds **3d** and **4g** as representative examples to investigate their respective fluorescence detection performance concerning metal ions.

Upon the incremental addition of Fe^{3+} solutions to a 10^{-5} M solution of compound **3d** (DMSO/H₂O, v/v, 40/60), the fluorescence intensity of probe **3d** at 445 nm exhibits a marked decrease. And when the concentration of Fe^{3+} is increased from 0 to 20 eq., there is a 97% quenching rate (**Fig. S113a**).

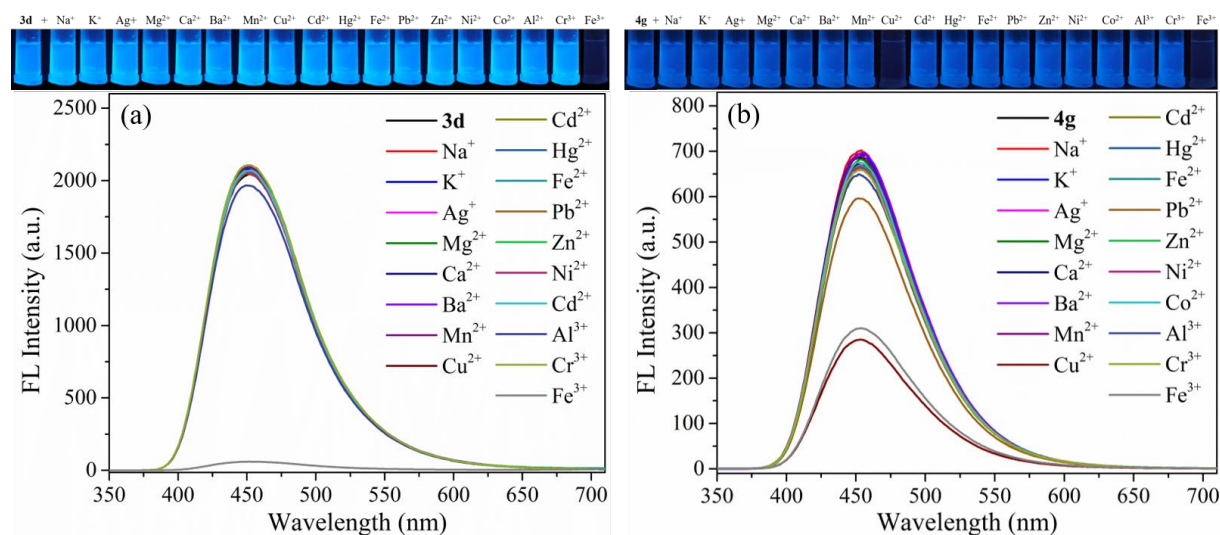


Fig. S113. Compounds **3d** and **4g** (10^{-5} M) were added 20.0 eq in DMSO/H₂O (v/v, 40/60) and DMSO solution.

To a 10^{-5} M solution of compound **4g** in DMSO, varying equivalents of Fe^{3+} and Cu^{2+} solutions were added. Upon increasing the analyte concentration from 0 to 20 eq., the fluorescence intensity of probe **4g** at 460 nm exhibits a significant decrease, with quenching efficiencies of 58% and 55%, respectively (Fig. S113b). The detection limits of probe **4g** for Fe^{3+} and Cu^{2+} can be determined to be 6.71×10^{-7} M and 7.62×10^{-7} M, respectively (Figs. S114 and S115).

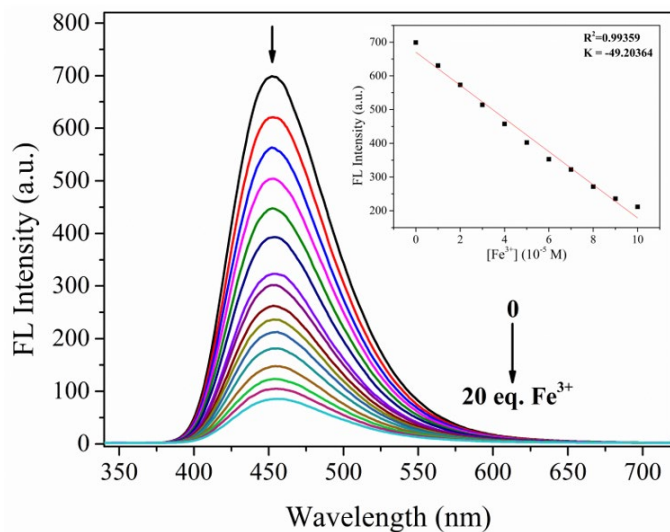


Fig. S114. Fluorescence emission spectra of compound **4g** (10^{-5} M, DMSO) upon interaction with varying concentrations (0-20 eq.) of Fe^{3+} . The inset illustrates the correlation between the maximum fluorescence intensity of **4g** and Fe^{3+} concentration.

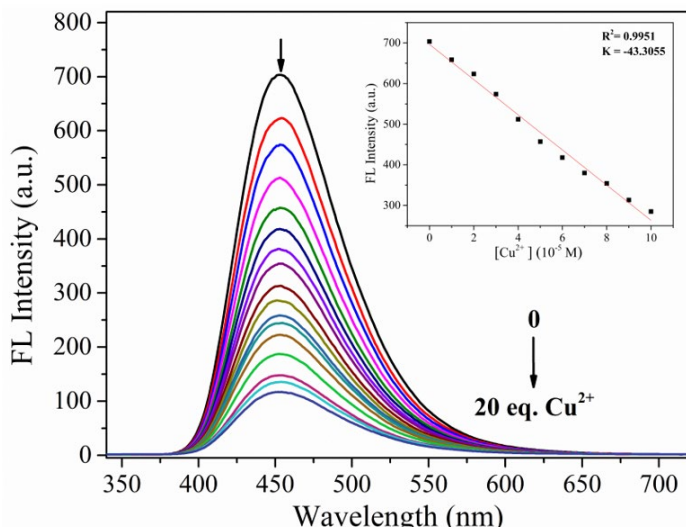


Fig. S115. Fluorescence emission spectra of compound **4g** (10^{-5} M, DMSO) upon interaction with varying concentrations (0-20 eq.) of Cu^{2+} . The inset illustrates the correlation between the maximum fluorescence intensity of **4g** and Cu^{2+} concentration.

Furthermore, the interference experiments were conducted on probes **3d** and **4g**. As illustrated in **Fig. S116**, upon the addition of 20 eq. of Fe^{3+} to the test solution of **3d**, followed by the introduction of other metal ions or anions, the majority of these ions exhibit negligible interference with the detection of Fe^{3+} .

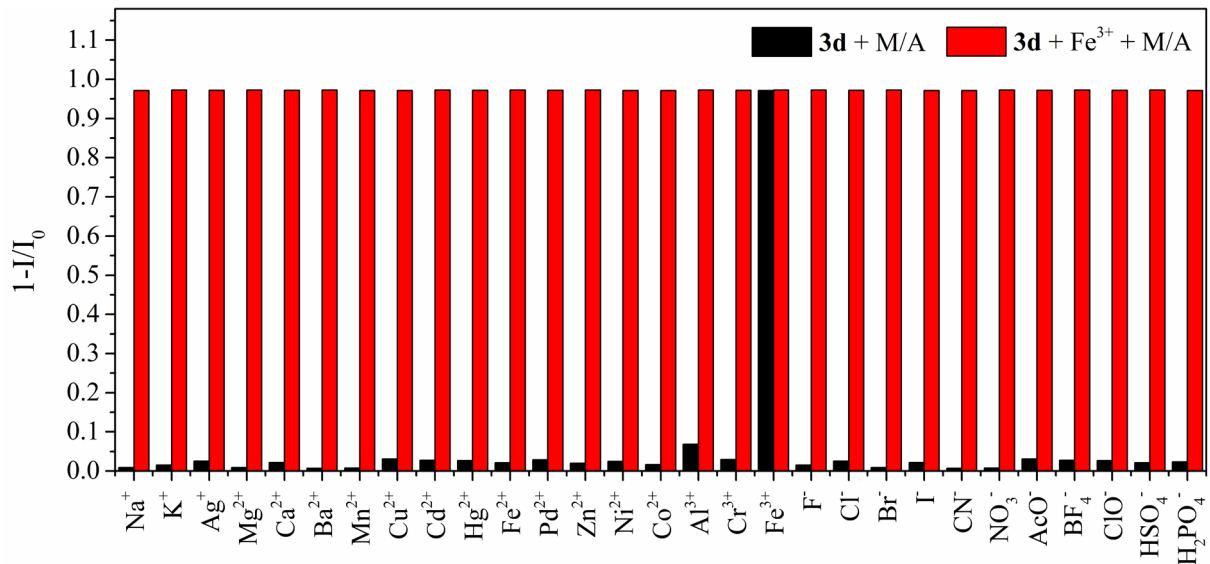


Fig. S116. The anti-interference of compound **3d** for the detection of Fe^{3+} (Fe^{3+} : 20 eq.; other ions: 20 eq.; M = metal ions; A = anions).

Similarly, the specific responses of other anions to **4g** with Fe^{3+} or Cu^{2+} does not exhibit significant interference (**Fig. S117** and **Fig. S118**). These findings demonstrate that probes **3d** and **4g** possess robust anti-interference capabilities in the detection of Fe^{3+} and Cu^{2+} .

This characteristic is advantageous for the reliable detection of Fe^{3+} and Cu^{2+} in actual water samples or other practical samples.

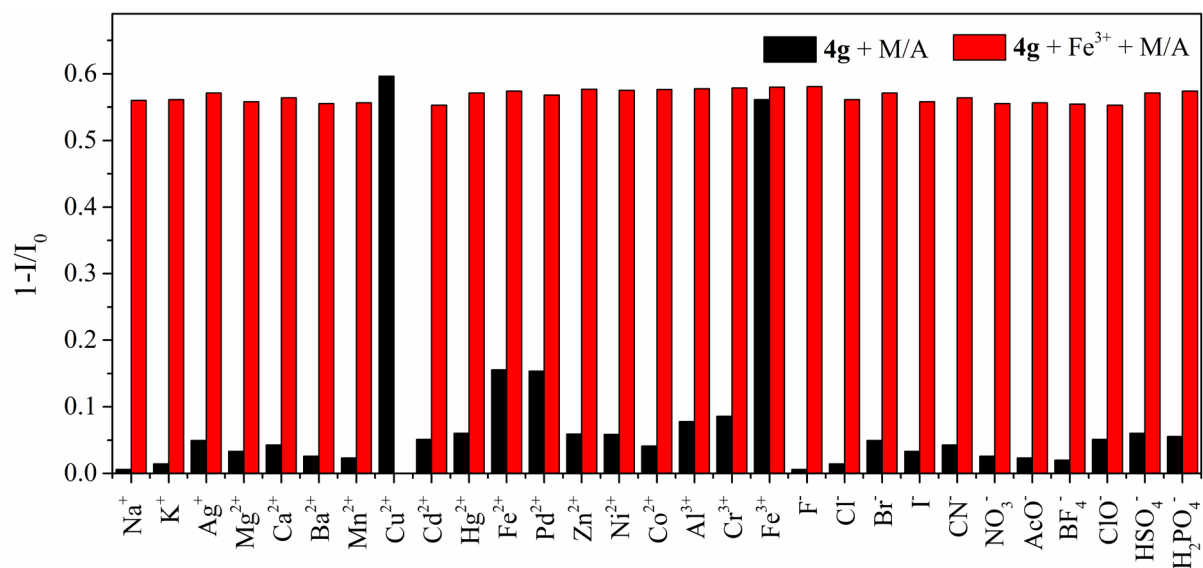


Fig. S117. The anti-interference of compound **4g** for the detection of Fe^{3+} (Fe^{3+} : 20 eq.; other ions: 20 eq.; M = metal ions; A = anions).

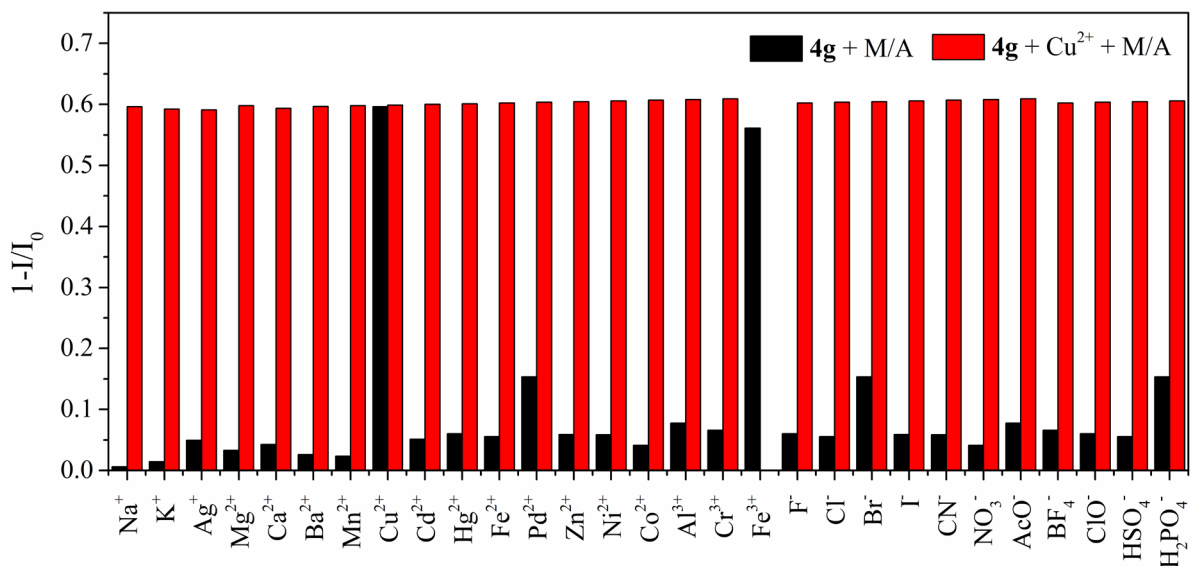


Fig. S118. The anti-interference of compound **4g** for the detection of Cu^{2+} (Cu^{2+} : 20 eq.; other ions: 20 eq.; M = metal ions; A = anions).

To ascertain the binding constants for **3d**-Fe³⁺, **4g**-Fe³⁺, and **4g**-Cu²⁺, Job's plots were initially constructed by utilizing the acquired fluorescence spectral data, thereby enabling the determination of the binding stoichiometry between the probe and the metal analytes.^[12-14]

The resultant data, as depicted in **Fig. S119**, reveal a 1:1 binding stoichiometry for **3d** with Fe³⁺; furthermore, **4g** exhibits 1:1 coordination with both Fe³⁺ and Cu²⁺.

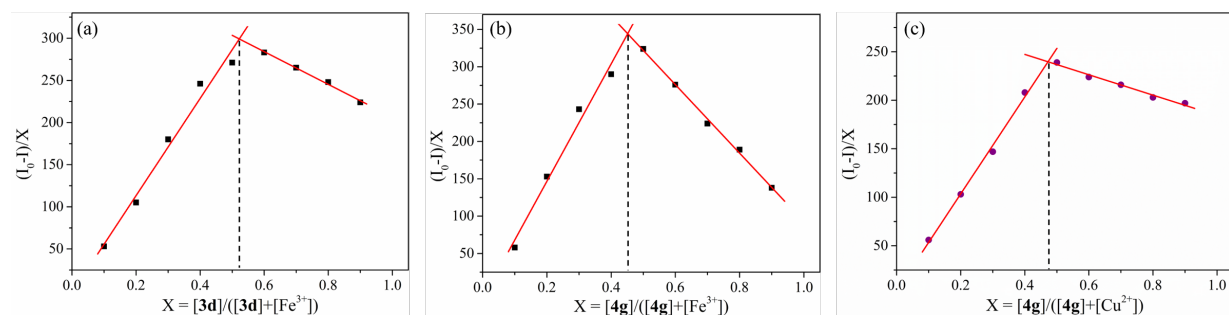


Fig. S119. The Job's plots of **3d**-Fe³⁺, **4g**-Fe³⁺ and **4g**-Cu²⁺.

In addition to the aforementioned analyses, the coordination behavior was further elucidated through HRMS testing of the **3d** and **4g** solutions subsequent to their interaction with metal ions, as detailed in the references.^[15, 16]

As illustrated in **Fig. S120**, a prominent peak emerges at *m/z* 437.1215, which exhibits a precise match with the molecular weight of **3d**+Fe³⁺+4H₂O+H⁺ (*m/z*: 437.1227), thereby corroborating the proposed coordination complex.

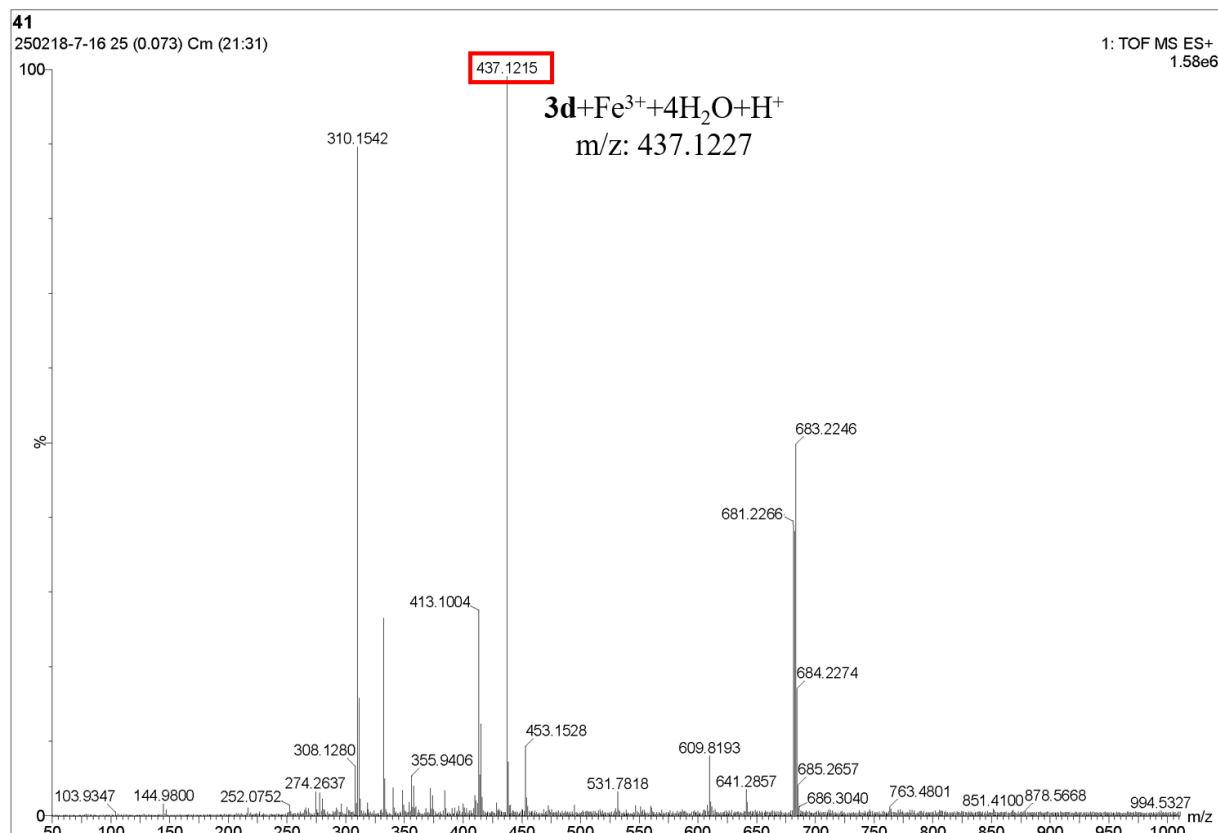


Fig. S120. HRMS spectra of **3d**+Fe³⁺.

Similarly, it can be seen from **Fig. S121** and **Fig. S122** that the molecular ion peaks after the interaction of **4g** with Fe³⁺ and Cu²⁺ are at *m/z* 441.0506 and 388.0686. These indicate that the probe **4g** forms a complex of **4g**+Fe³⁺+2H₂O+2H⁺+Na⁺ (*m/z*: 441.0930) and **4g**+Cu²⁺+H⁺ (*m/z*: 388.0706) with Fe³⁺ and Cu²⁺, respectively.

Therefore, the above HRMS test results strongly prove that **3d** is 1:1 complex with Fe³⁺, and **4g** is also 1:1 complex with Fe³⁺ and Cu²⁺, respectively.

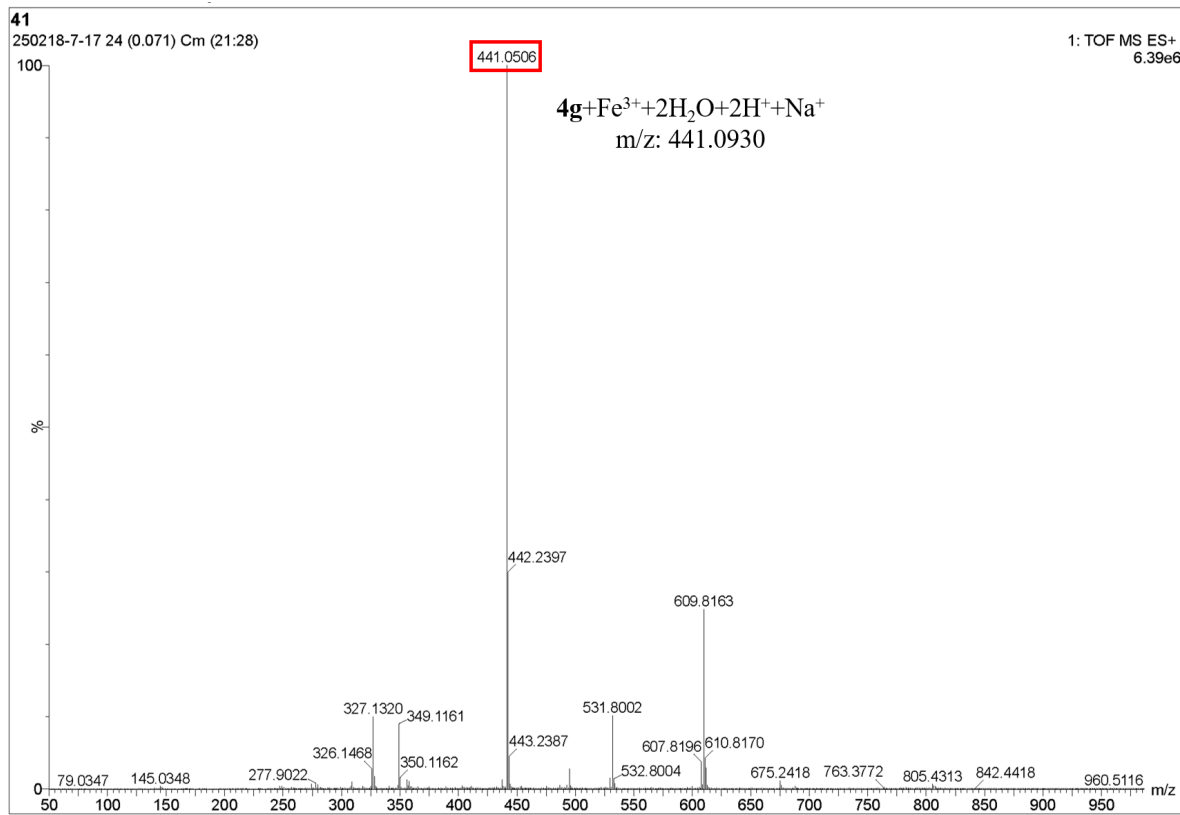


Fig. S121. HRMS spectra of **4g+Fe³⁺**.

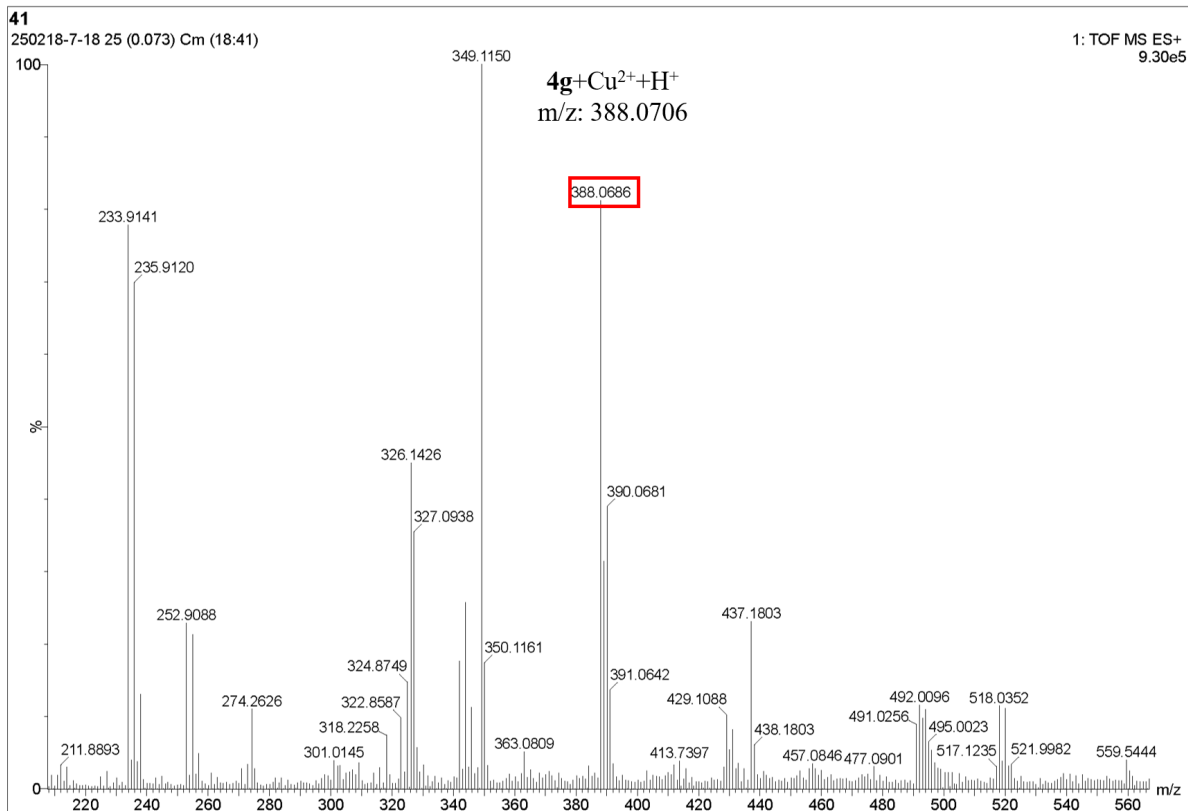


Fig. S122. HRMS spectra of **4g+Cu²⁺**.

Based on the Job's plot analysis, and in combination with the high-resolution mass spectrometry data obtained from the probe's interaction with metal ions, we have postulated potential coordination models for the probe's **3d** and **4g** sites with Fe^{3+} or Cu^{2+} .

These models were subsequently subjected to DFT calculations using Gaussian 09, as illustrated in **Fig. S123**.

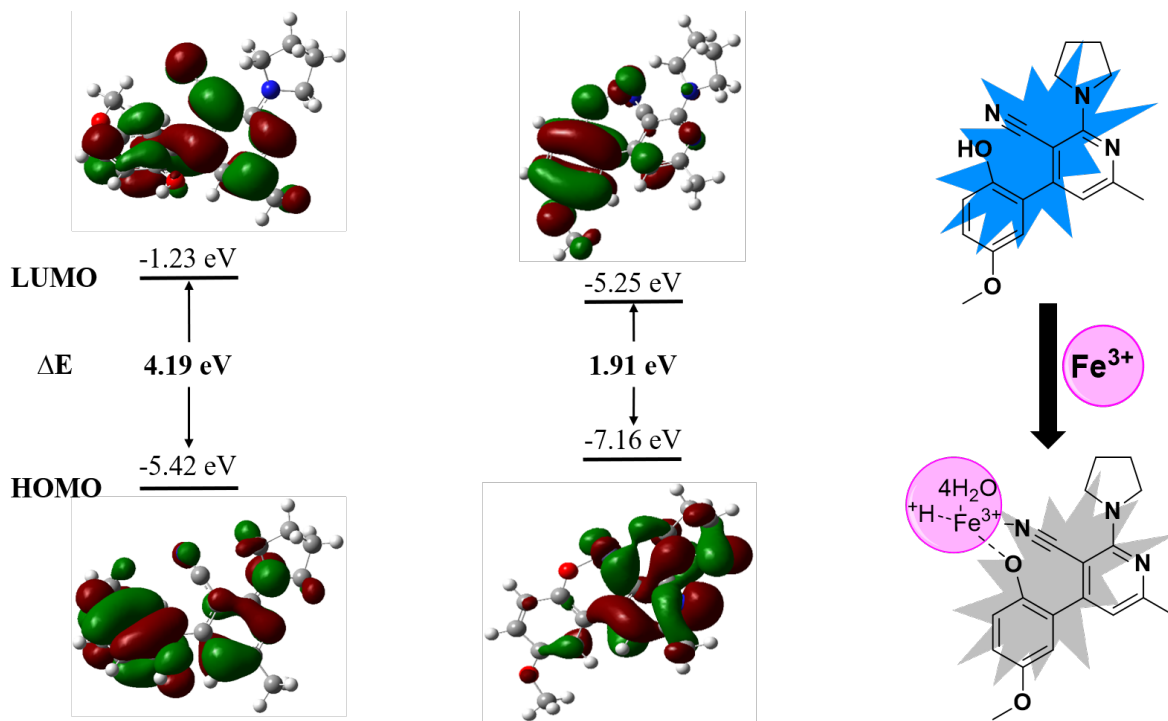


Fig. S123. Possible coordination models and DFT calculation results of **3d** with Fe^{3+} .

As illustrated in **Fig. S123**, the interaction between probe **3d** and Fe^{3+} results in a significant shift of the LUMO orbital towards the phenyl group, while the HOMO orbital predominantly localizes on the pyridine and pyrrolidine rings. This is accompanied by a more pronounced energy distribution compared to the pre-coordination state.

Furthermore, after coordination, the ΔE of the **3d**+ Fe^{3+} complex notably decreases.

These observations suggest an enhanced interaction between probe **3d** and Fe^{3+} , leading to the formation of a stable complex,^[17-19] which subsequently quenches fluorescence.

3.6. The Responses of Compounds **3d** and **4g** to NACs.

The addition of 20.0 or 10.0 eq. of NACs to test solutions of compounds **3d** and **4g** can result in the quenching of fluorescence for PA, DNP, NBA, NBAc, and NA. The quenching rates of the analytes on the fluorescence intensity of **3d** are 54.8%, 53.4%, 58.0%, 76.4%, and 57.4%, respectively (**Fig. S124a**), while the quenching rates on the fluorescence intensity of **4g** are 71.5%, 74.7%, 78.8%, 74.7%, and 82.7%, respectively (**Fig. S124b**).

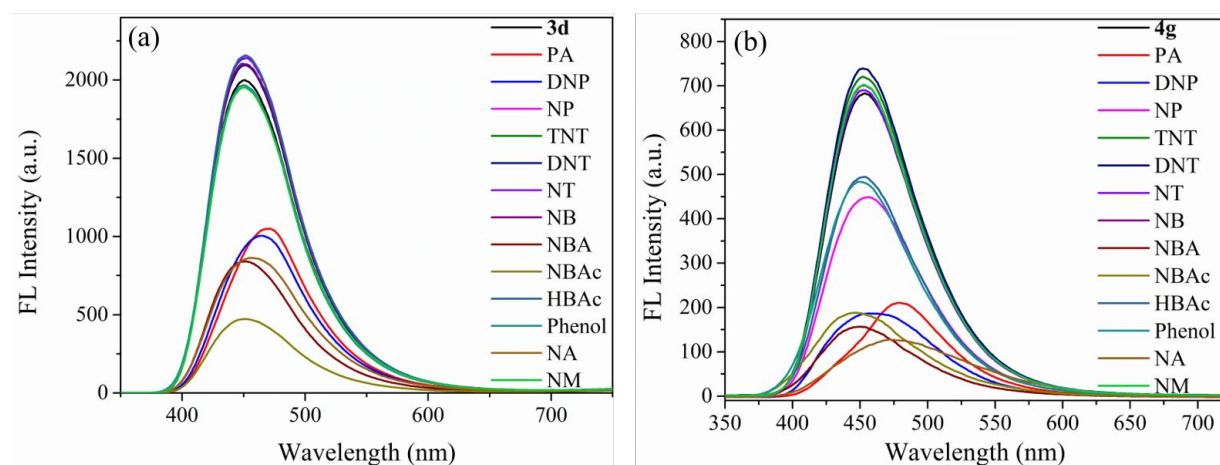


Fig. S124. The fluorescence spectra of (a) compounds **3d** (10^{-5} M, DMSO/H₂O, v/v, 40/60) and (b) **4g** (10^{-5} M, DMSO) before and after different the addition of 20 eq. and 10.0 eq. different NAC effects.

Comparative analysis of the test data indicates that the fluorescence quenching of probe **4g** is more pronounced than that of **3d** following interaction with NACs. Furthermore, **4g** can reach saturation with only 10.0 eq. of NACs, which may be attributed to the lone pair electrons provided by the hydroxyl group, facilitating enhanced interaction with NACs.

Upon the addition of varying equivalents of PA solution to a 10^{-5} M solution of compound **3d** in DMSO/H₂O (v/v, 40/60), the fluorescence intensity of probe **3d** at 445 nm exhibits a marked decrease over time. This can be observed as the eq. of PA is increased from 0 to 20. The observed quenching rate is 54.8% (**Fig. S125**).

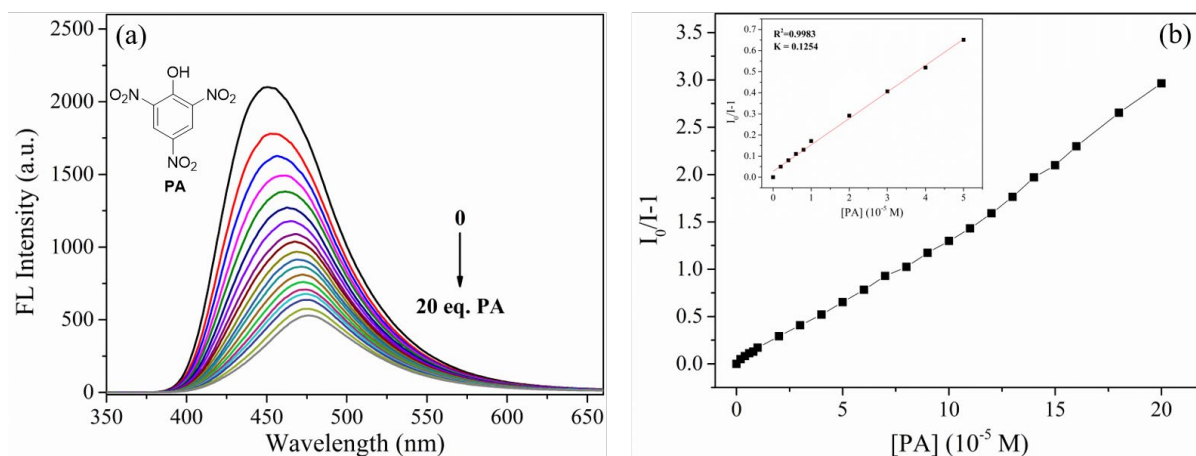


Fig. S125. (a) Fluorescence emission spectra of compound **3d** (10^{-5} M, DMSO/H₂O, v/v, 40/60) with different concentrations (0-20 eq.) of PA; (b) Stern-Volmer curve of compound **3d** response to PA. The insets show the Stern-Volmer plot (1-5 eq.) of the response of compound **3d** to low concentrations.

The fluorescence quenching of probe **3d** was analyzed using the Stern-Volmer equation.^[20] At low concentrations of PA (5×10^{-5} M), the fluorescence quenching of probe **3d** exhibits a good linear relationship with the amount of PA added, while the SV curve shows a nonlinear deviation as the concentration of PA is increased. This suggests that an energy transfer process may occur between probe **3d** and PA upon the addition of PA,^[21] and the quenching mechanism may be static quenching. The K_{sv} value between probe **3d** and PA can be determined to be $1.25 \times 10^4 \text{ M}^{-1}$ from the SV curve obtained at low PA concentrations.

Similarly, the other titration curves and Stern-Volmer plots were generated for DNP, NBA, NBAc, and NA (**Figs. S126-S129**), facilitating a parallel analysis. The K_{sv} values, representing the interaction of probe **3d** with the NACs, were subsequently calculated. The resultant data are presented in **Table S6**.

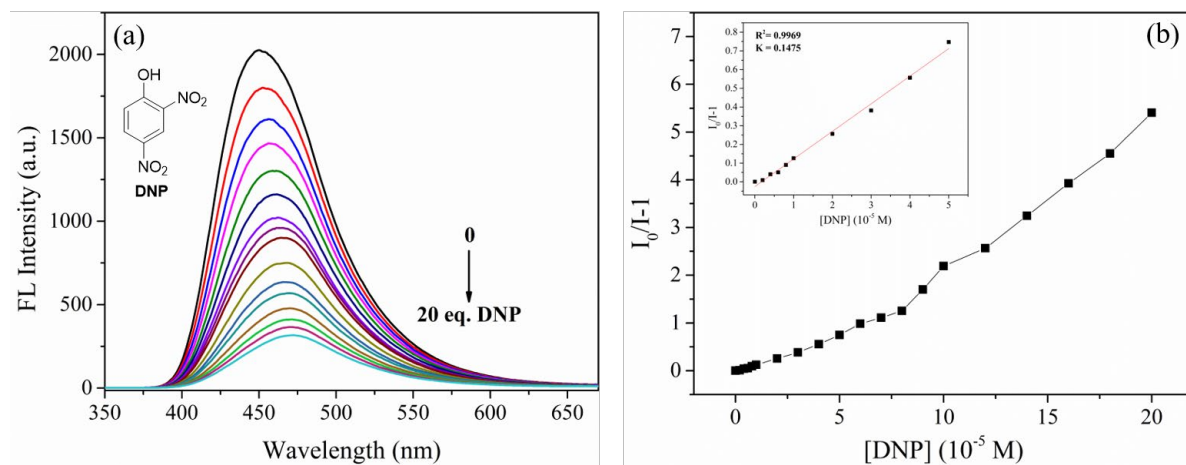


Fig. S126. (a) Fluorescence emission spectra of compound **3d** (10^{-5} M, DMSO/H₂O, v/v, 40/60) with different concentrations (0-20 eq.) of DNP; (b) Stern-Volmer curve of compound **3d** response to DNP. The insets show the Stern-Volmer plot (1-5 eq.) of the response of compound **3d** to low concentrations.

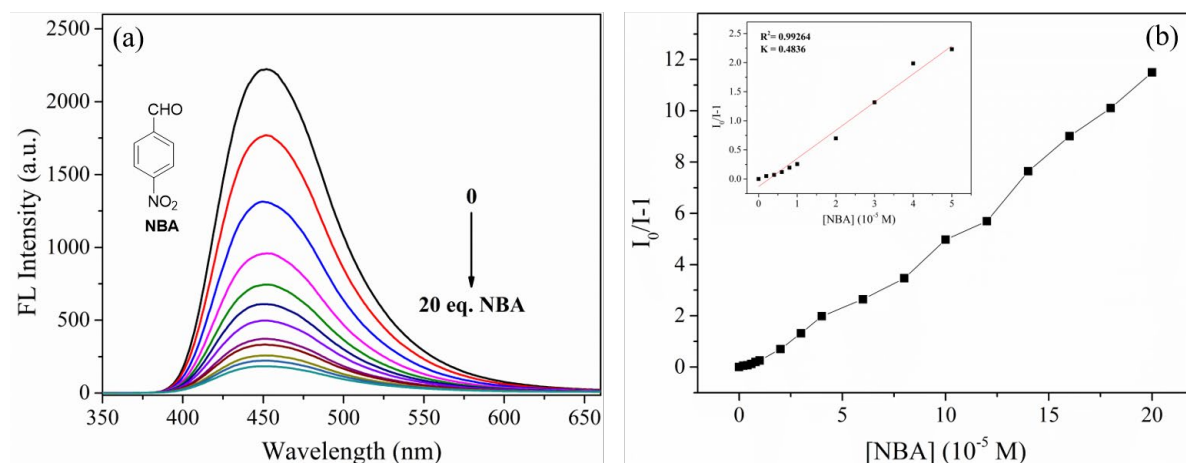


Fig. S127. (a) Fluorescence emission spectra of compound **3d** (10^{-5} M, DMSO/H₂O, v/v, 40/60) with different concentrations (0-20 eq.) of NBA; (b) Stern-Volmer curve of compound **3d** response to NBA. The insets show the Stern-Volmer plot (1-5 eq.) of the response of compound **3d** to low concentrations.

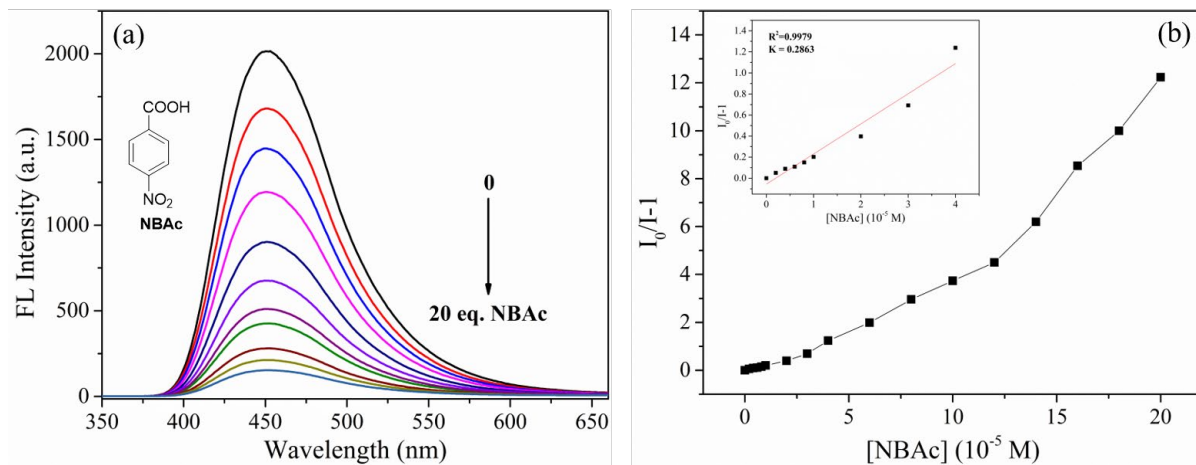


Fig. S128. (a) Fluorescence emission spectra of compound **3d** (10⁻⁵ M, DMSO/H₂O, v/v, 40/60) with different concentrations (0-20 eq.) of NBAc; (b) Stern-Volmer curve of compound **3d** response to NBAc. The insets show the Stern-Volmer plot (1-5 eq.) of the response of compound **3d** to low concentrations.

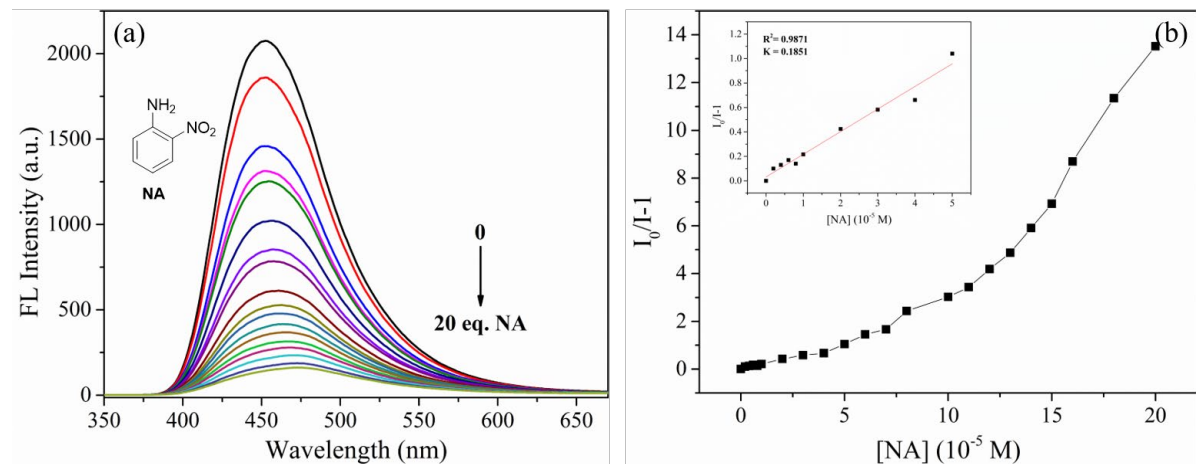


Fig. S129. (a) Fluorescence emission spectra of compound **3d** (10⁻⁵ M, DMSO/H₂O, v/v, 40/60) with different concentrations (0-20 eq.) of NA; (b) Stern-Volmer curve of compound **3d** response to NA. The insets show the Stern-Volmer plot (1-5 eq.) of the response of compound **3d** to low concentrations.

What's more, the fluorescence intensity of probe **4g** at 460 nm is decreased significantly with varying degrees of red-shift upon the addition of different equivalents of PA, DNP, NBA, NBAc, and NA solutions (**Figs. S130-S134**) to compound **4g** (10^{-5} M, DMSO) as the analyte amount is increased from 0 to 10 eq.

The Stern-Volmer plots for probe **4g** were generated *via* **4g** titration with the analyte, and the resulting fluorescence quenching was analyzed (see insets in **Figs. S130b-S134b**). It can be observed that at low analyte concentrations, the fluorescence quenching of probe **4g** exhibits a strong linear correlation with the amount of analyte added. This behavior is similar to that of probe **3d**, suggesting that the quenching mechanism between probe **4g** and the analyte may also be static quenching.

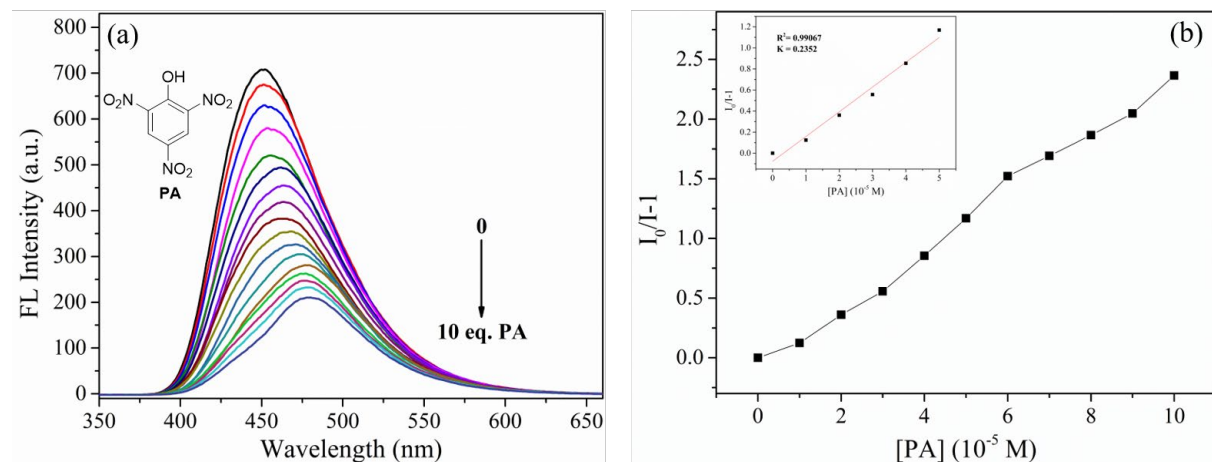


Fig. S130. (a) Fluorescence emission spectra of compound **4g** (10^{-5} M, DMSO) with different concentrations (0-10 eq.) of PA; (b) Stern-Volmer curve of compound **4g** response to PA. The insets show the Stern-Volmer plot (1-5 eq.) of the response of compound **4g** to low concentrations.

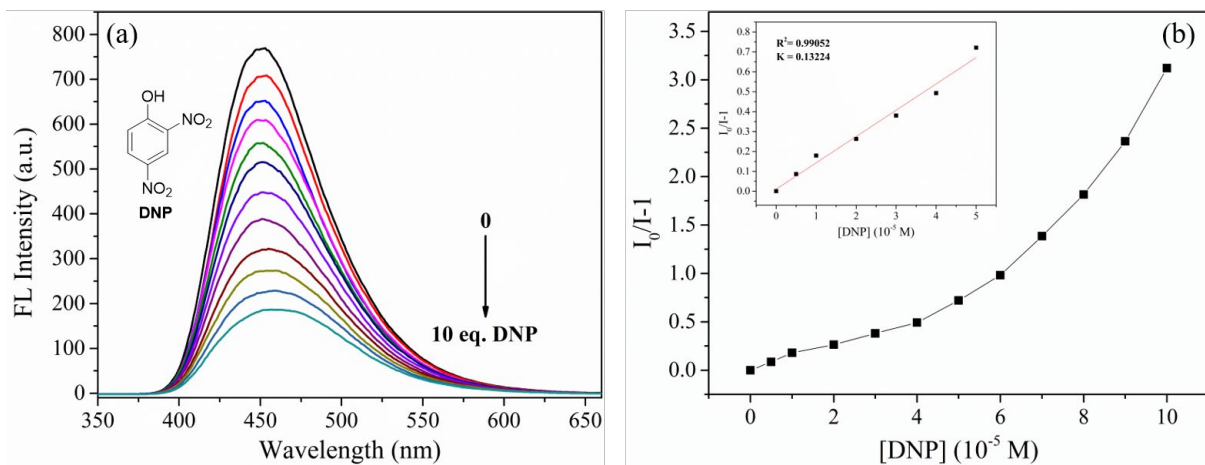


Fig. S131. (a) Fluorescence emission spectra of compound **4g** (10^{-5} M, DMSO) with different concentrations (0-10 eq.) of DNP; (b) Stern-Volmer curve of compound **4g** response to DNP. The insets show the Stern-Volmer plot (1-5 eq.) of the response of compound **4g** to low concentrations.

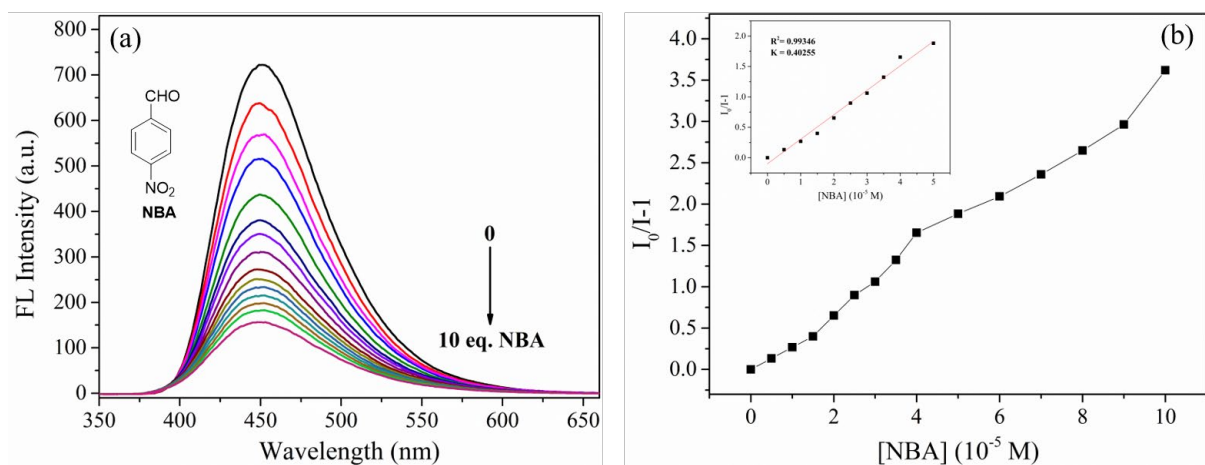


Fig. S132. (a) Fluorescence emission spectra of compound **4g** (10^{-5} M, DMSO) with different concentrations (0-10 eq.) of NBA; (b) Stern-Volmer curve of compound **4g** response to NBA. The insets show the Stern-Volmer plot (1-5 eq.) of the response of compound **4g** to low concentrations.

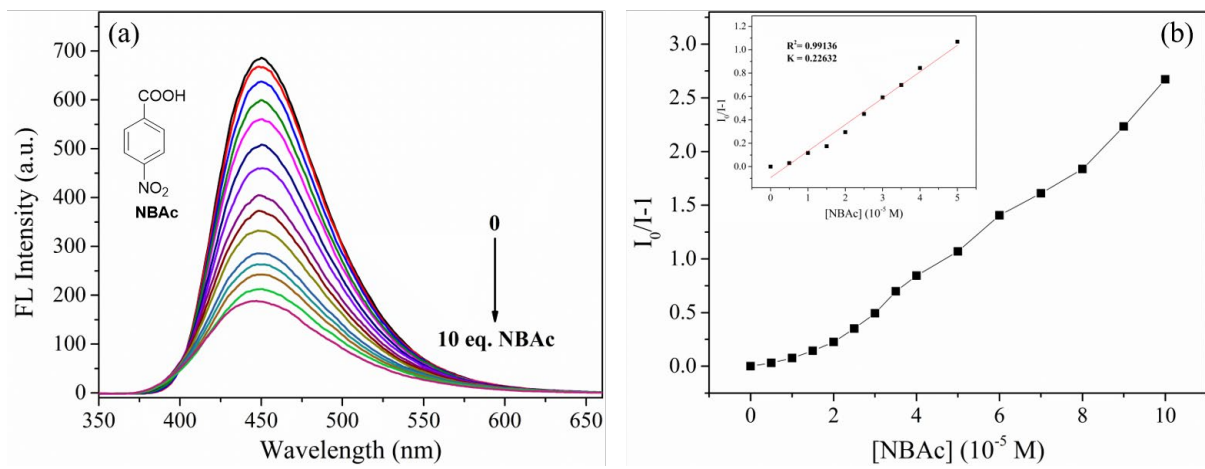


Fig. S133. (a) Fluorescence emission spectra of compound **4g** (10^{-5} M, DMSO) with different concentrations (0-10 eq.) of NBAc; (b) Stern-Volmer curve of compound **4g** response to NBAc. The insets show the Stern-Volmer plot (1-5 eq.) of the response of compound **4g** to low concentrations.

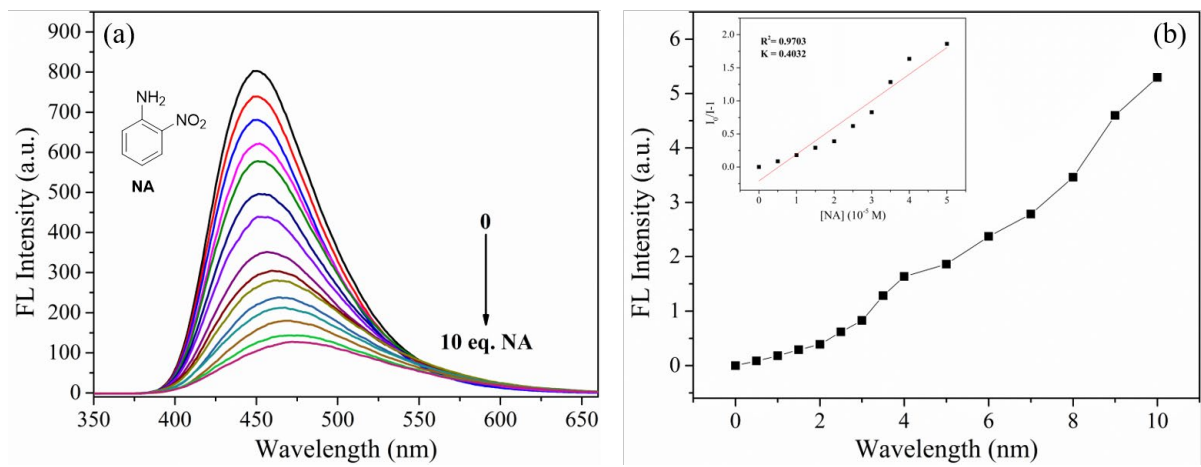


Fig. S134. (a) Fluorescence emission spectra of compound **4g** (10^{-5} M, DMSO) with different concentrations (0-10 eq.) of NA; (b) Stern-Volmer curve of compound **4g** response to NA. The insets show the Stern-Volmer plot (1-5 eq.) of the response of compound **4g** to low concentrations.

Subsequently, based on the fluorescence titration curves, the plots that used to illustrate the relationship between maximum fluorescence intensity and the concentrations of PA, DNP, NBA, NBAc, and NA for compounds **3d** and **4g** were generated (Figs. S135 and S136).

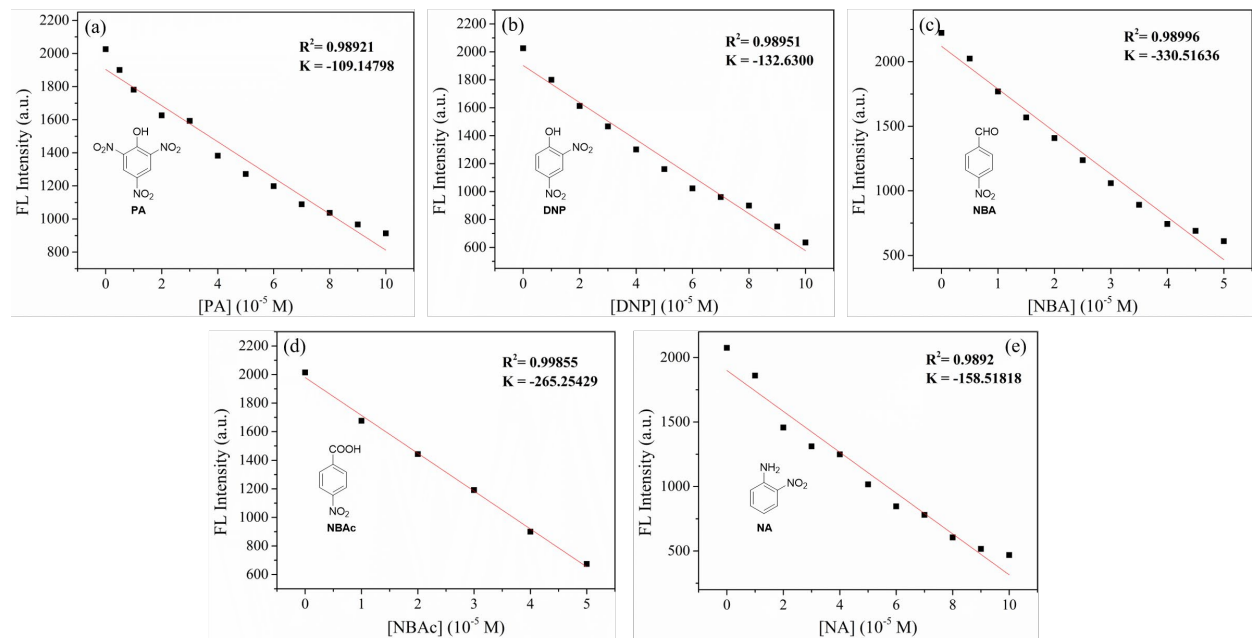


Fig. S135. The relationship between the maximum fluorescence intensity of compound **3d** (10^{-5} M, DMSO/H₂O, v/v, 40/60) and the concentrations of PA (a), DNP (b), NBA (c), NBAc (d) and NA (e).

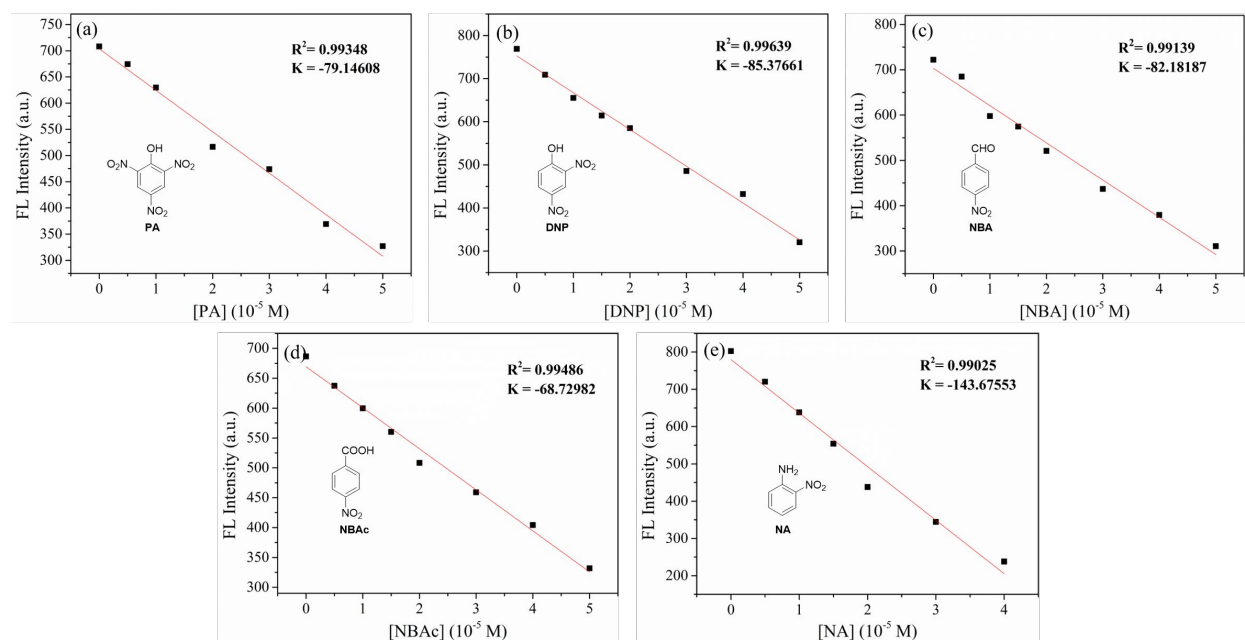
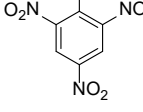
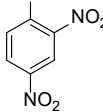
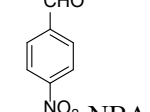
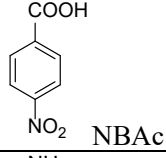
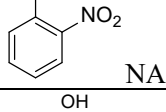
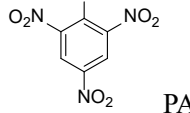
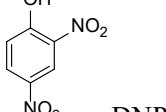
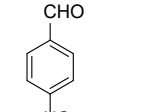
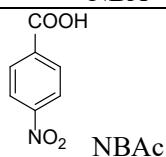
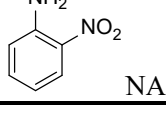


Fig. S136. The relationship between the maximum fluorescence intensity of compound **4g** (10^{-5} M, DMSO) and the concentrations of PA (a), DNP (b), NBA (c), NBAc (d) and NA (e).

Table S6. Comparison of NACs detection performance between probes **3d** and **4g**.

Probes	NACs structure	Quenching efficiency	$K_{sv} (\text{M}^{-1})$	LOD (M)
3d	 PA	54.8%	1.25×10^4	3.02×10^{-8}
	 DNP	53.4%	1.48×10^4	2.49×10^{-8}
	 NBA	58.0%	4.84×10^4	9.98×10^{-9}
	 NBAc	76.4%	2.86×10^4	1.24×10^{-8}
	 NA	57.4%	1.85×10^4	2.08×10^{-8}
4g	 PA	71.5%	2.35×10^4	4.17×10^{-8}
	 DNP	74.7%	1.32×10^4	3.87×10^{-8}
	 NBA	78.8%	4.03×10^4	4.02×10^{-8}
	 NBAc	74.7%	2.26×10^4	4.80×10^{-8}
	 NA	82.7%	4.03×10^4	2.30×10^{-8}

Given that compounds **3d** and **4g** are classified as dual-state emission (DSE) molecules, they exhibit robust fluorescence emission in both solution and solid states. Consequently, probes **3d** and **4g** should be loaded onto Whatman filter paper to fabricate straightforward test strips, thereby providing a portable, visually detectable tool.^[22, 23]

As anticipated, their visual detections of metal ions and NACs are successful, as shown as **Figs. S137-S140**. These indicate their good practical applications as probes.

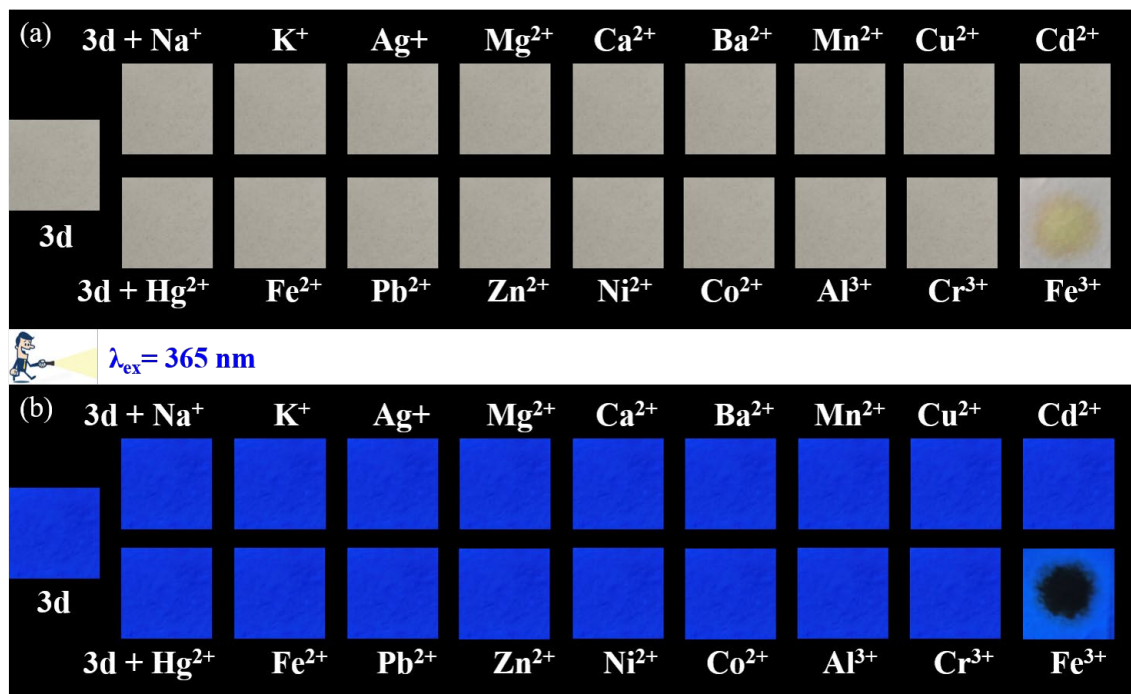


Fig. S137. Visualization of the **3d** loaded Whatman test strip under sunlight (a) and UV light (b).

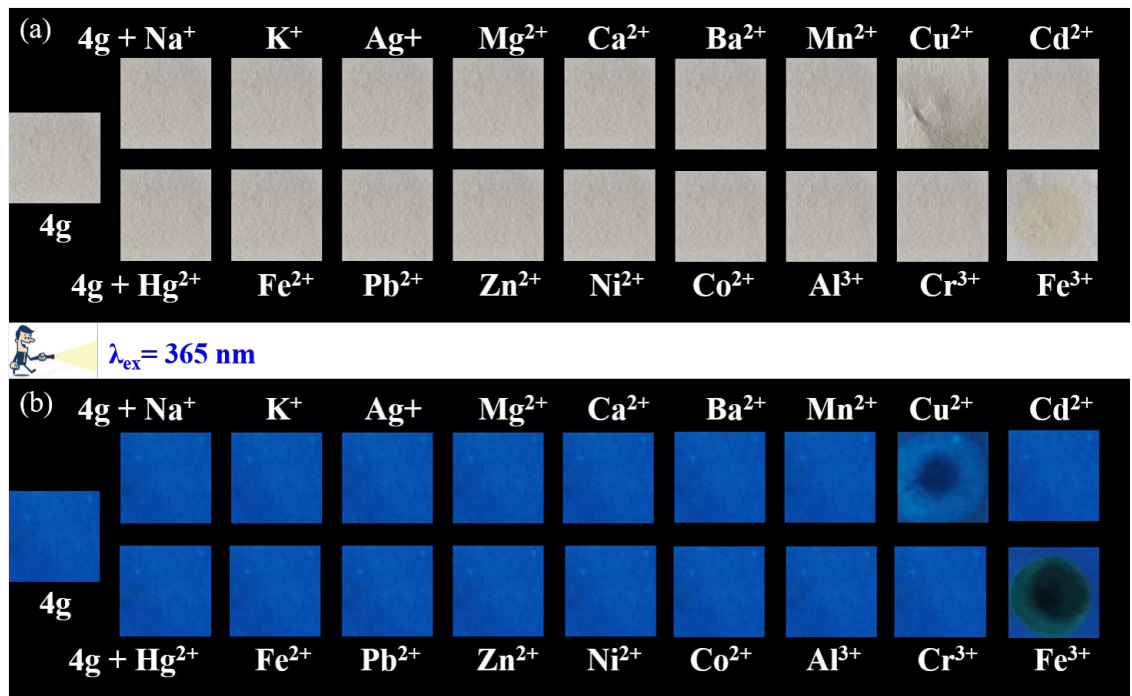


Fig. S138. Visualization of the **4g** loaded Whatman test strip under sunlight (a) and UV light (b).

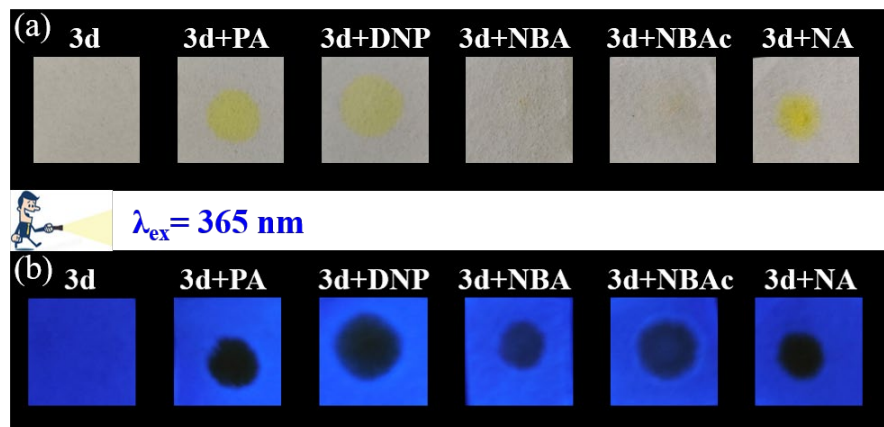


Fig. S139. Visual detection of NACs images of Whatman strips loaded with **3d** under sunlight (a) and UV light (b).

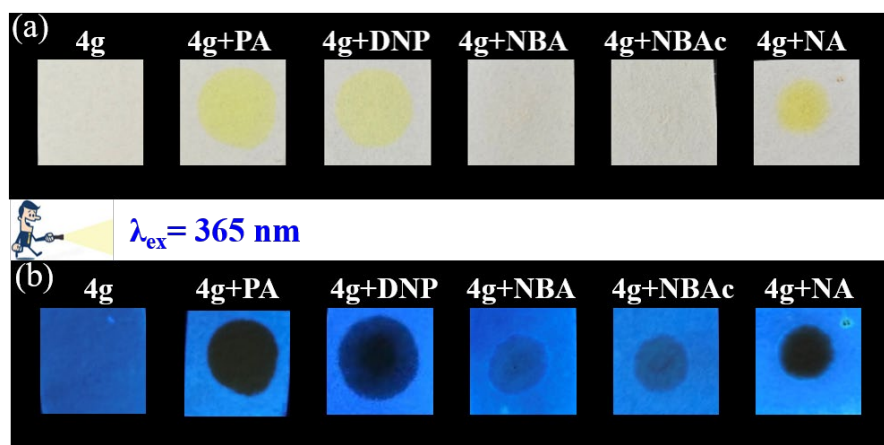


Fig. S140. Visual detection of NACs images of Whatman strips loaded with **4g** under sunlight (a) and UV light (b).

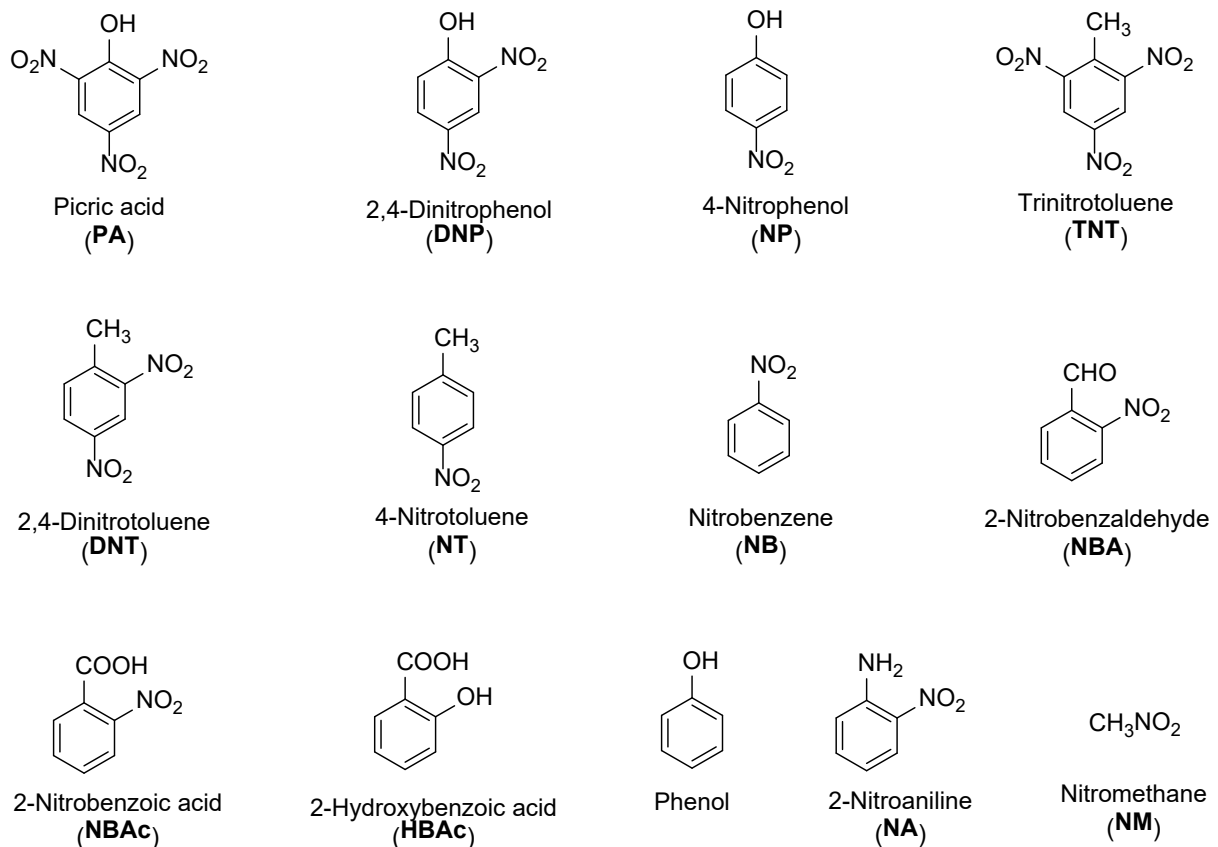


Fig. S141. The structures of nitroaromatic compounds (NACs).

5. Antimicrobial Activity Assays

Table S7. Antibacterial activity of 3-cyanopyridine compounds.

	<i>E. coli</i>		<i>S. aureus</i>	
	MIC $\mu\text{g/mL}$	MBC $\mu\text{g/mL}$	MIC $\mu\text{g/mL}$	MBC $\mu\text{g/mL}$
3a	500	> 1000	500	> 1000
3b	250	> 500	250	500
3c	250	> 500	250	500
3d	250	> 500	250	> 500
3e	250	> 500	250	> 500
3f	500	1000	500	1000
3g	250	> 500	125	500
3h	250	> 500	125	500
3i	250	> 500	62.5	125
3j	250	> 500	15.625	31.25
4a	500	1000	500	1000
4b	500	1000	500	1000
4c	500	1000	1000	2000
4d	500	1000	1000	2000
4e	500	1000	1000	2000
4f	500	1000	1000	2000
4g	500	1000	1000	2000
4h	500	1000	1000	2000
4i	500	1000	1000	2000
4j	500	1000	1000	2000
4k	500	1000	1000	2000
4l	500	1000	1000	2000
4m	2000	>2000	2000	>2000
4n	2000	>2000	2000	>2000
4o	1000	2000	500	1000
4p	1000	2000	500	1000
4q	1000	2000	125	500
4r	1000	2000	250	1000
4s	1000	2000	125	500
4t	1000	2000	125	500

6. References

- [1] X.-Y. Cao, Z.-H. Li, R.-R. Yu, Y.-Y. Ye, J.-Y. Xie, H. Li, and Wang Z.-Y. *Guangzhou Chem.*, 2025, DOI: [10.16560/j.cnki.gzhx.20250217](https://doi.org/10.16560/j.cnki.gzhx.20250217).
- [2] S. L. Liao, S. B. Shang, M. G. Shen, X. P. Rao, H. Y. Si, J. Song, and Z. Q. Song, *Bioorg. Med. Chem. Lett.*, 2016, **26**, 1512-1515.
- [3] J. Vassallo, A. Besinis, R. Boden, and R. Handy, D. *Ecotoxicol. Environ. Saf.*, 2018, **162**, 633-646.
- [4] C. M. Pang, Y. X. Tan, J. H. Ling, and L. Z. Hong, *Nanoscale*, 2024, **16**, 856-21868.
- [5] B.-W. Wang, K. Jiang, J.-X. Li, S.-H. Luo, Z.-Y. Wang, and H.-F. Jiang, *Angew. Chem., Int. Ed.*, 2020, **9**, 2338-2343.
- [6] M. J. Frisch, et al. *Gaussian 09, Revision D.01* (Gaussian, Inc.: Wallingford, CT, 2009).
- [7] P. Hohenberg, W. Kohn, *Phys. Rev.*, 1964, **136**, 864.
- [8] A. D. Becke, *J. Chem. Phys.*, 1993, **98**, 5648.
- [9] S. Grimme, S. Ehrlich, L. Goerigk, *J. Comput. Chem.*, 2011, **32**, 1456.
- [10] A. V. Marenich, C. J. Cramer, and D. G. Truhlar, *J. Phys. Chem. B*, 2009, **113**, 6378.
- [11] F. Weigend, R. Ahlrichs, *Phys. Chem. Chem. Phys.*, 2005, **7**, 3297.
- [12] Arushi, A. Sharma, A. Arora, N. Mehta, R. Kataria, and S. K. Mehta, *Chemosphere*, 2024, **363**, 142834.
- [13] X. B. Yu, Y. T. Xu, F. Liu, W. Zhang, Y. Sun, Y. J. Fang, L. Y. Fang, X. F. He, H. N. Na, and J. Zhu, *J. Mater. Chem. A*, 2023, **11**, 23511-23522.
- [14] J. P. Zhu, M. E. Graziotto, V. Cottam, T. Hawtrey, L. D. Adair, B. G. Trist, N. T. H. Pham, J. R. C. Rouaen, C. Ohno, M. Heisler, O. Vittorio, K. L. Double, and E. J. New, *ACS Sens.*, 2024, **9**, 2858-2868.
- [15] L. F. Li, S. H. Xu, X. Z. Li, H. C. Gao, L. Yang, and C. L. Jiang, *Chem. Eng. J.*, 2024, **493**, 152636.
- [16] B. X. Wang, J. Z. Shi, W. B. Zhai, L. Jiang, Y. M. Ma, Z. K. Zhang, F. Q. Zhao, X. T. Wu, J. Wu, J. F. Wang, L. D. Du, X. B. Pang, and L. Yan, *Sens. Actuators, B*, 2025, **432**, 136767.
- [17] S. N. K. Elmas, Z. E. Dincer, A. S. Erturk, A. Bostanci, A. Karagoz, M. Koca, G. Sadi, and I. Yilmaz, *Spectrochim. Acta, Part A*, 2020, **224**, 117402.
- [18] S. Lee, H. E. Kang, S. B. Park, X. Q. Chen, J. H. Shin, and S. Lee, *Sens. Actuators, B*, 2025, **423**, 136808.
- [19] H. Y. Niu, T. Q. Ye, L. Y. Yao, Y. F. Lin, K. Chen, Y. B. Zeng, L. Li, L. H. Guo, and J. B. Wang, *J. Hazard. Mater.*, 2024, **475**, 134914.
- [20] Q. Peng, and Y. X. Zhang, *J. Solid State Chem.*, 2024, **333**, 124596.

- [21] C. H. T. Nguyen, M. D. Hoang, T. T. Nguyen, T. H. Nguyen, T. P. L. Nguyen, L. T. Nguyen, H. L. Tran, M. H. Hoang, and H. Nguyen, *Synth. Met.*, 2025, **311**, 117828.
- [22] S. Suganya, E. Ravindran, M. K. Mahato, and E. Prasad, *Sens. Actuators, B*, 2019, **291**, 426-432.
- [23] H. F. Wu, Y. B. Chen, M. Q. Xu, Y. W. Ling, S. Y. Ju, Y. F. Tang, and C. L. Tong, *Sci. Total Environ.*, 2023, **860**, 160533.